INSIGHTS IN RESPIRATORY PHARMACOLOGY: 2021

EDITED BY: Paolo Montuschi and Irfan Rahman
PUBLISHED IN: Frontiers in Pharmacology

frontiers Research Topics

frontiers

ISSN 1664-8714
ISBN 978-2-83250-829-9
DOI 10.3389/978-2-83250-829-9

About Frontiers

Frontiers is more than just an open-access publisher of scholarly articles: it is a pioneering approach to the world of academia, radically improving the way scholarly research is managed. The grand vision of Frontiers is a world where all people have an equal opportunity to seek, share and generate knowledge. Frontiers provides immediate and permanent online open access to all its publications, but this alone is not enough to realize our grand goals.

Frontiers Journal Series

The Frontiers Journal Series is a multi-tier and interdisciplinary set of open-access, online journals, promising a paradigm shift from the current review, selection and dissemination processes in academic publishing. All Frontiers journals are driven by researchers for researchers; therefore, they constitute a service to the scholarly community. At the same time, the Frontiers Journal Series operates on a revolutionary invention, the tiered publishing system, initially addressing specific communities of scholars, and gradually climbing up to broader public understanding, thus serving the interests of the lay society, too.

Dedication to Quality

Each Frontiers article is a landmark of the highest quality, thanks to genuinely collaborative interactions between authors and review editors, who include some of the world's best academicians. Research must be certified by peers before entering a stream of knowledge that may eventually reach the public - and shape society; therefore, Frontiers only applies the most rigorous and unbiased reviews.
Frontiers revolutionizes research publishing by freely delivering the most outstanding research, evaluated with no bias from both the academic and social point of view. By applying the most advanced information technologies, Frontiers is catapulting scholarly publishing into a new generation.

What are Frontiers Research Topics?

Frontiers Research Topics are very popular trademarks of the Frontiers Journals Series: they are collections of at least ten articles, all centered on a particular subject. With their unique mix of varied contributions from Original Research to Review Articles, Frontiers Research Topics unify the most influential researchers, the latest key findings and historical advances in a hot research area! Find out more on how to host your own Frontiers Research Topic or contribute to one as an author by contacting the Frontiers Editorial Office: frontiersin.org/about/contact

INSIGHTS IN RESPIRATORY PHARMACOLOGY: 2021

Topic Editors:
Paolo Montuschi, Catholic University of the Sacred Heart, Italy
Irfan Rahman, University of Rochester, United States

The authors declare that the research was conducted in the absence of any commercial or financial relationships that could be construed as a potential conflict of interest.

Citation: Montuschi, P., Rahman, I., eds. (2022). Insights in Respiratory Pharmacology: 2021. Lausanne: Frontiers Media SA.
doi: 10.3389/978-2-83250-829-9

Table of Contents

frontiers | Frontiers in Pharmacology

TYPE Editorial
PUBLISHED 07 November 2022
DOI 10.3389/fphar.2022.1052994

OPEN ACCESS

EDITED AND REVIEWED BY
Jian Fu,
University of Kentucky, United States

*CORRESPONDENCE
Paolo Montuschi,
paolo.montuschi@unicatt.it

SPECIALTY SECTION
This article was submitted to Respiratory Pharmacology,
a section of the journal
Frontiers in Pharmacology

RECEIVED 24 September 2022
ACCEPTED 03 October 2022
PUBLISHED 07 November 2022

CITATION
Montuschi P and Rahman I (2022), Editorial: Insights in respiratory pharmacology: 2021.
Front. Pharmacol. 13:1052994.
doi: 10.3389/fphar.2022.1052994

Editorial: Insights in respiratory pharmacology: 2021

Paolo Montuschi[1,2]* and Irfan Rahman[3]

[1]Faculty of Medicine, Imperial College, National Heart and Lung Institute, London, United Kingdom, [2]Department of Pharmacology, Faculty of Medicine, Catholic University of the Sacred Heart, Roma, Italy, [3]Department of Environmental Medicine, School of Medicine and Dentistry, University of Rochester Medical Center, Rochester, NY, United States

KEYWORDS

respiratory pharmachology, personalised pharmacotherapy, personalised medicine, drug mechanism of action, pharmacological targets

Editorial on the Research Topic
Editorial: Insights in respiratory pharmacology: 2021

There is an unprecedented unmet need to understand the mechanisms and therapeutic targets of pulmonary diseases. In the past, several approaches have been used to identify the respiratory disease mechanisms involving acute and chronic exposures (e.g., tobacco smoke, bacteria, viruses, hyperoxia, bleomycin) and other factors. Some targets have been successfully pinpointed based on cell signaling, kinase mechanisms, nuclear signaling, and epigenetic changes. However, these achievements have only partially translated into clinical applications.

For this Research Topic, we solicited several top-class articles on the mechanisms of acute and chronic pulmonary diseases, with a view to prioritizing the understanding of potential therapeutic targets and pharmacotherapies. Some interesting and timely topics were chosen from key authors, and a series of original articles was compiled.

Regarding the mechanisms of *in vivo* acute lung injury in experimental animal models, one study describes the role of the mitochondrial protein AKAP1 in the regulation of endoplasmic reticulum function; Sidramagowda Patil et al.; another study demonstrates the anti-inflammatory role played by metformin through its regulation of the SIRT1/nuclear factor-kB (NF-kB)/NLRP3 pathway during endothelial cell pyroptosis; Zhang et al.; and another describes the role of aspirin in reducing hyperoxia-induced pulmonary inflammation by regulating the NF-kB signaling pathway Tung et al.

In terms of potential anti-remodeling effects, one study shows that chemerin is upregulated in the lungs in acute-exposure experimental animal models *in vivo*, that it promotes the proliferation and migration of arterial smooth muscle cells *in vitro* by regulating ERK1/2 signaling, and that its plasma concentrations are elevated in persons with idiopathic pulmonary hypertension compared with healthy controls Peng et al.

Another study shows that activation of midkine-Notch2 signaling promotes the proliferation of airway smooth muscle cells *in vitro*, and in a COPD experimental animal model *in vivo*, as an airway remodeling mechanism Deng et al.

In terms of clinical studies, one article describes the development and validation of the Respiratory Adherence Care Enhancer Questionnaire and assesses its utility for identifying self-management barriers to the use of inhaled corticosteroids, the mainstay of asthma maintenance pharmacotherapy Visser et al.

Another study presents the results of a prospective, controlled, randomized clinical trial that identified the optimal dose of ropivacain, a local anesthetic, in participants who received an ultrasound-guided rhombic intercostal block (RIB) as analgesia during video-assisted thoracoscopic surgery (VATS) Deng et al.

One article summarizes recent evidence regarding the role of COVID-19 vaccines and other therapeutic interventions, focusing on emerging variants Islam et al.

One study describes the development of nanoparticle drug delivery systems actively directed against molecular targets and their potential implications for lung cancer pharmacotherapy Wang et al.

Regarding the potential pharmacological modulation of the mechanisms of allergic diseases, one *in vitro* and *in vivo* study shows that house dust mite aeroallergen increases susceptibility to pneumococcal infection by reducing leukocyte phagocytosis and NETosis Papanicolaou et al.

Finally, in the context of the emerging usage of cannabis products, one article describes the development of a standardized method for the generation of a cannabis smoke extract to investigate its mechanism of action. It also shows the inflammatory effects of cannabis smoke extract *in vitro* Aloufi et al.

We are pleased to present this series of emerging topics in this Research Topic of the Respiratory Pharmacology section of *Frontiers in Pharmacology*. These topics have high translational potential. A better understanding of the pathogenesis and mechanisms of drug action are expected to lead to identification of new therapeutic targets, which will pave the way for more personalized pharmacotherapies for respiratory diseases.

Author contributions

PM and IR drafted and revised the manuscript.

Acknowledgments

To my Beloved Mamma Laura, Paolino. To my Beloved Mother Rabia Khatoon, Irfan.

Conflict of interest

The authors declare that the research was conducted in the absence of any commercial or financial relationships that could be construed as a potential conflict of interest.

Publisher's note

frontiers in Pharmacology

ORIGINAL RESEARCH
published: 22 December 2021
doi: 10.3389/fphar.2021.767092

Respiratory Adherence Care Enhancer Questionnaire: Identifying Self-Management Barriers of Inhalation Corticosteroids in Asthma

*Claire D. Visser[1], Jip M. Linthorst[2], Esther Kuipers[3], Jacob K. Sont[4], Joyca P. W. Lacroix[5], Henk-Jan Guchelaar[1] and Martina Teichert[1,2]**

[1]Department of Clinical Pharmacy and Toxicology, Leiden University Medical Center, Leiden, Netherlands, [2]Royal Dutch Pharmacists Association (KNMP), The Hague, Netherlands, [3]Community Pharmacy Empel, 's-Hertogenbosch, Netherlands, [4]Department of Biomedical Data Sciences, Section Medical Decision Making, Leiden University Medical Center, Leiden, Netherlands, [5]Department of Digital Engagement, Behavior and Cognition, Philips Research, Eindhoven, Netherlands

OPEN ACCESS

Edited by:
Paolo Montuschi,
Catholic University of the Sacred Heart, Italy

Reviewed by:
Antonio Molino,
University of Naples Federico II, Italy
Yuan-Pang Wang,
University of São Paulo, Brazil

***Correspondence:**
Martina Teichert
M.Teichert@lumc.nl

Specialty section:
This article was submitted to Respiratory Pharmacology, a section of the journal Frontiers in Pharmacology

Received: 30 August 2021
Accepted: 25 November 2021
Published: 22 December 2021

Citation:
Visser CD, Linthorst JM, Kuipers E, Sont JK, Lacroix JPW, Guchelaar H-J and Teichert M (2021) Respiratory Adherence Care Enhancer Questionnaire: Identifying Self-Management Barriers of Inhalation Corticosteroids in Asthma. Front. Pharmacol. 12:767092. doi: 10.3389/fphar.2021.767092

Introduction: Suboptimal self-management of inhaled corticosteroids (ICS) in asthma patients is frequently observed in clinical practice and associated with poor asthma control. Driving factors for suboptimal self-management are complex and consist of a range of behavioral barriers (cognitive, affective and practical) with a considerable inter-individual variability. Identification of individual barriers facilitates the use of corresponding behavior change techniques and tailored care to improve asthma treatment outcomes.

Objective: This study describes the development and validation of the 'Respiratory Adherence Care Enhancer' (RACE) questionnaire to identify individual barriers to self-management of ICS therapy in asthma patients.

Methods: The development included: 1) an inventory of self-management barriers based on a literature review, 2) expert assessment on relevance and completeness of this set, linking these barriers to behavioral domains of the Theoretical Domains Framework (TDF) and 3) the formulation of corresponding questions assessing each of the barriers. A cross-sectional study was performed for validation. Primary care asthma patients were invited to fill out the RACE-questionnaire prior to a semi-structured telephonic interview as golden standard. Barriers detected from the questionnaire were compared to those mentioned in the interview.

Results: The developed questionnaire is made up of 6 TDF-domains, covering 10 self-management barriers with 23 questions. For the validation 64 patients completed the questionnaire, of whom 61 patients were interviewed. Cronbach's alpha for the consistency of questions within the barriers ranged from 0.58 to 0.90. Optimal cut-off values for the presence of barriers were determined at a specificity between 67 and 92% with a sensitivity between 41 and 83%. Significant Areas Under the Receiver Operating Curves values were observed for 9 barriers with values between 0.69 and 0.86 (p-value <0.05), except for 'Knowledge of ICS medication' with an insignificant value of 0.53.

Conclusion: The RACE-questionnaire yields adequate psychometric characteristics to identify individual barriers to self-management of ICS therapy in asthma patients, facilitating tailored care.

Keywords: asthma, inhaled corticosteroids (ICS), self-management (self-care), theoretical domains framework (TDF), tailored care, adherence–compliance–persistance

INTRODUCTION

Asthma is a chronic respiratory disease affecting an estimated 300 million individuals worldwide (GBD 2017 Disease and Injury Incidence and Prevalence Collaborators, 2018). It is a public health problem placing a significant socioeconomic burden on patients, caregivers and healthcare systems (Dharmage et al., 2019; Dierick et al., 2020). Inhaled corticosteroids (ICS) are considered the cornerstone of controller therapy for asthma according to the recommendations of the Global Initiative For Asthma (GINA) guideline (Global Initiative for Ast, 2020). These drugs have the ability to effectively control asthma by suppressing airway inflammation, reducing bronchoconstriction and concomitant asthma symptoms such as breathlessness and wheezing (Barnes, 2010; Global Initiative for Ast, 2020). However, approximately 50% of asthma patients do not follow the prescribed ICS regimen due to factors related to self-management including poor adherence, awareness of the disease or the lacking of practical skills (World Health Organisation, 2021). This phenomenon has been associated with an increased risk of exacerbations, impaired quality of life, hospitalization, and mortality (Bårnes and Ulrik, 2015).

Healthcare professionals interact with asthma patients in the field of respiratory health during consultations or prescription refills and have an important role in providing long-term care for effective self-management. They educate patients on their disease and inhalation medication, provide training on the use of inhalation devices, address patients' concerns and beliefs in order to guide optimal self-management of ICS therapy (Bridgeman and Wilken, 2021; Murray and O'Neill, 2018). However, identifying and overcoming barriers to self-management of ICS therapy is a major challenge in clinical practice (Murray and O'Neill, 2018). Driving factors are complex and consist of a range of cognitive, affective and practical barriers with a considerable inter-individual variability (Boulet et al., 2012; World Health Organisation, 2021). Healthcare professionals often lack good insight into this multitude of barriers and therefore apply a "one size fits all" approach, frequently focusing on adherence and practical skills without addressing the underlying individual behavioral barriers (Plaza et al., 2016; Dima et al., 2017; Anghel et al., 2019; Toelle et al., 2020). Enabling healthcare professionals with a tool to identify individual barriers to self-management of ICS therapy may be of added value to facilitate tailored care to optimize self-management and treatment outcomes.

Based on psychological behavioral change theories, the Theoretical Domains Framework (TDF) offers a set of domains with associated constructs composed of cognitive, affective, social and environmental factors. This validated framework can be applied to identify individual behavioral challenges and to develop corresponding interventions as a strategy to overcome behavioral barriers (Cane et al., 2012; French et al., 2012). Thus, the TDF is appropriate as a theoretical underpinning for asthma patient behavior, enhancing existing interventions in their effectiveness to overcome individual barriers to self-management of ICS therapy in clinical practice (Allemann et al., 2016; Presseau et al., 2017; Patton et al., 2018).

Hence, the aim of this study was to develop and validate a questionnaire based on the TDF for identification of individual barriers to self-management of ICS therapy in primary care asthma patients: the "Respiratory Adherence Care Enhancer" (RACE) questionnaire.

METHODS

Study Design

A mixed-methodology approach was conducted in this study to develop and validate the RACE questionnaire (**Supplementary 1.1**). The development of the questionnaire was based on a literature review. The questionnaire was validated by the assessment of the content and face validity as part of the development phase. To validate the questionnaire on internal consistency and criterion validity of the barriers with asthma patients, a cross-sectional study was performed. Primary care asthma patients were invited to fill out the questionnaire, followed by a telephonic semi-structured interview as a golden standard method within a 2-week period. The study protocol (N19.097) was declared to not fall within the scope of the Dutch Medical Research Involving Human Subjects Act by the Medical Ethics Committee (MEC) of the Leiden University Medical Center (LUMC). The study was approved by the scientific committee of the division of Clinical Pharmacy and Toxicology of the LUMC and was conducted according to the principles of the World Medical Association Declaration of Helsinki. Written informed consent was obtained from all included patients prior to participation.

Development

Systematic Literature Review

A systematic literature review was performed to identify articles published between January 2000 and October 2018 concerning barriers to self-management or adherence of ICS therapy in asthma patients. The search was performed in PubMed and the Web of Science database using a combination of the following keywords and Medical Subject Headings (MeSH): "asthma", "barriers", "self-management" and "adherence". All obtained records were screened by two independent researchers

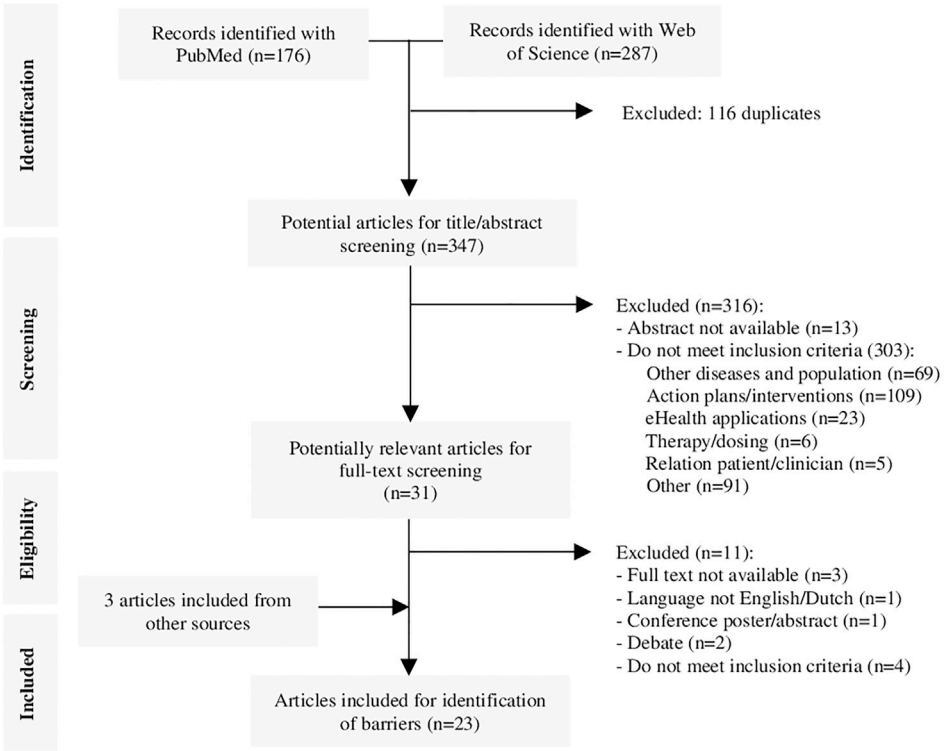

FIGURE 1 | Systematic literature review flowchart.

(RM, MT) according to predefined inclusion criteria including "asthma patients receiving ICS therapy" and "barriers concerning non-adherence, beliefs or self-management" to determine their eligibility in a three-stage screening process which consisted of title, abstract- and full-text screening. Duplicates, commentaries, editorials, poster abstracts, letters without original data and publications in other languages other than English or Dutch were excluded. Consensus on discrepancies of the included articles was achieved through discussion. Subsequently, barriers to self-management or adherence of ICS therapy were extracted and summarized according to the TDF.

Content and Face Validity

An expert panel was consulted in two Delphi rounds to assess the clinical relevance, completeness and feasibility of the set of extracted barriers and to cluster these barriers into TDF-domains. Pharmacists of the Special Interest Group (SIG) Lung from the Royal Dutch Pharmacists Association (KNMP) and General Practitioners (GP) were invited to this panel. In round 1, participants were requested to rate the barriers on the abovementioned with a scale from 0 to 10 (low to high). In round 2 participants reappraised the results from round 1 through the same method. Subsequently, questions were formulated to address the barriers identified (JML, MT). Questions were framed as negative and positive statements to limit social-desirability bias (Larson, 2018). For the responses, a 5-point Likert scale was provided ranging from complete disagreement to complete agreement. Questions on medication use and the validated "Control of Allergic Rhinitis and Asthma Test" (CARAT10) were added to assess asthma control (Fonseca et al., 2010). The final questionnaire was tested for face validity by pharmacists of the SIG Lung and researchers with experience in the development of questionnaires, to assess the readability, feasibility and comprehensive understanding of the questions.

Forward-backward translation was performed on the original Dutch version of the RACE questionnaire, providing an English version. Forward translation was conducted by a native English speaker and backward translation by a native Dutch speaker. These two processes were performed independently of each other, after which the two Dutch versions were compared and discrepancies were resolved in a consultation session.

Validation

For the assessment of the internal consistency and criterion validity of the barriers, a cross-sectional study was performed in primary care asthma patients. As there were no other comparable measuring tools available, all respondents to the RACE questionnaire were invited for semi-structured interviews. The barriers identified from these interviews were considered as golden standard to validate the barriers as detected from the scores on the RACE questionnaire.

Study Participants

A total of 20 community pharmacists from the SIG lung and the internship database of the Leiden University were invited to each

TABLE 1 | RACE questionnaire construct for the identification of self-management barriers.

TDF-domains	Barriers	Questions (n)[a]	Total score[b]
Knowledge	Knowledge of asthma	2	0–8
	Knowledge of ICS medication	3	0–12
Beliefs about consequences	Expectations of ICS medication	2	0–8
	Experience of side-effects	2	0–8
Emotion	Concerns about ICS inhaler	3	0–12
	Social discomfort of inhaling with ICS in public	1	0–4
Skills	Understanding and application of ICS inhaler techniques	3	0–12
Memory, attention and decision process	(Un)Conscious adherence to prescribed ICS medication regimen	3	0–12
	Shared treatment decision making	3	0–12
Behavioural regulation	Existence of structure in ICS medication intake	1	0–4

[a]*Responses to the questions are provided on a 5-point Likert scale with the following options: I disagree completely, I disagree mostly, I agree somewhat, I agree mostly and I agree completely. Scores to these options vary from 0 to 4 or 4 to 0 dependent on the question.*

[b]*Sum scores were computed per barrier by adding the scores of the corresponding questions. Total scores achievable for a barrier differ for the number of questions included, with a maximum of 4 points to be obtained per question.*

Abbreviations: RACE: respiratory adherence care enhancer; TDF: theoretical domains framework; ICS: inhaled corticosteroids.

recruit 10 asthma patients with ICS dispensing's between October and December 2019. The aim of this study was to include 100 patients at a non-response rate of 50%. Patients were eligible for inclusion when ≥18 years, diagnosed with asthma and treated with ICS according to dispensing data present in the pharmacy information systems. Patients with Chronic Obstructive Pulmonary disease (COPD), suspicions hereof or diagnosed with other significant lung diseases were excluded. Likewise, the incapability to speak, write and comprehend the Dutch language were exclusion criteria.

Data-Collection

An online version of the RACE questionnaire was built within the facilities of Castor Electronic Data Capture (EDC) to safeguard the collected data in the LUMC surroundings according to the Data Protection Act. If requested by the patient, a paper version of the questionnaire was provided.

Semi-structured interviews were performed with the responders to the questionnaire. An interview guide was developed with comparable components, prompts and recommendations as presented in the TDF-based interview topic guides of earlier studies (**Supplementary 2.1**) (Presseau et al., 2017; DeJonckheere and Vaughn, 2019). This method was applied to elicit and encourage patients to provide overt information concerning their feelings, thoughts and beliefs on the TDF domains and barriers. To retain the objectivity of the provided information in the interviews, the components of the questionnaire were presented in a different order and posed through an open dialogue approach. The interviews were conducted in the Dutch language by a member of the research team (JML) who did not have any prior contact with the participants and no access to the scores of the questionnaire. The interviews were recorded, transcribed verbatim and independently categorized for barriers with the aid of a predefined coding framework by two other members of the research team (CV, MT). This framework was developed to provide a clear distinction between the presence or absence of each barrier, ensuring a complete and comprehensive understanding of existing barriers in the participants (**Supplementary 2.2**). The interrater reliability was assessed between the coding appraisals. Any discrepancies of the coded data were resolved through discussions. The recordings and transcripts were safeguarded within the LUMC password-secured surroundings.

Patient's judgements on the questionnaire were queried as last question in the semi-structured interview and taken into consideration in the final RACE questionnaire.

Data-Analysis

Descriptive analysis was performed to describe demographic characteristics and the distribution of barriers of the overall included sample population.

Cronbach's alpha test was used to determine the internal consistency of the questions within each barrier. Values between 0.6 and 0.7 were considered as acceptable and values between 0.7 and 0.9 indicated a good level of reliability (Taber, 2018). Cohen's kappa statistic was performed to assess the inter-rater reliability between the coding appraisals of the semi-structured interview data. Values of at least 0.6 were considered acceptable (Landis and Koch, 1977).

The identification of cut-off values for the presence of barriers were determined for optimal specificity and sensitivity values by receiver operating characteristic (ROC) analysis. The sum scores of the questions per barrier obtained from the RACE questionnaire and the binary outcomes from the interviews were used for the ROC curves. Furthermore, criterion validity was assessed with the optimal sensitivity and specificity values. If necessary, higher specificity was preferred to higher sensitivity to reduce the number of false positives, maintaining practicability in clinical practice. Additionally, the area under the curve (AUROC) was calculated per barrier to determine the ability of the barrier scores to discriminate between barrier presence or absence by comparing the AUROC values to a chance value of 0.5. Two-tailed p-values ≤ 0.05 were considered significant.

Statistical analyses were performed using SPSS statistical software (version 26.0, IBM corp., Armonk, NY).

TABLE 2 | Demographic characteristics of the included study participants (n = 64).

Variables	Number (Percentages)
Gender (Female)	45 (70.3%)
Type of inhaler used	
pMDI	25 (39.1%)
DPI	38 (59.4%)
Unknown	1 (1.6%)
Reliever ICS therapy	6 (9.4%)
Maintenance ICS therapy	58 (90.6%)
Adequate asthma control	25 (39.1%)

Abbreviations: pMDI: pressurized Metered Dose Inhaler; DPI: dry powder inhaler; ICS: inhaled corticosteroids.

RESULTS

Development

A total of 347 potentially relevant articles were identified from the systematic literature review, of which 316 were excluded based on their titles and/or abstract. Full-text screening was conducted on the remaining 31 articles, resulting in the exclusion of 11 articles and the addition of 3 articles identified from reference lists. The final review included 23 articles (**Figure 1**) containing 32 barriers to self-management of ICS therapy in asthma patients, which could be related to 8 TDF-domains. The clinical relevance of the extracted barriers and their relation to the TDF-domains were assessed by a panel of 9 pharmacists from the SIG Lung and 1 GP in Delphi-rounds, resulting in the addition of 1 barrier and exclusion of 13 barriers and 2 TDF-domains. The final version of the RACE questionnaire included 6 TDF domains, covering 10 self-management barriers with 23 corresponding questions (**Table 1**). The RACE questionnaire is provided as additional material (**Table 4**).

Validation

Participating Patients

Eligible asthma patients were invited by 16 community pharmacies. An informed consent was provided by 73 patients of whom 8 patients did not respond to the RACE questionnaire and 1 patient was excluded due to mentioning diagnosis with COPD during the interview. Therefore, 64 patients were enrolled in this study. Semi-structured interviews were conducted in 63 of these patients of which 2 interviews were excluded due to an unclear record and 1 interview was excluded due to record failure. This resulted in 61 patients available for assessment of criterion validity.

Demographic characteristics of the included patients are presented in **Table 2**. Of the 64 patients 70.3% were female. With regard to their ICS therapy, 39.1% of the patients were reported to use pressurized metered dose inhalers (pMDI's) and 59.4% dry powder inhalers (DPI's). The majority of the patients used their ICS on a daily basis as maintenance therapy (90.6%) and a small number of patients as reliever therapy (9.4%). Adequate asthma control, as established by a CARAT-score of >24, was present in 39.1% of the patients. The presence of the barriers ranged between 16.4 and 57.4% according to the semi-structured interviews (**Figure 2**). The majority of the barriers detected concerned 'Shared treatment decision making' (57.4%), 'Knowledge of asthma' (44.3%) and 'Knowledge of ICS medication' (36.1%).

Psychometric Characteristics

Cronbach's alpha values ranged from 0.58 to 0.89 (**Table 3**). Three barriers were considered good Cronbach's alpha values, including 'Expectations of ICS medication' (0.89), 'Concerns about ICS inhaler' (0.80) and '(Un)conscious adherence to prescribed ICS medication regimen' (0.77). The barriers 'Knowledge of asthma' (0.67), 'Knowledge of ICS medication' (0.65), 'Experience of side-effects' (0.66) and 'Shared treatment decision making' (0.66) were considered acceptable. For the barrier 'Understanding and application of ICS inhaler techniques' Cronbach's alpha was just below the acceptable range (0.58). Cohen's kappa values ranged between 0.35 and 0.96 for the inter-rater reliability of the coding of the barriers from the interviews, with a total of 5 barriers above 0.6 (**Table 5**).

Optimal cut-off values for the presence of a barrier were determined at specificity values between 67.3 and 91.8% with sensitivity values between 40.9 and 83.3% for the 10 barriers (**Table 3**). In addition, significant AUROC values were determined for the barriers ranging between 0.69 and 0.86 (p-value <0.05), except for the barrier 'Knowledge of ICS medication' with an AUROC value of 0.53 (**Figure 3**). Further investigation of this barrier revealed a poorly comprehensible question on knowledge of the difference between bronchodilator and anti-inflammatory inhalers which has been revised. Also, after evaluation of the patient's judgements, the terminology for 'shame' was adjusted in the question corresponding to the barrier 'Social discomfort of inhaling with ICS in public' (**Table 4**).

DISCUSSION

This study described the development and validation of the RACE questionnaire to identify individual barriers to self-management of ICS therapy in primary care asthma patients.

The concise set of barriers addressed has shown associations with decreased self-management, adherence and poor treatment outcomes with ICS therapy in asthma patients (Ponieman et al., 2009; Wilson et al., 2010; Dima et al., 2015; Foster et al., 2017; George and Bender, 2019). Clinical relevance of these barriers has also been verified by a panel of experts during the development of the questionnaire. At present multiple questionnaires are available for asthma patients, mainly emphasizing on barriers related to (un) conscious adherence and side-effects (Plaza et al., 2016; Dima et al., 2017; Toelle et al., 2020). However, these questionnaires often consider adherence as a single outcome without acknowledging that adherence is influenced by a set of underlying behavioral barriers that need to be overcome to optimize adherence. Other questionnaires as the Self-Management Screening (SeMaS) questionnaire signal essential individual barriers to self-

TABLE 3 | Psychometric characteristics of the self-management barriers on the RACE questionnaire.

TDF-domain	Barrier	Reliability	Criterion validity				
		Cronbach's α[a]	Cut-off	Sensitivity (%)	Specificity (%)	AUROC	*p*-value[b]
Knowledge	Knowledge of asthma	0.67	3.5	59.3	70.6	0.70	**0.007**
	Knowledge of ICS medication	0.65	3.5	40.9	71.8	0.53	0.724
Beliefs about consequences	Expectations of ICS medication	0.89	3.5	60.0	82.4	0.81	**0.002**
	Experience of side-effects	0.66	2.5	58.3	91.8	0.73	**0.014**
Emotion	Concerns about inhaler medication	0.80	3.5	75.0	73.3	0.77	**0.002**
	Social discomfort of inhaling with ICS in public	N.A[c]	1.5	47.1	83.7	0.69	**0.022**
Skills	Understanding and application of ICS inhaler techniques	0.58	2.5	50.0	67.3	0.69	**0.042**
Memory, attention and decision process	(Un)conscious adherence to prescribed ICS medication regimen	0.77	3.5	83.3	79.1	0.86	**0.000**
	Shared treatment decision making	0.66	5.5	65.7	73.1	0.76	**0.001**
Behavioural regulation	Existence of structure in ICS medication intake	N.A[c]	1.5	64.3	89.4	0.80	**0.001**

[a]*Cronbach's alpha values between 0.6 and 0.7 indicate an acceptable level of reliability and values between 0.7 and 0.9 indicate a good level of reliability.*
[b]*p-value ≤ 0.05 was set as statistically significant for the assessment of the accuracy of the barriers to discriminate between the presence and absence of the barrier and are printed in bold.*
[c]*The internal consistency test was not applicable (N.A.) as only one question was included in the barrier.*
Abbreviations: RACE: respiratory adherence care enhancer; TDF: theoretical domains framework; ICS: inhaled corticosteroids; AUROC: area under the receiver operating characteristic; N.A.: not applicable.

management (Eikelenboom et al., 2015). Nevertheless, the contents of this questionnaire are generic and aimed at a range of chronic conditions. The Nijmegen Clinical Screening Instrument (NCSI) for patients with COPD also provides a tailored approach measuring disease-specific characteristics that determine their health status (Vercoulen, 2012). Yet, these questionnaires do not highlight specific underlying barriers concerning inhalation therapy or asthma requiring behavior change. Moreover, interventions targeting self-management or adherence of ICS therapy lack a theoretical underpinning which may clarify their disappointing effectiveness (Normansell et al., 2017). The applied TDF in the RACE questionnaire may therefore aid in the identification of individual behavioral challenges and support matching interventions with behavior change techniques (BCTs) (Cane et al., 2012; French et al., 2012). This may enable healthcare professionals to provide tailored care in a multidisciplinary setting with barrier-specific interventions to overcome or prevent suboptimal self-management of ICS therapy. The study of Patton et al. (2018) has demonstrated potential for the use of TDF to identify and overcome non-adherence to multiple medications in elderly patients.

The RACE questionnaire has shown acceptable to good reliability for the internal consistency of the questions per barrier, except for the barrier 'Understanding and application of ICS inhaler techniques' with a value just below the acceptable range. These observed values are in conformity with previous studies addressing comparable screening questionnaires with multiple constructs (Cramm et al., 2012; Eikelenboom et al., 2015). Additionally, any variation in internal consistency of the barriers can be explained by differences in the extent of heterogeneity of the corresponding questions per barrier and the limited number of questions presented per barrier (Tavakol and Dennick, 2011). Whereas the RACE questionnaire was developed to receive relevant information at a concise number of questions, minimizing respondent burden (Turner et al., 2007).

The RACE questionnaire is developed as tool to complement the usual care for asthma patients. It is intended for consultations between patients and healthcare professionals to identify potential barriers to self-management of ICS therapy, facilitating tailored care to improve self-management and

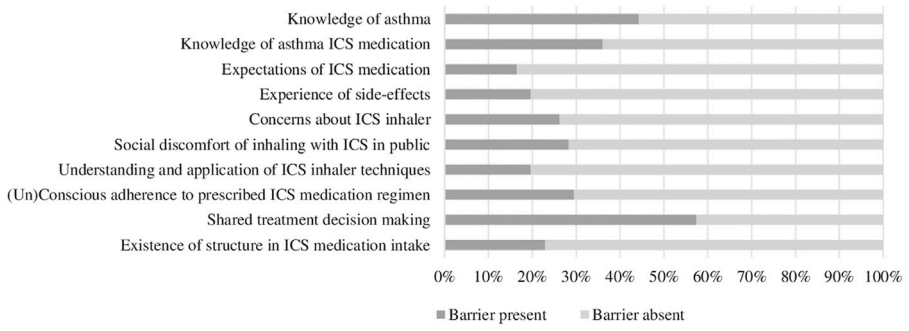

FIGURE 2 | Percentages of barriers present identified from the semi-structured interviews (*n* = 61). Abbreviations: ICS: Inhaled Corticosteroids.

TABLE 4 | Description of the RACE questionnaire identifying individual barriers to self-management of ICS therapy.

TDF-domains	Barriers	Questions	Score[a]	Total score[ab]	Interpretation
Knowledge	Knowledge of asthma	1a. I know what triggers an asthma attack	4–0	0–8	BA:0–3
		1b. I know how to prevent an asthma attack	4–0		BP: 4–8
	Knowledge of ICS medication	2a. I know that my anti-inflammatory inhaler reduces the swelling of the lining in my airways	4–0	0–12	BA: 0–3
		2b. I know that my anti-inflammatory inhaler improves the condition of my airways	4–0		BP: 4–12
		2c. I know that my anti-inflammatory does not provide quick relief of my asthma symptoms but it tackles the cause of my asthma[c]	4–0		
Beliefs about consequences	Expectations of ICS medication	3a. I need my anti-inflammatory inhaler to keep my asthma stable	4–0	0–8	BA: 0–3
		3b. I need my anti-inflammatory inhaler to prevent my asthma from getting worse	4–0		BP: 4–8
	Experience of side-effects	4a. I experience side-effects from my anti-inflammatory inhaler	0–4	0–8	BA: 0–2
		4b. The side-effects of my anti-inflammatory inhaler reduce my daily functioning	0–4		BP: 3–8
Emotion	Concerns about ICS inhaler	5a. I am concerned about possible side-effects from my anti-inflammatory inhaler	0–4	0–12	BA: 0–3
		5b. I am concerned about long-term side-effects from my anti-inflammatory inhaler	0–4		BP: 4–12
		5c. I dread having to inhale regularly with an anti-inflammatory inhaler for my asthma	0–4		
	Social discomfort of inhaling with ICS in public	6. I prefer not to use my inhaler in public[d]	0–4	0–4	BA: 0–1 BP: 2–4
Skills	Understanding and application of ICS inhaler techniques	7a. I understand the instructions on how to use my anti-inflammatory inhaler	4–0	0–12	BA: 0–2
		7b. With the instructions I am capable of using my anti-inflammatory inhaler properly	4–0		BP: 3–12
		7c. I find it difficult to inhale properly with my anti-inflammatory inhaler	0–4		
Memory, attention and decision process	(Un)conscious adherence to prescribed ICS medication regimen	8a. I use my anti-inflammatory inhaler every day	4–0	0–12	BA: 0–3
		8b. I use my anti-inflammatory inhaler as prescribed by my healthcare provider	4–0		BP: 4–12
		8c. Sometimes I forget to use my anti-inflammatory inhaler	0–4		
	Shared treatment decision making	9a. My healthcare provider (doctor, nurse, pharmacist or lung specialist) has discussed with me in which way my asthma can best be treated	4–0	0–12	BA: 0–5
		9b. My healthcare provider (doctor, nurse, pharmacist or lung specialist) has asked me which type of inhaler I prefer	4–0		BP: 6–12
		9c. My healthcare provider (doctor, nurse, pharmacist or lung specialist) has discussed with me how I can best use my anti-inflammatory inhaler to prevent an asthma attack	4–0		
Behavioral regulation	Existence of structure in ICS medication intake	10. I inhale at a fixed time of the day	4–0	0–4	BA: 0–1 BP: 2–4

[a]*Responses to the questions are provided on a 5-point Likert scale with the following options: I disagree completely, I disagree mostly, I agree somewhat, I agree mostly and I agree completely. Scores to these options vary from 0 to 4 or 4 to 0 dependent on the question.*

[b]*Sum scores per barrier can be computed by adding the scores of the responses on the questions per barrier.*

[c]*Additional adjustments have been implemented on this question after validation. Former question: I know how to use my ICS inhaler.*

[d]*Additional adjustments have been implemented on this question after validation. Former question: I am embarrassed to use my inhaler in public.*

Abbreviations: RACE: respiratory adherence care enhancer; TDF: theoretical domains framework; ICS: inhaled corticosteroids; BA: barrier absent; BP: barrier present.

treatment outcomes. In this context, higher specificity values were aimed at for the barriers to avoid high false positives, partly at the expense of sensitivity. The barriers 'Knowledge of asthma medication', 'Social discomfort of ICS inhaler in public' and 'Understanding and application of ICS inhaler techniques' presented the lowest sensitivity values with values between 40.9 and 50.0%. However, this does not affect their usefulness and still provides the opportunity to identify approximately half of the asthma patients who have these barriers, that might otherwise remain unnoticed. The accuracy of the questionnaire to discriminate between the presence or absence of the barriers was significant, except for 'Knowledge of ICS medication'. This may be due to an identified incomprehensible question which has been adjusted in the final RACE questionnaire, requiring further validation.

The personal barrier profiles obtained from the RACE questionnaire should be discussed in consultations between patients and their healthcare professionals. Moreover, this tool might facilitate multidisciplinary cooperation on the provision of

TABLE 5 | The inter-rater reliability test results of the appraisals on the presence/absence of self-management barriers according to the interview coding's of two analysts.

TDF-domains	Barriers	Cohen's kappa[a]
Knowledge	Knowledge of asthma	**0.77**
	Knowledge of ICS medication	0.35
Beliefs about consequences	Expectations of ICS medication	0.52
	Experience of side-effects	0.54
Emotion	Concerns about ICS inhaler	0.41
	Social discomfort of inhaling with ICS in public	**0.88**
Skills	Understanding and application of ICS inhaler techniques	**0.58**
Memory, attention and decision process	(Un)Conscious adherence to prescribed ICS medication regimen	**0.68**
	Shared treatment decision making	**0.64**
Behavioral regulation	Existence of structure in ICS medication intake	**0.96**

[a]*Cohen's kappa values higher or equal to 0.6 were considered acceptable and are printed in bold.*

Abbreviations: RACE: respiratory adherence care enhancer; TDF: theoretical domains framework; ICS: inhaled corticosteroids; AUROC: area under the receiver operating characteristic.

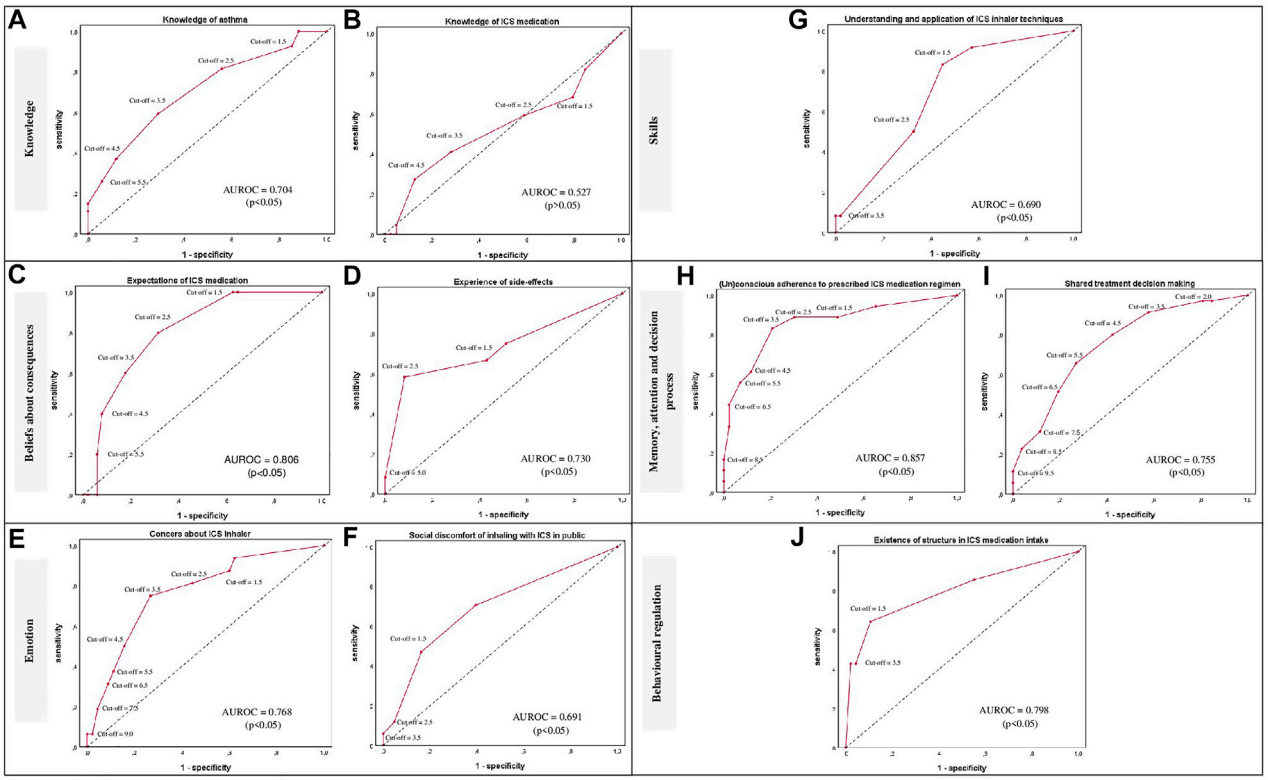

FIGURE 3 | ROC curves per barrier **(A–J)** are provided per TDF-domain for the classification of patients in presence or absence of a self-management barrier using various cut-off points of the sum scores per barrier. The ROC curves are presented as red lines. The diagonal dashed line represents the line that is no better than chance at discriminating between the presence or absence of a self-management barrier. Adjuvant AUROC values are presented per graph providing an indication of the accuracy of the scores at discriminating between the presence or absence of a self-management barrier. Corresponding *p*-values ≤ 0.05 were considered statistically significant; Abbreviations: ROC: Receiver operating characteristic; TDF: Theoretical Domains Framework; AUROC: Area under the ROC; ICS: Inhaled Corticosteroids.

tailored interventions, joining the efforts of healthcare professionals. Completion of the questionnaire by the patient might take place prior to the consultation and can be used to monitor potential self-management barriers, behavior change and disease control. Further research will focus on an additional guide with interventions to overcome identified barriers.

There are also some potential limitations in this study which need to be addressed. First, patients were not part of the development of the RACE questionnaire. However, the experts involved were all active in clinical practice. Second, the validation of the questionnaire was performed in a voluntary sample of asthma patients which may not be representative for all asthma patients. Nevertheless, a variability in asthma control, ICS inhaler types and self-management barriers were observed. Also, the possibility of the inclusion of a convenience sample of asthma patients is kept

to a minimum as community pharmacists involved are members of special interest and/or university groups and are eager to improve care for lung patients, therefore being more inclined to an objective approach and acknowledging potential pitfalls. Third, less patients than intended could be included in the validation. Yet, these numbers were sufficient to obtain statistically significant AUROC values for nearly all barriers. Fourth, the semi-structured interviews as golden standard for the criterion validity may contain a level of subjectivity. However, other comparable measurements were not available, which was the reason for conducting this study. To retain the objectivity of these interviews, an interview guide was used to encourage patients to provide overt information about their feelings, thoughts and beliefs (Presseau et al., 2017; DeJonckheere and Vaughn, 2019). In this guide, questions were presented in a different order in comparison to the RACE questionnaire. To assure the reliability of the data collected and analyzed, qualitative research standards were applied (Edwards and Holland, 2013).

CONCLUSION

The newly developed RACE questionnaire yields adequate psychometric properties for the identification of individual barriers to self-management of ICS therapy in primary care asthma patients. It is therefore ready to be applied in consultations, providing insights into the multitude of barriers that can prevent optimal ICS use in patients. As these barriers are based upon a theoretical underpinning, the next step is to address and overcome these barriers in consultations with tailored advise from healthcare professionals. Subsequently, these efforts should become visible in improved self-management and disease stability of asthma patients.

DATA AVAILABILITY STATEMENT

The raw data supporting the conclusions of this article will be made available by the authors, without undue reservation.

ETHICS STATEMENT

The studies involving human participants were reviewed and approved by Medical Ethics Committee (MEC) of the Leiden University Medical Center (LUMC). The patients/participants provided their written informed consent to participate in this study.

AUTHOR CONTRIBUTIONS

MT designed, conducted and led the project, participated in data collection and data-analysis and contributed to writing the manuscript. CV participated in the analysis and interpretation of the data and contributed to writing the manuscript. JL participated in the validation part of the questionnaire. JS, JL, EK, and H-JG revised the manuscript and contributed to the interpretation of the data.

FUNDING

This work was supported by AstraZeneca and the Royal Dutch Pharmacists Association (KNMP) with an unconditional research grant.

ACKNOWLEDGMENTS

The authors would like to thank Rahima Mesdar (RM) for her contribution in the development phase of the RACE questionnaire in this study.

SUPPLEMENTARY MATERIAL

The Supplementary Material for this article can be found online at: https://www.frontiersin.org/articles/10.3389/fphar.2021.767092/full#supplementary-material

REFERENCES

Allemann, S. S., Nieuwlaat, R., van den Bemt, B. J., Hersberger, K. E., and Arnet, I. (2016). Matching Adherence Interventions to Patient Determinants Using the Theoretical Domains Framework. *Front. Pharmacol.* 7, 429. doi:10.3389/fphar.2016.00429

Anghel, L. A., Farcas, A. M., and Oprean, R. N. (2019). An Overview of the Common Methods Used to Measure Treatment Adherence. *Med. Pharm. Rep.* 92 (2), 117–122. doi:10.15386/mpr-1201

Bårnes, C. B., and Ulrik, C. S. (2015). Asthma and Adherence to Inhaled Corticosteroids: Current Status and Future Perspectives. *Respir. Care* 60 (3), 455–468. doi:10.4187/respcare.03200

Barnes, P. J. (2010). Inhaled Corticosteroids. *Pharmaceuticals* 3 (3), 514–540. doi:10.3390/ph3030514

Boulet, L. P., Vervloet, D., Magar, Y., and Foster, J. M. (2012). Adherence: the Goal to Control Asthma. *Clin. Chest Med.* 33 (3), 405–417. doi:10.1016/j.ccm.2012.06.002

Bridgeman, M. B., and Wilken, L. A. (2021). Essential Role of Pharmacists in Asthma Care and Management. *J. Pharm. Pract.* 34 (1), 149–162. doi:10.1177/0897190020927274

Cane, J., O'Connor, D., and Michie, S. (2012). Validation of the Theoretical Domains Framework for Use in Behaviour Change and Implementation Research. *Implement Sci.* 7, 37. doi:10.1186/1748-5908-7-37

Cramm, J. M., Strating, M. M., de Vreede, P. L., Steverink, N., and Nieboer, A. P. (2012). Validation of the Self-Management Ability Scale (SMAS) and Development and Validation of a Shorter Scale (SMAS-S) Among Older Patients Shortly after Hospitalisation. *Health Qual. Life Outcomes* 10, 9. doi:10.1186/1477-7525-10-9

DeJonckheere, M., and Vaughn, L. M. (2019). Semistructured Interviewing in Primary Care Research: a Balance of Relationship and Rigour. *Fam. Med. Community Health* 7 (2), e000057. doi:10.1136/fmch-2018-000057

Dharmage, S. C., Perret, J. L., and Custovic, A. (2019). Epidemiology of Asthma in Children and Adults. *Front. Pediatr.* 7, 246. doi:10.3389/fped.2019.00246

Dierick, B. J. H., van der Molen, T., Flokstra-de Blok, B. M. J., Muraro, A., Postma, M. J., Kocks, J. W. H., et al. (2020). Burden and Socioeconomics of Asthma, Allergic Rhinitis, Atopic Dermatitis and Food Allergy. *Expert Rev. Pharmacoecon Outcomes Res.* 20 (5), 437–453. doi:10.1080/14737167.2020.1819793

Dima, A. L., Hernandez, G., Cunillera, O., Ferrer, M., and de Bruin, M.ASTRO-LAB group (2015). Asthma Inhaler Adherence Determinants in Adults: Systematic

Review of Observational Data. *Eur. Respir. J.* 45 (4), 994–1018. doi:10.1183/09031936.00172114

Dima, A. L., van Ganse, E., Laforest, L., Texier, N., and de Bruin, M. (2017). Measuring Medication Adherence in Asthma: Development of a Novel Self-Report Tool. *Psychol. Health* 32 (10), 1288–1307. doi:10.1080/08870446.2017.1290248

Edwards, R., and Holland, J. (2013). *What Is Qualitative Interviewing*. New York: A&C Black.

Eikelenboom, N., Smeele, I., Faber, M., Jacobs, A., Verhulst, F., Lacroix, J., et al. (2015). Validation of Self-Management Screening (SeMaS), a Tool to Facilitate Personalised Counselling and Support of Patients with Chronic Diseases. *BMC Fam. Pract.* 16, 165. doi:10.1186/s12875-015-0381-z

Fonseca, J. A., Nogueira-Silva, L., Morais-Almeida, M., Azevedo, L., Sa-Sousa, A., Branco-Ferreira, M., et al. (2010). Validation of a Questionnaire (CARAT10) to Assess Rhinitis and Asthma in Patients with Asthma. *Allergy* 65 (8), 1042–1048. doi:10.1111/j.1398-9995.2009.02310.x

Foster, J. M., McDonald, V. M., Guo, M., and Reddel, H. K. (2017). "I Have Lost in Every Facet of My Life": the Hidden burden of Severe Asthma. *Eur. Respir. J.* 50 (3), 1700765. doi:10.1183/13993003.00765-2017

French, S. D., Green, S. E., O'Connor, D. A., McKenzie, J. E., Francis, J. J., Michie, S., et al. (2012). Developing Theory-Informed Behaviour Change Interventions to Implement Evidence into Practice: a Systematic Approach Using the Theoretical Domains Framework. *Implement Sci.* 7, 38. doi:10.1186/1748-5908-7-38

GBD 2017 Disease and Injury Incidence and Prevalence Collaborators (2018). Global, Regional, and National Incidence, Prevalence, and Years Lived with Disability for 354 Diseases and Injuries for 195 Countries and Territories, 1990-2017: a Systematic Analysis for the Global Burden of Disease Study 2017. *Lancet* 392 (10159), 1789–1858. doi:10.1016/S0140-6736(18)32279-7

George, M., and Bender, B. (2019). New Insights to Improve Treatment Adherence in Asthma and COPD. *Patient Prefer Adherence* 13, 1325–1334. doi:10.2147/PPA.S209532

Global Initiative for Asthma (2020). *Global Strategy for Asthma Management and Prevention*. Available at: www.ginasthma.org (Accessed March 10, 2021).

Landis, J. R., and Koch, G. G. (1977). The Measurement of Observer Agreement for Categorical Data. *Biometrics* 33 (1), 159–174. doi:10.2307/2529310

Larson, R. B. (2018). Controlling Social Desirability Bias. *Int. J. Market Res.* 61, 534–547. doi:10.1177/1470785318805305

Murray, B., and O'Neill, M. (2018). Supporting Self-Management of Asthma through Patient Education. *Br. J. Nurs.* 27 (7), 396–401. doi:10.12968/bjon.2018.27.7.396

Normansell, R., Kew, K. M., and Stovold, E. (2017). Interventions to Improve Adherence to Inhaled Steroids for Asthma. *Cochrane Database Syst. Rev.* 4 (4), CD012226. doi:10.1002/14651858.CD012226.pub2

Patton, D. E., Cadogan, C. A., Ryan, C., Francis, J. J., Gormley, G. J., Passmore, P., et al. (2018). Improving Adherence to Multiple Medications in Older People in Primary Care: Selecting Intervention Components to Address Patient-Reported Barriers and Facilitators. *Health Expect.* 21 (1), 138–148. doi:10.1111/hex.12595

Plaza, V., Fernández-Rodríguez, C., Melero, C., Cosío, B. G., Entrenas, L. M., de Llano, L. P., et al. (2016). Validation of the 'Test of the Adherence to Inhalers' (TAI) for Asthma and COPD Patients. *J. Aerosol Med. Pulm. Drug Deliv.* 29 (2), 142–152. doi:10.1089/jamp.2015.1212

Ponieman, D., Wisnivesky, J. P., Leventhal, H., Musumeci-Szabó, T. J., and Halm, E. A. (2009). Impact of Positive and Negative Beliefs about Inhaled Corticosteroids on Adherence in Inner-City Asthmatic Patients. *Ann. Allergy Asthma Immunol.* 103 (1), 38–42. doi:10.1016/S1081-1206(10)60141-X

Presseau, J., Schwalm, J. D., Grimshaw, J. M., Witteman, H. O., Natarajan, M. K., Linklater, S., et al. (2017). Identifying Determinants of Medication Adherence Following Myocardial Infarction Using the Theoretical Domains Framework and the Health Action Process Approach. *Psychol. Health* 32 (10), 1176–1194. doi:10.1080/08870446.2016.1260724

Taber, K. S. (2018). The Use of Cronbach's Alpha when Developing and Reporting Research Instruments in Science Education. *Res. Sci. Educ.* 48, 1273–1296. doi:10.1007/s11165-016-9602-2

Tavakol, M., and Dennick, R. (2011). Making Sense of Cronbach's Alpha. *Int. J. Med. Educ.* 2, 53–55. doi:10.5116/ijme.4dfb.8dfd

Toelle, B. G., Marks, G. B., and Dunn, S. M. (2020). Validation of the Inhaler Adherence Questionnaire. *BMC Psychol.* 8 (1), 95. doi:10.1186/s40359-020-00461-x

Turner, R. R., Quittner, A. L., Parasuraman, B. M., Kallich, J. D., and Cleeland, C. S. (2007). Patient-reported Outcomes: Instrument Development and Selection Issues. *Value Health* 10 (Suppl. 2), S86–S93. doi:10.1111/j.1524-4733.2007.00271.x

Vercoulen, J. H. (2012). A Simple Method to Enable Patient-Tailored Treatment and to Motivate the Patient to Change Behaviour. *Chron. Respir. Dis.* 9 (4), 259–268. doi:10.1177/1479972312459974

Wilson, S. R., Strub, P., Buist, A. S., Knowles, S. B., Lavori, P. W., Lapidus, J., et al. (2010). Shared Treatment Decision Making Improves Adherence and Outcomes in Poorly Controlled Asthma. *Am. J. Respir. Crit. Care Med.* 181 (6), 566–577. doi:10.1164/rccm.200906-0907OC

World Health Organisation (2021). *Adherence to Long-Term Therapies: Evidence for Action*. Available at: http://www.who.int/chp/knowledge/publications/adherence_report/en/(Accessed March 10, 2021).

Conflict of Interest: MT received unconditional research grants from AstraZeneca and the Royal Dutch Pharmacist Association on the advancement of pharmacy. The PhD projects of CV and EK were paid from these unconditional research grants. JL contributed to this manuscript as a master pharmacy student at the Leiden University; she is employed by GlaxoSmithKline. JL is employed by Philips Research. The content of the current manuscript may or may not relate to future products and services supporting the health and well-being of people.

The remaining authors declare that the research was conducted in the absence of any commercial or financial relationships that could be construed as a potential conflict of interest.

Publisher's Note: All claims expressed in this article are solely those of the authors and do not necessarily represent those of their affiliated organizations, or those of the publisher, the editors and the reviewers. Any product that may be evaluated in this article, or claim that may be made by its manufacturer, is not guaranteed or endorsed by the publisher.

frontiers in Pharmacology

REVIEW
published: 23 December 2021
doi: 10.3389/fphar.2021.778219

Molecular and Clinical Aspects of COVID-19 Vaccines and Other Therapeutic Interventions Apropos Emerging Variants of Concern

Khursheed Ul Islam[1], Thoraya Mohamed Elhassan A-Elgadir[2], Sarah Afaq[2], Tanveer Ahmad[1] and Jawed Iqbal[1]**

[1]Multidisciplinary Centre for Advanced Research and Studies, Jamia Millia Islamia, New Delhi, India, [2]Department of Clinical Biochemistry, College of Medicine, King Khalid University, Abha, Saudi Arabia

Coronavirus disease 2019 (COVID-19) has overwhelmed the healthcare and economy of the world, with emerging new variants of severe acute respiratory syndrome coronavirus 2 (SARS-CoV-2) posing an everlasting threat to humanity. While most COVID-19 vaccines provide adequate protective immunological response against the original SARS-CoV-2 variant, there is a pressing need to understand their biological and clinical responses. Recent evidence suggests that some of the new variants of SARS-CoV-2 evade the protection conferred by the existing vaccines, which may impede the ongoing efforts to expedite the vaccination programs worldwide. These concerns have also highlighted the importance of a pan-COVID-19 vaccine, which is currently in the making. Thus, it is imperative to have a better molecular and clinical understanding of the various COVID-19 vaccines and their immunological trajectory against any emerging variant of concerns (VOCs) in particular to break this vicious cycle. Furthermore, other treatment regimens based on cellular therapies and monoclonal antibodies should be explored systematically as an alternative and readily available option considering the possibility of the emergence of more virulent SARS-CoV-2 mutants. In this review, we shed light on the various molecular mechanisms and clinical responses of COVID-19 vaccines. Importantly, we review the recent findings of their long-term immune protection and efficacy against emerging VOCs. Considering that other targeted and effective treatments will complement vaccine therapy, we provide a comprehensive understanding of the role of cell-based therapies, monoclonal antibodies, and immunomodulatory agents as alternative and readily available treatment modalities against any emerging SARS-CoV-2 variant.

Keywords: SARS-CoV-2, COVID-19, vaccines, variant of concern, therapeutics

OPEN ACCESS

Edited by:
Irfan Rahman,
University of Rochester, United States

Reviewed by:
Manish Kumar,
Augusta University, United States
Syed M. Moin,
National Institutes of Health (NIH), United States

***Correspondence:**
Jawed Iqbal
jiqbal1@jmi.ac.in
Tanveer Ahmad
tahmad7@jmi.ac.in

Specialty section:
This article was submitted to Respiratory Pharmacology, a section of the journal Frontiers in Pharmacology

Received: *16 September 2021*
Accepted: *08 November 2021*
Published: *23 December 2021*

Citation:
Islam KU, A-Elgadir TME, Afaq S, Ahmad T and Iqbal J (2021) Molecular and Clinical Aspects of COVID-19 Vaccines and Other Therapeutic Interventions Apropos Emerging Variants of Concern. Front. Pharmacol. 12:778219. doi: 10.3389/fphar.2021.778219

INTRODUCTION

Severe acute respiratory syndrome coronavirus-2 (SARS-CoV-2) emerged as a new virus from a wild market in Wuhan City, China, and had spread rapidly to almost every part of the world (Zheng 2020). Due to its highly contagious nature, the SARS-CoV-2 outbreak was declared as pandemic on March 11, 2020 by the World Health Organization (WHO) (Cucinotta and Vanelli 2020). SARS-CoV-2 causes a coronavirus disease called COVID-19 that has resulted in more than 4.87 million

deaths worldwide as per the WHO report on October 15, 2021 (https://covid19.who.int/). The COVID-19 outbreak and its widespread disruption in health and the economy have prompted scientists to look for different therapeutic strategies to minimize viral spread and the morbidities associated with it. Different therapeutic approaches such as convalescent therapy, monoclonal antibody treatment, immunotherapies, cell-based therapies, and vaccine therapeutics are available and used to combat SARS-CoV-2 infection (Ali et al., 2020). Passive immunotherapy in the form of convalescent therapy has been used since the late 19th century against infectious diseases, recently reviewed by Katz (2021). Convalescent plasma has also shown moderate success in a subset of COVID-19 patients, while in others this treatment offered very little respite (Nagoba et al., 2020).

Owing to the novelty of SARS-CoV-2 and its rapid spread, it was a challenging task to develop a new drug or a therapeutic agent at the earliest. In this challenging situation, some repurposed drugs and later immunotherapeutic options were introduced to limit hospitalizations due to COVID-19. The immunotherapeutic approaches were based on recombinant proteins or monoclonal antibodies generated against various antigens of SARS-CoV-2 (Wang et al., 2020). These antibody-based therapies became available as intravenous injection and, in some cases, as easy-to-use nasal sprays (Kwon 2021; Taylor et al., 2021). However, the major breakthrough treatment came in the form of the much anticipated COVID-19 vaccines (Kyriakidis et al., 2021). History tells us that developing a vaccine against a novel pathogen is a time-consuming process. However, the early development of the COVID-19 vaccines took the whole world by surprise, and the scientific community as well, as the general public had apprehensions about the safety, efficacy, and long-term health impact of these vaccines. About 126 COVID-19 vaccine candidates are currently in various stages of clinical development and around 194 in the preclinical stage according to the WHO report in August 2021 (https://www.who.int/publications/m/item/draft-landscape-of-covid-19-candidate-vaccines).

Now, as large populations worldwide are getting vaccinated, we have data regarding the safety, efficacy, and immunological response of these vaccines and other therapeutic interventions. Thus, in this review, we will discuss the molecular and clinical responses of various immunotherapeutic modalities, specifically the COVID-19 vaccine-based therapeutic interventions that are currently used to limit SARS-CoV-2 infection and treat COVID-19.

IMMUNOMODULATORY-BASED THERAPEUTIC APPROACHES FOR COVID-19

Considering the complexity of the immune response developed due to COVID-19, it is imperative to contemplate on the underlying immune response while designing the best possible therapeutic interventions (Roberts et al., 2020). As most of the complications seem to arise due to hyperactivated immune response-associated acute respiratory distress syndrome (ARDS), drugs modulating the pro-inflammatory responses may be effective (Gibson and Qin, 2020). In this regard, immunotherapies and cell-based therapies are emerging as the promising therapeutic modality for the treatment of severe and critically ill patients (AminJafari and Ghasemi 2020). Immunotherapies targeting the cytokines implicated as the hallmark in cytokine storm and adoptive cell-based therapies such as mesenchymal stem cells (MSCs), T cells, and natural killer (NK) cell-based therapies are in various phases of clinical testing for the treatment of COVID-19 (Saeedi and Halabian, 2019; Musial and Gorska-Ponikowska 2021).

Convalescent Plasma Therapy

An immediate and readily available source to treat severe and critically ill COVID-19 patients is by taking advantage of traditional convalescent plasma therapy (CPT). The presence of virus-specific antibodies has been detected in most of the patients who have successfully eliminated the virus (Ahmad et al., 2020; Casadevall and Pirofski 2020). The plasma containing antibodies from the recovered patients are thus given to the infected patients who could not mount an adequate humoral response (Luke et al., 2006). This traditional approach is based on the principle that the neutralizing antibodies from the recovered patients will provide a similar and durable response in the infected patients who receive the CPT. Antibodies will either neutralize the virus or enhance their uptake by phagocytosis. Additionally, these antibodies will also activate other effector immune cells to eliminate the virus-infected cells by activating other immune functions such as NK cells. Considering the high success rate of CPT in previous SARS-CoV-1-infected patients (Cheng et al., 2005; Yeh et al., 2005), it is plausible to use a similar approach for COVID-19. The ease of availability of plasma from a large number of infected COVID-19 donors seems a rational therapeutic option at hand before any other potential therapies become available for emerging variants of concern (VOCs), which escape the immunity conferred by the existing vaccines (Lopez Bernal et al., 2021). Previous data from SARS-CoV-2-infected individuals treated with CPT showed moderate success in a subset of patients. In a small cohort of 10 severe cases of COVID-19, Duan et al. showed that all patients successfully recovered after convalescent plasma transfusion (Duan et al., 2020). Similarly, the study by Shen et al. demonstrated 100% recovery in five critically ill patients after they received the plasma transfusion (Shen et al., 2020). Furthermore, in a case study on a single critically ill patient who exhibited respiratory distress, CPT along with remdesivir showed a promising recovery rate (Anderson et al., 2020). Many other early clinical reports have shown promising results with CPT, reviewed by Casadevall et al. (2020). Besides, more than 100 clinical trials are registered in ClinicalTrials.gov.in. These early clinical findings thus suggest that CPT is a potential therapeutic intervention for severe and critically ill patients and should be explored in cases of emergent new variants, where vaccines are not available or have failed to provide protection (Kanj and Al-Omari 2021). However, caution should be exercised while using this approach as many studies have shown contradicting results (Zhao and He 2020; Tiberghien

et al., 2020). Particularly, to ensure virus-free plasma, optimization of the dosage and time of delivery should be critically evaluated (Duan et al., 2020).

Targeted Immunotherapy Approaches for COVID-19

Consistently, the levels of interleukin 6 (IL-6) are increased in severe and critically ill COVID-19 patients, which is thus being considered as the prognostic and predictive disease biomarker along with the numbers of neutrophil/lymphocytes (Liu et al., 2020; Santa Cruz, 2021). The presence of increased levels of IL-6 are detected in blood and in the bronchoalveolar lavage fluid (BALF), thus making this cytokine as a potential therapeutic target. Approaches to neutralize IL-6 usually rely on the use of anti-IL6R antibody to inhibit IL-6 signaling. Previous studies on cytokine release syndrome (CRS) during cancer immunotherapy have shown clinical success of the anti-IL6R-directed antibody tocilizumab (TCZ) (Khadka et al., 2019). Furthermore, TCZ is an approved drug for the treatment of other inflammatory conditions such as rheumatoid arthritis (Yazici et al., 2012). Thus, it was rational to test this drug for the treatment of COVID-19. Several reports have suggested the beneficial effect of TCZ in severe and critical COVID-19 patients. The study by Luo et al. found that out of 15 patients, 11 responded well to the treatment and showed stable disease condition and a marked decrease in C-reactive protein (CRP) levels (Luo et al., 2020).

In a cohort of 100 critically ill patients, TCZ treatment was associated with a high recovery rate and a significant improvement in cytokine storm and clinical symptoms (Toniati et al., 2020) Similarly, a 92% recovery rate was observed in patients who received TCZ treatment in comparison to the 42.1% recovery rate in patients who received a combination therapy of hydroxychloroquine, lopinavir, and ritonavir (Chen et al., 2020). Surprisingly, in a very recent study by Xu et al., a 100% recovery rate was observed in 20 severe and critically ill patients who received TCZ treatment (Xu et al., 2020). Similarly, others have also observed the beneficial effect of TCZ (Luo et al., 2020). On the contrary, TCZ was shown to exhibit no added benefit in intensive care unit (ICU) admissions or mortality rate in a cohort of 21 patients who were compared with a combination therapy of hydroxychloroquine, azithromycin, and a prophylactic dose of low-molecular-weight heparin (Colaneri et al., 2020). Similarly, the study carried out by Carlo Salvarani et al. compared TCZ treatment with standard care on the clinical worsening of COVID-19 patients. In this study, it was found that clinical worsening in COVID-19 patients was not effectively prevented by the administration of TCZ (Salvarani et al., 2021). The probable reason for this discrepancy could be the dose, time, and the combinatorial effect of other drugs, which were given along with TCZ. Furthermore, the underlying health conditions and comorbidities may have an impact on the therapeutic outcome of this treatment, which needs further exploration. Overall, the results with TCZ have been mostly promising so far, but its use in combination with other antiviral and anti-inflammatory drugs has shown better results (Zhao et al., 2021). Currently, there are more than 50 clinical trials registered in ClinicalTrials.gov evaluating the potential efficacy of TCZ to minimize the cytokine storm and associated immunopathology. These studies will provide a detailed account of the therapeutic efficacy of TCZ for the treatment of COVID-19.

Approaches handling angiogenesis such as anti-VEGF (vascular endothelial growth factor) antibody (bevacizumab) or complement activation inhibitors such as anti-C5a antibody (eculizumab and avdoralimab) are also being explored (Billioti de Gage et al., 2021). Other immunotherapy approaches that were investigated include blocking the inhibitory T-cell receptors by anti-PD-1 (programmed cell death 1) or anti-CTLA4 (cytotoxic T-lymphocyte-associated protein 4) antibody (Pardoll and Drew, 2012). These approaches have been successfully used in cancer immunotherapy and other viral infections (Velu et al., 2009). Similarly, immunotherapeutic approaches to handle cytokine storm are in various phases of clinical trials or already approved for emergency use, such as therapies based on anti-IL-6, anti-GM-CSF (granulocyte–macrophage colony-stimulating factor), anti-IL-1β, anti-JAK (Janus kinase), anti-CCR5, anti-TIGIT [T-cell immunoreceptor with immunoglobulin (Ig) and immunoreceptor tyrosine-base inhibitory motif (ITIM) domains], and anti-IFN-γ (Buckley et al., 2020). Thus, exploring the use of these targeted therapies for emergency use seems a rational and feasible approach, considering that T-cell exhaustion is highly prevalent in COVID-19 (De Biasi et al., 2020).

Mesenchymal Stem Cell-Based Therapy for COVID-19

Owing to their immunomodulatory activity, MSCs exhibit greater potential to modulate the immunological response. Over the years, MSCs have shown greater promise for the treatment of chronic lung disease such as asthma, chronic obstructive pulmonary disease (COPD), pulmonary fibrosis, and acute lung injury (Harrell et al., 2019). The therapeutic potential of these cells is largely exhibited by their paracrine secretion of a range of anti-inflammatory molecules. Our own work has also established the therapeutic efficacy of MSCs in preclinical animal models of various lung diseases (Ahmad et al., 2014). MSCs have been used for the treatment of acute lung diseases such as ARDS, as reviewed by Rogers et al. (2020). Also, early studies in ARDS models have also strengthened this notion that MSCs have an impressive potential to be used as a therapeutic approach to manage the consequences of a hyperactive immune system (Mei et al., 2010). Previous studies have established the safety and efficacy of these cells in patients with ARDS (Simonson, 2015; Wilson et al., 2015; Matthay et al., 2019). Thus, owing to their safety profile and immunomodulatory activity, MSCs can be tested as a viable therapeutic option for the treatment of hyper-inflammatory state in COVID-19 patients. Clinical studies have suggested the early efficacy of these cells in COVID-19 patients (Wang et al., 2021). Last year, a 65-year-old COVID-19 patient showed recovery from ICU in about a week after treatment with umbilical cord-derived MSCs. In

another study of seven patients, MSCs resulted in the improvement of disease after just 2 days of treatment. MSC treatment was associated with a significant decline in TNF-α and CRP, with a concomitant increase in anti-inflammatory IL-10 levels (Leng et al., 2020). Besides their direct immunomodulatory potential, MSC-derived products such as exosomes also hold great therapeutic promise. Sengupta et al. evaluated the effect of exosomes derived from allogeneic bone marrow MSCs. Interestingly, these immunomodulatory molecules showed 71% recovery rate in a cohort of 24 severe and critically ill patients (Sengupta et al. 2020). Thus, it is plausible that MSCs may hold promise in alleviating the hyper-inflammatory state in COVID-19 patients infected with new variants of SARS-CoV-2. Several ongoing clinical trials are currently underway to explore in a holistic manner the protective effects of MSCs against COVID-19 (Leng et al., 2020; Moll et al., 2020; Saleh et al., 2021).

Other Adoptive Cell Transfer-Based Therapies for COVID-19

Adoptive cell transfer (ACT) is emerging as the most promising approach for the treatment of cancer. The current approach uses chimeric antigen-expressing T cells called CAR-T cells for the treatment of hematological malignancies, reviewed by Landoni and Savoldo (2018). The overwhelming success rate of this approach has encouraged researchers to use a similar approach for the treatment of COVID-19. However, limitations associated with this approach may hamper its use in COVID-19, specifically the associated high cost and CRS, which may additionally contribute to hyper-inflammatory response. Besides, CAR-T cell therapy has mostly remained confined to autologous approaches, while it is difficult to obtain the optimal functional T cells from severe and critically ill COVID-19 patients due to lymphopenia and lymphocyte exhaustion (Zheng et al., 2020). Thus, an alternative approach based on NK cells is currently being investigated, as NK cell-based therapy is not associated with CRS and can be used as an allogeneic source owing to their low graft-*versus*-host disease (GvHD) (Liu et al., 2021). There are ongoing trials based on NK adoptive cell treatment (NCT04900454). One such elegant approach using chimeric receptor-expressing NK cells is being evaluated. In this, off-the-shelf IL-15 superagonist and GM-CSF neutralizing single-chain variable fragment (scFv) NK cells are being evaluated (Kundu et al., 2021). These dual cytokine-secreting cells will ensure the regulated activation of the adoptively transferred NK cells by the IL-15 superagonist and also handle the cytokine storm by neutralizing GM-CSF. Additionally, many more clinical trials are reported in ClinicalTrials.gov.in, which are evaluating the therapeutic potential of NK cells for COVID-19, the success of which will determine the application of this approach against any emerging SARS-CoV-2 VOCs.

MONOCLONAL ANTIBODY-BASED THERAPY

Monoclonal antibody-based therapy is currently considered the most successful treatment for COVID-19 besides the protection conferred by vaccines, reviewed by Zhou et al. (2021). A large repertoire of therapeutic monoclonal antibodies has been developed using various approaches, such as humanized animals, chimeric animals, phage display assay, and direct use of B cells from COVID-19 patients. In the next section, we will briefly discuss about the recent developments in the clinical application of therapeutic antibodies for COVID-19 treatment.

Nasal Delivery of Antibody to Combat SARS-CoV-2

The delivery of neutralizing antibodies (IgG1 and isotypes) is usually carried out intravenously; however, these circulating antibodies lack efficient access to mucosal compartments, as is evident from a research carried out by DeFrancesco et al., where they have observed less antibody titer in the lungs as compared to the serum (DeFrancesco 2021). Delivering antibodies through the nasal route is an alternative to this approach and has an advantage for a pathogen causing respiratory tract infection such as SARS-CoV-2 because antibodies, if nebulized, can have greater access to the target cells compared to the intravenously delivered antibodies. Antibodies such as IgG and IgA1 have been reported to be nebulized through nasal inhalation (Vonarburg et al., 2019). The major challenge for antibody-based therapy is the resistance attained by newly emerging SARS-CoV-2 variants to different neutralizing IgG1 antibodies (Wibmer et al., 2021). To overcome such resistance encountered by IgG-based antibody therapeutics, an engineered IgM neutralizing antibody (IgM-14) was developed by Ku et al. (2021a). Compared to its parent counterpart (IgG-14), IgM-14 (engineered antibody) was observed to be >230-fold potent in neutralizing the SARS-CoV-2 pathogen. The resistant strains of SARS-CoV-2 and the VOCs, including the UK (B.1.1.7), Brazilian (P.1), and South African (B.1.351) strains, were shown to be neutralized by IgM-14 (Ku et al., 2021b).

Antibody Cocktail Against SARS-CoV-2 Infection

The emergence of resistant strains due to antibody treatment interventions against pathogens such as respiratory syncytial virus (RSV) became the basis to developing an antibody cocktail approach against the SARS-CoV-2 pathogen (Simões et al., 2020). The antibody cocktail approach was observed to be beneficial against the rapid emergence of resistant mutations due to the single use of neutralizing antibody (Baum et al., 2020). Regeneron Pharmaceuticals developed an antibody cocktail with the trade name REGN-COV2 that contains a combination of two SARS-CoV-2 neutralizing antibodies: casirivimab (REGN10933) and imdevimab (REGN10987). The antibody cocktail containing two neutralizing and non-competing human IgG1 antibodies target the receptor binding domain of the SARS-CoV-2 spike protein, thus preventing viral entry *via* ACE2 (Baum et al., 2020; Hansen et al., 2020; Weinreich et al., 2021). A phase 1/3 clinical trial was conducted to determine the efficacy and safety of REGN-COV2, which involved hospitalized and asymptomatic COVID-19 patients. A total of 269 patients received REGN-COV2 and

placebo, among which 90 patients were assigned to receive high-dose (8.0 g) REGN-COV2, 92 patients received a low dose (2.4 g), and 93 received placebo. Interim results showed low-grade and a few toxic effects of both low- and high-dose REGN-COV2. Adverse effects of special interest were reported in 2 out of 93 patients in the placebo group and 2 out of 176 patients in the REGN-COV2 group (Weinreich et al., 2021). Exogenous antibody treatment was better suited to those patients whose immune system had not yet been activated. However, patients who were already found serum-positive for neutralizing antibodies against SARS-CoV-2 were able to clear the virus efficiently. Based on these clinical findings, emergency use of this cocktail was granted in the 2021 for the treatment of COVID-19 in patients with mild to moderate symptoms. Similar antibody cocktails are being explored in various preclinical or clinical trials, and their success will determine the availability of this therapeutic modality against any emerging SARS-CoV-2 VOCs (Taylor et al., 2021).

VACCINE THERAPEUTICS

Vaccine is a substance, usually an inactivated pathogen or its component [protein or a messenger RNA (mRNA)], that, when introduced into the host, can elicit an immune response by imitating the pathogen's infection process. This imitation of the infection lasts for a short duration until the body has developed long-term memory against the specific infection (Pulendran and Ahmed 2011). The aim of the vaccination is to prepare the body so that, in future, if there is an infection of the specific pathogen against which the vaccine was administered, memory cells will recognize and destroy the pathogen by releasing neutralizing antibodies. Vaccination, as a deliberate attempt at pathogen exposure, began in the lab of Louis Pasteur *via* his discovery of attenuated vaccine. He administered an aged culture of *Pasteurella multocida* to chickens that did not develop any disease-like symptoms; to his surprise, he observed that, on treating the same chickens with fresh culture of *P. multocida*, none of the subjects developed the disease (Pasteur, 1880). This observation led him to infer that aged culture had developed resistance against the pathogen in the chicken, which helped the subjects to fight against the infection of fresh bacterial culture. This observation led Pasteur to hypothesize that pathogens can be attenuated by any kind of environmental insults such as chemicals and high temperature, and the attenuated pathogen can bring immunity in healthy individuals against the disease-causing pathogen. Louis Pasteur confirmed his hypothesis further by working on rabies and anthrax (Pasteur, 1881). Due to the increased understanding regarding vaccine development, new endeavors of vaccine were brought into use, among which "antitoxin therapy," also known as "serum therapy," was an important discovery in the later part of the 19th century. Antitoxin preparations were first applied on animals, and the immunization studies on animals paved the way to applying this preparation in humans, which was utilized in 1931 (Moss 2020). The development of toxoid (inactivated toxin by formalin) took place in the early 1920s and is being used with certain minor modifications. Over the decades, knowledge regarding vaccine development has increased at an enormous pace, which paved the way to developing new vaccines within a short span of time and with better specificity and effectiveness against a particular pathogen.

Types of Vaccines

Vaccines and vaccine development strategies have evolved with time, from traditional to new-generation vaccines. Traditional vaccines include whole pathogen vaccines, which can either be live-attenuated or inactivated vaccines. Live-attenuated vaccines consist of the pathogen with a highly reduced virulence (e.g., yellow fever/smallpox). On the other hand, inactivated vaccines are the chemically or thermally inactivated pathogens (Polack et al., 2020a). Developing live-attenuated or inactivated vaccines is an age-old and well-established strategy harboring rapid immunogenic property and providing immunological memory against specific pathogens. However, the drawback related to their use is the safety concern, which is due to live-attenuated vaccines having the potential to revert back to the virulent form and may infect immune-compromised subjects (Bazin 2003). Similarly, attenuated vaccines do not exhibit durable immunological memory and, hence, may not show long-term safety. Inactivation of a pathogen must neutralize the virulence without compromising its immunogenicity, as evident from previous research conducted to solve the mystery of why children in Washington, DC, developed disease after receiving the vaccine against RSV infection in the late 1960s. The research has highlighted the ineffective activation of immune response against the pathogen, as the RSV vaccine was not able to produce specific antibody response; rather, a hyper-immune response condition, also called enhanced respiratory disease (ERD), was elicited (Polack 2007). Advanced knowledge at the molecular level has highlighted an opportunity to identify and suppress the virulent genes of the pathogen to combat the problem of reversion of pathogenic virulence; however, safety concerns and short-term immunological memory persisted. Another approach is the subunit vaccine that consists of a part of the pathogen projected as an antigen to elicit immune response in the host organism. Adenoviral vectors are also being used to deliver some specific viral genes that can produce viral antigenic peptides in the host cells to elicit immune response (Kremer 2020b). Adenoviruses are non-fatal viruses that can infect humans and other organisms. Their exploitation as a vector for delivering viral antigens in host cells is a promising tool for the development of vaccines (Tatsis and Ertl 2004). Other vaccine types directly use the nucleic acids (mRNA and DNA) integrated with nano-technological approaches for delivery, as used by Moderna and Pfizer for COVID-19 vaccines, which will be discussed in the later section (Polack et al., 2020a; Corbett et al., 2020).

General Mechanism of Vaccine Immunity

The immune system reacts against challenges, whether it is from a pathogen or from an immunization, by activating its diverse components. Detection is carried out by the innate immune system by antigen-presenting cells (APCs). Within an APC, the antigen is processed to generate small protein fragments

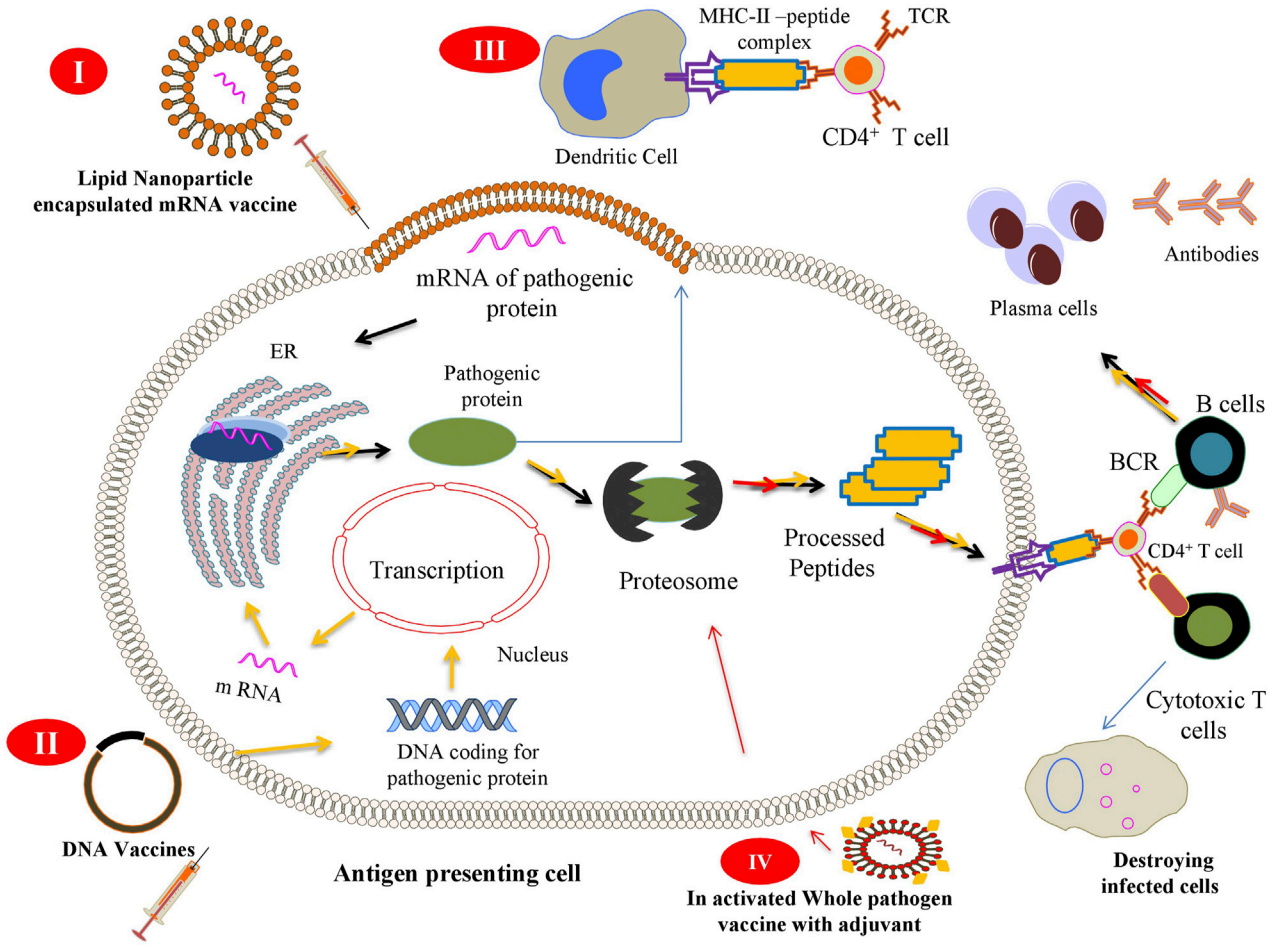

FIGURE 1 | Scheme of the different vaccine strategies: (*I*) Messenger RNA (mRNA) vaccines contain mRNA encoding a pathogenic protein that acts as an immunogen to elicit cellular and humoral immune responses. The vaccine is injected as a lipid nanoparticle encapsulation that, once released inside (depicted by *black arrow*), the antigen-presenting cell (APC) is translated by cellular ribosomes and further presented on the surface of APCs. (*II*) DNA vaccines encoding a specific sequence for a pathogenic gene are captured by APCs that express and present the antigen to immune cells to elicit immune response (process depicted by the *yellow arrow*). (*III*) After expression of pathogenic proteins inside APCs, it may be secreted in the surrounding tissues (depicted by *cyan arrow*) where different other APCs can engulf, process, and present it to immune cells. (*IV*) Inactivated whole pathogen vaccines contain whole pathogens that have been subjected to heat or chemical inactivation when introduced into the body (depicted by *red arrow*) and stay avirulent, but pathogenic. This strategy is not able to bring an effective cellular immune response because of the inactivation of immunogenic proteins, thus needing an adjuvant (*yellow dots*) to bring about such a response in the cells.

(peptides) that form a complex with major histocompatibility complex (MHC) molecules. This peptide–MHC complex is expressed on these cells, which further elicit an immune reaction by specifically engaging innate immune cells such as T or B cells. During immunization, either a whole pathogen or its component (protein) is introduced into the body in the form of a vaccine. This vaccine is detected as a non-self-entity by the APCs, which process it in the same way the pathogen is processed and subjected for antigen presentation to immune cells. Briefly, the peptide–MHC complex is expressed on the cell surface as an antigenic determinant (epitope), which activates T and B cells to neutralize the specific antigen. During this course, some T and B cells differentiate into memory cells and provide long-term memory against a particular pathogen (Clem 2011). **Figure 1** shows a general scheme of a vaccine-mediated immune response after its delivery inside the human body.

The protective immunity against any viral infection has been attributed to the function of antibodies, especially neutralizing antibodies (Corti and Lanzavecchia 2013). These antibodies block the entry of viruses into the host cell, thus preventing infection. It has been the prime goal of vaccination to elicit adequate neutralizing antibodies. Different vaccines elicit different levels of serum antibodies serving as surrogates of protective immunity. These antibodies are measured using ELISA, lateral flow assay, hemagglutination assays, and live/pseudoviral-based neutralization assays (Amanat et al., 2020). The activation of immune cells against the vaccines depends upon the type of vaccine and its route of administration. Certain vaccines, like the cholera and typhoid fever vaccines that were designed to promote IgA response through oral administration, show lower efficacies. In contrast, parenterally administered vaccines elicit long-term immunity (Clemens et al., 2011).

The molecular players in vaccine-mediated immunity involve B cells, which are activated by the binding of antigenic determinants (from a pathogen or immunization) to B-cell receptors (BCRs) or by antigen-specific T helper cells. Pathogens like viruses have highly repetitive structures that can efficiently crosslink BCRs. However, soluble antigens lack such property and are usually ignored by B cells (Bachmann and Zinkernagel 1997). After the binding of antigen to the receptors, B cells interact with T helper cells and macrophages to differentiate in the clones of antibody-secreting cells, also called plasma cells and memory B cells. Plasma cells constitutively secrete antigen-specific antibodies, right after the pathogen attack. However, memory B cells are responsible for long-term antibody response (Amanna and Slifka 2011). Viruses usually bind to cell receptors; thus, the neutralizing antibody is directed against the viral protein that binds to the host cell receptor, thereby limiting the viral entry into the cells (Murin et al., 2019).

Long-term T-cell memory is a collaborative response of all T-cell populations against any cognate pathogen. $CD4^+$ and $CD8^+$ cells represent the specific cellular arm of adaptive immune response against viral infection or immunization. A subset of $CD4^+$ T cells, also called T helper cells, recognizes processed antigens presented by APCs, especially dendritic cells (DCs). This process mounts a better immune response and memory compared to the immune response elicited by direct antigen binding by B cells (Kim et al., 2005). Detection of vaccine-associated signals by DCs conditions them to express molecules like interleukin 12 (IL-12), which further help T cells to proliferate and differentiate into various phenotypes (Alcaide et al., 2021).

COVID-19 VACCINES

The COVID-19 pandemic has put pharmaceutical companies and laboratories in a race to develop an effective and rapid COVID-19 vaccine. Both traditional as well as modern vaccine development strategies have been employed to develop an effective and safe vaccine for COVID-19. This becomes imperative when there is no suitable drug available in the market, owing to the novelty of the pathogen causing COVID-19. As of October 2021, around 194 vaccine candidates have been in the preclinical phase and 126 vaccine candidates in the advanced clinical phases (https://www.who.int/publications/m/item/draft-landscape-of-covid-19-candidate-vaccines). Due to the availability of prior knowledge regarding the pathogenesis and immune responses of SARS-CoV and Middle East respiratory syndrome-related coronavirus (MERS CoV), the vaccine development against SARS CoV-2 started at a remarkable pace (Folegatti et al., 2020a). Early pieces of evidence have suggested that neutralizing antibodies against the spike protein might be an important hallmark for immunity against SARS-CoV-2 infection (Wajnberg et al., 2020). These reports thus formed the basis for developing the COVID-19 vaccine, many of which have successfully passed clinical trials and are currently available in the market, as reviewed recently (Kyriakidis et al., 2021). Most COVID-19 vaccines that obtained an emergency approval for their therapeutic use have been recommended for the population beyond the age of 18 years, and in most countries, these vaccines are yet to be tested in children below 18 years. Certain vaccines that are in the early stage of drug trials are reported to be intranasally administered, including ChAdOx1-S, AdCOVID, BBV154, and COVI-VAC, which may become the leading vaccines to be used for those below 18 years old (Lund and Randall 2021). Such vaccines have been used in the past to treat respiratory pathogens in children (Mohn et al., 2018). There are challenges that can be encountered in the future regarding the efficacy of the COVID-19 vaccines, as the SARS-CoV-2 pathogen is rapidly evolving owing to its RNA genome (MacLean et al., 2020). Thus, many COVID-19 vaccines are being tested for their efficacy against the different VOCs currently circulating in places where drug trials are being carried out. **Table 1** summarizes certain important and approved vaccines and their status of efficacy and the drug trial stages. In the next section, we will discuss the basic biological features and clinical information of the candidate vaccines currently approved or undergoing the final phase of clinical trials for COVID-19.

mRNA-Based COVID-19 Vaccines

Pfizer/BioNTech mRNA Vaccine: Tozinameran, code named BNT162b2, is more commonly known as Pfizer/BioNTech COVID-19 vaccine. It is being sold in the market with the trade name Comirnaty. This vaccine is based on mRNA (encoding the full-length SARS-CoV-2 spike protein) encapsulated in a lipid nanoparticle formulation (Polack et al., 2020a). The first country to authorize Tozinameran for emergency use was the UK. This vaccine is administered as a two-dose regimen (30 μg each), given 21 days apart. The dosage regimen has been observed to elicit optimal immune response in the form of neutralizing antibodies and effective T-cell responses after 28 days of administration (Mahase 2020). A local and short-term reactogenicity profile was observed in the second phase of drug trials at the injection site. An early trial report indicated that, initially, a total of 44,820 people (with mean age of ≥16 years) were screened, among which 43,548 underwent randomization at different sites round the globe. In the phase 2/3 trial, 43,448 participants received injection, among which 21,728 were administered placebo and 21,720 participants received BNT162b2 (NCT04368728). During the follow-up, around 27% of BNT162b2 recipients and 12% of placebo recipients reported adverse but manageable side effects. Lymphadenopathy was reported in 0.3% of vaccine recipients and <0.1% placebo recipients. In terms of efficacy, it was observed that BNT162b2 had an impressive 95.0% efficacy in the early trial results (Polack et al., 2020a). However, the major limitation of this vaccine is the need for storage at lower temperatures ranging from −80°C to −60°C, which is challenging for most of the developing countries. Drug trial 2/3, which was carried out to assess the safety and immunogenicity of 30 μg BNT162b2 (given 21 days apart) among participants 16 years of age or older, found the vaccine to be safe with an efficacy of 95% (Polack et al., 2020b). This is the first vaccine to obtain stringent regulatory

TABLE 1 | Trial stages of some important COVID-19 vaccines and their efficacy with respect to different SARS-CoV-2 variants

S/No.	Vaccine	Phase of drug trial	Trial number	Effectiveness against VOCs	Reference
1	Pfizer	Phase III trial completed	NCT04368728	B.1.351, P.1, B.1.427/B.1.419, P.2, and B.1.526	Polack et al. (2020b)
2	Moderna	Under phase III drug trial	NCT04470427	B.1.427/B.1.429 and B.1.526	Baden et al. (2021)
3	CoronaVac	Under phase III drug trial	NCT04582344	P.1 and P.2	Tanriover et al. (2021)
4	BBIBP-CorV	Under phase III drug trial	NCT04984408	No information	Al et al. (2021)
5	BBV152	Under phase III drug trial	NCT04641481	B.1.617.2 and B.1.617.1	Ella, Reddy, et al. (2021)
6	Sputnik	Under phase III drug trial	NCT04656613	No information	Callaway (2020)
7	Ad26.CoV2.S	Under phase III drug trial	NCT04505722	B.1.351, P.1, B.1.427/B.1.429, P.2, B.1.526, and C.37	Sadoff et al. (2021)
8	Covisheild	Under phase III drug trial	NCT04324606, NCT04400838 NCT04444674	B.1.1.7, B.1.351, P.1, B.1.427/B.1.429, P.2, B.1.526, and C.37	Voysey et al. (2021)
9	NVX-CoV2373	Under phase III drug trial	NCT04611802	B.1.1.7, B.1.351, B.1.427/B.1.429, and B.1.526	Heath et al. (2021b)

VOCs, variants of concern

authorization and clearance for its emergency and regular use in the United States. It is fully authorized in five countries and has an emergency use authorization in around 108 countries.

mRNA-1273 vaccine: The joint collaboration of Moderna, Biomedical Advanced Research and Development Authority (BARDA), and National Institute of Allergy and Infectious Diseases (NIAID) led to the development of another mRNA-based SARS-CoV-2 vaccine, more commonly called Moderna COVID-19 vaccine and code named mRNA-1273. It is sold in the market under the brand name Spikevax. This vaccine also contains an mRNA encoding the SARS-CoV-2 spike glycoprotein enclosed in a lipid nanoparticle encapsulation (Corbett et al., 2020). This vaccine is administered intramuscularly in two doses of 0.5 ml within a gap of 2 weeks.

In the first phase of the drug trial, 45 participants were enrolled to receive the mRNA-1273 vaccine, which was initially given in three different concentrations (25, 100, and 250 μg) in 15 participants each (NCT04283461). The vaccine was provided in the form of a sterile liquid for injection at a concentration of 0.5 mg/ml. Two consecutive doses of each concentration were given with a gap of 28 days. No participant developed any serious complication immediately after the first vaccination. In the second vaccination process, no participant reported any adverse effect in the 25-μg group; however, 40% of the participants in the 100-μg group and 57% of the participants given 250 μg reported minor complications such as fever, mild fatigue, chills, and pain at the injection site. The published drug trial reports indicated that mRNA-1273 was effective enough to develop immune response *via* virus-neutralizing antibodies in the recipients (Jackson and ColerMcCullough, 2020). Rapid seroconversion was observed 2 weeks after the administration of the first vaccine dose. However, pseudoviral neutralization was found to be low in the first dose, which signifies the need for a second dose of this vaccine. Drug trial III was conducted at 99 centers across the United States, and 30,420 volunteers took part in the trial. mRNA-1273 showed 94.1% efficacy in preventing COVID-19 illness (NCT04470427) (Baden et al., 2021). Unlike BNT162b2, mRNA-1273 does not need to be stored at −80°C, but instead can be stored between −25 and −15°C. However, the thawed vaccine cannot be refrozen and should be stored between 2°C and 8°C for use within a short time frame. This vaccine obtained emergency use authorization by the Food and Drug Administration (FDA) on December 18, 2020. Since then, the health ministries of various other countries, including the European Union, United States, and Canada, have also approved its emergency use.

Advantages and Limitations

mRNA vaccines are developed in a microbial-free environment and are also non-infectious molecules. These features discriminate them from the other vaccine regimens such as inactivated viral vaccines, live attenuated viral vaccines, and vector-based vaccines in terms of safety and efficacy. mRNA vaccines are free from the issue of anti-vector immunity and are inexpensive compared to the other vaccines. As the mRNA is restricted to the cytosolic region, there is no chance of integration within the host genome, thus ensuring that cells do not get transformed (Pardi et al., 2018). Their adaptability and simple design provide rapid and easy production for any emerging strain, which thus makes mRNA-based vaccines more attractive.

Certain limitations may be associated with their use, as the formulation of modified mRNA-based vaccines is being employed for the first time on large populations; thus, it is too early to discuss their long-term safety concerns and complications. Specifically, the nanoparticle conjugates used to deliver mRNA into the cells need further investigation. According to a few studies, mRNA-based vaccines formulated with nanoparticles may induce type I interferon response associated with potential autoimmunity and inflammation, which warrants further study (Zhang et al., 2019).

Inactivated Whole Pathogen Vaccines

CoronaVac: The vaccine candidate formerly known as PiCoVacc is an inactivated vaccine (CNO2 strain of virus) developed against SARS-CoV-2 by the China-based biotechnology company Sinovac Biotech. This vaccine is being sold under the trade name "CoronaVac." The vaccine was derived from African green monkey kidney cells (Vero cells) inoculated with SARS-CoV-2. The virus was inactivated by β-propiolactone and adsorbed onto aluminum hydroxide. The vaccine is

administered in two doses with a gap of 14 days and has obtained an emergency use approval by the Chinese government for high-risk groups and frontline COVID-19 warriors. Doses of 3 and 6 μg of the vaccine are administered intramuscularly as per the dosing schedule (Zhang et al., 2020). Some participants have reported mild adverse effects, and the incidence of these reactions was dose-independent, signifying that there is no dose-related safety concern for this vaccine (NCT04352608) (Gao et al., 2020). This inactivated vaccine candidate is under phase III trial, currently ongoing in Brazil, Chile, Turkey, and Indonesia. On January 12, 2021, Brazil announced an efficacy of 50.38% from a study on 12,508 participants, whereas the trial reports from Turkey showed 91.25% efficacy. However, the data from Turkey were based on only 29 COVID-19 cases among 1,322 trial participants; thus, further results from enrolled participants will provide more explicit data on the efficacy of this vaccine (Mallapaty 2021).

BBIBP-CorV: BBIBP-CorV (Biotech Group and Beijing Institute of Biological Products—Coronavirus Vaccine) is another promising vaccine candidate developed by Beijing Institute of Biological Products, China. It is also a whole inactivated virus vaccine developed using the HBO2 strain of SARS-CoV-2 derived from Vero cells. Inactivation was carried out by treating the viral supernatant with β-propiolactone. This vaccine can be stored and transported at refrigeration temperatures (2–8°C). An early trial report conducted at Shangqiu City Liangyuan District Center for Disease Control and Prevention, Henan Province, China, has suggested that BBIP-CorV is an effective vaccine in all the age groups enrolled in the study. Vaccine/placebo recipients were separated randomly into two age groups: 18–59 and 60 years. The vaccine was administered at a two-dose schedule (2, 4, or 8 μg) with a gap of 4 weeks. The same immunogenicity profile was observed for the vaccine in both age groups. The anti-SARS-CoV-2 neutralizing antibody titer was higher at day 42 in the age group 18–59 years. BBIBP-CorV was also found to induce sufficient amount of immune response in participants 60 years and older (Xia et al., 2021). Adverse reactions were reported within 7 days of vaccine inoculation in 29% of the participants; however, these adverse reactions were found to be mild. BBIBP-CorV is currently tested in trial III, which started on October 1, 2021 with the estimated date of completion on September 30, 2024. The study will involve volunteers aged 18 years (NCT04984408).

BBV152: BBV152, with the trade name "Covaxin," is an inactivated whole pathogen vaccine against SARS-CoV-2. It was developed by Bharat Biotech in collaboration with the Indian Council of Medical Research (ICMR). Bharat Biotech obtained an approval to conduct its early phase drug trials on June 20, 2020. BBV152 is a whole SARS-CoV-2 virus inactivated by β-propiolactone and developed from a strain of SARS-CoV-2 (NIV-2020-770) isolated and sequenced from the National Institute of Virology of ICMR, Pune, and provided to Bharat Biotech for vaccine development. NIV-2020-770 contains a D614G mutation at its spike protein. The whole pathogen vaccines were formulated with alum, which is reportedly less likely to induce cell-mediated immunity. However, considering the desirability of cell-mediated immune response, an imidazoquinoline molecule, a Toll-like receptor (TLR7/8) agonist was used to induce cell-mediated immune response (Philbin et al., 2012). To deliver the vaccine antigen directly to the lymph nodes and avoid direct diffusion into systemic circulation, imidazoquinoline chemisorbed on alum (Algel-IMDG) was designed. Preclinical trials conducted in non-human primates showed enough viral clearance in vaccinated subjects using this strategy (Yadav et al. 2020).

Between July 13 and 30, 2020, a total of 375 participants took part in the first drug trial, among which 100 participants were assigned randomly to receive either one of the three formulations of the vaccine (3 μg Algel-IMDG, 6 μg Algel-IMDG, or 6 μg Algel) and 75 comprised the control group given Algel only (without antigen; NCT04471519). Two doses of the vaccine were administered intramuscularly with a gap of 14 days. Common adverse effects after vaccine administration were injection site pain, headache, vomiting, fever, and nausea. All the adverse effects were mild or moderate and were frequent after the first dose only. The tolerable safety outcomes and the enhanced immune response led both vaccine formulations (3 and 6 μg) to enter phase II of immunogenicity trials (EllaRachers et al., 2021a). This vaccine can be stored at 2–8°C, making it compatible to the cold chain requirements. The Lancet reported interim findings of the safety and immunogenicity of BBV152 at three different formulations and the control group Algel (EllaRachers et al., 2021a). Phase III of the drug trials was conducted between November 16, 2020 and January 7, 2021. In this trial 25,798 participants took part, among which 12,221 received the vaccine (two doses) and 12,198 participants received placebo (NCT04641481). BBV152 was found to be 77.8% efficient against the Wuhan strain of SARS-CoV-2; however, efficacy against a VOC (B.1.617.2, Delta) was observed to be only 65. 2% (EllaRachers et al., 2021b). This vaccine obtained emergency use approval in India on January 2, 2021 (Mohapatra and Mishra 2021).

Advantages and Limitations

In an inactivated vaccine, the pathogen loses the infectivity potential faster than in other vaccine types, but the antigenicity profile is maintained for longer. Thus, these vaccines are considered relatively safer than the vaccines based on live pathogens. Furthermore, the immunogenicity of inactivated viruses is lower and needs a booster dose to be administered, which usually increases the cost. The use of adjuvants can cause unwanted inflammatory responses (Gendon 2004). In the past, inactivated vaccines have been known to induce enhanced disease among the recipients. In fact, the trials for formalin-inactivated RSV had disastrous outcomes, as 80% of the vaccine recipients were hospitalized and two recipients died as a consequence of enhanced disease (Kapikian et al., 1969). However, considering the early success of the use of these vaccines for COVID-19, similar approaches may be used for developing vaccines against the emerging VOCs, if needed.

Adenovirus Vector-Based Vaccines

Russian Sputnik V SARS-CoV-2 Vaccine: Gam-COVID-Vac, with the trade name Sputnik V was the first vaccine against COVID-19

announced by the Russian Government on August 11, 2020. The vaccine is based on two human non-replicating adenoviral vectors—recombinant adenovirus 26 (rAd26-S) and recombinant adenovirus 5 (rAd5-S)—both of them carrying the gene related to the spike protein of SARS-CoV-2. It was developed by Gamaleya National Center of Epidemiology and Microbiology, Moscow, Russia (Burki 2020). This approach has been used in the past to develop a vaccine against Ebola (Dolzhikova et al., 2017). The vaccine was made in two formulations, frozen and lyophilized, and is administered intramuscularly. Both formulations require different storage temperatures: −18°C for the frozen formulation and 2–8°C for the lyophilized one. To assess the safety and immunogenicity of both vaccine formulations, a non-randomized study was carried out at Burdenko Hospital and Sechenov University, Moscow, Russia, which included 120 healthy participants aged 18–60 years (NCT04530396). A full dose contained 10^{11} viral particles, and every participant under study was given a full dose of the vaccine. The volume of the frozen vaccine was 0.5 ml and that of the lyophilized vaccine needed to be reconstituted in 1 ml of sterile water (Logunov et al., 2020). The findings of the phase 1/2 drug trial, as reported by The Lancet, have provided feasible results (Logunov et al., 2020). The vaccine was found safe and well tolerated, with adequate cellular and humoral immune response in healthy volunteers. On day 14 post-administration of rAd26-S and rAd5-S, SARS-CoV-2 receptor-binding domain (RBD)-specific IgGs (neutralizing antibodies) were detected in 88.9% and 84.2% of participants, respectively. The adverse effects reported post-vaccine administration included hyperthermia, headache, muscle and joint pain, and pain at the injection site. No serious adverse effects were reported during the study (Logunov et al., 2020). The neutralizing antibody titer was lower compared to that of mRNA-based vaccines (Jackson ColerMcCullough, 2020). Based on the successful clinical trial results, Sputnik V was approved in more than 60 countries for COVID-19 (Lawton 2021).

Ad26.COV2.S vaccine by Johnson & Johnson: Ad26.COV2.S is a vaccine candidate developed by Janssen Pharmaceuticals of Johnson & Johnson in collaboration with Leiden University Medical Center, Netherlands. It is a replication-defective vaccine expressing the full-length spike glycoprotein of SARS-CoV-2 (Poland et al., 2020). Ad26.COV2.S is in phase 3 trial involving 60,000 participants aged 18 years or older. Induction of strong neutralizing antibodies was observed after a single immunization (1×10^{11} viral particles introduced intramuscularly) of this adenovirus-based vaccine in rhesus macaques (Mercado et al. 2020). This vaccine can be stored at 2–8°C. Drug trial 1/2a was conducted among healthy adults aged 18–55 years (cohort 1) and 65 years and above (cohort 3). The vaccine was administered in a single- or two-dose regimen (5×10^{10} or 1×10^{11} viral particles per vaccination) within an interval of 56 days. Interim results indicated that there was a paramount development of S-binding antibody titer in 90% of the participants regardless of age and vaccine dose (NCT04436276). Detectable neutralizing antibodies were observed in 98% of the participants 29 days after vaccination (Sadoff et al., 2020). Phase 3 trial reports involving around 40,000 participants indicated that a single dose of the Ad26.COV2.S vaccine provides protection against symptomatic and asymptomatic SARS-CoV-2 infections (NCT04505722). Vaccine efficacy was found to be higher against severe to critical COVID-19, around 76.7% for onset at >14 days (Sadoff et al., 2021). The FDA issued emergency use authorization of the Johnson & Johnson COVID-19 vaccine on February 27, 2021.

ChAdOx1 nCoV-19: ChAdOx1 nCoV-19 is a chimpanzee adenovirus-based SARS-CoV-2 vaccine developed by Oxford University (ChAdOx1) and is in the market under the trade name "Covishield." It is a replication-deficient adenoviral vector carrying the SARS-CoV-2 surface glycoprotein antigen gene (spike protein). This strategy has already been tested in the past for other pathogens such as MERS CoV (Jia et al., 2019). Since the use of human adenoviral vaccines may have a reduced immunogenicity profile due to preexisting immunity to human adenoviruses, using chimpanzee-derived vectors was thus a better strategy of developing a vaccine with better immunogenicity against the SARS-CoV-2 antigen owing to the low seroprevalence of antibodies against chimpanzee-derived adenoviral vectors (Ramasamy et al., 2020). As per previous studies, the prevalence of antibodies against chimpanzee adenoviruses was found to be 0% in tested individuals among the UK population and 9% in the Gambia population, which provided an insight into the safe usage of adenoviral vectors for vaccine delivery (Morris et al., 2016).

Phase 1/2 trial reports published in The Lancet indicated acceptable profiles of immunogenicity and safety related to the ChAdOx1 vaccine (Folegatti et al., 2020a). The report was published from a phase 1/2 trial conducted in the UK on 1,077 participants (18–55 years old) who have received the vaccine (NCT04324606) (Folegatti et al., 2020b). In the phase 2 trial, older participants (>65 years) received the vaccine, and a 62% efficacy was observed in the two full-dose regimen administered with a gap of 1 month (Ramasamy et al., 2020). However, better efficacy was observed when a lower dose of the vaccine was used followed by a full dose. No COVID-19-related hospitalization was reported in the ChAdOx1 vaccine recipients, while 10 volunteers from the control (placebo recipients) group were hospitalized due to unrelated complications (Knoll and Wonodi 2020). Considerable binding and neutralizing antibody induction were observed after the administration of the second dose. This vaccine has been observed to be better tolerated in older participants with uniform immunological profile in all age groups after administration of a booster dose, thus becoming a ray of hope for the elderly population who are at greater risk of severe COVID-19 (Folegattiet al., 2020b). Drug trial 2/3 carried out between May 30 and August 8, 2020 has highlighted the safety and efficacy of ChAdOx1 nCoV-19 in different age groups, especially in the age group 70 years and above (NCT04400838). The vaccine was administered either as a single dose or as a two-dose regimen at a low dose (2.2×10^{10} viral particles) or a standard dose ($3.5–6.5\ 10^{10}$ viral particles). Multiplex immunoassay was used to determine the total IgG levels against the trimeric spike protein and RBD. At both dose levels, the anti-spike IgG response was found to be decreased with increasing age. However, participants who received a booster dose

had similar antibody titers regardless of age or vaccine dose, and the titer was higher compared to that in participants who did not receive a booster dose. A similar trend was observed with the anti-RBD IgG (Ramasamy et al., 2020). In India, the vaccine is sold under the brand name Covishield and was first approved on December 30, 2020.

Advantages and Limitations

Adenoviral-based vectors are considered relatively safe due to their low immunogenicity in humans. These vectors are efficient in inducing antibody- and cell-mediated immune responses, probably due to the efficient expression of the encoded gene of interest. Long-term immunity requires prime booster doses. Thus, usually, a two-dose regimen is followed for adenoviral vectors to induce memory T- and B-cell immune responses (Geisbert et al., 2011).

Human adenoviruses have long since been known to mankind; thus, preexisting antibodies against these vectors can be a drawback for vaccine development. Certain rare but grave adverse reactions after administration of human adenoviral-based vaccines have been observed, which could be the cause of the preexisting anti-adenoviral immunity in the subjects who have been previously infected by multiple adenoviruses (Kremer 2020a). To induce a stringent amount of immune response and memory cells, adenovirus-based vaccines need booster doses, which may increase the cost of their preparation. Thus, to overcome these limitations, it is imperative to use adenovirus vectors from other species, such as the chimpanzee adenovirus used in ChAdOx1. The long-term side effects of these vaccines will be monitored over the years.

Protein Subunit Vaccines

NVX-CoV2373 vaccine: Novavax developed a recombinant SARS-CoV-2 (rSARS-CoV-2) nanoparticle vaccine against the S-protein also known as NVX-CoV2373. The vaccine was manufactured at Emergent BioSolutions and constructed from the full-length, wild-type SARS-CoV-2 trimeric S-protein with the Matrix-M1 adjuvant. Optimization was done in the already established baculovirus *Spedoptera frugiperda* (Sf9) insect cell expression system (Tian et al., 2020). The rSARS-CoV-2 vaccine has been modified, wherein certain mutations such as 682QQAQ685 at the S1/S2 cleavage site of the S-protein confer protease resistance to the vaccine and at the same time two proline substitutions in residues K986P and V987P in the S2 subunit help in stabilizing the construct in a profusion conformation. This strategy makes NVX-CoV2373 resistant to proteolytic cleavage and allows it to bind to hACE2 receptors with high affinity. The Matrix-M1 adjuvant is a saponin-based adjuvant, a product of Novavax (Wrapp et al., 2020). Trial 1/2 was initiated to evaluate the safety and immunogenicity of the NVX-CoV2373 vaccine given in 5 and 25 μg doses with or without the adjuvant (NCT04368988). The trial started on May 26, 2020 on 134 study participants, among which 83 participants received the vaccine with adjuvant, 25 without adjuvant, and 23 participants were assigned to receive placebo (0.9% normal saline). Three participants served as a backup during the trial run. Mild side effects were seen, and a few cases of adverse events in different groups were observed, which became stable after a few days (less than 7 days). Thus, overall, no severe adverse events were reported in the early trial results. The primary immunogenicity profile of the 5- and 25-μg doses of the vaccine plus adjuvant showed acceptable neutralizing antibody response correlating with anti-spike IgG (Keech et al., 2020). Both vaccine and adjuvant can be stored at 2–8°C.

Furthermore, in a phase 3 trial, 14,039 participants (7,020 in the vaccine group and 7,019 in the placebo group) were enrolled as per protocol and included for population efficacy (NCT04583995). A two-dose regimen of the NVX-CoV2373 vaccine was given 21 days apart, and an efficacy of 89.7% was observed (Heath et al., 2021a). There were no hospitalizations or deaths among the 10 cases in the vaccine group: however, five cases of severe infection were reported among 96 in the placebo group. It was also worth observing that this vaccine was effective against variant B.1.1.7 and the non-B.1.1.7 variants, and the efficacy rates were observed to be 86.3% and 96.4%, respectively, using a *post-hoc* analysis (Heath et al., 2021a). Shinde et al. carried out a study on the efficacy of NVX-CoV2373 against the B.1.351 variant of SARS-CoV-2. This was a phase 2-a trial that started in South Africa, where 6,324 participants received a single dose of vaccine/placebo. The recruited participants were either HIV-negative or medically stable HIV-positive. The vaccine was found to be efficacious in preventing COVID-19, with a higher efficacy rate among HIV-negative participants (NCT04533399) (Shinde et al., 2021).

Advantages and Limitations

As the vaccine is devoid of any infectious particle, it is thus safe for use. The benefit of using an adjuvant was clear in terms of the high magnitude of antibody- and cell-mediated immune responses compared to the antigenicity profile of the vaccine without adjuvant. This vaccine can be stored at 2–8°C, thus mitigating cold chain storage and transport demands. The vaccines contain purified antigenic peptides to elicit immune response, thus avoiding the use of live components of the pathogen.

The limitation, as with all other vaccines, is that it needs booster doses to provide long-term immune response against the pathogen. The immune response remains low without the adjuvant; thus, the need of an adjuvant increases the cost of vaccine formulation. Since the isolated peptide is used to design the vaccine, the other limitations related to this technique is that the isolated protein, if denatured, may bind to nonspecific antibodies.

FUTURE PERSPECTIVES

After the onset of the COVID-19 pandemic, an immediate need for treatment arose to limit the spread of the disease. Initially, repurposed antiviral drugs and other anti-inflammatory treatment regimens were tested. Antiviral drugs such as remdesivir had a significant effect of minimizing the hospitalization in a subset of patients, but this drug also fell short of expectations (Hoek and Sarahanne, 2021; Masoomikarimi et al., 2021). Similarly, CPT showed promising results in earlier clinical trials, but this therapy was also limited

due to technical difficulties and safety concerns. However, antibody-based therapies presented a promising approach in dealing with SARS-CoV-2 infection, and many therapeutic antibodies were approved for the treatment of patients with mild and moderate symptoms (Ning et al., 2021). Besides the existing approaches for developing therapeutic antibodies, several engineered antibody-based therapies, including antibody cocktails and nasal sprays, showed promising clinical outcomes (Baum et al., 2020). These short-term protective therapeutic modalities may also work against the emerging SARS-CoV-2 VOCs, but a long-term and sustainable treatment is what would change the COVID-19 infection landscape. In this direction, vaccines will remain the mainstay therapeutic modalities for COVID-19, which has already documented successful and lasting protective immunity. Modern vaccines such as those based on mRNAs designate a new era in vaccinology as the approach is being used against infectious diseases, and they appear ideal for use against any emerging SARS-CoV-2 variants and non-pathogenic diseases such as cancer (Pardi et al., 2018). Notably, the pan-COVID-19 vaccine (Saunders et al., 2021), which is in the making, holds an enormous promise to target multiple and any new variants of coronaviruses—a hope for the future.

AUTHOR CONTRIBUTIONS

JI and TA conceived the idea, wrote some parts of the manuscript, and modified and corrected the manuscript. KI wrote the major part of this manuscript and arranged ideas accordingly. TME and SA compiled table and figures and helped in overall formatting of manuscript text. All authors contributed to the article and approved the final version for submission.

ACKNOWLEDGMENTS

The support of Ramalingaswami Fellowship Grant (BT/RLF/Re-entry/09/2015) from the Department of Biotechnology (DBT) and Early Career Research Award Grant (file no. ECR/2018/002114) from the Science and Engineering Research Board (SERB), Department of Science and Technology, Govt. of India, to JI, is acknowledged. TA is acknowledged to UGC early career grant (F.4/2018/FRP-Start-up-grant) and SERB Core research grant (CRG/2020/002294). The authors are thankful to Mehwish Nafiz for critical proofreading.

REFERENCES

Ahmad, T., Chaudhuri, R., Joshi, M. C., Almatroudi, A., Rahmani, A. H., and Ali, S. M. (2020). COVID-19: The Emerging Immunopathological Determinants for Recovery or Death. *Front. Microbiol.* 11, 588409. doi:10.3389/fmicb.2020.588409

Ahmad, Tanveer., Mukherjee, Shravani., Pattnaik, Bijay., Kumar, Manish., Singh, Suchita., Kumar, Manish., et al. (2014). Miro1 Regulates Intercellular Mitochondrial Transport & Enhances Mesenchymal Stem Cell Rescue Efficacy. *EMBO J.*, n/a, 2014 . January, n/a. doi:10.1002/embj.201386030

Al Kaabi, N., Zhang, Y., Xia, S., Yang, Y., Al Qahtani, M. M., Abdulrazzaq, N., et al. (2021). Effect of 2 Inactivated SARS-CoV-2 Vaccines on Symptomatic COVID-19 Infection in Adults: A Randomized Clinical Trial. *JAMA* 326 (1), 35–45. doi:10.1001/jama.2021.8565

Alcaide, E. G., Krishnarajah, S., Junker, F., and Junker, Fabian. (2021). Dendritic Cell Tumor Vaccination via Fc Gamma Receptor Targeting: Lessons Learned from Pre-clinical and Translational Studies. *Vaccines (Basel)* 9 (4), 409. doi:10.3390/vaccines9040409

Ali, M. J., Hanif, M., Haider, M. A., Ahmed, M. U., Sundas, F., Hirani, A., et al. (2020). Treatment Options for COVID-19: A Review. *Front. Med. (Lausanne)* 7 (July), 480. doi:10.3389/fmed.2020.00480

Amanat, F., Stadlbauer, D., Strohmeier, S., Nguyen, T. H. O., Chromikova, V., McMahon, M., et al. (2020). A Serological Assay to Detect SARS-CoV-2 Seroconversion in Humans. *Nat. Med.* 26 (7), 1033–1036. doi:10.1038/s41591-020-0913-5

Amanna, I. J., and Slifka, M. K. (2011). Contributions of Humoral and Cellular Immunity to Vaccine-Induced Protection in Humans. *Virology* 411 (2), 206–215. doi:10.1016/j.virol.2010.12.016

AminJafari, A., and Ghasemi, S. (2020). The Possible of Immunotherapy for COVID-19: A Systematic Review. *Int. Immunopharmacol* 83 (June), 106455. doi:10.1016/j.intimp.2020.106455

Anderson, J., Schauer, J., Bryant, S., and Graves, C. R. (2020). The Use of Convalescent Plasma Therapy and Remdesivir in the Successful Management of a Critically Ill Obstetric Patient with Novel Coronavirus 2019 Infection: A Case Report. *Case Rep. Women's Health* 27 (July), e00221. doi:10.1016/j.crwh.2020.e00221

Bachmann, M. F., and Zinkernagel, R. M. (1997). Neutralizing Antiviral B Cell Responses. *Annu. Rev. Immunol.* 15 (1), 235–270. doi:10.1146/annurev.immunol.15.1.235

Baden, L. R., El Sahly, H. M., Essink, B., Kotloff, K., Frey, S., Novak, R., et al. (2021). Efficacy and Safety of the MRNA-1273 SARS-CoV-2 Vaccine. *N. Engl. J. Med.* 384 (5), 403–416. doi:10.1056/NEJMoa2035389

Baum, A., Fulton, B. O., Wloga, E., Copin, R., Pascal, K. E., Russo, V., et al. (2020). Antibody Cocktail to SARS-CoV-2 Spike Protein Prevents Rapid Mutational Escape Seen with Individual Antibodies. *Science* 369 (6506), 1014–1018. doi:10.1126/science.abd0831

Bazin, Hervé. (2003). A Brief History of the Prevention of Infectious Diseases by Immunisations. *Comp. Immunol. Microbiol. Infect. Dis.* 26 (5–6), 293–308. doi:10.1016/S0147-9571(03)00016-X

Billioti de Gage, S., Drouin, J., Desplas, D., Cuenot, F., Dray-Spira, R., Weill, A., et al. (2021). Intravitreal Anti-vascular Endothelial Growth Factor Use in France during the Coronavirus Disease 2019 Pandemic. *JAMA Ophthalmol.* 139 (2), 240–242. doi:10.1001/jamaophthalmol.2020.5594

Buckley, L. F., Wohlford, G. F., Ting, C., Alahmed, A., Van Tassell, B. W., Abbate, A., et al. (2020). Role for Anti-cytokine Therapies in Severe Coronavirus Disease 2019. *Crit. Care Explor* 2 (8), e0178. doi:10.1097/CCE.0000000000000178

Burki, T. K. (2020). The Russian Vaccine for COVID-19. *Lancet Respir. Med.* 8 (11), e85–86. doi:10.1016/S2213-2600(20)30402-1

Callaway, E. (2020). Russia Announces Positive COVID-Vaccine Results from Controversial Trial. *Nature*. November, d41586-020-03209–0. doi:10.1038/d41586-020-03209-0

Casadevall, A., Joyner, M. J., and Pirofski, L. A. (2020). A Randomized Trial of Convalescent Plasma for COVID-19-Potentially Hopeful Signals. *JAMA* 324 (5), 455–457. doi:10.1001/jama.2020.10218

Casadevall, A., and Pirofski, L-A. (2020). The Convalescent Sera Option for Containing COVID-19. *J. Clin. Invest.* 130 (4), 1545–1548. doi:10.1172/JCI138003

Chen, P. L., Lee, N. Y., Cia, C. T., Ko, W. C., and Hsueh, P. R. (2020). A Review of Treatment of Coronavirus Disease 2019 (COVID-19): Therapeutic Repurposing and Unmet Clinical Needs. *Front. Pharmacol.* 11 (November), 584956. doi:10.3389/fphar.2020.584956

Cheng, Y., Wong, R., Soo, Y. O. Y., Wong, W. S., Lee, C. K., Ng, M. H. L., et al. (2005). Use of Convalescent Plasma Therapy in SARS Patients in Hong Kong.

Eur. J. Clin. Microbiol. Infect. Dis. 24 (1), 44–46. doi:10.1007/s10096-004-1271-9

Clem, A. S. (2011). Fundamentals of Vaccine Immunology. *J. Glob. Infect. Dis.* 3 (1), 73–78. doi:10.4103/0974-777X.77299

Clemens, J., Shin, S., Sur, D., Nair, G. B., and Holmgren, J. (2011). New-Generation Vaccines against Cholera. *Nat. Rev. Gastroenterol. Hepatol.* 8 (12), 701–710. doi:10.1038/nrgastro.2011.174

Colaneri, M., Bogliolo, L., Valsecchi, P., Sacchi, P., Zuccaro, V., Brandolino, F., et al. (2020). Tocilizumab for Treatment of Severe COVID-19 Patients: Preliminary Results from SMAtteo COvid19 REgistry (SMACORE). *Microorganisms* 8 (5), 695. doi:10.3390/microorganisms8050695

Corbett, K. S., Flynn, B., Foulds, K. E., Francica, J. R., Boyoglu-Barnum, Seyhan., Boyoglu-Barnum, S., et al. (2020). Evaluation of the MRNA-1273 Vaccine against SARS-CoV-2 in Nonhuman Primates. *N. Engl. J. Med.* 383 (16), 1544–1555. doi:10.1056/NEJMoa2024671

Corti, D., and Lanzavecchia, A. (2013). Broadly Neutralizing Antiviral Antibodies. *Annu. Rev. Immunol.* 31, 705–742. doi:10.1146/annurev-immunol-032712-095916

Cucinotta, D., and Vanelli, M. (2020). WHO Declares COVID-19 a Pandemic. *Acta Biomed.* 91 (1), 157–160. doi:10.23750/abm.v91i1.9397

De Biasi, S., Meschiari, M., Gibellini, L., Bellinazzi, C., Borella, R., Fidanza, L., et al. (2020). Marked T Cell Activation, Senescence, Exhaustion and Skewing towards TH17 in Patients with COVID-19 Pneumonia. *Nat. Commun.* 11 (1), 3434. doi:10.1038/s41467-020-17292-4

DeFrancesco, L. (2021). Publisher Correction: COVID-19 Antibodies on Trial. *Nat. Biotechnol.* 39 (2), 246. doi:10.1038/s41587-021-00813-x

Dolzhikova, I. V., Zubkova, O. V., Tukhvatulin, A. I., Dzharullaeva, A. S., Tukhvatulina, N. M., Shcheblyakov, D. V., et al. (2017). Safety and Immunogenicity of GamEvac-Combi, a Heterologous VSV- and Ad5-Vectored Ebola Vaccine: An Open Phase I/II Trial in Healthy Adults in Russia. *Hum. Vaccin. Immunother.* 13 (3), 613–620. doi:10.1080/21645515.2016.1238535

Duan, K., Liu, B., Li, C., Zhang, H., Yu, T., Qu, J., et al. (2020). Effectiveness of Convalescent Plasma Therapy in Severe COVID-19 Patients. *Proc. Natl. Acad. Sci. USA* 117 (17), 9490–9496. doi:10.1073/pnas.2004168117

Ella, R., Mohan Vadrevu, K., Jogdand, H., Prasad, S., Reddy, S., Sarangi, V., et al. (2021a). Safety and Immunogenicity of an Inactivated SARS-CoV-2 Vaccine, BBV152: A Double-Blind, Randomised, Phase 1 Trial. *Lancet Infect. Dis.* January, S1473309920309427. doi:10.1016/S1473-3099(20)30942-7

EllaRaches, R., Reddy, S., Blackwelder, W., Potdar, V., Yadav, P., Sarangi, V., et al. (2021b). Efficacy, Safety, and Lot to Lot Immunogenicity of an Inactivated SARS-CoV-2 Vaccine (BBV152): A, Double-Blind, Randomised, Controlled Phase 3 Trial. *Preprint. Infect. Dis. (except HIV/AIDS)*. doi:10.1101/2021.06.30.21259439

Folegatti, P. M., Bittaye, M., Flaxman, A., Lopez, F. R., Bellamy, D., Kupke, A., et al. (2020a). Safety and Immunogenicity of a Candidate Middle East Respiratory Syndrome Coronavirus Viral-Vectored Vaccine: A Dose-Escalation, Open-Label, Non-randomised, Uncontrolled, Phase 1 Trial. *Lancet Infect. Dis.* 20 (7), 816–826. doi:10.1016/S1473-3099(20)30160-2

Folegatti, P. M., Ewer, K. J., Aley, P. K., Aley, Angus. B., Becker, S., Belij-Rammerstorfer, S., et al. (2020b). Safety and Immunogenicity of the ChAdOx1 NCoV-19 Vaccine against SARS-CoV-2: A Preliminary Report of a Phase 1/2, Single-Blind, Randomised Controlled Trial. *Lancet* 396 (10249), 467–478. doi:10.1016/S0140-6736(20)31604-4

Geisbert, T. W., Bailey, M., Hensley, L., Asiedu, C., Geisbert, J., Stanley, D., et al. (2011). Recombinant Adenovirus Serotype 26 (Ad26) and Ad35 Vaccine Vectors Bypass Immunity to Ad5 and Protect Nonhuman Primates against Ebolavirus Challenge. *J. Virol.* 85 (9), 4222–4233. doi:10.1128/JVI.02407-10

Gendon, Iu. Z. (2004). Advantages and Disadvantages of Inactivated and Live Influenza Vaccine. *Vopr Virusol* 49 (4), 4–12.

Gibson, P. G., Qin, L., and Puah, S. H. (2020). COVID-19 Acute Respiratory Distress Syndrome (ARDS): Clinical Features and Differences from Typical Pre-COVID-19 ARDS. *Med. J. Aust.* 213 (2), 54–e1. doi:10.5694/mja2.50674

Hansen, J., Baum, A., Pascal, K. E., Russo, V., Giordano, S., Wloga, E., et al. (2020). Studies in Humanized Mice and Convalescent Humans Yield a SARS-CoV-2 Antibody Cocktail. *Science* 369 (6506), 1010–1014. doi:10.1126/science.abd0827

Harrell, C. R., Sadikot, R., Pascual, J., Fellabaum, C., Jankovic, M. G., Jovicic, N., et al. (2019). Mesenchymal Stem Cell-Based Therapy of Inflammatory Lung Diseases: Current Understanding and Future Perspectives. *Stem Cell Int* 2019 (May), 1–14. doi:10.1155/2019/4236973

Heath, P. T., Galiza, E. P., Baxter, D. N., Boffito, M., Browne, D., Burns, F., et al. (2021a). Safety and Efficacy of NVX-CoV2373 Covid-19 Vaccine. *N. Engl. J. Med.* 385, 1172–1183. June. doi:10.1056/NEJMoa2107659

Heath, P. T., Galiza, E. P., Baxter, D. N., Boffito, M., Browne, D., Burns, F., et al. (2021b). Safety and Efficacy of NVX-CoV2373 Covid-19 Vaccine. *N. Engl. J. Med.* 385 (13), 1172–1183. doi:10.1056/NEJMoa2107659

Hoek, J. M., Field, S. M., de Vries, Y. A., Linde, M., Pittelkow, M.-M., Muradchanian, J., et al. (2021). Rethinking Remdesivir for COVID-19: A Bayesian Reanalysis of Trial findings"Rethinking Remdesivir for COVID-19: A Bayesian Reanalysis of Trial Findings." Edited by Alan D Hutson. *PLOS ONE* 16 (7), e0255093. doi:10.1371/journal.pone.0255093

Jackson, L. A., Anderson, E. J., Rouphael, N. G., Roberts, P. C., Makhene, M., Coler, R. N., et al. (2020). An mRNA Vaccine against SARS-CoV-2 - Preliminary Report. *N. Engl. J. Med.* 383 (20), 1920–1931. doi:10.1056/NEJMoa2022483

Jia, W., Channappanavar, R., Zhang, C., Li, M., Zhou, H., Zhang, S., et al. (2019). Single Intranasal Immunization with Chimpanzee Adenovirus-Based Vaccine Induces Sustained and Protective Immunity against MERS-CoV Infection. *Emerg. Microbes Infect.* 8 (1), 760–772. doi:10.1080/22221751.2019.1620083

Kanj, S., and Al-Omari, B. (2021). Convalescent Plasma Transfusion for the Treatment of COVID-19 in Adults: A Global Perspective. *Viruses* 13 (5), 849. doi:10.3390/v13050849

Kapikian, A. Z., Mitchell, R. H., Chanock, R. M., Shvedoff, R. A., and Stewart, C. E. (1969). An Epidemiologic Study of Altered Clinical Reactivity to Respiratory Syncytial (Rs) Virus Infection in Children Previously Vaccinated with an Inactivated Rs Virus Vaccine. *Am. J. Epidemiol.* 89 (4), 405–421. doi:10.1093/oxfordjournals.aje.a120954

Katz, L. M. (2021). (A Little) Clarity on Convalescent Plasma for Covid-19. *N. Engl. J. Med.* 384 (7), 666–668. doi:10.1056/NEJMe2035678

Keech, C., Albert, G., Cho, I., Robertson, A., Reed, P., Neal, S., et al. (2020). Phase 1-2 Trial of a SARS-CoV-2 Recombinant Spike Protein Nanoparticle Vaccine. *N. Engl. J. Med.* 383 (24), 2320–2332. doi:10.1056/NEJMoa2026920

Khadka, R. H., Sakemura, R., Kenderian, S. S., and Johnson, A. J. (2019). Management of Cytokine Release Syndrome: An Update on Emerging Antigen-specific T Cell Engaging Immunotherapies. *Immunotherapy* 11 (10), 851–857. doi:10.2217/imt-2019-0074

Kim, H. S., Choi, E. H., Khan, J., Roilides, E., Francesconi, A., Kasai, M., et al. (2005). Expression of Genes Encoding Innate Host Defense Molecules in Normal Human Monocytes in Response to Candida Albicans. *Infect. Immun.* 73 (6), 3714–3724. doi:10.1128/IAI.73.6.3714-3724.2005

Knoll, Maria. Deloria., and Wonodi, Chizoba. (2020). December, S0140673620326234. doi:10.1016/S0140-6736(20)32623-4Oxford–AstraZeneca COVID-19 Vaccine Efficacy*The Lancet*

Kremer, E. J. (2020a). Pros and Cons of Adenovirus-Based SARS-CoV-2 Vaccines. *Mol. Ther.* 28 (11), 2303–2304. doi:10.1016/j.ymthe.2020.10.002

Kremer, E. J. (2020b). Pros and Cons of Adenovirus-Based SARS-CoV-2 Vaccines. *Mol. Ther.* 28 (11), 2303–2304. doi:10.1016/j.ymthe.2020.10.002

Ku, Z., Xie, X., Davidson, E., Ye, X., Su, H., Menachery, V. D., et al. (2021a). Molecular Determinants and Mechanism for Antibody Cocktail Preventing SARS-CoV-2 Escape. *Nat. Commun.* 12 (1), 469. doi:10.1038/s41467-020-20789-7

Ku, Z., Xie, X., Hinton, P. R., Liu, X., Ye, X., Muruato, A. E., et al. (2021b). Nasal Delivery of an IgM Offers Broad Protection from SARS-CoV-2 Variants. *Nature* 595 (7869), 718–723. doi:10.1038/s41586-021-03673-2

Kundu, S., Gurney, M., and O'Dwyer, M. (2021). Generating Natural Killer Cells for Adoptive Transfer: Expanding Horizons. *Cytotherapy* 23 (7), 559–566. doi:10.1016/j.jcyt.2020.12.002

Kwon, D. (2021). Antibody-laden Nasal spray Could Provide COVID protection - and Treatment. *Nature*. June, d41586-021-01481–82. doi:10.1038/d41586-021-01481-2

Kyriakidis, N. C., López-Cortés, A., González, E. V., Grimaldos, A. B., and Prado, E. O. (2021). SARS-CoV-2 Vaccines Strategies: A Comprehensive Review of Phase 3 Candidates. *Npj Vaccin.* 6 (1), 28. doi:10.1038/s41541-021-00292-w

Landoni, E., and Savoldo, B. (2018). Treating Hematological Malignancies with Cell Therapy: Where Are We Now?. *Expert Opin. Biol. Ther.* 18 (1), 65–75. doi:10.1080/14712598.2018.1384810

Lawton, G. (2021). Sputnik V Vaccine Goes Global. *New Scientist* 250 (3331), 10–11. doi:10.1016/S0262-4079(21)00671-0

Leng, Z., Zhu, R., Hou, W., Feng, Y., Yang, Y., Han, Q., et al. (2020). Transplantation of ACE2- Mesenchymal Stem Cells Improves the Outcome of Patients with COVID-19 Pneumonia. *Aging Dis.* 11 (2), 216–228. doi:10.14336/AD.2020.0228

Liu, J., Li, S., Liu, J., Liang, B., Wang, X., Wang, H., et al. (2020). Longitudinal Characteristics of Lymphocyte Responses and Cytokine Profiles in the Peripheral Blood of SARS-CoV-2 Infected Patients. *EBioMedicine* 55 (May), 102763. doi:10.1016/j.ebiom.2020.102763

Liu, S., Galat, V., Galat4, Y., Lee, Y. K. A., Wainwright, D., and Wu, J. (2021). NK Cell-Based Cancer Immunotherapy: From Basic Biology to Clinical Development. *J. Hematol. Oncol.* 14 (1), 7. doi:10.1186/s13045-020-01014-w

Logunov, D. Y., Dolzhikova, I. V., Zubkova, O. V., Tukhvatullin, A. I., Shcheblyakov, D. V., Dzharullaeva, A. S., et al. (2020). Safety and Immunogenicity of an RAd26 and RAd5 Vector-Based Heterologous Prime-Boost COVID-19 Vaccine in Two Formulations: Two Open, Non-randomised Phase 1/2 Studies from Russia. *Lancet* 396 (10255), 887–897. doi:10.1016/S0140-6736(20)31866-3

Lopez Bernal, J., Andrews, N., Gower, C., Gallagher, E., Simmons, R., Thelwall, S., et al. (2021). Effectiveness of Covid-19 Vaccines against the B.1.617.2 (Delta) Variant. *N. Engl. J. Med.* 385 (7), 585–594. doi:10.1056/NEJMoa2108891

Luke, T. C., Kilbane, E. M., Jackson, J. L., and Hoffman, S. L. (2006). Meta-Analysis: Convalescent Blood Products for Spanish Influenza Pneumonia: A Future H5N1 Treatment?. *Ann. Intern. Med.* 145 (8), 599–609. doi:10.7326/0003-4819-145-8-200610170-00139

Lund, F. E., and Randall, T. D. (2021). Scent of a Vaccine. *Science* 373 (6553), 397–399. doi:10.1126/science.abg9857

Luo, P., Liu, Y., Qiu, L., Liu, X., Liu, D., and Li, J. (2020). Tocilizumab Treatment in COVID-19: A Single center Experience. *J. Med. Virol.* 92 (7), 814–818. doi:10.1002/jmv.25801

MacLean, O. A., Lytras, S., Weaver, S., Singer, J. B., Boni, Maciej. F., Boni, M. F., et al. (2020). Natural Selection in the Evolution of SARS-CoV-2 in Bats, Not Humans, Created a Highly Capable Human Pathogen. *Preprint. Evol. Biol.* doi:10.1101/2020.05.28.122366

Mahase, E. (2020)., 371. December, m4714. doi:10.1136/bmj.m4714Covid-19: UK Approves Pfizer and BioNTech Vaccine with Rollout Due to Start Next Week*BMJ*

Mallapaty, S. (2021). China COVID Vaccine Reports Mixed Results - what Does that Mean for the Pandemic?. *Nature*. January, d41586-021-00094-z. doi:10.1038/d41586-021-00094-z

Masoomikarimi, M., Garmabi, B., Alizadeh, J., Kazemi, E., Azari Jafari, A., Mirmoeeni, S., et al. (2021). Advances in Immunotherapy for COVID-19: A Comprehensive Review. *Int. Immunopharmacol* 93 (April), 107409. doi:10.1016/j.intimp.2021.107409

Matthay, M. A., Calfee, C. S., Zhuo, H., Thompson, B. T., Wilson, J. G., Levitt, J. E., et al. (2019). Treatment with Allogeneic Mesenchymal Stromal Cells for Moderate to Severe Acute Respiratory Distress Syndrome (START Study): A Randomised Phase 2a Safety Trial. *Lancet Respir. Med.* 7 (2), 154–162. doi:10.1016/S2213-2600(18)30418-1

Mei, S. H., Haitsma, J. J., Dos Santos, C. C., Deng, Y., Lai, P. F., Slutsky, A. S., et al. (2010). Mesenchymal Stem Cells Reduce Inflammation while Enhancing Bacterial Clearance and Improving Survival in Sepsis. *Am. J. Respir. Crit. Care Med.* 182 (8), 1047–1057. doi:10.1164/rccm.201001-0010OC

Mercado, N. B., Zahn, R., Wegmann, F., Loos, C., Chandrashekar, A., Yu, J., et al. (2020). Single-Shot Ad26 Vaccine Protects against SARS-CoV-2 in Rhesus Macaques. *Nature* 586 (7830), 583–588. doi:10.1038/s41586-020-2607-z

Mohapatra, P. R., and Mishra, B. (2021). Regulatory Approval of COVID-19 Vaccine for Restricted Use in Clinical Trial Mode. *Lancet Infect. Dis.* 21 (5), 599–600. doi:10.1016/S1473-3099(21)00045-1

Mohn, K. G.-I., Smith, I., Sjursen, H., and Cox, R. J. (2018). Immune Responses after Live Attenuated Influenza Vaccination. *Hum. Vaccin. Immunother.* 14 (3), 571–578. doi:10.1080/21645515.2017.1377376

Moll, G., Hoogduijn, M. J., and Ankrum, J. A. (2020). Editorial: Safety, Efficacy and Mechanisms of Action of Mesenchymal Stem Cell Therapies. *Front. Immunol.* 11 (February), 243. doi:10.3389/fimmu.2020.00243

Morris, S. J., Sebastian, S., Spencer, A. J., and Gilbert, S. C. (2016). Simian Adenoviruses as Vaccine Vectors. *Future Virol.* 11 (9), 649–659. doi:10.2217/fvl-2016-0070

Moss, S. W. (2020). Vulgarly Called the Throat-Distemper: New Jersey's Two-Century Struggle against Diphtheria. *njs* 6 (2), 56–84. doi:10.14713/njs.v6i2.213

Murin, C. D., Wilson, I. A., and Ward, A. B. (2019). Antibody Responses to Viral Infections: A Structural Perspective across Three Different Enveloped Viruses. *Nat. Microbiol.* 4 (5), 734–747. doi:10.1038/s41564-019-0392-y

Musial, C., and Gorska-Ponikowska, M. (2021). Medical Progress: Stem Cells as a New Therapeutic Strategy for COVID-19. *Stem Cel Res* 52 (April), 102239. doi:10.1016/j.scr.2021.102239

Nagoba, B., Gavkare, A., Jamadar, N., Mumbre, S., and Selkar, S. (2020). Positive Aspects, Negative Aspects and Limitations of Plasma Therapy with Special Reference to COVID-19. *J. Infect. Public Health* 13 (12), 1818–1822. doi:10.1016/j.jiph.2020.08.011

Ning, L., Abagna, H. B., Jiang, Q., Liu, S., and Huang, J. (2021). Development and Application of Therapeutic Antibodies against COVID-19. *Int. J. Biol. Sci.* 17 (6), 1486–1496. doi:10.7150/ijbs.59149

Pardi, N., Hogan, M. J., Porter, F. W., and Weissman, D. (2018). mRNA Vaccines - a new era in Vaccinology. *Nat. Rev. Drug Discov.* 17 (4), 261–279. doi:10.1038/nrd.2017.243

Pardoll, D. M., and Drew, M. (2012). The Blockade of Immune Checkpoints in Cancer Immunotherapy. *Nat. Rev. Cancer* 12 (4), 252–264. doi:10.1038/nrc3239

Pasteur, L. (1880). De L'attenuation Du Virus. *Du Cholera Des Poules"* 91, 673–680.

Pasteur, L., Chamberland. 1881. "Sur La Vaccination Charbonneuse" 92: 1378–1383.

Philbin, V. J., Dowling, D. J., Gallington, Leighanne. C., Gallington, L. C., Cortés, G., Tan, Z., et al. (2012). Imidazoquinoline Toll-like Receptor 8 Agonists Activate Human Newborn Monocytes and Dendritic Cells through Adenosine-Refractory and Caspase-1-dependent Pathways. *J. Allergy Clin. Immunol.* 130 (1), 195–e9. doi:10.1016/j.jaci.2012.02.042

Polack, F. P. (2007). Atypical Measles and Enhanced Respiratory Syncytial Virus Disease (ERD) Made Simple. *Pediatr. Res.* 62 (1), 111–115. doi:10.1203/PDR.0b013e3180686ce0

Polack, F. P., Thomas, S. J., Kitchin, N., Absalon, J., Gurtman, A., Lockhart, S., et al. (2020a). December, NEJMoa2034577. doi:10.1056/NEJMoa2034577Safety and Efficacy of the BNT162b2 MRNA Covid-19 Vaccine*N. Engl. J. Med.*

Polack, F. P., Thomas, S. J., Kitchin, N., Absalon, J., Gurtman, A., Lockhart, S., et al. (2020b). Safety and Efficacy of the BNT162b2 MRNA Covid-19 Vaccine. *N. Engl. J. Med.* 383 (27), 2603–2615. doi:10.1056/NEJMoa2034577

Poland, G. A., Ovsyannikova, I. G., and Kennedy, R. B. (2020). SARS-CoV-2 Immunity: Review and Applications to Phase 3 Vaccine Candidates. *The Lancet* 396 (10262), 1595–1606. doi:10.1016/S0140-6736(20)32137-1

Pulendran, B., and Ahmed, R. (2011). Immunological Mechanisms of Vaccination. *Nat. Immunol.* 12 (6), 509–517. doi:10.1038/ni.2039

Ramasamy, M. N., Minassian, A. M., Ewer, K. J., Flaxman, A. L., Folegatti, P. M., Owens, D. R., et al. (2020). Safety and Immunogenicity of ChAdOx1 NCoV-19 Vaccine Administered in a Prime-Boost Regimen in Young and Old Adults (COV002): A Single-Blind, Randomised, Controlled, Phase 2/3 Trial. *Lancet* 396 (10267), 1979–1993. doi:10.1016/S0140-6736(20)32466-1

Roberts, C. M., Levi, M., McKee, M., Schilling, R., Lim, W. S., Grocott, M. P. W., et al. (2020). COVID-19: A Complex Multisystem Disorder. *Br. J. Anaesth.* 125 (3), 238–242. doi:10.1016/j.bja.2020.06.013

Rogers, C. J., Harman, R. J., Bunnell, B. A., Schreiber, M. A., Xiang, C., Wang, F. S., et al. (2020). Rationale for the Clinical Use of Adipose-Derived Mesenchymal Stem Cells for COVID-19 Patients. *J. Transl Med.* 18 (1), 203. doi:10.1186/s12967-020-02380-2

Sadoff, J., Gars, M. L., Shukarev, G., Heerwegh, D., Truyers, C., de Groot, A. M., et al. (2020). Safety and Immunogenicity of the Ad26.COV2.S COVID-19 Vaccine Candidate: Interim Results of a Phase 1/2a, Double-Blind, Randomized, Placebo-Controlled Trial. *Infect. Dis. (except HIV/AIDS)*. doi:10.1101/2020.09.23.20199604

Sadoff, J., Gray, G., Vandebosch, A., Cárdenas, V., Shukarev, G., Grinsztejn, B., et al. (2021). Safety and Efficacy of Single-Dose Ad26.COV2.S Vaccine against Covid-19. *N. Engl. J. Med.* 384 (23), 2187–2201. doi:10.1056/NEJMoa2101544

Saeedi, P., Halabian, R., and Imani Fooladi, A. A. (2019). A Revealing Review of Mesenchymal Stem Cells Therapy, Clinical Perspectives and Modification Strategies. *Stem Cel Investig* 6 (September), 34. doi:10.21037/sci.2019.08.11

Saleh, M., Vaezi, A. A., Aliannejad, R., Sohrabpour, A. A., Kiaei, S. Z. F., Shadnoush, M., et al. (2021). Cell Therapy in Patients with COVID-19 Using Wharton's Jelly Mesenchymal Stem Cells: a Phase 1 Clinical Trial. *Stem Cel Res Ther* 12 (1), 410. doi:10.1186/s13287-021-02483-7

Salvarani, C., Dolci, G., Massari, M., Merlo, D. F., Cavuto, S., Savoldi, L., et al. (2021). Effect of Tocilizumab vs Standard Care on Clinical Worsening in Patients Hospitalized with COVID-19 Pneumonia: A Randomized Clinical Trial. *JAMA Intern. Med.* 181 (1), 24–31. doi:10.1001/jamainternmed.2020.6615

Santa Cruz, A., Mendes-Frias, A., Oliveira, A. I., Dias, L., Matos, A. R., Carvalho, A., et al. (2021). André, Ana Mendes-Frias, Ana Isabel Oliveira, Luís Dias, Ana Rita Matos, Alexandre Carvalho, Carlos Capela, Jorge Pedrosa, António Gil Castro, and Ricardo SilvestreInterleukin-6 Is a Biomarker for the Development of Fatal Severe Acute Respiratory Syndrome Coronavirus 2 Pneumonia. *Front. Immunol.* 12 (February), 613422. doi:10.3389/fimmu.2021.613422

Saunders, K. O., Lee, E., Parks, R., Martinez, D. R., Li, D., Chen, H., et al. (2021). Neutralizing Antibody Vaccine for Pandemic and Pre-emergent Coronaviruses. *Nature* 594 (7864), 553–559. doi:10.1038/s41586-021-03594-0

Sengupta, V., Sengupta, S., Lazo, A., Woods, P., Nolan, A., and Bremer, N. (2020). Exosomes Derived from Bone Marrow Mesenchymal Stem Cells as Treatment for Severe COVID-19. *Stem Cell Dev* 29 (12), 747–754. doi:10.1089/scd.2020.0080

Shen, M., Zhou, Y., Ye, J., Abdullah Al-maskri, A. A., Kang, Y., Zeng, S., et al. (2020). Recent Advances and Perspectives of Nucleic Acid Detection for Coronavirus. *J. Pharm. Anal.* 10 (2), 97–101. doi:10.1016/j.jpha.2020.02.010

Shinde, V., Bhikha, S., Hoosain, Z., Archary, M., Bhorat, Q., Fairlie, L., et al. (2021). Efficacy of NVX-CoV2373 Covid-19 Vaccine against the B.1.351 Variant. *N. Engl. J. Med.* 384 (20), 1899–1909. doi:10.1056/NEJMoa2103055

Simões, E. A. F., Forleo-Neto, E., Geba, G. P., Kamal, M., Yang, F., Cicirello, H., et al. (2020). Suptavumab for the Prevention of Medically Attended Respiratory Syncytial Virus Infection in Preterm Infants. *Clin. Infect. Dis.*, ciaa951, 2020 . September. doi:10.1093/cid/ciaa951

Simonson, O. E., Mougiakakos, D., Heldring, N., Bassi, G., Johansson, H. J., Dalén, M., et al. (2015). *In Vivo* Effects of Mesenchymal Stromal Cells in Two Patients with Severe Acute Respiratory Distress SyndromeIn Vivo Effects of Mesenchymal Stromal Cells in Two Patients with Severe Acute Respiratory Distress Syndrome: Effects of Mesenchymal Stromal Cells in ARDS. *STEM CELLS Translational Med.* 4 (10), 1199–1213. doi:10.5966/sctm.2015-0021

Tanriover, M. D., Doğanay, H. L., Akova, M., Güner, H. R., Azap, A., Akhan, S., et al. (2021). Efficacy and Safety of an Inactivated Whole-Virion SARS-CoV-2 Vaccine (CoronaVac): Interim Results of a Double-Blind, Randomised, Placebo-Controlled, Phase 3 Trial in Turkey. *The Lancet* 398 (10296), 213–222. doi:10.1016/S0140-6736(21)01429-X

Tatsis, N., and Ertl, H. C. (2004). Adenoviruses as Vaccine Vectors. *Mol. Ther.* 10 (4), 616–629. doi:10.1016/j.ymthe.2004.07.013

Taylor, P. C., Adams, A. C., HuffordInmaculada de la Torre, M. M., de la Torre, I., Winthrop, K., and Gottlieb, R. L. (2021). Neutralizing Monoclonal Antibodies for Treatment of COVID-19. *Nat. Rev. Immunol.* 21 (6), 382–393. doi:10.1038/s41577-021-00542-x

Tian, J.-H., Patel, N., Haupt, R., Zhou, H., Weston, S., Hammond, H., et al. (2020). SARS-CoV-2 Spike Glycoprotein Vaccine Candidate NVX-CoV2373 Elicits Immunogenicity in Baboons and Protection in Mice. *Preprint. Microbiol.* doi:10.1101/2020.06.29.178509

Tiberghien, P., de Lamballerie, X., Morel, P., Gallian, P., Lacombe, K., and Yazdanpanah, Y. (2020). Collecting and Evaluating Convalescent Plasma for COVID-19 Treatment: Why and How?. *Vox Sang* 115 (6), 488–494. doi:10.1111/vox.12926

Toniati, P., Piva, S., Cattalini, M., Garrafa, E., Regola, F., Castelli, F., et al. (2020). Tocilizumab for the Treatment of Severe COVID-19 Pneumonia with Hyperinflammatory Syndrome and Acute Respiratory Failure: A Single Center Study of 100 Patients in Brescia, Italy. *Autoimmun. Rev.* 19 (7), 102568. doi:10.1016/j.autrev.2020.102568

Velu, V., Titanji, K., Zhu, B., Husain, S., Pladevega, A., Lai, L., et al. (2009). Enhancing SIV-specific Immunity *In Vivo* by PD-1 Blockade. *Nature* 458 (7235), 206–210. doi:10.1038/nature07662

Vonarburg, C., Loetscher, M., Spycher, M. O., Kropf, A., Illi, M., Salmon, S., et al. (2019). Topical Application of Nebulized Human IgG, IgA and IgAM in the Lungs of Rats and Non-human Primates. *Respir. Res.* 20 (1), 99. doi:10.1186/s12931-019-1057-3

Voysey, Merryn., Clemens, Sue. Ann. Costa., Madhi, Shabir. A., Weckx, Lily. Y., Folegatti, Pedro. M., Parvinder, K. A., et al. (2021). Safety and Efficacy of the ChAdOx1 NCoV-19 Vaccine (AZD1222) against SARS-CoV-2: An Interim Analysis of Four Randomised Controlled Trials in Brazil, South Africa, and the UK. *The Lancet* 397 (10269), 99–111. doi:10.1016/S0140-6736(20)32661-110.1016/s0140-6736(21)00976-4

Wajnberg, A., Amanat, F., Firpo, A., Altman, D. R., Bailey, M. J., Mansour, M., et al. (2020). Robust Neutralizing Antibodies to SARS-CoV-2 Infection Persist for Months. *Science* 370 (6521), 1227–1230. doi:10.1126/science.abd7728

Wang, C., Li, W., Drabek, D., Okba, N. M. A., van Haperen, R., Osterhaus, A. D. M. E., et al. (2020). A Human Monoclonal Antibody Blocking SARS-CoV-2 Infection. *Nat. Commun.* 11 (1), 2251. doi:10.1038/s41467-020-16256-y

Wang, H., Zhang, Y., Huang, B., Deng, W., Quan, Y., Wang, W., et al. (2020). Development of an Inactivated Vaccine Candidate, BBIBP-CorV, with Potent Protection against SARS-CoV-2. *Cell* 182 (6499), 713–e9. doi:10.1126/science.abc193210.1016/j.cell.2020.06.008

Wang, S. H., Shetty, A. K., Jin, K., and Chunhua Zhao, R. (2020). Combating COVID-19 with Mesenchymal Stem/Stromal Cell Therapy: Promise and Challenges. *Front Cel Dev Biol* 8 (January), 627414. doi:10.3389/fcell.2020.627414

Weinreich, D. M., Sivapalasingam, S., Norton, T., Ali, S., Gao, H., Bhore, R., et al. (2021). REGN-COV2, a Neutralizing Antibody Cocktail, in Outpatients with Covid-19. *N. Engl. J. Med.* 384 (3), 238–251. doi:10.1056/NEJMoa2035002

Wibmer, C. K., Ayres, F., Hermanus, T., Madzivhandila, M., Kgagudi, P., Oosthuysen, B., et al. (2021). SARS-CoV-2 501Y.V2 Escapes Neutralization by South African COVID-19 Donor Plasma. *Nat. Med.* 27 (4), 622–625. doi:10.1038/s41591-021-01285-x

Wilson, J. G., Liu, K. D., Zhuo, H., Caballero, L., McMillan, M., Fang, X., et al. (2015). Mesenchymal Stem (Stromal) Cells for Treatment of ARDS: A Phase 1 Clinical Trial. *Lancet Respir. Med.* 3 (1), 24–32. doi:10.1016/S2213-2600(14)70291-7

Wrapp, D., Wang, N., Corbett, K. S., Goldsmith, J. A., Hsieh, C. L., Abiona, O., et al. (2020). Cryo-EM Structure of the 2019-NCoV Spike in the Prefusion Conformation. *bioRxiv* 367 (6483), 1260–1263. doi:10.1126/science.abb250710.1101/2020.02.11.944462

Xia, S., Zhang, Y., Wang, Y., Wang, H., Yang, Y., Gao, G. F., et al. (2021). Safety and Immunogenicity of an Inactivated SARS-CoV-2 Vaccine, BBIBP-CorV: A Randomised, Double-Blind, Placebo-Controlled, Phase 1/2 Trial. *Lancet Infect. Dis.* 21 (1), 39–51. doi:10.1016/S1473-3099(20)30831-8

Xu, X., Han, M., Li, T., Sun, W., Wang, D., Fu, B., et al. (2020). Effective Treatment of Severe COVID-19 Patients with Tocilizumab. *Proc. Natl. Acad. Sci. USA* 117 (20), 10970–10975. doi:10.1073/pnas.2005615117

Yadav, P., Ella, R., Kumar, S., Patil, D., Mohandas, S., Shete, A., et al. (2020). Remarkable Immunogenicity and Protective Efficacy of BBV152, an Inactivated SARS-CoV-2 Vaccine in Rhesus Macaques. *Nat. Commun.* 12 (1), 1–11. doi:10.1038/s41467-021-21639-w

Yazici, Y., Curtis, J. R., Ince, A., Baraf, H., Malamet, R. L., Teng, L. L., et al. (2012). Efficacy of Tocilizumab in Patients with Moderate to Severe Active Rheumatoid Arthritis and a Previous Inadequate Response to Disease-Modifying Antirheumatic Drugs: The ROSE Study. *Ann. Rheum. Dis.* 71 (2), 198–205. doi:10.1136/ard.2010.148700

Yeh, K.-M., Chiueh, T.-S., Siu, L. K., Lin, J.-C., Chan, P. K. S., Peng, M.-Y., et al. (2005). Experience of Using Convalescent Plasma for Severe Acute Respiratory Syndrome Among Healthcare Workers in a Taiwan Hospital. *J. Antimicrob. Chemother.* 56 (5), 919–922. doi:10.1093/jac/dki346

Zhang, C., Maruggi, G., Shan, H., and Li, J. (2019). Advances in MRNA Vaccines for Infectious Diseases. *Front. Immunol.* 10 (March), 594. doi:10.3389/fimmu.2019.00594

Zhang, Yanjun., Zeng, Gang., Pan, Hongxing., Li, Changgui., Hu, Yaling., Chu, Kai., et al. (2020). November, S1473309920308434. doi:10.1016/S1473-3099(20)30843-4Safety, Tolerability, and Immunogenicity of an Inactivated SARS-CoV-2 Vaccine in Healthy Adults Aged 18–59 Years: A Randomised, Double-Blind, Placebo-Controlled, Phase 1/2 Clinical Trial*Lancet Infect. Dis.*

Zhao, H., Zhu, Q., Zhang, C., Li, J., Wei, M., Qin, Y., et al. (2021). Tocilizumab Combined with Favipiravir in the Treatment of COVID-19: A Multicenter Trial in a Small Sample Size. *Biomed. Pharmacother.* 133 (January), 110825. doi:10.1016/j.biopha.2020.110825

Zhao, Q., and He, Y. (2020). Challenges of Convalescent Plasma Therapy on COVID-19. *J. Clin. Virolthe Official Publ. Pan Am. Soc. Clin. Virol.* 127 (June), 104358. doi:10.1016/j.jcv.2020.104358

Zheng, J. (2020). SARS-CoV-2: An Emerging Coronavirus that Causes a Global Threat. *Int. J. Biol. Sci.* 16 (10), 1678–1685. doi:10.7150/ijbs.45053

Zheng, M., Gao, Y., Wang, G., Song, G., Liu, S., Sun, D., et al. (2020). Functional Exhaustion of Antiviral Lymphocytes in COVID-19 Patients. *Cell Mol Immunol* 17 (5), 533–535. doi:10.1038/s41423-020-0402-2

Zhou, Y. W., Xie, Y., Tang, L. S., Pu, D., Zhu, Y. J., Liu, J. Y., et al. (2021). Therapeutic Targets and Interventional Strategies in COVID-19: Mechanisms and Clinical Studies. *Signal. Transduct Target. Ther.* 6 (1), 317. doi:10.1038/s41392-021-00733-x

Conflict of Interest: The authors declare that the research was conducted in the absence of any commercial or financial relationships that could be construed as a potential conflict of interest.

Publisher's Note: All claims expressed in this article are solely those of the authors and do not necessarily represent those of their affiliated organizations, or those of the publisher, the editors, and the reviewers. Any product that may be evaluated in this article, or claim that may be made by its manufacturer, is not guaranteed or endorsed by the publisher.

frontiers in Pharmacology

REVIEW
published: 10 January 2022
doi: 10.3389/fphar.2021.781425

Application of Nanoparticles in the Treatment of Lung Cancer With Emphasis on Receptors

*Jingyue Wang[1†], Tong Zhou[2†], Ying Liu[3], Shuangmin Chen[3] and Zhenxiang Yu[3]**

[1]Department of Cardiology, The First Hospital of Jilin University, Changchun, China, [2]Department of Endocrinology and Metabolism, The First Hospital of Jilin University, Changchun, China, [3]Department of Respiration, The First Hospital of Jilin University, Changchun, China

Lung cancer is one of the malignant tumors that has seen the most rapid growth in terms of morbidity and mortality in recent years, posing the biggest threat to people's health and lives. In recent years, the nano-drug loading system has made significant progress in the detection, diagnosis, and treatment of lung cancer. Nanomaterials are used to specifically target tumor tissue to minimize therapeutic adverse effects and increase bioavailability. It is achieved primarily through two mechanisms: passive targeting, which entails the use of enhanced penetration and retention (EPR) effect, and active targeting, which entails the loading recognition ligands for tumor marker molecules onto nanomaterials. However, it has been demonstrated that the EPR effect is effective in rodents but not in humans. Taking this into consideration, researchers paid significant attention to the active targeting nano-drug loading system. Additionally, it has been demonstrated to have a higher affinity and specificity for tumor cells. In this review, it describes the development of research into active targeted nano-drug delivery systems for lung cancer treatment from the receptors' or targets' perspective. We anticipate that this study will help biomedical researchers use nanoparticles (NPs) to treat lung cancer by providing more and novel drug delivery strategies or solid ligands.

Keywords: lung cancer, nanoparticle, active targeting, receptors, biological ligands, drug delivery

OPEN ACCESS

Edited by:
Irfan Rahman,
University of Rochester, United States

Reviewed by:
Inmaculada Posadas,
University of Castilla-La Mancha, Spain
Leli Zeng,
Sun Yat-sen University, China

****Correspondence:***
Zhenxiang Yu
yuzx@jlu.edu.cn

†These authors have contributed equally to this work and share first authorship

Specialty section:
This article was submitted to Respiratory Pharmacology, a section of the journal Frontiers in Pharmacology

Received: *22 September 2021*
Accepted: *06 December 2021*
Published: *10 January 2022*

Citation:
Wang J, Zhou T, Liu Y, Chen S and Yu Z (2022) Application of Nanoparticles in the Treatment of Lung Cancer With Emphasis on Receptors. Front. Pharmacol. 12:781425. doi: 10.3389/fphar.2021.781425

1 INTRODUCTION

Cancer is a major cause of mortality worldwide, with over 200 distinct types, the most common of which is lung cancer, which is also the leading cause of cancer-related deaths. Lung cancer accounted for 11.6% of the 2.09 million new cancer cases diagnosed in 2018 and 18.4% of the 1.76 million cancer deaths. Among all malignant tumors, men have the highest incidence and mortality rates for lung cancer, while women have the third and second highest incidence and mortality rates for lung cancer, respectively (Bade and Dela Cruz, 2020). Lung cancer is classified as small cell lung cancer (SCLC) or non-small cell lung cancer (NSCLC), with about 80% of cases being NSCLC and 20% being SCLC. NSCLC can be divided into adenocarcinoma, squamous cell carcinoma, large cell carcinoma, and mixtures. SCLC is classified into three subtypes: small cell carcinoma, mixed small cell and large cell carcinoma, and mixed small cell carcinoma, each of which has a distinct therapeutic profile and clinical prognosis (Khanmohammadi et al., 2020). Lung cancer is often treated with surgery, chemotherapy, radiotherapy, and adjuvant therapy (Zappa and Mousa, 2016). Traditional chemotherapy treatments for lung cancer are unable to specifically target tumor cells and cause significant damages to normal cells, including bone marrow arrest, gastrointestinal reactions, and phlebophlogosis (Jin et al., 2018), thus limiting the development of anticancer drugs. In the 20th

TABLE 1 | Receptors: principal categories, functions, and applications.

Major categories of receptors	Functions and applications
VEGFR	Functions: increase vascular permeability; make lung cancer drug-resistant Tran et al. (2002), Herbst et al. (2005) • tLYP-1(NRP-1)enhanced the tumor inhibitory effect and reduced the side effects Jin et al. (2018) • Flk-1(VEGFR-2)enhanced the tumor inhibitory effect and reduced the side effects on heart and kidney Liu et al. (2011)
αvβ3 Integrin	Functions: promoting tumor angiogenesis and tumor metastasis Marelli et al. (2013) • GRGDSP(αvβ3 and α5β1)inhibited tumor growth and reduced side effectsBabu et al. (2017) • RGD (Integrin) improved the anti-tumor activity and delayed the release of loaded drugs Wang et al. (2018) • cRGD (Integrin) -PS-DOX was more likely to accumulate in tumors Zou et al. (2018)
EGFR	Functions: involve in tumor growth and progression, including proliferation, angiogenesis, invasion and metastasis Singh et al. (2016) • ER (EGFR) enhanced the targeting effect on PC-9 (Zhang et al., 2019) • EGF (EGFR) increased the distribution of NPs in tumor tissues, enhanced the uptake of NPs by lung cancer cells, and greatly enhanced the tumor-killing effect of drugs Zhang et al. (2016) • APT improved tumor inhibition, induced apoptosis, and had more minor side effects Lv et al. (2018)
σ Receptor	Functions: overexpressed in rapidly proliferating normal cells and cancer cells such as malignant melanoma, glioma, breast cancer, prostate cancer, SCLC and NSCLC van Waarde et al. (2015) • AA improved the delivery efficiency of siRNA by 9 times Yang et al. (2012) • AA can target the overexpressed σ receptor Xiong et al. (2016)
Folate Receptor	Functions: tumor tissue specificity; tumor marker • Improved the effectiveness and specificity of photodynamic therapy (PDT) Kato et al. (2017) • Den NPs:suitable carrier for co-delivery of siRNA and chemotherapeutic drugs in lung cancer cells Amreddy et al. (2018) • Efficacy of folate receptor-α (FRA)-targeted DOTAP Muralidharan et al. (2016) • FA modified amphiphilic PEG-PLGA copolymer NPs carried with CDDP and PTX He et al. (2015); also effective for the combined delivery of cisplatin and paclitaxel He et al. (2016)
Transferrin Receptor	Functions: expression level is higher in cells with a high proliferation rate, especially in tumor cells Daniels et al. (2006), Cheng et al. (2011), Dev and Babitt, (2017) • As a monitoring index of gambogic acid therapy sensitivity Zhu et al. (2009) • Combination of TFR and artemisinin could reduce small cell lung cancer drug resistance Sadava et al. (2002) • Thymoquinone-NP modified transferrin successfully couples two different miRNA pathways Upadhyay et al. (2019)
CD44	Functions: plays an important role in malignant tumor-related activities • HA-PCL- CAP nanoparticles identified the potential for the treatment of non-small cell lung cancer Parashar et al. (2019)

century, Paul Ehrlich, inspired by Karl Maria von Weber's opera "DerFreischutz," coined the term "magic bullet" for the first time and later expanded on the concepts of nanoparticles (NPs) and drug targeting in medicine (Kreuter, 2007). In recent years, advancements in drug nanotechnology have effectively overcome the drawbacks of traditional chemotherapy drugs. NPs have a small particle size, large specific surface area, and good biocompatibility and degradability. The critical point is that NPs may passively target tumor cells, and active targeting can be achieved by modifying the surface of NPs to enhance the therapeutic impact and decrease the toxicity of anticancer drugs (Ahmad et al., 2015).

Nanomedicine is a relatively new form of treatment that focuses on replacing drug delivery and improving therapeutic effects while minimizing adverse effects on normal tissues (Markman et al., 2013). NPs used in the treatment of lung cancer can be divided into two categories: organic and inorganic NPs. The following are the major classes of organic NPs: 1) liposome-cholesterol and phospholipid-like biofilm-like NPs, 2) solid lipid NPs, 3)nanostructured lipid carriers-NPs mixed with solid lipids and liquid lipids, 4) polymeric NPs composed of polymers such as sodium alginate, chitosan, gelatin, polycaprolactone, polylactide, and polylactic acid, 5) Polymeric micelles-colloidal NPs composed of amphiphilic block copolymers, 6) dendrimer-highly branched, symmetrical, radiating NPs. Inorganic NPs are classified into three types: 1) magnetic NPs-superparamagnetic materials with size > 25 nm, 2) carbon nanotubes-hydrophobic tubular structure made by carbon atoms diameters between 4 nm and 100 mm, and 3) quantum dots-colloidal NPs with atomic properties (Sharma et al., 2019). There are three passive targeting techniques. One is to use tumors' enhanced penetration and retention (EPR) effect to induce NPs to accumulate in tumor tissue, which does not work in humans (Danhier, 2016). The second technique is to use the acidic microenvironment of tumors to limit the action of NPs to acidic conditions (In and Nieva, 2015). Thirdly, tumor cells can be used to carry additional negative charges, since NPs are positively charged (Prabhu et al., 2015). Active targeting couples ligands to NPs via the receptors overexpressed explicitly on the surface of tumor cells or blood vessels, providing NPs with a more precise targeting effect than passive targeting. Additionally, the interaction of certain receptors and ligands has been shown to facilitate cell endocytosis and inhibit tumor multi-drug resistance (Bazak et al., 2015). Antibodies, fragments, aptamers (APTs), or small molecules are frequently used as ligands. Numerous previous studies (Landesman-Milo et al., 2015; Hussain, 2016; Mangal et al., 2017; Yu et al., 2017; Crintea et al., 2021) have described the

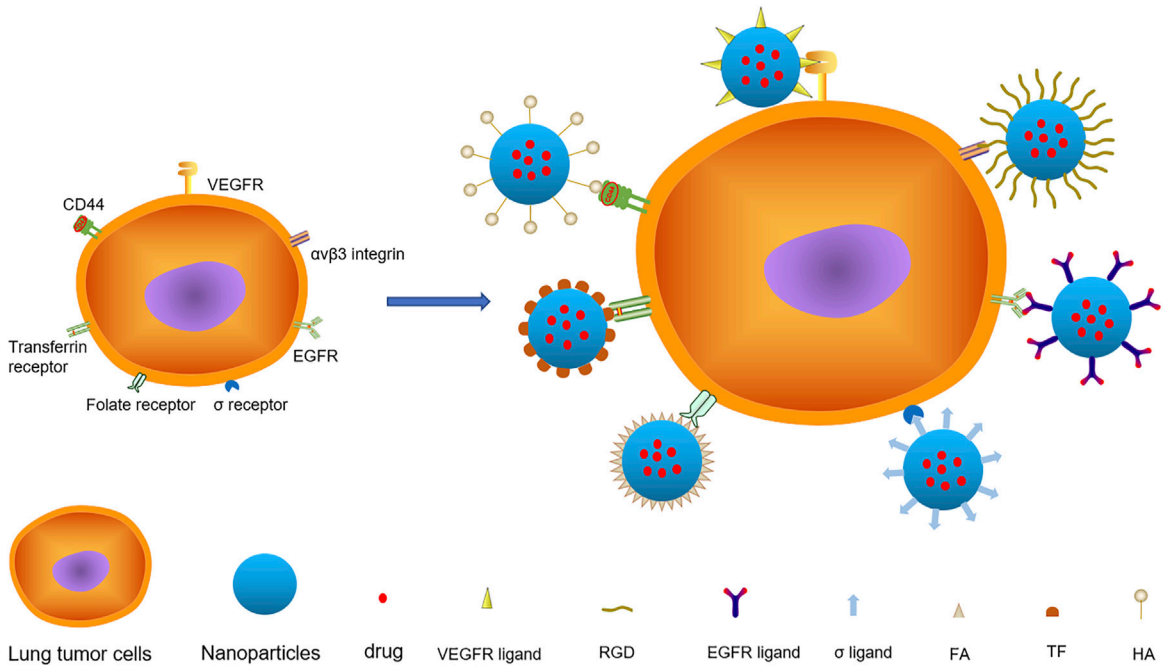

FIGURE 1 | There are various targets on lung cancer cells, among which VEGFR, αvβ3 Integrin, EGFR, σ Receptor, Folate Receptor, Transferrin Receptor and CD44 are important targets. The nanoparticles with specific ligand structure loaded with anticancer drugs specifically bind to the receptors on the surface of lung cancer and deliver the drugs to the cells.

characteristics and applications of current NPs and ligands for lung cancer treatment. Thus, this review mainly focused on several nanocarriers with active targeting functions for lung cancer treatment in detail from the receptors' perspective. The studies related to the major biological receptors and their applications are summarized in **Table 1**. The combined application of biological ligands and NPs are summarized in **Figure 1**. The oncogenic signaling pathways and drugs targeting abnormal signals in lung cancer therapy are summarized in **Table 2**.

2 BIOLOGICAL RECEPTORS AND THEIR APPLICATIONS FOR NANOPARTICLES

2.1 Vascular Endothelial-Derived Growth Factor Receptors

Due to gene mutation and tissue hypoxia in lung cancer, the expression level of vascular endothelial-derived growth factor (VEGF) is increased by hypoxia-inducible factor-1α (HIF-1α) and matrix metalloproteinase (MMP), resulting in an overexpression of vascular endothelial-derived growth factor receptors (VEGFRs) in lung cancer cells and endothelial cells (Prabhu et al., 2015). The primary function of VEGFs is to induce angiogenesis, chemotactic endothelial cells and increase vascular permeability by binding and activating VEGFRs signal cascade. Additionally, VEGF can promote lung cancer metastasis and induce survivin expression, conferring lung cancer drug-resistant (Tran et al., 2002; Herbst et al., 2005). VEGFs are a family of glycoproteins that include VEGF-A, VEGF-B, VEGF-C, VEGF-D, VEGF-E, and placenta growth factor (PGF). VEGFRs have several receptor subtypes: VEGFR-1/Flt-1, VEGFR-2/Flk-1/KDR, VEGFR-3/Flt-4, neuropilin-1(NRP-1), and neuropilin-2(NRP-2), among which VEGFR-2 is the most important and prevalent subtype. VEGFRs consist of an extracellular ligand-binding domain, a transmembrane domain, and a cytoplasmic domain encoding a tyrosine kinase. NRPs consist of extracellular domains, single transmembrane domains, and short intracellular domains lacking intrinsic catalytic function (Frezzetti et al., 2017). VEGFRs are overexpressed on the surface of a wide range of tumor cells and *in situ* tumor neovasculature, making them prospective targets for "double targeting" (tumor and vascular targeting) tumor therapy (Liu et al., 2011). VEGFRs, in particular, is the better target for overexpression on the cell membrane surface (Liu et al., 2011).

Jin et al. (2018) designed a new type of liposome nanoparticles with an active targeting function for loading parthenolide and ginsenoside compound K (CK) for the treatment of NSCLC. The NPs used tumor homing peptide tLYP-1 (sequence CGNKRTR) as the ligand and had a hydrophilic PEG shell. The particle size was 188 nm. The encapsulation efficiency of CK and parthenolide was 83.4 and 70.7%, respectively, while the drug loading efficiency was 14.8 and 2.9%, respectively. The PEG shell of new NPs can improve its stability, prolong cycle time, and increase solubility. tLYP-1 can enhance its tissue penetration ability, selectively target the over-expressed NRP-1 on the surface of lung cancer cells, and enter the cells via receptor-mediated endocytosis, causing

TABLE 2 | Some drugs and their mechanism of action in lung cancer therapy.

Major categories of lung cancer drug therapy	Mechanism of action	Drugs
Chemotherapy	Platinum: By binding to the DNA in the nucleus, it destroys the DNA of tumor cells and induces apoptosis (Dilruba and Kalayda, 2016).	Platinum: cisplatin, carboplatin and oxaliplatin
	Taxane-type anticancer drugs: Through the unique microtubule stabilization mechanism, they act on the mitotic process, thus reducing the proliferation of cancer cells (Wen et al., 2016).	Taxane-type anticancer drugs: paclitaxel, docetaxel and cabazitaxel
	Gemcitabine: By infiltrating the intracellular DNA, it inhibits DNA synthesis, and ultimately leads to apoptosis (Mlak et al., 2016).	Gemcitabine
	Etoposide(VP-16): It acts on DNA topoisomerase II, causing DNA damage and promoting apoptosis (Nam et al., 2010).	Etoposide (VP-16)
Targeted therapy	Tyrosine kinase inhibitors (TKIs): It can inhibit the growth and induce apoptosis of tumor cells by inhibiting the two signal transduction pathways of RAS/RAF/MAPK/ERK and PI3K/AKT/mTOR. (Dienstmann et al., 2011).	Tyrosine kinase inhibitors (TKIs): gefitinib and erlotinib
	Receptor tyrosine kinase (RTK) inhibitor: Anti-tumor angiogenesis by selectively inhibiting vascular endothelial growth factor receptor-2 (EGFR-2) (Li et al., 2010; Ding et al., 2013).	Apatinib
Immunotherapy	Programmed cell death (PD)-1 immune checkpoint inhibitors: By combining with PD-1 receptor highly expressed on T cells, it can block the signal pathway induced by PD-L1 and PD-L2, and restore the function of T cells (Wang et al., 2014; Oya et al., 2017).	Nivolumab,pembrolizumab
Natural antitumor products	Combining the tumor targeting carriers with natural anti-tumor drugs in an appropriate way can improve the anti-tumor efficacy (Jin et al., 2018). • Parthenolide: It can achieve anti-tumor effect by inhibiting B-Raf/MAPK/Erk signaling pathway, inhibiting NF-κB activation, and inhibiting PI3K/AKT signaling pathway (Jeyamohan et al., 2016; Kim et al., 2017; Lin et al., 2017). • CK: It can induce apoptosis through glycogen synthase kinase 3β(GSK3β) signaling pathway and regulating reactive oxygen species (ROS). It can inhibit angiogenesis by inhibiting sphingosine kinase -1 (Kim et al., 2013; Shin et al., 2014; Kwak et al., 2015)	Parthenolide,ginsenoside compound K

mitochondrial swelling and apoptosis, increasing the level of reactive oxygen species and inducing apoptosis. *In vivo* studies illustrated that the presence of tLYP-1 can undoubtedly increase the tumor inhibitory effect while minimizing adverse effects by increasing the selectivity of the tumor. It also suggests that researchers can further develop this new strategy for the effective treatment of cancer by using the combination of low-toxic natural products. Liu et al. (2011) developed a nanostructured lipid carrier with active targeting properties for docetaxel (DTX) loading. They studied its uptake in tumor and endothelial cells, as well as its therapeutic effect *in vivo* and biological distribution. Nanostructured lipid carriers (NLC) was found to be linked to the ligand (VEGFR-2 antibody) through DSPE-PEG-NH2. The average particle size of targeted NLC (tNLC) was 68.70 ± 2.07 nm; the encapsulation efficiency of DTX was 98.43 ± 0.51%; the drug loading rate was 5.55 ± 0.06%, and the average ligand coupling efficiency was 3.34 ± 2.63%. The findings indicated that tNLC first accumulated in tumor tissues via the EPR effect. It was then internalized by tumor cells and endothelial cells via the specific binding of Flk-1 with VEGFR-2, resulting in effective anti-tumor activity. tNLC has little influence on the growth of A549 and HUVEC cells, however, its polyethylene glycol coating can prevent interaction with serum proteins. Flk-1 can undoubtedly boost the tumor inhibitory effect while minimizing adverse effects by binding specifically on and internalization of tumor cells and tumor microvasculature. This study advances the targeted therapy strategy using VEGFR-2, but the precise metastasis mechanism of tNLC remains to be further studied.

Tumor neovascularization not only supplies nutrients to the tumor but also acts as a conduit for tumor diffusion and metastasis. VEGFR inhibition as a target for angiogenesis has become a research hotspot in tumor therapy. The purpose of this review was to summarize previous research on active targeted therapy for lung cancer using VEGFR ligands and NPs. A comparison is made between the new active targeting strategies for targeted-NPs (tNPs) (**Table 3**). More NPs-targeted drugs will be introduced to anti-lung cancer clinical therapy in the future, providing patients with more precise treatment options with fewer adverse effects.

2.2 αvβ3 Integrin

Integrin is a transmembrane glycoprotein heterodimer composed of 18 α and 8 β subunits. There have been 24 distinct subtypes identified thus far, 11 of which specifically bind to the arginine-glycine-aspartic acid (Arg-Gly-Asp, RGD) sequence. The RGD sequence widely exists in extracellular matrix proteins, such as collagen, fibronectin, fibrinogen, laminin, von Willebrand factor, thrombospondin, osteopontin, and vitreous connective protein. Combining the extracellular domain of integrin with an extracellular matrix protein alters the conformation of its transmembrane domain and intracellular domain connected to

TABLE 3 | VEGFR antibody for active targeting of nanoparticle drug delivery systems.

Types	Encapsulation percentage,EN%	Loading efficiency,LE%	Size (nm)
tLYP-1-PEG-NP Jin et al. (2018)	CK:83.4 Parthenolide:70.7	14.8 2.9	188
Flk-1-DSPE-PEG-NH2-NLC Liu et al. (2011)	CTX:98.43 + 0.51	3.34 ± 2.63	168.70 ± 2.07

the actin skeleton, hence regulating cell adhesion, migration, differentiation, proliferation, and survival (Aksorn and Chanvorachote, 2019). avβ3 integrin subtype is highly overexpressed on the surface of lung cancer cells and endothelial cells, promoting tumor angiogenesis and metastasis. Because the RGD sequence can specifically bind to αvβ3 integrin, numerous RGD peptides have been developed. avβ3 integrin biological and kinetic features can be altered by cyclizing, connecting other amino acids on both sides, and altering the stereo configuration or N-methylation. RGD peptides can improve the adherence of nanomaterials to lung cancer and mediate endocytosis into target cells (Marelli et al., 2013).

Babu et al. (2017) developed an RGD peptide modified polylactic acid-glycolic acid (PLGA)- chitosan-based nanoparticle system (CSNP)-RGD, loaded with paclitaxel (PTX) and used for NSCLC targeted drug delivery. The NPs were mainly drug-loaded PLGA, coated with positively charged chitosan, and linked to linear RGD peptides (GRGDSP). Chitosan can improve the stability of particles, control drug release, and increase adhesion. GRGDSP is a linear peptide with strong adhesion that recognizes the cell surface integrins αvβ3 and α5β1. PLGA-CSNP-RGD has an average particle size of 217 nm; the average entrapment efficiency of PTX is 93.7%, and the drug loading rate is 6.5%. The findings indicate that NPs have favorable physical and chemical properties and that NPs without drugs exhibit no apparent cytotoxicity. PTX-PLGA-CSNP-RGD is extremely selective for NSCLC cells such as A549 and H1299, which are overexpressed by integrin αvβ3. It penetrates cells via endocytosis mediated by integrin αvβ3, which inhibits the G2/M cell cycle and induces apoptosis of tumor cells, but has almost no toxicity to normal bronchial epithelial cells. GRGDSP has been shown to suppress tumor growth and alleviate adverse effects *in vivo*. This study shows PLGA-CSNP-RGD is expected to become a tool for priority drug delivery in lung cancer cells. And what deserves the attention of the researchers is that different normal cell lines need to be wisely evaluated when studying the efficacy of targeted nano-drug delivery systems in the treatment of cancer. Wang et al. (2018) synthesized RGD-modified lipid polymer NPs loaded with PTX and cisplatin (CDDP) (RGD-ss-PTX-CDDP LPNs) and investigated their anti-lung cancer effect in lung cancer cells and tumor-bearing animal models. RGD-ss-PTX-CDDP LPNs are mostly composed of PLGA loaded with PTX and CDDP and coated with soybean lecithin (SL). PTX is linked to the RGD peptide via PEG disulfide bonds, and disulfide bonds utilize a high concentration of glutathione (GSH) in tumor cells to allow specific intracellular drug release. The particle size was 191.3 ± 5.3 nm; the zeta potential was -37.2 ± 3.9 mV; the drug loading rates of PTX and CDDP were 5.4 ± 0.6% and 12.3 ± 1.1% respectively; the encapsulation rates were 85.3 ± 3.3% and 82.7 ± 4.1%, respectively. The results indicated that the NPs' properties were stable and the structure remained unchanged after 30 days in phosphate buffered saline (PBS) and 5 days in the culture medium. At 100 μg/ml, the drug-free NPs exhibited no apparent cytotoxicity and rarely accumulated in normal tissues. RGD can enhance anti-tumor activity and delay drug release. This study provides a scheme for the preparation of specific RGD modified, redox sensitive, prodrug-based lipid polymer NPs, which can be used in the synergistic combination chemotherapy of PTX and CDDP. RGD-ss-PTX-CDDP LPNs has synergistic anti-tumor effect and low systemic toxicity. The resulting system may become a promising targeted nano-drug for the treatment of lung cancer. Zou et al. (2018) synthesized the cyclic RGD peptide disulfide cross-linked polymer doxorubicin (cRGD-PS-DOX) and studied its targeted therapeutic effect on NSCLC. cRGD-PS-DOX utilizes PEG-P (TMC-DTC), loaded with DOX, as the primary linking ligand cRGD. The particle size of cRGD-PS-DOX was 96nm and the drug loading rate of DOX was 15.2%. It was determined that the release of cRGD-PS-DOX was less than 15% at 37°C, pH = 7.4, and GSH concentration = 2 m within 24 h. The release amount increased with the increase in GSH concentration, demonstrating that NPs had excellent stability in circulation and the capacity to deliver drugs rapidly into cells. The 3-(4,5-dimethylthiazol-2-yl)-2,5-diphenyltetrazolium bromide (MTT) assay demonstrated that drug-free NPs were non-toxic to A549 cells, but drug-loaded NPs had a strong inhibitory effect. Flow cytometry analysis revealed that cRGD-PS-DOX had stronger DOX·HCl intensity than PS-DOX when A549 cells with αvβ3 integrin overexpression were treated respectively. In MCF-7 cells with decreased αvβ3 integrin expression, the two intensities were comparable, demonstrating that cRGD-PS-DOX exhibited a high degree of specificity for NSCLC. Pharmacokinetics analysis revealed that cRGD-PS-DOX accumulates more readily tumors than in normal tissues.

To date, several RGD peptides and their analogues have been developed for targeting integrin αvβ3. However, there are certain drawbacks, including low affinity, poor specificity, and so on. Therefore, the combination of NPs with targeted peptides is critical for lung cancer treatment. A comparison of the tNPs listed above was performed (**Table 4**).

2.3 Epidermal Growth Factor Receptor

The epidermal growth factor receptor (EGFR) is a member of the class I transmembrane receptor tyrosine kinase superfamily, which is composed of EGFR/ERBB1/HER1, ERBB2/HER2, ERBB3/HER3, and ERBB4/HER4. EGFR is composed of an extracellular ligand-binding region, a

TABLE 4 | avβ3 antibody for active targeting of nanoparticle drug delivery systems.

Types	Encapsulation percentage,EN%	Loading efficiency,LE%	Size (nm)
PLGA-CSNP-RGD Babu et al. (2017)	PTX 93.7	6.5	217
RGD-ss-PTX/CDDP LPNs Wang et al. (2018)	PTX 85.3 ± 3.3	5.4 ± 0.6	191.3 ± 5.3
	CDDP 82.7 ± 4.1	12.3 ± 1.1	
cRGD-PS-Dox Zou et al. (2018)		15.2	96

transmembrane region, and an intracellular kinase region, which plays an essential role in the physiological process of cell growth, proliferation, and differentiation. EGFR is widely distributed on the surface of mammalian epithelial cells, fibroblasts, glial cells, keratinocytes, etc., and is overexpressed in many cancers. Although the EGFR gene is not overexpressed in SCLC, it is overexpressed in more than 60% of NSCLC (Zhang et al., 2010). The EGFR may bind to seven different ligands: EGF, transforming growth factor-alpha (TGFA), heparin-bound EGF-like growth factor (HBEGF), betamycin (BTC), amphotericin (AREG), insulin (EREG), and epigenetic gene (EPGN). EGF, TGFA, HBEGF, and BTC are considered high-affinity ligands, while AREG, EREG, and EPGN are low-affinity ligands. These ligands activate EGFR to stimulate intracellular signaling processes involved in tumor growth and progression, including proliferation, angiogenesis, invasion, and metastasis (Singh et al., 2016). In addition, EGFR tyrosine kinase inhibitors (EGFRTKIs) such as erlotinib (ER), gefitinib, and afatinib are often utilized targeting ligands (Zhang et al., 2019). Additionally, the anti-EGFR APT is a frequently used targeting ligand (Lv et al., 2018).

Kim and Huang (2012) studied a peptide-based therapy aimed at blocking intracellular protein-protein interactions in EGFR signal transduction. They also evaluated a targeted lipid carrier system capable of delivering peptides to intracellular targets in human cancer cells, thereby validating the concept of intracellular peptide-mediated cancer therapy delivered via well-designed NPs. Zhang et al. (2019) successfully synthesized a redox/pH double reaction nano thermosensitive agent (ECMI) for targeted molecular imaging and synergistic EGFR mutant lung cancer treatment. ECMI utilizes mesoporous silica (MSN) as the main body, supports indocyanine green (ICG) through electrostatic interactions, and fills the pores of MSNs with ZnO quantum dots (QDs). To form a shell, the drug-loaded MSNs were coated with chitosan (Cs) modified by ER, a cross-linked disulfide ligand. The diameter of ECMI was 220.0 ± 3.5 nm; polydispersity indexes (PDI) was 0.41 ± 0.03; Zeta potential was −18.5 ± 1.7 mV; drug loading rate was 15 ± 2 μg/mg, and ER conjugation efficiency was 35 ± 1 μg/mg. *In vitro* and *in vivo* studies indicated that EMCI has good biocompatibility and degradability and can accumulate in wild-type A549, ER-sensitive PC-9, and ER-resistant H1975 tumor cells. In PC-9 cells, the average fluorescence intensity of ECMI is more potent than that of CMI, indicating that ER can significantly enhance the targeting effect on PC-9. Zhang et al. (2016) successfully developed a PEG- PLGA-PLL targeting nanoparticle (EGF-PEAL NPs) using EGF as a ligand and loaded DOX and Bcl-2 small interfering RNA (siRNA), respectively, to study the synergistic effect anti-lung cancer effect of DOX-EGF-PEAL NPs and BCL-2-EGF- PEAL NPs. Particle sizes of DOX-EGF-PEAL NPs and Bcl-2-EGF-PEAL NPs were 203.7 ± 7.42 nm and 206.5 ± 6.37 nm; Zeta potentials were 3.5 ± 0.88 mV, and 2.1 ± 1.24 mV; PDI were 0.182 and 0.217, respectively. The results indicated that EGF-PEAL NPs were biodegradable and compatible with H1299 cells and exhibited low toxicity. EGF-PEAL NPs loaded with DOX or Bcl-2-siRNA showed a drug slow-release mode. EGF can significantly boost the dispersion of NPs in tumor tissues, enhance the uptake of NPs by lung cancer cells, and greatly enhance the tumor-killing effect of drugs. At the same time, EGF can decrease the concentration of NPs in the liver, spleen, and kidney and reduce the phagocytosis of NPs by the reticuloendothelial system and mononuclear phagocytic system. AnnexinV/PI staining showed that the combination of DOX-EGF-PEAL NPs and Bcl-2-EGF-PEAL NPs may have the most significant therapeutic effect. Lv et al. (2018) synthesized targeted NPs (AP/ES) with anti-EGFR,APT as ligand, polyamine dendrimer (PAMAM) as the main body, and simultaneously loaded ER and Survivin-short hairpin (shRNA), and studied the therapeutic effects of AP/ES and AP/ES combined with chloroquine (CQ) on EGFR mutant NSCLC. AP/ES exhibits favorable physical and chemical properties, including average particle size of 383.1 ± 0.4 nm, zeta potential of 12.1 ± 0.1 mV, ER drug loading rate of 10.4 ± 0.7%, encapsulation efficiency of 18.7 ± 0.4%, and PDI of 0.27 ± 0.01. The results demonstrate that anti-EGFR APT modified NPs can specifically recognize, bind, and deliver drugs and genes to EGFR overexpressed in NSCLC cells simultaneously. They can significantly improve tumor inhibition, induce apoptosis, and have fewer adverse side effects when compared with non-targeted NPs. The combined use of CQ and AP/ES improves tumor microcirculation and gene transfection efficiency, hence promoting drug delivery and efficacy of AP/ES, and has shown promising results in patients with ER-resistant NSCLC.

With the continuous development of tumor cytology and molecular biology, the potential of EGFR as a targeted therapy for lung cancer has been shown. However, several issues and technological difficulties persist. A comparison of these tNPs was performed (**Table 5**).

2.4 σ Receptor

σ receptor is one of the important targets of lung cancer, which is classified into two subtypes: σ1 and σ2. They are not genetically related, but their functions are similar. Recent studies have shown that the σ1 receptor is a single-channel transmembrane protein, whereas the σ2 receptor is TMEM97, a four-channel

TABLE 5 | EGFR antibody for active targeting of nanoparticle drug delivery systems.

Types	PDI	Zeta potential (mV)	Size (nm)
ECMI Zhang et al. (2019)	0.41 ± 0.03	−18.5 ± 1.7	220.0 ± 3.5
Dox-EGF-PEAL NPs	0.182	3.5 ± 0.88	203.7 ± 7.42
Bcl-2-EGF-PEAL NPs Zhang et al. (2016)	0.217	2.1 ± 1.24	206.5 ± 6.37
AP/ES Lv et al. (2018)	0.27 ± 0.01	12.1 ± 0.1	383.1 ± 0.4

transmembrane protein. σ receptor is mainly expressed in the intracellular membrane system, with a small amount expressed in the cell membrane (Schmidt and Kruse, 2019). Additionally, the σ receptor, especially σ2 receptor, is rapidly overexpressed in proliferating normal cells and cancer cells such as malignant melanoma, glioma, breast cancer, prostate cancer, SCLC, and NSCLC. Surprisingly, σ ligands can only cause cancer cell death (van Waarde et al., 2015). σ1 ligand can reduce the invasiveness of tumors, while σ2 ligand can mediate cancer cells' death via autophagy, cell cycle interference, and apoptosis (Ramzy et al., 2017). σ1 ligand can be classified into Gilligan and Glennon/Ablordeppey models, while σ2 ligand can be classified as amine derivatives with limited conformation, indole analogs related to Siramesine, and amine derivatives with flexible conformation (Georgiadis et al., 2017). Anisamide (AA) is a benzamide derivative with a small molecular weight and is the most common σ ligand.

Yang et al. (2012) developed lipid-calcium-phosphate (LCP) targeting NPs with AA as the ligand and simultaneously loaded three siRNAs (HDM2: c-myc: VEGF = 1: 1: 1, weight ratio) to study the therapeutic effect of AA-siRNA-LCP NPs on NSCLC. With calcium phosphate (CaP)-siRNA as the core, the NPs were stabilized with dioleoylphosphatidic acid (DOPA), coated with 1,2-dioleoyl-3-trimethylammonium-propane chloride salt (DOTAP), and further linked to 2-Distearoryl-sn-glycero-3-phosphoethanol-amine-N-[methoxy (polyethyleneglycol-2000) ammonium salt (DSPE-PEG_{2000})-AA, and reported a particle size of 38.6 ± 3.6 nm and Zeta potential of 29.1 ± 1.3 mV. The results showed that AA-LCP NPs have a high affinity for nucleic acid. They are biocompatible and biodegradable, and dissolve rapidly in acidic pH. AA-LCP NPs can significantly reduce the reticuloendothelial system (RES) uptake, increase tumor accumulation, and effectively deliver siRNA to NSCLC cells overexpressing the σ receptor. AA can improve the delivery efficiency of siRNA by 9 times, which significantly enhance the inhibition of HDM2/c-myc/VEGF expression, inhibit tumor proliferation and angiogenesis, and induce tumor apoptosis. Targeted LCP is a promising carrier that can deliver multiple siRNA to NSCLC, realize multi-target blocking, and effectively inhibit tumor growth, which suggests pooled siRNA formulated in targeted LCP may become a useful tool for NSCLC therapy. Xiong et al. (2016) designed a cationic liposome (LP) targeted nanocomposite with AA as the ligand and used it to load cisplatin (CDDP) and metformin. Using H460 cell xenotransplantation as a model, the synergistic anticancer effect on NSCLC was studied. Electrostatic complexation of anionic polyglutamic acid (PGA) and cationic polymer metformin (Polymet) created the core of NPs, which is covered with polyglycolic cationic LP and coupled to the ligand AA through DSPE-PEG. The NPs had a particle size of 145 ± 1 nm and a zeta potential of 49 ± 1 mV. The results showed that NPs had a high degree of stability, biocompatibility, and biodegradability. While the combination of CDDP and PGA inhibits medication release and impairs the therapeutic effect, NPs greatly inhibit RES absorption and promote tumor accumulation. AA can target the overexpressed σ receptor, and Polymet and CDDP work synergistically. These improvements not only render drug-loaded NPs statistically equivalent to or even better than free CDDP in terms of effectiveness but also significantly lower systemic toxicity and CDDP resistance. Haloperidol (Hal) is a ligand targeting σ2 receptor overexpressed in NSCLC. Varshosaz et al. (2015) synthesized Hal targeting bovine serum albumin (BSA) NPs for pulmonary delivery of DOX. The tNP size was 218 nm, the zeta potential was −25.4 mV, the drug entrapment efficiency was 89%, and the 2 h release rate was 56%.

TABLE 6 | σ Receptor antibody for active targeting of nanoparticle drug delivery systems.

Types	Size (nm)	Zeta potential (mV)
AA-siRNA-LCP NPs Yang et al. (2012)	38.6 ± 3.6	29.1 ± 1.3
AA-Cationic-LP NPs Xiong et al. (2016)	145 ± 1	49 ± 1
Hal-BSA NPs Varshosaz et al. (2015)	218	−25.4

There have been few studies on the σ receptor ligands to far, and the most often used ligand is AA. **Table 6** compares the binding of AA to NPs. In the future, more researches on the mechanism which causes lung cancer are required to identify additional ligands.

2.5 Folate Receptor

Folate acid (FA) is a water-soluble vitamin commonly known as vitamin B9. It is required for the body to utilize carbohydrates and amino acids in cell division and growth, nucleic acid, and protein synthesis. Together with vitamin B12, it is known that FA functions *in vivo* as tetrahydrofolate acid and contributes to the synthesis and transformation of purine and pyrimidine nucleotides, aids in protein metabolism, and promotes the formation and maturation of erythrocytes. Due to the low relative molecular weight of FA, it is easy to modify and penetrate tumor cells and has low immunogenicity. FA offers several benefits, including a short time to reach the target, fast blood clearance, intense penetration, low human immune response, and so on (Prabhu et al., 2015; Sharma et al., 2019). FA be utilized as a tumor-targeting agent and is frequently used in

the clinic. The folate receptor (FR) is a 38 kDa glycosyl-phosphatidylinositol binding glycoprotein, which often binds to FA, FA coupling drugs or FA anchored nanocarriers with high affinity, and internalizes FA into cells by mediating the endocytosis of FR. Studies have confirmed that FR is highly expressed on the surface of some tumor cells but has no or little expression in normal tissues, indicating that it has a reasonable tumor tissue specificity and is the most extensively researched tumor marker. In recent years, FRs have gained increasing interest in the domains of targeted drug delivery, cancer, and immunotherapy of rheumatoid arthritis. It is well established that FRs exist in three isomers: FRα, FR β, and FR γ (Bazak et al., 2015). FR α is highly expressed in epithelial cell line tumors, such as ovarian cancer, colorectal cancer, lung adenocarcinoma, etc. FR β is often highly expressed on the surface of tumor cells derived from non-epithelial tissues, such as sarcoma and acute myeloid leukemia. It is a potential target for FR-mediated targeted myeloid leukemia therapy, and FR γ can be used as a serum marker for lymphoma because it is not detected in normal serum (Jin et al., 2018). With the increasing understanding of FRs on the cell membrane, an FA-binding protein that is anchored to the cell membrane by phosphatidylinositol and can be removed by specific phospholipase C or D, it was discovered that the activity and number of FRs on the membrane surface of many types of tumor cells (such as ovarian cancer, colorectal cancer, breast cancer, lung cancer, and renal cell carcinoma) were significantly higher than those of normal cells. It lays a foundation for the study of drug targeting of tumor cells mediated by FA. Due to the high level of expression of FR on the surface of a variety of cancer cells, particularly the surface of malignant epithelial tumors, it is critical in the targeted therapy of nasopharyngeal carcinoma, lung cancer, colon cancer, gastric cancer, and gynecological tumors. By precisely binding to the overexpressed FR on the surface of tumor cells, the FR-mediated targeted drug delivery system can increase the drug's toxicity to the target and reduce the side effects. However, at present, the targeting evaluation of this kind of targeted drug delivery system is mainly based on *in vitro* cytotoxicity test and cell uptake rate test; there is a dearth of experimental data in animals, and the targeted therapeutic effect in humans people requires additional investigation.

Kato et al. (2017) found that novel porphyrin lipid NPs targeting folate receptor 1 (FOLR1) can improve the effectiveness and specificity of photodynamic therapy (PDT), which is helpful for the minimally invasive intervention of peripheral lung cancer and advanced lung cancer metastatic lymph nodes. They constructed subcutaneous and *in situ* lung cancer models in mice and constructed targeted NPs with FA and porphysomes. Porphysomes are unique NPs made of two naturally occurring molecules (chlorophyll and lipids) that have the potential to be used in a wide range of biological photon applications. This nanostructure is like a miniature colorful water balloon through which the drug-loaded NPs may be delivered to the tumor for targeted treatment. These NPs exhibit a broad range of variable absorptivity, structure-dependent fluorescence self-quenching, and unique photothermal and photoacoustic properties (Lovell et al., 2011). Amreddy et al. (2018) demonstrated that the dendrimer (Den) nanoparticle system targeting the FR-α is a suitable carrier for co-delivery of siRNA and chemotherapeutic drugs in lung cancer cells. Den-Polyethlyeneimine (PEI)- cis-diamine platinum (CDDP)-siRNA-FA NPs have low molecular weight (800 MW), well-dispersed spherical particles less than 10 nm in size, encapsulation efficiencies for CDDP 40.52 ± 4.18%, zeta potential +17.2 mV. Muralidharan et al. (2016) established the effectiveness of FR-α (FRA)-targeted DOTAP: Human lung cancer cells were treated with cholesterol lipid NPs containing HuR siRNA (HuR-FNP). HuR-FNP particle size had a diameter of 303.3 nm. Compared with normal lung fibroblast (CCD 16) cells, human lung cancer (H1299) cells had significantly higher uptake of FNP, indicating the existence of receptor dose effect. HuR-FNP zeta potential was 4.3 mV. About 39% of siRNA was released in an acetic acid buffer for the first hour. He et al. (2015) found that the FA modified amphiphilic PEG-PLGA copolymer NPs combined with CDDP and PTX may be used to guide efficient and safe cancer chemotherapy, particularly in tumors with high FA receptor expression. The particle size of Co-FA-NPs (CDDP: PTX = 2:1) was 171.36 ± 8.67 nm, PDI was 0.133 ± 0.008, and zeta potential was 21.50 ± 0.88 mV. The targeted NPs are also effective for the combined delivery of cisplatin and paclitaxel in the treatment of non-small cell lung cancer. Additionally, the tNPs are also effective for delivering cisplatin and paclitaxel in the treatment of NSCLC (He et al., 2016).

Table 7 compares FA binding to NPs. FA combined with NPs provides a new solution to toxicity and side effects, treatment drug resistance, and poor detection strategies of cancer treatment, making it a promising theragnostic ligand.

2.6 Transferrin Receptor

Human transferrin (TF) is an iron-binding protein with a molecular weight of 79.57 kDa. It may bind to the transferrin receptor (TFR) to transfer iron absorbed via the digestive tract and iron released by red blood cell degradation into bone marrow in the form of TFR-Fe3+ complex to generate mature red blood cells. Additionally, it is capable of transporting iron into cells that express TFRs. TF is biodegradable, non-toxic, non-immunogenic, and may be used to target particular sites via TFR expression on the cell surface (Vaidya and Vyas, 2012). TFR is expressed at a modest level in all normal nucleated cells. Studies have shown that the expression level is higher in cells with a high proliferation rate, especially in tumor cells, such as liver cancer, chronic lymphocytic leukemia, lung cancer (Daniels et al., 2006; Cheng et al., 2011; Dev and Babitt, 2017), as evidenced by increased cell membrane expression and blood concentration (Feelders et al., 1999). This phenomenon is referred to as iron addiction (Manz et al., 2016), as iron is required for a variety of key biological functions, including cell proliferation and growth (Dev and Babitt, 2017). Because TFR is overexpressed in a variety of tumor cells, TF/TFR-mediated cell events have been used to deliver therapeutic drugs to malignant tumor cells (Tros de Ilarduya and Düzgüneş, 2013).

Zhu et al. (2009) found that the histopathological quantification of TFR expression in lung cancer may be employed in clinical practice to monitor gambogic acid treatment susceptibility. Multi-drug resistance is a

TABLE 7 | Folate Receptor antibody for active targeting of nanoparticle drug delivery systems.

Types	Size (nm)	Zeta potential (mV)
Den-PEI-CDDP-siRNA-FA NPs Amreddy et al. (2018)	<10	17.2
HuR-FNP Muralidharan et al. (2016)	Diameter 303.3	4.3
Co-FA-NPs He et al. (2015)	171.36 ± 8.67	21.50 ± 0.88

fundamental problem in SCLC. Sadava et al. (2002) found that the combination of TFR and artemisinin could reduce small cell lung cancer drug resistance. The low molar concentration of artemisinin after pretreatment could kill the cells in SCLC. Upadhyay et al. (2019) found that thymoquinone-NP modified transferrin successfully couples two distinct miRNA pathways, enhances the apoptosis and death cascade of extremely lethal NSCLC cells, and limits these migration cells without producing any significant toxicity like the widely used combination of chemotherapeutic drugs.

In a nutshell, the transferrin receptor plays an important role in the abnormal iron metabolism of lung cancer cells. Although its mechanism is not fully understood, we can reduce the iron intake of cancer cells through transferrin receptors, thus interfering with the iron metabolism of lung cancer cells and limiting their proliferation, thereby enabling novel therapy options for the treatment of lung cancer diseases. Transferrin receptors will have a good application prospect in the treatment of tumor diseases.

2.7 CD44

CD44 is a membrane-bound glycoprotein that plays an important role in malignant tumor-related activities. It has been demonstrated that it can be used as a cancer stem cell (CSC)/tumor-initiating cells (TIC) marker (Fasano et al., 1997; Du et al., 2008; Ghosh et al., 2012). CSC theory suggests that cancer is composed of tumor cell subsets with the characteristics of stem cells or progenitor cells. These cells are capable of initiating tumor formation and differentiation via a variety of effective pathways and exhibiting a high level of resistance to conventional chemotherapy (Leung et al., 2010). The receptor is overexpressed in various solid tumors, such as pancreatic cancer, breast cancer, and lung cancer (Mattheolabakis et al., 2015). In mechanism, the invasive and metastatic growth of cancer cells can be mediated by the interaction between CD44 on the cell surface and extracellular matrix components such as hyaluronic acid and then induce changes in the cytoskeleton of cancer cells (Marhaba et al., 2008). CD44 is also involved in many signal cascades that mediate tumor enhancement. As a co-receptor with adjacent EGFR or other ErbB family receptor tyrosine kinases, it can indirectly activate cell proliferation pathways through ligands (Bourguignon et al., 2007). Additionally, it can activate anti-apoptotic pathways, such as phosphatidylinositol-3-kinase (PI3K)/protein kinase B (AKT) signal cascade (Bourguignon et al., 2007) and B lymphocyte tumor-2 gene (Bcl-2) and Bcl-xl transcription to enhance the survival ability of tumor cells (Madjd et al., 2009). According to research on SCLC, activation of CD44-MAPK-PI3K signal transduction results in increased expression of urokinase plasminogen activator (uPA)/uPA receptor (uPAR) and multi-drug resistance gene (MDR) 1, resulting in increased invasiveness and multi-drug resistance phenotype of lung cancer cells (Gutova et al., 2007).

Jeannot et al. (2016) proved that the size of hyaluronic acid (HA) NPs plays an important role in cellular uptake and biological distribution. Small NPs exhibit a positive targeting effect on tumors overexpressing CD44, implying that they might be employed as drug delivery systems. Poly-ε-caprolactone (PCL) is a commonly used polymer. Due to its biocompatibility and biodegradability, it has become the preferred targeted drug delivery system for scientists (Amreddy et al., 2017). The anticancer activity of Capsaicin (CAP) has been extensively examined for its anticancer activity in a variety of cancers, including lung cancer, where it has been shown to operate as an anticancer and anti-proliferative agent on a variety of human cancer cell lines (Galano and Martínez, 2012). Parashar et al. (2019) demonstrated that HA-PCL- CAP NPs identified the potential for the treatment of NSCLC and showed enhanced cytotoxicity, anti-proliferation, and apoptosis properties of CAP in A549.

In the future, drug targeted approaches based on CD44 expression on CSCs/TICs should be developed, including cytotoxic drugs now employed in clinics (Ghosh et al., 2012). Increasing our understanding of the molecular function of specific CD44 isoforms, the transcriptional regulation of CD44 expression, and the molecular regulation of CD44 alternative splicing will contribute to targeted therapy (Orian-Rousseau and Ponta, 2015; Yan et al., 2015).

2.8 Others

Overall, the main players in the field of nanomaterial-assisted lung cancer therapy are summarized. Still some new receptors or therapies are worth giving an update. Hsu et al. (2017) concluded estrogen and its receptor may be a predictor and therapeutic target for lung cancer after evaluating the expression and prognostic effects of estrogen receptor in lung cancer and clinical trials of a combination of estrogen receptor antagonist and EGFR antagonist. Madan et al. (2014) established the feasibility of using estrogen-coupled NPs to target breast cancer cells. Orphan receptors play important roles in development, cellular homeostasis, and diseases, including cancer, and overexpression or underexpression of some receptors has prognostic implications for patient survival, suggesting that they may be novel targets for lung cancer therapy (Safe et al., 2014; Moreno et al., 2018). Currently, immunotherapy has been widely used to treat lung cancer. Lung cancer-borne immunological targets like T-lymphocytes, myeloid-derived suppressor cells (MDSCs), tumor-associated

macrophages (TAMs), and dendritic cells (DCs) may be used to modulate tumor activity by targeting various surface-expressed receptors or by interfering with immune cell-specific pathways (Jeanson et al., 2019; Xia et al., 2019; Larionova et al., 2020; Yang et al., 2020; Yu et al., 2020). Nano-drug delivery targeting tumor microenvironment components may enhance the efficacy of immune checkpoint blocking (Kim et al., 2021). Kang et al. (2020) confirmed the anti-tumor effect of T-cell-membrane-coated nanoparticles (TCM NPs) in the treatment of lung cancer in an antigenic non-specific way. The combined application of PD-1/PD-L1 inhibitors and novel platinum-loaded composite NPs has been shown to have a positive synergistic effect (Xue et al., 2021). Cui et al. (2018) demonstrated that glutathione-triggered NPs can enhance the chemotherapy of lung cancer by reconstructing the tumor microenvironment. Zhou et al. (2020) found that the nano-vaccine was very effective in enhancing cell uptake through macrophage phagocytosis, and significantly promoted DCs maturation and antigen presentation.

3 CONCLUSION

To date, we have summarized representative examples of biological targets or receptors regarding lung cancer. Numerous receptors, including VEGFR, integrin, EGFR, FR, TFR, CD44, and σ receptor capable of increasing the specific binding of NPs containing drugs to disease cells, thereby increase the efficacy of chemotherapy. For example, σ ligands induce significant cell death and apoptosis only in tumor tissue, but not in proliferating normal cells such as stem cells (Georgiadis et al., 2017). The weak expression of the TFR in normal lung tissue and the high expression in lung adenocarcinoma tissue indicate that the expression of TFR is related to the histological type of lung cancer, and the expression in lung adenocarcinoma is significantly higher than that in other histological types. Numerous trials have established that TF plays an important role in the abnormal iron metabolism of lung cancer cells; however, the mechanism by which it does so is unknown; we can reduce iron uptake by cancer cells via TF, thereby interfering with the iron metabolism of lung cancer cells, inhibiting lung cancer cell proliferation, and providing new ideas for the treatment of lung cancer diseases. TF has good application prospects in the treatment of tumor diseases. Additionally, the evidence demonstrated that the activity and number of FRs on the membrane surface of a variety of tumor cells (such as ovarian cancer, colorectal cancer, breast cancer, lung cancer, and renal cell carcinoma) were significantly higher than those of normal cells, laying the foundation for the study of drug targeting tumor cells mediated by FA. Reuter et al. (2015) demonstrated that RGD peptide-modified NPs accumulate less in tumors than control PEG-modified NPs. It indicated that researchers should avoid exaggerating the influence of biological ligands. Rather than that, researchers might focus their efforts on receptors to identify more qualified and high-quality ligands. Another important consideration of receptors is the fact that many are overexpressed in tumor cells. We anticipate that specificity comparison trials will become increasingly common as they provide greater benefit in terms of reducing side effects and improving treatment effectiveness. Additionally, several novel targets were investigated that previously received little attention, such as the orphan receptor, bombesin receptor subtype-3 (Moreno et al., 2018).

As we all know, nanotechnology has fundamentally altered the way carriers are used to treat lung cancer and holds enormous possibilities for the future (Parvanian et al., 2017; Sivarajakumar et al., 2018; Mottaghitalab et al., 2019). Physicochemical properties such as size, shape, rigidity, or surface properties, all play a significant role in determining their large-scale distribution (Yoo et al., 2019). NPs of 10–100 nm with a molecular weight above 50 kDa are ideal nanoparticle drug delivery systems (In and Nieva, 2015), considering that tumor blood vessels have wide gap connections with a size of 100–600 nm (Maeda and Matsumura, 1989; Yuan et al., 1995; Maeda, 2012), NPs smaller than 150 nm might escape capture by macrophages in the RES (Aderem and Underhill, 1999; Feelders et al., 1999) and NPs larger than 10nm might avoid leakage into capillaries (Gaucher et al., 2005), but the restriction on size is not absolute and needs to be further studied. It is also important for nanocarriers to overcome the lung's physiological and anatomical barrier and precisely deliver drugs to tumor cells. Meanwhile, it also faces difficulties in transforming pragmatic medical technology like many new techniques. Additional researches or trials, whether animal or human, are required.

AUTHOR CONTRIBUTIONS

JW and TZ searched the literature and drafted the manuscript. SC and YL made the figure and tables. ZY critically revised the manuscript. All authors listed have made a substantial, direct, and intellectual contribution to the work and approved it for publication.

FUNDING

This study was supported by Fund of Science and Technology Development Project of Jilin Province (No. 20190701004GH).

REFERENCES

Aderem, A., and Underhill, D. M. (1999). Mechanisms of Phagocytosis in Macrophages. *Annu. Rev. Immunol.* 17, 593–623. doi:10.1146/annurev.immunol.17.1.593

Ahmad, J., Akhter, S., Rizwanullah, M., Amin, S., Rahman, M., Ahmad, M. Z., et al. (2015). Nanotechnology-based Inhalation Treatments for Lung Cancer: State of the Art. *Nanotechnol Sci. Appl.* 8, 55–66. doi:10.2147/nsa.S49052

Aksorn, N., and Chanvorachote, P. (2019). Integrin as a Molecular Target for Anti-cancer Approaches in Lung Cancer. *Anticancer Res.* 39 (2), 541–548. doi:10.21873/anticanres.13146

Amreddy, N., Babu, A., Muralidharan, R., Munshi, A., and Ramesh, R. (2017). Polymeric Nanoparticle-Mediated Gene Delivery for Lung Cancer Treatment. *Top. Curr. Chem. (Cham)* 375 (2), 35. doi:10.1007/s41061-017-0128-5

Amreddy, N., Babu, A., Panneerselvam, J., Srivastava, A., Muralidharan, R., Chen, A., et al. (2018). Chemo-biologic Combinatorial Drug Delivery Using Folate Receptor-Targeted Dendrimer Nanoparticles for Lung Cancer Treatment. *Nanomedicine* 14 (2), 373–384. doi:10.1016/j.nano.2017.11.010

Babu, A., Amreddy, N., Muralidharan, R., Pathuri, G., Gali, H., Chen, A., et al. (2017). Chemodrug Delivery Using Integrin-Targeted PLGA-Chitosan Nanoparticle for Lung Cancer Therapy. *Sci. Rep.* 7 (1), 14674. doi:10.1038/s41598-017-15012-5

Bade, B. C., and Dela Cruz, C. S. (2020). Lung Cancer 2020: Epidemiology, Etiology, and Prevention. *Clin. Chest Med.* 41 (1), 1–24. doi:10.1016/j.ccm.2019.10.001

Bazak, R., Houri, M., El Achy, S., Kamel, S., and Refaat, T. (2015). Cancer Active Targeting by Nanoparticles: a Comprehensive Review of Literature. *J. Cancer Res. Clin. Oncol.* 141 (5), 769–784. doi:10.1007/s00432-014-1767-3

Bourguignon, L. Y., Gilad, E., and Peyrollier, K. (2007). Heregulin-mediated ErbB2-ERK Signaling Activates Hyaluronan Synthases Leading to CD44-dependent Ovarian Tumor Cell Growth and Migration. *J. Biol. Chem.* 282 (27), 19426–19441. doi:10.1074/jbc.M610054200

Cheng, Z., Liu, Y. F., Song, Y. N., Dai, L. L., Kang, Y., Xia, J., et al. (2011). Regulating Action of Iron Regulatory Protein-2 in Iron Metabolism of Lung Cancer. *Zhonghua Yi Xue Za Zhi* 91 (28), 1992–1995.

Crintea, A., Dutu, A. G., Samasca, G., Florian, I. A., Lupan, I., and Craciun, A. M. (2021). The Nanosystems Involved in Treating Lung Cancer. *Life (Basel)* 11 (7). doi:10.3390/life11070682

Cui, T., Li, X., Shu, Y., Huang, X., Wang, Y., and Zhang, W. (2018). Utilizing Glutathione-Triggered Nanoparticles to Enhance Chemotherapy of Lung Cancer by Reprograming the Tumor Microenvironment. *Int. J. Pharm.* 552 (1-2), 16–26. doi:10.1016/j.ijpharm.2018.09.050

Danhier, F. (2016). To Exploit the Tumor Microenvironment: Since the EPR Effect Fails in the Clinic, what Is the Future of Nanomedicine? *J. Control. Release* 244 (Pt A), 108–121. doi:10.1016/j.jconrel.2016.11.015

Daniels, T. R., Delgado, T., Rodriguez, J. A., Helguera, G., and Penichet, M. L. (2006). The Transferrin Receptor Part I: Biology and Targeting with Cytotoxic Antibodies for the Treatment of Cancer. *Clin. Immunol.* 121 (2), 144–158. doi:10.1016/j.clim.2006.06.010

Dev, S., and Babitt, J. L. (2017). Overview of Iron Metabolism in Health and Disease. *Hemodial Int.* 21 Suppl 1 (Suppl. 1Suppl 1), S6–s20. doi:10.1111/hdi.12542

Dienstmann, R., Martinez, P., and Felip, E. (2011). Personalizing Therapy with Targeted Agents in Non-small Cell Lung Cancer. *Oncotarget* 2 (3), 165–177. doi:10.18632/oncotarget.245

Dilruba, S., and Kalayda, G. V. (2016). Platinum-based Drugs: Past, Present and Future. *Cancer Chemother. Pharmacol.* 77 (6), 1103–1124. doi:10.1007/s00280-016-2976-z

Ding, J., Chen, X., Gao, Z., Dai, X., Li, L., Xie, C., et al. (2013). Metabolism and Pharmacokinetics of Novel Selective Vascular Endothelial Growth Factor Receptor-2 Inhibitor Apatinib in Humans. *Drug Metab. Dispos* 41 (6), 1195–1210. doi:10.1124/dmd.112.050310

Du, L., Wang, H., He, L., Zhang, J., Ni, B., Wang, X., et al. (2008). CD44 Is of Functional Importance for Colorectal Cancer Stem Cells. *Clin. Cancer Res.* 14 (21), 6751–6760. doi:10.1158/1078-0432.Ccr-08-1034

Fasano, M., Sabatini, M. T., Wieczorek, R., Sidhu, G., Goswami, S., and Jagirdar, J. (1997). CD44 and its V6 Spliced Variant in Lung Tumors: a Role in Histogenesis? *Cancer* 80 (1), 34–41. doi:10.1002/(sici)1097-0142(19970701)80:1<34::aid-cncr5>3.0.co;2-f

Feelders, R. A., Kuiper-Kramer, E. P., and van Eijk, H. G. (1999). Structure, Function and Clinical Significance of Transferrin Receptors. *Clin. Chem. Lab. Med.* 37 (1), 1–10. doi:10.1515/cclm.1999.001

Frezzetti, D., Gallo, M., Maiello, M. R., D'Alessio, A., Esposito, C., Chicchinelli, N., et al. (2017). VEGF as a Potential Target in Lung Cancer. *Expert Opin. Ther. Targets* 21 (10), 959–966. doi:10.1080/14728222.2017.1371137

Galano, A., and Martínez, A. (2012). Capsaicin, a Tasty Free Radical Scavenger: Mechanism of Action and Kinetics. *J. Phys. Chem. B* 116 (3), 1200–1208. doi:10.1021/jp211172f

Gaucher, G., Dufresne, M. H., Sant, V. P., Kang, N., Maysinger, D., and Leroux, J. C. (2005). Block Copolymer Micelles: Preparation, Characterization and Application in Drug Delivery. *J. Control. Release* 109 (1-3), 169–188. doi:10.1016/j.jconrel.2005.09.034

Georgiadis, M. O., Karoutzou, O., Foscolos, A. S., and Papanastasiou, I. (2017). Sigma Receptor (σR) Ligands with Antiproliferative and Anticancer Activity. *Molecules* 22 (9). doi:10.3390/molecules22091408

Ghosh, S. C., Neslihan Alpay, S., and Klostergaard, J. (2012). CD44: a Validated Target for Improved Delivery of Cancer Therapeutics. *Expert Opin. Ther. Targets* 16 (7), 635–650. doi:10.1517/14728222.2012.687374

Gutova, M., Najbauer, J., Gevorgyan, A., Metz, M. Z., Weng, Y., Shih, C. C., et al. (2007). Identification of uPAR-Positive Chemoresistant Cells in Small Cell Lung Cancer. *PLoS One* 2 (2), e243. doi:10.1371/journal.pone.0000243

He, Z., Huang, J., Xu, Y., Zhang, X., Teng, Y., Huang, C., et al. (2015). Co-delivery of Cisplatin and Paclitaxel by Folic Acid Conjugated Amphiphilic PEG-PLGA Copolymer Nanoparticles for the Treatment of Non-small Lung Cancer. *Oncotarget* 6 (39), 42150–42168. doi:10.18632/oncotarget.6243

He, Z., Shi, Z., Sun, W., Ma, J., Xia, J., Zhang, X., et al. (2016). Hemocompatibility of Folic-Acid-Conjugated Amphiphilic PEG-PLGA Copolymer Nanoparticles for Co-delivery of Cisplatin and Paclitaxel: Treatment Effects for Non-small-cell Lung Cancer. *Tumour Biol.* 37 (6), 7809–7821. doi:10.1007/s13277-015-4634-1

Herbst, R. S., Onn, A., and Sandler, A. (2005). Angiogenesis and Lung Cancer: Prognostic and Therapeutic Implications. *J. Clin. Oncol.* 23 (14), 3243–3256. doi:10.1200/jco.2005.18.853

Hsu, L. H., Chu, N. M., and Kao, S. H. (2017). Estrogen, Estrogen Receptor and Lung Cancer. *Int. J. Mol. Sci.* 18 (8). doi:10.3390/ijms18081713

Hussain, S. (2016). Nanomedicine for Treatment of Lung Cancer. *Adv. Exp. Med. Biol.* 890, 137–147. doi:10.1007/978-3-319-24932-2_8

In, G. K., and Nieva, J. (2015). Emerging Chemotherapy Agents in Lung Cancer Nanopa. *Transl. Cancer Res.* 4 (4), 340–355. doi:10.3978/j.issn.2218-676X.2015.08.05

Jeannot, V., Mazzaferro, S., Lavaud, J., Vanwonterghem, L., Henry, M., Arboléas, M., et al. (2016). Targeting CD44 Receptor-Positive Lung Tumors Using Polysaccharide-Based Nanocarriers: Influence of Nanoparticle Size and Administration Route. *Nanomedicine* 12 (4), 921–932. doi:10.1016/j.nano.2015.11.018

Jeanson, A., Tomasini, P., Souquet-Bressand, M., Brandone, N., Boucekine, M., Grangeon, M., et al. (2019). Efficacy of Immune Checkpoint Inhibitors in KRAS-Mutant Non-small Cell Lung Cancer (NSCLC). *J. Thorac. Oncol.* 14 (6), 1095–1101. doi:10.1016/j.jtho.2019.01.011

Jeyamohan, S., Moorthy, R. K., Kannan, M. K., and Arockiam, A. J. (2016). Parthenolide Induces Apoptosis and Autophagy through the Suppression of PI3K/Akt Signaling Pathway in Cervical Cancer. *Biotechnol. Lett.* 38 (8), 1251–1260. doi:10.1007/s10529-016-2102-7

Jin, X., Zhou, J., Zhang, Z., and Lv, H. (2018). The Combined Administration of Parthenolide and Ginsenoside CK in Long Circulation Liposomes with Targeted tLyp-1 Ligand Induce Mitochondria-Mediated Lung Cancer Apoptosis. *Artif. Cell Nanomed Biotechnol* 46 (Suppl. 3), S931–s942. doi:10.1080/21691401.2018.1518913

Kang, M., Hong, J., Jung, M., Kwon, S. P., Song, S. Y., Kim, H. Y., et al. (2020). T-Cell-Mimicking Nanoparticles for Cancer Immunotherapy. *Adv. Mater.* 32 (39), e2003368. doi:10.1002/adma.202003368

Kato, T., Jin, C. S., Ujiie, H., Lee, D., Fujino, K., Wada, H., et al. (2017). Nanoparticle Targeted Folate Receptor 1-enhanced Photodynamic Therapy for Lung Cancer. *Lung Cancer* 113, 59–68. doi:10.1016/j.lungcan.2017.09.002

Khanmohammadi, A., Aghaie, A., Vahedi, E., Qazvini, A., Ghanei, M., Afkhami, A., et al. (2020). Electrochemical Biosensors for the Detection of Lung Cancer Biomarkers: A Review. *Talanta* 206, 120251. doi:10.1016/j.talanta.2019.120251

Kim, A. D., Kang, K. A., Kim, H. S., Kim, D. H., Choi, Y. H., Lee, S. J., et al. (2013). A Ginseng Metabolite, Compound K, Induces Autophagy and Apoptosis via Generation of Reactive Oxygen Species and Activation of JNK in Human colon Cancer Cells. *Cell Death Dis* 4, e750. doi:10.1038/cddis.2013.273

Kim, J., Hong, J., Lee, J., Fakhraei Lahiji, S., and Kim, Y. H. (2021). Recent Advances in Tumor Microenvironment-Targeted Nanomedicine Delivery Approaches to Overcome Limitations of Immune Checkpoint Blockade-Based Immunotherapy. *J. Control. Release* 332, 109–126. doi:10.1016/j.jconrel.2021.02.002

Kim, S. K., and Huang, L. (2012). Nanoparticle Delivery of a Peptide Targeting EGFR Signaling. *J. Control. Release* 157 (2), 279–286. doi:10.1016/j.jconrel.2011.08.014

Kim, S. L., Kim, S. H., Park, Y. R., Liu, Y. C., Kim, E. M., Jeong, H. J., et al. (2017). Combined Parthenolide and Balsalazide Have Enhanced Antitumor Efficacy through Blockade of NF-Kb Activation. *Mol. Cancer Res.* 15 (2), 141–151. doi:10.1158/1541-7786.Mcr-16-0101

Kreuter, J. (2007). Nanoparticles--a Historical Perspective. *Int. J. Pharm.* 331 (1), 1–10. doi:10.1016/j.ijpharm.2006.10.021

Kwak, C. W., Son, Y. M., Gu, M. J., Kim, G., Lee, I. K., Kye, Y. C., et al. (2015). A Bacterial Metabolite, Compound K, Induces Programmed Necrosis in MCF-7 Cells via GSK3β. *J. Microbiol. Biotechnol.* 25 (7), 1170–1176. doi:10.4014/jmb.1505.05057

Landesman-Milo, D., Ramishetti, S., and Peer, D. (2015). Nanomedicine as an Emerging Platform for Metastatic Lung Cancer Therapy. *Cancer Metastasis Rev.* 34 (2), 291–301. doi:10.1007/s10555-015-9554-4

Larionova, I., Tuguzbaeva, G., Ponomaryova, A., Stakheyeva, M., Cherdyntseva, N., Pavlov, V., et al. (2020). Tumor-Associated Macrophages in Human Breast, Colorectal, Lung, Ovarian and Prostate Cancers. *Front. Oncol.* 10, 566511. doi:10.3389/fonc.2020.566511

Leung, E. L., Fiscus, R. R., Tung, J. W., Tin, V. P., Cheng, L. C., Sihoe, A. D., et al. (2010). Non-small Cell Lung Cancer Cells Expressing CD44 Are Enriched for Stem Cell-like Properties. *PLoS One* 5 (11), e14062. doi:10.1371/journal.pone.0014062

Li, J., Zhao, X., Chen, L., Guo, H., Lv, F., Jia, K., et al. (2010). Safety and Pharmacokinetics of Novel Selective Vascular Endothelial Growth Factor Receptor-2 Inhibitor YN968D1 in Patients with Advanced Malignancies. *Bmc Cancer* 10, 529. doi:10.1186/1471-2407-10-529

Lin, M., Bi, H., Yan, Y., Huang, W., Zhang, G., Zhang, G., et al. (2017). Parthenolide Suppresses Non-small Cell Lung Cancer GLC-82 Cells Growth via B-Raf/MAPK/Erk Pathway. *Oncotarget* 8 (14), 23436–23447. doi:10.18632/oncotarget.15584

Liu, D., Liu, F., Liu, Z., Wang, L., and Zhang, N. (2011). Tumor Specific Delivery and Therapy by Double-Targeted Nanostructured Lipid Carriers with Anti-VEGFR-2 Antibody. *Mol. Pharm.* 8 (6), 2291–2301. doi:10.1021/mp200402e

Lovell, J. F., Jin, C. S., Huynh, E., Jin, H., Kim, C., Rubinstein, J. L., et al. (2011). Porphysome Nanovesicles Generated by Porphyrin Bilayers for Use as Multimodal Biophotonic Contrast Agents. *Nat. Mater.* 10 (4), 324–332. doi:10.1038/nmat2986

Lv, T., Li, Z., Xu, L., Zhang, Y., Chen, H., and Gao, Y. (2018). Chloroquine in Combination with Aptamer-Modified Nanocomplexes for Tumor Vessel Normalization and Efficient erlotinib/Survivin shRNA Co-delivery to Overcome Drug Resistance in EGFR-Mutated Non-small Cell Lung Cancer. *Acta Biomater.* 76, 257–274. doi:10.1016/j.actbio.2018.06.034

Madan, J., Gundala, S. R., Kasetti, Y., Bharatam, P. V., Aneja, R., Katyal, A., et al. (2014). Enhanced Noscapine Delivery Using Estrogen-Receptor-Targeted Nanoparticles for Breast Cancer Therapy. *Anticancer Drugs* 25 (6), 704–716. doi:10.1097/cad.0000000000000098

Madjd, Z., Mehrjerdi, A. Z., Sharifi, A. M., Molanaei, S., Shahzadi, S. Z., and Asadi-Lari, M. (2009). CD44+ Cancer Cells Express Higher Levels of the Anti-apoptotic Protein Bcl-2 in Breast Tumours. *Cancer Immun.* 9, 4.

Maeda, H. (2012). Macromolecular Therapeutics in Cancer Treatment: the EPR Effect and beyond. *J. Control. Release* 164 (2), 138–144. doi:10.1016/j.jconrel.2012.04.038

Maeda, H., and Matsumura, Y. (1989). Tumoritropic and Lymphotropic Principles of Macromolecular Drugs. *Crit. Rev. Ther. Drug Carrier Syst.* 6 (3), 193–210.

Mangal, S., Gao, W., Li, T., and Zhou, Q. T. (2017). Pulmonary Delivery of Nanoparticle Chemotherapy for the Treatment of Lung Cancers: Challenges and Opportunities. *Acta Pharmacol. Sin* 38 (6), 782–797. doi:10.1038/aps.2017.34

Manz, D. H., Blanchette, N. L., Paul, B. T., Torti, F. M., and Torti, S. V. (2016). Iron and Cancer: Recent Insights. *Ann. N. Y Acad. Sci.* 1368 (1), 149–161. doi:10.1111/nyas.13008

Marelli, U. K., Rechenmacher, F., Sobahi, T. R., Mas-Moruno, C., and Kessler, H. (2013). Tumor Targeting via Integrin Ligands. *Front. Oncol.* 3, 222. doi:10.3389/fonc.2013.00222

Marhaba, R., Klingbeil, P., Nuebel, T., Nazarenko, I., Buechler, M. W., and Zoeller, M. (2008). CD44 and EpCAM: Cancer-Initiating Cell Markers. *Curr. Mol. Med.* 8 (8), 784–804. doi:10.2174/156652408786733667

Markman, J. L., Rekechenetskiy, A., Holler, E., and Ljubimova, J. Y. (2013). Nanomedicine Therapeutic Approaches to Overcome Cancer Drug Resistance. *Adv. Drug Deliv. Rev.* 65 (13-14), 1866–1879. doi:10.1016/j.addr.2013.09.019

Mattheolabakis, G., Milane, L., Singh, A., and Amiji, M. M. (2015). Hyaluronic Acid Targeting of CD44 for Cancer Therapy: from Receptor Biology to Nanomedicine. *J. Drug Target.* 23 (7-8), 605–618. doi:10.3109/1061186x.2015.1052072

Mlak, R., Krawczyk, P., Ciesielka, M., Kozioł, P., Homa, I., Powrózek, T., et al. (2016). The Relationship between RRM1 Gene Polymorphisms and Effectiveness of Gemcitabine-Based First-Line Chemotherapy in Advanced NSCLC Patient. *Clin. Transl Oncol.* 18 (9), 915–924. doi:10.1007/s12094-015-1461-1

Moreno, P., Mantey, S. A., Lee, S. H., Ramos-Álvarez, I., Moody, T. W., and Jensen, R. T. (2018). A Possible New Target in Lung-Cancer Cells: The Orphan Receptor, Bombesin Receptor Subtype-3. *Peptides* 101, 213–226. doi:10.1016/j.peptides.2018.01.016

Mottaghitalab, F., Farokhi, M., Fatahi, Y., Atyabi, F., and Dinarvand, R. (2019). New Insights into Designing Hybrid Nanoparticles for Lung Cancer: Diagnosis and Treatment. *J. Control. Release* 295, 250–267. doi:10.1016/j.jconrel.2019.01.009

Muralidharan, R., Babu, A., Amreddy, N., Basalingappa, K., Mehta, M., Chen, A., et al. (2016). Folate Receptor-Targeted Nanoparticle Delivery of HuR-RNAi Suppresses Lung Cancer Cell Proliferation and Migration. *J. Nanobiotechnology* 14 (1), 47. doi:10.1186/s12951-016-0201-1

Nam, C., Doi, K., and Nakayama, H. (2010). Etoposide Induces G2/M Arrest and Apoptosis in Neural Progenitor Cells via DNA Damage and an ATM/p53-related Pathway. *Histol. Histopathol* 25 (4), 485–493. doi:10.14670/HH-25.485

Orian-Rousseau, V., and Ponta, H. (2015). Perspectives of CD44 Targeting Therapies. *Arch. Toxicol.* 89 (1), 3–14. doi:10.1007/s00204-014-1424-2

Oya, Y., Yoshida, T., Kuroda, H., Mikubo, M., Kondo, C., Shimizu, J., et al. (2017). Predictive Clinical Parameters for the Response of Nivolumab in Pretreated Advanced Non-small-cell Lung Cancer. *Oncotarget* 8 (61), 103117–103128. doi:10.18632/oncotarget.21602

Parashar, P., Tripathi, C. B., Arya, M., Kanoujia, J., Singh, M., Yadav, A., et al. (2019). A Facile Approach for Fabricating CD44-Targeted Delivery of Hyaluronic Acid-Functionalized PCL Nanoparticles in Urethane-Induced Lung Cancer: Bcl-2, MMP-9, Caspase-9, and BAX as Potential Markers. *Drug Deliv. Transl Res.* 9 (1), 37–52. doi:10.1007/s13346-018-0575-8

Parvanian, S., Mostafavi, S. M., Aghashiri, M., and Research, B.-S. (2017). Multifunctional Nanoparticle Developments in Cancer Diagnosis and Treatment. *Sensing Bio-Sensing Res.* 13, 81–87. doi:10.1016/j.sbsr.2016.08.002

Prabhu, R. H., Patravale, V. B., and Joshi, M. D. (2015). Polymeric Nanoparticles for Targeted Treatment in Oncology: Current Insights. *Int. J. Nanomedicine* 10, 1001–1018. doi:10.2147/ijn.S56932

Ramzy, L., Nasr, M., Metwally, A. A., and Awad, G. A. S. (2017). Cancer Nanotheranostics: A Review of the Role of Conjugated Ligands for Overexpressed Receptors. *Eur. J. Pharm. Sci.* 104, 273–292. doi:10.1016/j.ejps.2017.04.005

Reuter, K. G., Perry, J. L., Kim, D., Luft, J. C., Liu, R., and DeSimone, J. M. (2015). Targeted PRINT Hydrogels: The Role of Nanoparticle Size and Ligand Density on Cell Association, Biodistribution, and Tumor Accumulation. *Nano Lett.* 15 (10), 6371–6378. doi:10.1021/acs.nanolett.5b01362

Sadava, D., Phillips, T., Lin, C., and Kane, S. E. (2002). Transferrin Overcomes Drug Resistance to Artemisinin in Human Small-Cell Lung Carcinoma Cells. *Cancer Lett.* 179 (2), 151–156. doi:10.1016/s0304-3835(02)00005-8

Safe, S., Jin, U. H., Hedrick, E., Reeder, A., and Lee, S. O. (2014). Minireview: Role of Orphan Nuclear Receptors in Cancer and Potential as Drug Targets. *Mol. Endocrinol.* 28 (2), 157–172. doi:10.1210/me.2013-1291

Schmidt, H. R., and Kruse, A. C. (2019). The Molecular Function of σ Receptors: Past, Present, and Future. *Trends Pharmacol. Sci.* 40 (9), 636–654. doi:10.1016/j.tips.2019.07.006

Sharma, P., Mehta, M., Dhanjal, D. S., Kaur, S., Gupta, G., Singh, H., et al. (2019). Emerging Trends in the Novel Drug Delivery Approaches for the Treatment of Lung Cancer. *Chem. Biol. Interact* 309, 108720. doi:10.1016/j.cbi.2019.06.033

Shin, K. O., Seo, C. H., Cho, H. H., Oh, S., Hong, S. P., Yoo, H. S., et al. (2014). Ginsenoside Compound K Inhibits Angiogenesis via Regulation of Sphingosine Kinase-1 in Human Umbilical Vein Endothelial Cells. *Arch. Pharm. Res.* 37 (9), 1183–1192. doi:10.1007/s12272-014-0340-6

Singh, B., Carpenter, G., and Coffey, R. J. (2016). EGF Receptor Ligands: Recent Advances. *F1000Res* 5, 2270. doi:10.12688/f1000research.9025.1

Sivarajakumar, R., Mallukaraj, D., Kadavakollu, M., Neelakandan, N., Chandran, S., Bhojaraj, S., et al. (2018). Nanoparticles for the Treatment of Lung Cancers. *Jyp* 10 (3), 276–281. doi:10.5530/jyp.2018.10.62

Tran, J., Master, Z., Yu, J. L., Rak, J., Dumont, D. J., and Kerbel, R. S. (2002). A Role for Survivin in Chemoresistance of Endothelial Cells Mediated by VEGF. *Proc. Natl. Acad. Sci. U S A.* 99 (7), 4349–4354. doi:10.1073/pnas.072586399

Tros de Ilarduya, C., and Düzgüneş, N. (2013). Delivery of Therapeutic Nucleic Acids via Transferrin and Transferrin Receptors: Lipoplexes and Other Carriers. *Expert Opin. Drug Deliv.* 10 (11), 1583–1591. doi:10.1517/17425247.2013.837447

Upadhyay, P., Sarker, S., Ghosh, A., Gupta, P., Das, S., Ahir, M., et al. (2019). Transferrin-decorated Thymoquinone-Loaded PEG-PLGA Nanoparticles Exhibit Anticarcinogenic Effect in Non-small Cell Lung Carcinoma via the Modulation of miR-34a and miR-16. *Biomater. Sci.* 7 (10), 4325–4344. doi:10.1039/c9bm00912d

Vaidya, B., and Vyas, S. P. (2012). Transferrin Coupled Vesicular System for Intracellular Drug Delivery for the Treatment of Cancer: Development and Characterization. *J. Drug Target.* 20 (4), 372–380. doi:10.3109/1061186x.2012.662687

van Waarde, A., Rybczynska, A. A., Ramakrishnan, N. K., Ishiwata, K., Elsinga, P. H., and Dierckx, R. A. (2015). Potential Applications for Sigma Receptor Ligands in Cancer Diagnosis and Therapy. *Biochim. Biophys. Acta* 1848 (10 Pt B), 2703–2714. doi:10.1016/j.bbamem.2014.08.022

Varshosaz, J., Hassanzadeh, F., Mardani, A., and Rostami, M. (2015). Feasibility of Haloperidol-Anchored Albumin Nanoparticles Loaded with Doxorubicin as Dry Powder Inhaler for Pulmonary Delivery. *Pharm. Dev. Technol.* 20 (2), 183–196. doi:10.3109/10837450.2013.852576

Wang, C., Thudium, K. B., Han, M., Wang, X. T., Huang, H., Feingersh, D., et al. (2014). *In Vitro* Characterization of the Anti-PD-1 Antibody Nivolumab, BMS-936558, and *In Vivo* Toxicology in Non-human Primates. *Cancer Immunol. Res.* 2 (9), 846–856. doi:10.1158/2326-6066.Cir-14-0040

Wang, G., Wang, Z., Li, C., Duan, G., Wang, K., Li, Q., et al. (2018). RGD Peptide-Modified, Paclitaxel Prodrug-Based, Dual-Drugs Loaded, and Redox-Sensitive Lipid-Polymer Nanoparticles for the Enhanced Lung Cancer Therapy. *Biomed. Pharmacother.* 106, 275–284. doi:10.1016/j.biopha.2018.06.137

Wen, G., Qu, X. X., Wang, D., Chen, X. X., Tian, X. C., Gao, F., et al. (2016). Recent Advances in Design, Synthesis and Bioactivity of Paclitaxel-Mimics. *Fitoterapia* 110, 26–37. doi:10.1016/j.fitote.2016.02.010

Xia, L., Liu, Y., and Wang, Y. (2019). PD-1/PD-L1 Blockade Therapy in Advanced Non-small-cell Lung Cancer: Current Status and Future Directions. *Oncologist* 24 (Suppl. 1), S31–s41. doi:10.1634/theoncologist.2019-IO-S1-s05

Xiong, Y., Zhao, Y., Miao, L., Lin, C. M., and Huang, L. (2016). Co-delivery of Polymeric Metformin and Cisplatin by Self-Assembled Core-Membrane Nanoparticles to Treat Non-small Cell Lung Cancer. *J. Control. Release* 244 (Pt A), 63–73. doi:10.1016/j.jconrel.2016.11.005

Xue, Y., Gao, S., Gou, J., Yin, T., He, H., Wang, Y., et al. (2021). Platinum-based Chemotherapy in Combination with PD-1/pd-L1 Inhibitors: Preclinical and Clinical Studies and Mechanism of Action. *Expert Opin. Drug Deliv.* 18 (2), 187–203. doi:10.1080/17425247.2021.1825376

Yan, Y., Zuo, X., and Wei, D. (2015). Concise Review: Emerging Role of CD44 in Cancer Stem Cells: A Promising Biomarker and Therapeutic Target. *Stem Cell Transl Med* 4 (9), 1033–1043. doi:10.5966/sctm.2015-0048

Yang, Y., Hu, Y., Wang, Y., Li, J., Liu, F., and Huang, L. (2012). Nanoparticle Delivery of Pooled siRNA for Effective Treatment of Non-small Cell Lung Cancer. *Mol. Pharm.* 9 (8), 2280–2289. doi:10.1021/mp300152v

Yang, Z., Guo, J., Weng, L., Tang, W., Jin, S., and Ma, W. (2020). Myeloid-derived Suppressor Cells-New and Exciting Players in Lung Cancer. *J. Hematol. Oncol.* 13 (1), 10. doi:10.1186/s13045-020-0843-1

Yoo, J., Park, C., Yi, G., Lee, D., and Koo, H. (2019). Active Targeting Strategies Using Biological Ligands for Nanoparticle Drug Delivery Systems. *Cancers (Basel)* 11 (5). doi:10.3390/cancers11050640

Yu, H. P., Aljuffali, I. A., and Fang, J. Y. (2017). Injectable Drug-Loaded Nanocarriers for Lung Cancer Treatments. *Curr. Pharm. Des.* 23 (3), 481–494. doi:10.2174/1381612822666161027113654

Yu, S., Sha, H., Qin, X., Chen, Y., Li, X., Shi, M., et al. (2020). EGFR E746-A750 Deletion in Lung Cancer Represses Antitumor Immunity through the Exosome-Mediated Inhibition of Dendritic Cells. *Oncogene* 39 (13), 2643–2657. doi:10.1038/s41388-020-1182-y

Yuan, F., Dellian, M., Fukumura, D., Leunig, M., Berk, D. A., Torchilin, V. P., et al. (1995). Vascular Permeability in a Human Tumor Xenograft: Molecular Size Dependence and Cutoff Size. *Cancer Res.* 55 (17), 3752–3756.

Zappa, C., and Mousa, S. A. (2016). Non-small Cell Lung Cancer: Current Treatment and Future Advances. *Transl Lung Cancer Res.* 5 (3), 288–300. doi:10.21037/tlcr.2016.06.07

Zhang, X., Wang, Q., Qin, L., Fu, H., Fang, Y., Han, B., et al. (2016). EGF-modified mPEG-PLGA-PLL Nanoparticle for Delivering Doxorubicin Combined with Bcl-2 siRNA as a Potential Treatment Strategy for Lung Cancer. *Drug Deliv.* 23 (8), 2936–2945. doi:10.3109/10717544.2015.1126769

Zhang, Y., Zhang, L., Lin, X., Ke, L., Li, B., Xu, L., et al. (2019). Dual-responsive Nanosystem for Precise Molecular Subtyping and Resistant Reversal of EGFR Targeted Therapy. *Chem. Eng. J.* 372, 483–495. doi:10.1016/j.cej.2019.04.140

Zhang, Z., Stiegler, A. L., Boggon, T. J., Kobayashi, S., and Halmos, B. (2010). EGFR-mutated Lung Cancer: a Paradigm of Molecular Oncology. *Oncotarget* 1 (7), 497–514. doi:10.18632/oncotarget.186

Zhou, S., Huang, Y., Chen, Y., Liu, S., Xu, M., Jiang, T., et al. (2020). Engineering ApoE3-Incorporated Biomimetic Nanoparticle for Efficient Vaccine Delivery to Dendritic Cells via Macropinocytosis to Enhance Cancer Immunotherapy. *Biomaterials* 235, 119795. doi:10.1016/j.biomaterials.2020.119795

Zhu, X., Zhang, H., Lin, Y., Chen, P., Min, J., Wang, Z., et al. (2009). Mechanisms of Gambogic Acid-Induced Apoptosis in Non-small Cell Lung Cancer Cells in Relation to Transferrin Receptors. *J. Chemother.* 21 (6), 666–672. doi:10.1179/joc.2009.21.6.666

Zou, Y., Wei, J., Xia, Y., Meng, F., Yuan, J., and Zhong, Z. (2018). Targeted Chemotherapy for Subcutaneous and Orthotopic Non-small Cell Lung Tumors with Cyclic RGD-Functionalized and Disulfide-Crosslinked Polymersomal Doxorubicin. *Signal. Transduct Target. Ther.* 3, 32. doi:10.1038/s41392-018-0032-7

Conflict of Interest: The authors declare that the research was conducted in the absence of any commercial or financial relationships that could be construed as a potential conflict of interest.

Publisher's Note: All claims expressed in this article are solely those of the authors and do not necessarily represent those of their affiliated organizations, or those of the publisher, the editors and the reviewers. Any product that may be evaluated in this article, or claim that may be made by its manufacturer, is not guaranteed or endorsed by the publisher.

GLOSSARY

AA anisamide
AKT protein kinase B
APT aptamer
CK compound K
CSC cancer stem cell
CSNP chitosan-based nanoparticle system
DOTAP 1,2-dioleoyl-3-trimethylammonium-propane chloride salt
DOX doxorubicin
DTX docetaxel
EGFR epidermal growth factor receptor
EPR enhanced penetration and retention
ER erlotinib
FR folate receptor
GSH glutathione
HA hyaluronic acid
HIF-1α hypoxia-inducible factor -1α
LCP lipid-calcium-phosphate
LP liposome
LPN lipid polymer nanoparticle
MMP matrix metalloproteinase
NLC nanostructured lipid carriers
NPs nanoparticles
NRP neuropilin
NSCLC non-small cell lung cancer
PBS phosphate buffered saline
PDI polydispersity indexes
PGF placenta growth factor
PLGA polylactic acid-glycolic acid
PTX paclitaxel
RES reticuloendothelial system
RGD arginine-glycine-aspartic acid
SCLC small cell lung cancer
SL soybean lecithin
TFR transferrin receptor
TIC tumor initiating cells
VEGF vascular endothelial-derived growth factor

frontiers in Pharmacology

ORIGINAL RESEARCH
published: 17 January 2022
doi: 10.3389/fphar.2021.793107

Aspirin Attenuates Hyperoxia-Induced Acute Respiratory Distress Syndrome (ARDS) by Suppressing Pulmonary Inflammation via the NF-κB Signaling Pathway

Yu-Tang Tung[1,2,3,4†], Chi-Hsuan Wei[1,5†], Chih-Ching Yen[6†], Po-Ying Lee[7], Lorraine B. Ware[8], Hao-En Huang[4], Wei Chen[9] and Chuan-Mu Chen[1,10,11]**

[1]Department of Life Sciences and Ph.D. Program in Translational Medicine, National Chung Hsing University, Taichung, Taiwan, [2]Graduate Institute of Biotechnology, National Chung Hsing University, Taichung, Taiwan, [3]Cell Physiology and Molecular Image Research Center, Wan Fang Hospital, Taipei Medical University, Taipei, Taiwan, [4]Nutrition Research Center, Taipei Medical University Hospital, Taipei, Taiwan, [5]Institute of Biomedical Sciences, National Chung Hsing University, Taichung, Taiwan, [6]Department of Internal Medicine, China Medical University Hospitaland College of Health Care, China Medical University, Taichung, Taiwan, [7]Department of Surgery, Division of Plastic Surgery, Cathay General Hospital, Taipei, Taiwan, [8]Departments of Medicine and Pathology, Microbiology and Immunology, Vanderbilt University School of Medicine, Nashville, TN, United States, [9]Division of Pulmonary and Critical Care Medicine, Chia-Yi Christian Hospital, Chiayi, Taiwan, [10]The IEGG and Animal Biotechnology Center, National Chung Hsing University, Taichung, Taiwan, [11]Rong Hsing Research Center for Translational Medicine, Taichung Veterans General Hospital, Taichung, Taiwan

OPEN ACCESS

Edited by:
Paolo Montuschi,
Catholic University of the Sacred Heart, Italy

Reviewed by:
Erzsébet Bartolák-Suki,
Boston University, United States
Qinghe Meng,
Upstate Medical University, United States

***Correspondence:**
Wei Chen
peteralfa2004@gmail.com
Chuan-Mu Chen
chchen1@dragon.nchu.edu.tw

†These authors have contributed equally to this work

Specialty section:
This article was submitted to Respiratory Pharmacology, a section of the journal Frontiers in Pharmacology

Received: 11 October 2021
Accepted: 16 December 2021
Published: 17 January 2022

Citation:
Tung Y-T, Wei C-H, Yen C-C, Lee P-Y, Ware LB, Huang H-E, Chen W and Chen C-M (2022) Aspirin Attenuates Hyperoxia-Induced Acute Respiratory Distress Syndrome (ARDS) by Suppressing Pulmonary Inflammation via the NF-κB Signaling Pathway. Front. Pharmacol. 12:793107. doi: 10.3389/fphar.2021.793107

Acute respiratory distress syndrome (ARDS) is a common destructive syndrome with high morbidity and mortality rates. Currently, few effective therapeutic interventions for ARDS are available. Clinical trials have shown that the effectiveness of aspirin is inconsistent. The contribution of platelets to the inflammatory response leading to the development of ARDS is increasingly recognized. The antiplatelet agent aspirin reportedly exerts a protective effect on acid- and hyperoxia-induced lung injury in murine models. Our previous study showed that pretreatment with aspirin exerts protective effects on hyperoxia-induced lung injury in mice. However, the mechanisms and therapeutic efficacy of aspirin in the posttreatment of hyperoxia-induced acute lung injury (ALI) remain unclear. In this study, we used a homozygous NF-κB-luciferase$^{+/+}$ transgenic mouse model and treated mice with low-dose (25 μg/g) or high-dose (50 μg/g) aspirin at 0, 24, and 48 h after exposure to hyperoxia (inspired oxygen fraction (FiO_2) > 95%). Hyperoxia-induced lung injury significantly increased the activation of NF-κB in the lung and increased the levels of macrophages infiltrating the lung and reactive oxygen species (ROS), increased the HO-1, NF-κB, TNF-α, IL-1β, and IL-4 protein levels, and reduced the CC10, SPC, eNOS, Nrp-1, and IκBα protein levels in the lung tissue. Pulmonary edema and alveolar infiltration of neutrophils were also observed in the lung tissue of mice exposed to hyperoxia. However, *in vivo* imaging revealed that posttreatment with aspirin reduced luciferase expression, suggesting that aspirin might reduce NF-κB activation. Posttreatment with aspirin also reduced hyperoxia-induced increases in the numbers of lung macrophages, intracellular ROS levels, and the expression of TNF-α, IL-1β, and IL-4; it also increased CC10, SPC and Nrp-1 levels compared with hyperoxia exposure alone.

Lung histopathology also indicated that the aspirin posttreatment significantly reduced neutrophil infiltration and lung edema compared with hyperoxia exposure alone. Aspirin effectively induces an anti-inflammatory response in a model of hyperoxia-induced lung injury. Thus, aspirin may have potential as a novel treatment for hyperoxia-induced ALI.

Keywords: acute lung injury, acute respiratory distress syndrome, aspirin, hyperoxia, therapeutic efficacy

INTRODUCTION

Acute respiratory distress syndrome (ARDS) is a common destructive clinical syndrome characterized by alveolar-capillary membrane injury and hypoxemic respiratory failure that leads to mechanical ventilation and often to multiple organ failure. Due to endothelial injury and epithelial injury, alveolar epithelium and obvious hyaline membranes are observed (Ware and Herridge, 2013; Matthay et al., 2019). The strong inflammatory response is driven by oxidants, proteases and other potentially toxic substances released by activated white blood cells (Babior et al., 2003).

Few effective interventions for ARDS are available (Boyle et al., 2013; Boyle et al., 2014). Currently, mechanical ventilation with a lower tidal volume (Oba and Salzman, 2000) and early application of prolonged prone-positioning sessions (Guérin et al., 2013) result in decreased mortality in patients with ARDS. Emerging evidence has also suggested the effectiveness of extracorporeal therapies (Fitzgerald et al., 2014). Platelets play a profound role in the inflammatory response leading to the development of ARDS. The possible mechanisms of platelet-induced ARDS include activation of endothelial cells through the release of proinflammatory mediators (Kiefmann et al., 2004; Yadav and Kor, 2015) and adhesion of platelets to pulmonary capillary endothelial cells, which lead to the activation of attached white blood cells (Zarbock and Ley, 2009). Based on accumulating evidence, platelets are instrumental in both the onset (Zarbock and Ley, 2009) and resolution (Ortiz-Muñoz et al., 2014) of acute lung injury (ALI). Previous studies indicated a potential preventive effect of antiplatelet therapy on high-risk patients with ARDS (Ortiz-Muñoz et al., 2014; Boyle et al., 2015; Chen et al., 2015).

Aspirin is an irreversible and noncompetitive inhibitor of arachidonic acid cyclooxygenase metabolism and is widely used in the clinic. Aspirin inhibits platelet activation to mediate the recruitment of neutrophils to the lungs of rats with acid-induced lung injury (Zarbock et al., 2006). We previously reported that an aspirin pretreatment exerted protective effects on hyperoxia-induced lung injury in mice (Chen C. M. et al., 2020). Preclinical studies have shown that aspirin prevents neutrophil activation and recruitment to the lungs, and reduces TNF-α expression in macrophages in pulmonary blood vessels, thromboxane B2 levels in plasma, and platelet isolation in the lungs (Looney et al., 2009; Eickmeier et al., 2013; Tuinman et al., 2013). Aspirin also reduces the severity of edema and vascular permeability in individuals with ALI caused by oxidative stress (Wahn and Hammerschmidt, 2001). In human studies, the results of aspirin therapy have been inconsistent because of heterogeneity of the patient's performance, course, and outcome that meet the clinical definition of ARDS. Kor et al. (Kor et al., 2016) found that aspirin use did not reduce the risk of ARDS at 7 days after hospitalization compared to the placebo. As shown in our previous study, aspirin pretreatment exerted protective effects on hyperoxia-induced lung injury in mice (Chen C. M. et al., 2020). However, most people do not have the habit of taking aspirin, except for people with cardiovascular disease and Western populations (Antithrombotic Trialists, 2002; Gao and Li, 2010). To the best of our knowledge, no study has focused on the mechanism and therapeutic efficacy of an aspirin posttreatment on hyperoxia-induced ALI. Thus, we investigated the therapeutic efficacy of an aspirin posttreatment in terms of its anti-inflammatory effects.

MATERIALS AND METHODS

Murine Models

NF-κB-luciferase$^{+/+}$ transgenic mice express the luciferase gene driven by the NF-κB promoter; therefore, luciferase activity reflects NF-κB activity, according to previous studies (Ho et al., 2007; Hsiang et al., 2009). NF-κB-luciferase$^{+/+}$ transgenic mice on the FVB/NJNarl background were bred in our laboratory, provided a standard laboratory diet and distilled water ad libitum and housed in a temperature-controlled (24°C ± 2°C) animal center with a 12:12 h light–dark cycle. This study was approved by the Institutional Animal Care and Utilization Committee (IACUC) of National Chung Hsing University, Taichung, Taiwan (Approval No: IACUC-102–77). Eight-week-old NF-κB-luciferase$^{+/+}$ transgenic mice were randomly assigned to four groups (n = 6 mice per group) as follows: 1) intraperitoneal injection of phosphate-buffered saline (PBS) at 0, 24, and 48 h and exposure to normoxia (negative control); 2) intraperitoneal injection of PBS at 0, 24, and 48 h after hyperoxia exposure (mock group); 3) intraperitoneal injection of low-dose aspirin (25 μg/g) at 0, 24, and 48 h after hyperoxia exposure (A25 group); and 4) intraperitoneal injection of high-dose aspirin (50 μg/g) at 0, 24, and 48 h after hyperoxia exposure (A50 group). At the end of the experiment after 72 h of hyperoxia exposure, we anesthetized each mouse and collected pulmonary tissues for bronchoalveolar lavage, pathological histology, and protein extraction.

Hyperoxia-Induced ALI in Mice

As described in our previous study (Yen et al., 2011), mice exposed to hyperoxia were housed in a hyperoxia chamber under normal pressure with 99% oxygen. The mice were sacrificed after oxygen exposure and aspirin treatment.

Imaging of Luciferase Activity

As described in our previous study (Yen et al., 2020), NF-κB-luciferase$^{+/+}$ transgenic mice were imaged after the intraperitoneal injection of luciferin (150 mg/kg) using the IVIS Imaging System (IVIS Imaging System 200 Series; Xenogen Corp, Alameda, CA, United States). Photon intensity was recorded as photons/s/cm^2 using Living Image software (Xenogen).

Histopathological Analysis

Lung tissues were perfused to remove red blood cells (RBCs) and then preserved in 4% formaldehyde overnight, dehydrated through a graded series of alcohol solutions and embedded in paraffin wax. Serial sections with a thickness of approximately 4 μm were stained with hematoxylin and eosin (H&E) for histological examinations, as described in a previous study (Chen Y. H. et al., 2020). The frequency of neutrophils in the alveolar space, neutrophils in the interstitial space, and hyaline membranes in lung tissues was blindly evaluated by a pathologist.

Analysis of Inflammation in Bronchoalveolar Lavage Fluid

Bronchoalveolar lavage fluid (BALF) was collected by lavaging the lungs with 500 μL of sterile endotoxin-free saline and centrifuging the samples at 500 g at 4°C. The cell pellet was resuspended, and the number of BALF cells was determined using an automatic cell counter (Yen et al., 2011). Approximately 5×10^2 BALF cells were centrifuged, transferred to a glass slide and stained with Liu's stain. Lymphocytes and macrophages were subsequently classified.

Measurement of Extracellular and Intracellular Reactive Oxygen Species Generation

BALF was centrifuged at 500 g at 4°C to obtain the supernatant and cell pellet for measurements of extracellular and intracellular reactive oxygen species (ROS) levels. ROS generation in the BALF of perfused lungs was monitored using 2′,7′-dichlorodihydrofluorescein diacetate (H2DCF-DA) fluorescence, as described in a previous study (al-Mehdi et al., 1994).

Western Blot Analysis

Protein expression in the pulmonary tissues was measured using Western blot analysis as previously described (Chen et al., 2021). In the present study, the primary antibodies were anti-CC10 (clone EPR19846, 1:2000, Abcam, Cambridge, UK), anti-SP-C (clone EPR19839, 1:2000, Abcam), anti-p-ERK (clone E4, 1:500, Santa Cruz Biotech. Inc, Santa Cruz, CA, United States), anti-p-p38 (clone E1, 1:500, Santa Cruz Biotech. Inc.), anti-HO-1 (clone P249, 1:2000, Cell Signaling Technology, Danvers, MA, United States), anti-eNOS (clone M221, 1:2000, Abcam), anti-NRP-1 (clone BGO-14, 1:1000, BosterBio, Pleasanton, CA, United States), anti-NF-κB (clone D14E12, 1:2000, Cell Signaling Technology), anti-IκBα (clone 44D4, 1:2000, Cell Signaling Technology), anti-TNF-α (clone TN3-19.12, 1:500, Santa Cruz Biotech. Inc.), anti-IL-1β (clone 3A6, 1:2000, Cell Signaling Technology), anti-IL-4 (clone C1, 1:2000, Abcam), and anti-β-actin (clone C4, 1:10,000, Santa Cruz Biotech. Inc.). The membranes were developed using an enhanced chemiluminescence detection system (GE Health Care, Mississauga, Canada). The bands were quantified relative to β-actin bands using ImageJ software.

Immunohistochemical Staining

Lung tissue sections were examined using immunohistochemical (IHC) staining as previously described (Tung et al., 2011). Primary rabbit monoclonal antibodies against CXCL4 and CC10 were used. The reactions were visualized using the Vectastain ABC kit (universal, Vector Laboratories, CA, United States). Diaminobenzidine (DAB) was used as the chromogen, and hematoxylin was used as the counterstain.

Statistical Analysis

Data are presented as the means ± standard errors of the means (SEM). Differences between groups were analyzed using one-way ANOVA followed by Tukey's test, and p values <0.05 were considered significant.

RESULTS

Therapeutic Efficacy of Aspirin in Hyperoxia-Induced NF-?b Activation

NF-κB-luciferase$^{+/+}$ transgenic mice express a luciferase gene driven by an NF-κB response element in the promoter. Therefore, the luciferase signal reflects the activity of NF-κB (Hsiang et al., 2009). Mice were treated with 25 or 50 μg/g aspirin at 0, 24, and 48 h after exposure to hyperoxia. Hyperoxia stimulated the luminescent signal in the lung tissue; however, the luciferase signals in the A50 group were lower than those in the mock group (**Figure 1**). Therefore, posttreatment with 50 μg/g aspirin at 0, 24, and 48 h after hyperoxia exposure in NF-κB-luciferase$^{+/+}$ transgenic mice reduced ALI caused by hyperoxia (FiO_2 > 95%).

Therapeutic Efficacy of Aspirin Against Hyperoxia-Induced Histological Changes in the Lung

A histopathological examination of the lung was performed after 72 h of hyperoxia to further confirm the therapeutic effect of aspirin on hyperoxia-induced ALI. Erythematous swelling and bleeding were more obvious in the lungs of the mock group, and these changes were ameliorated in the A25 and A50 groups (**Figure 2**). Histological evidence revealed that the mock group developed ALI, with a greater degree of pulmonary edema and alveolar infiltration of neutrophils than the negative control group (**Figure 2**). However, mice posttreated with 25 or 50 μg/g aspirin exhibited reduced neutrophil infiltration and lung edema. As revealed in **Figure 2B** and **Table 1**, mice in the A25 ($p < 0.05$) and A50 groups ($p < 0.01$) presented

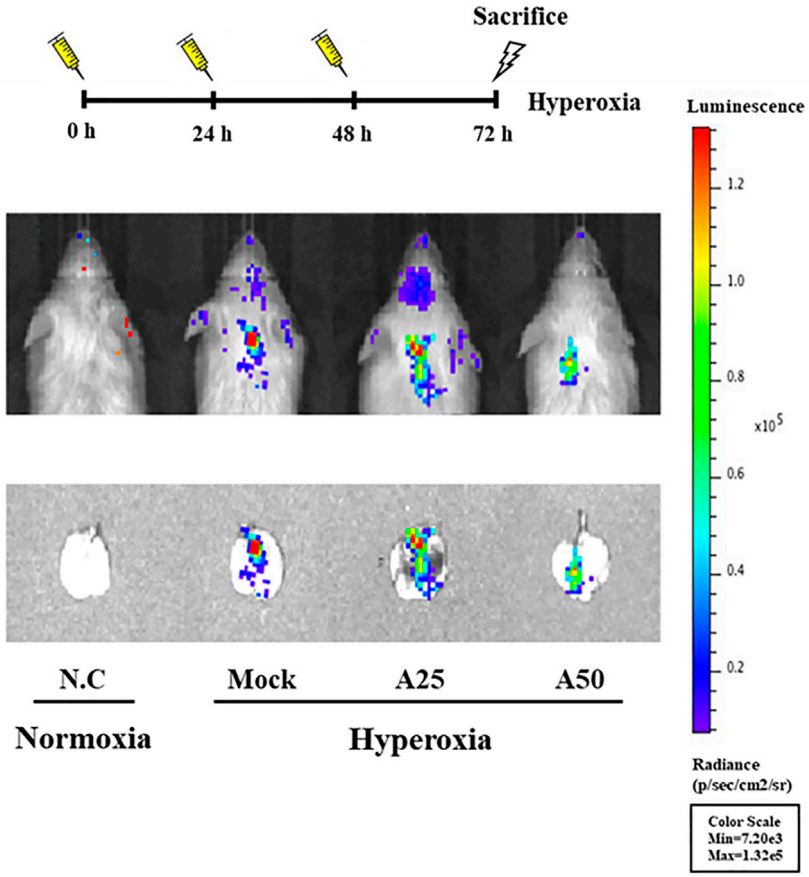

FIGURE 1 | Bioluminescence imaging indicating the therapeutic efficacy of aspirin in the lung tissues of NF-κB-luciferase$^{+/+}$ transgenic mice exposed to hyperoxia. NF-κB-luciferase$^{+/+}$ transgenic mice were assigned to four groups (n = 6 mice per group): N.C, treatment with PBS at 0, 24, and 48 h and exposure to normoxia; Mock, treatment with PBS at 0, 24, and 48 h and exposure to 72 h of hyperoxia; A25, treatment with 25 μg/g aspirin at 0, 24, and 48 h and exposure to 72 h of hyperoxia; and A50, treatment with 50 μg/g aspirin at 0, 24, and 48 h and exposure to 72 h of hyperoxia.

significantly lower lung-to-body weight ratios and lung damage (neutrophils in the alveolar space, neutrophils in the interstitial space, and hyaline membranes) than those in the mock group.

Therapeutic Efficacy of Aspirin in Reducing the Numbers of Total Cells, Macrophages and Lymphocytes and Extracellular and Intracellular ROS Generation in Lung Tissue Induced by Hyperoxia

Macrophages are essential cellular effectors of innate immune defenses, and circulating monocytes also play a critical role in defending against inflammation. Total cell counts and the relative cell counts of macrophages and lymphocytes in the BALF were analyzed (**Figures 3A–C**). Hyperoxia significantly increased the total cell counts and relative cell counts of macrophages and significantly reduced the numbers of lymphocytes compared with the negative control group. Following lung injury, monocytes are rapidly recruited into the lungs, where they differentiate into macrophages. However, compared with the mock group, treatment with 25 or 50 μg/g aspirin slightly reduced the number of macrophages and increased the number of lymphocytes. Extracellular and intracellular ROS generation in the BALF was significantly increased in the mock group compared with the negative control group (**Figures 3D,E**). However, only posttreatment with 50 μg/g aspirin resulted in a significant decrease in intracellular ROS generation compared with the mock group ($p < 0.05$). Thus, aspirin posttreatment reduced the number of circulating macrophages and intracellular ROS levels. The decrease in the number of macrophages and intracellular ROS levels might rescue the lung from a severe inflammatory response.

Effect of Aspirin on the Hyperoxia-Induced Expression of Proteins Related to Survival and Stress Response in the Lung Tissue

In this study, cell death and the induction of stress responses were analyzed. Hyperoxia-induced changes in the mRNA levels of lung epithelial proteins (CC10 and SP-C) have previously been shown to play an important role in the pathways involved

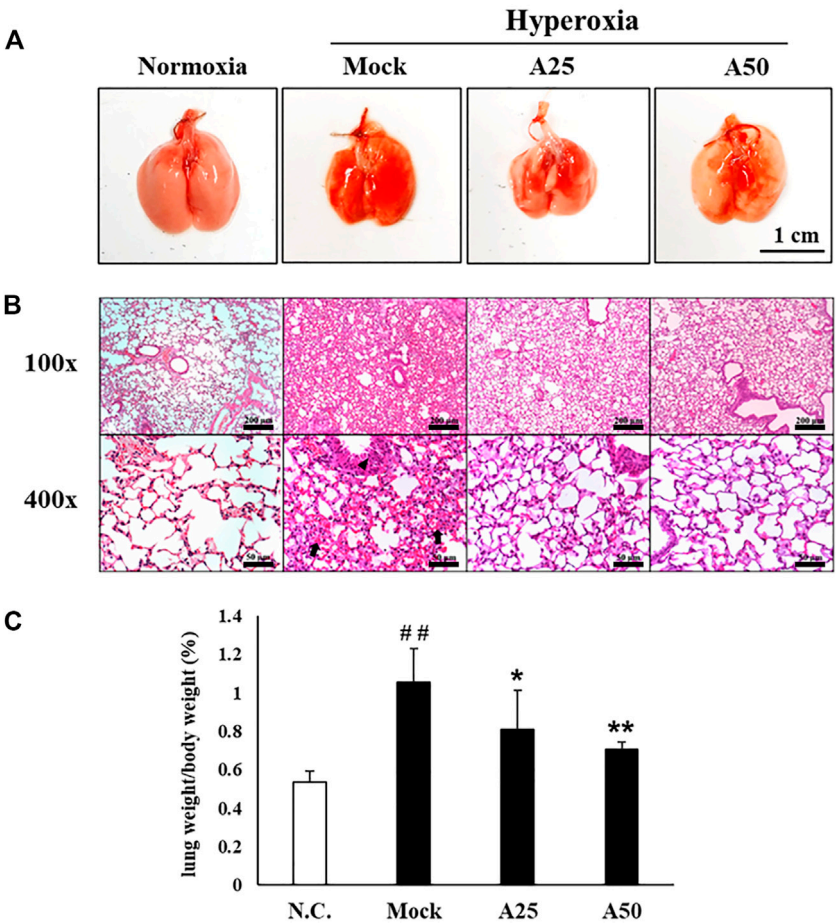

FIGURE 2 | Therapeutic efficacy of aspirin against lung inflammation in mice **(A)** Gross appearance of the lungs from NF-κB-luciferase$^{+/+}$ transgenic mice exposed to hyperoxia. Scale bar: 1 cm **(B)** Histological changes in the lungs of NF-κB-luciferase$^{+/+}$ transgenic mice exposed to hyperoxia. Scale bars for the upper panel represent 200 μm and lower panel represent 50 μm **(C)** Lung-to-body weight ratio of NF-κB-luciferase$^{+/+}$ transgenic mice exposed to hyperoxia. The values are reported as the means ± SEM (n = 6 mice per group). $^{\#\#}p < 0.01$ compared with the N.C. group; $^{*}p < 0.05$ and $^{**}p < 0.01$ compared with the Mock group. N.C, treatment with PBS at 0, 24, and 48 h and exposure to normoxia; Mock, treatment with PBS at 0, 24, and 48 h and exposure to hyperoxia for 72 h; A25, treatment with 25 μg/g aspirin at 0, 24, and 48 h and exposure to hyperoxia for 72 h; A50, treatment with 50 μg/g aspirin at 0, 24, and 48 h and exposure to hyperoxia for 72 h. Arrow: red blood cells in the intra-alveolar space, consistent with hemorrhage. Triangle: intrapulmonary hemorrhage with some histiocyte aggregation.

TABLE 1 | Histopathological scoring of the therapeutic effect of aspirin on hyperoxia-induced acute lung injury in lung tissues (n = 6) of NF-κB-luciferase$^{+/+}$ transgenic mice.

Variable	N.C[a]	Mock	A25	A50
Neutrophils in the alveolar space	1 (16.7%)	6 (100%)	2 (33.3%)	2 (33.3%)
Neutrophils in the interstitial space	1 (16.7%)	4 (66.7%)	3 (50%)	1 (16.7%)
Hyaline membranes	1 (16.7%)	5 (83.3%)	4 (66.7%)	2 (33.3%)

[a]*Abbreviations: N.C, treatment with PBS, at 0, 24, and 48 h and exposure to normoxia; Mock, treatment with PBS, at 0, 24, and 48 h and exposure to hyperoxia for 72 h; A25, treatment with 25 μg/g aspirin at 0, 24, and 48 h and exposure to hyperoxia for 72 h; A50, treatment with 50 μg/g aspirin at 0, 24, and 48 h and exposure to hyperoxia for 72 h.*

in hyperoxia-induced injury or oxidative stress (Matthew et al., 2003). The CC10 and SP-C levels in the mock group were decreased compared with those in the negative control group. However, posttreatment with 50 μg/g aspirin significantly restored the expression of the CC10 and SP-C proteins compared with the mock group (**Figure 4** and **Supplementary Figure S1**). Compared with the negative control group, the expression level of the p-p38 protein was increased in the mock group. However, posttreatment with 25 μg/g aspirin significantly reduced the level of the p-p38 protein (**Figure 4**). A significant increase in the nuclear localization of NF-κB was observed in the mock group compared with the negative control group. However, posttreatment with 25 or 50 μg/g aspirin resulted in a

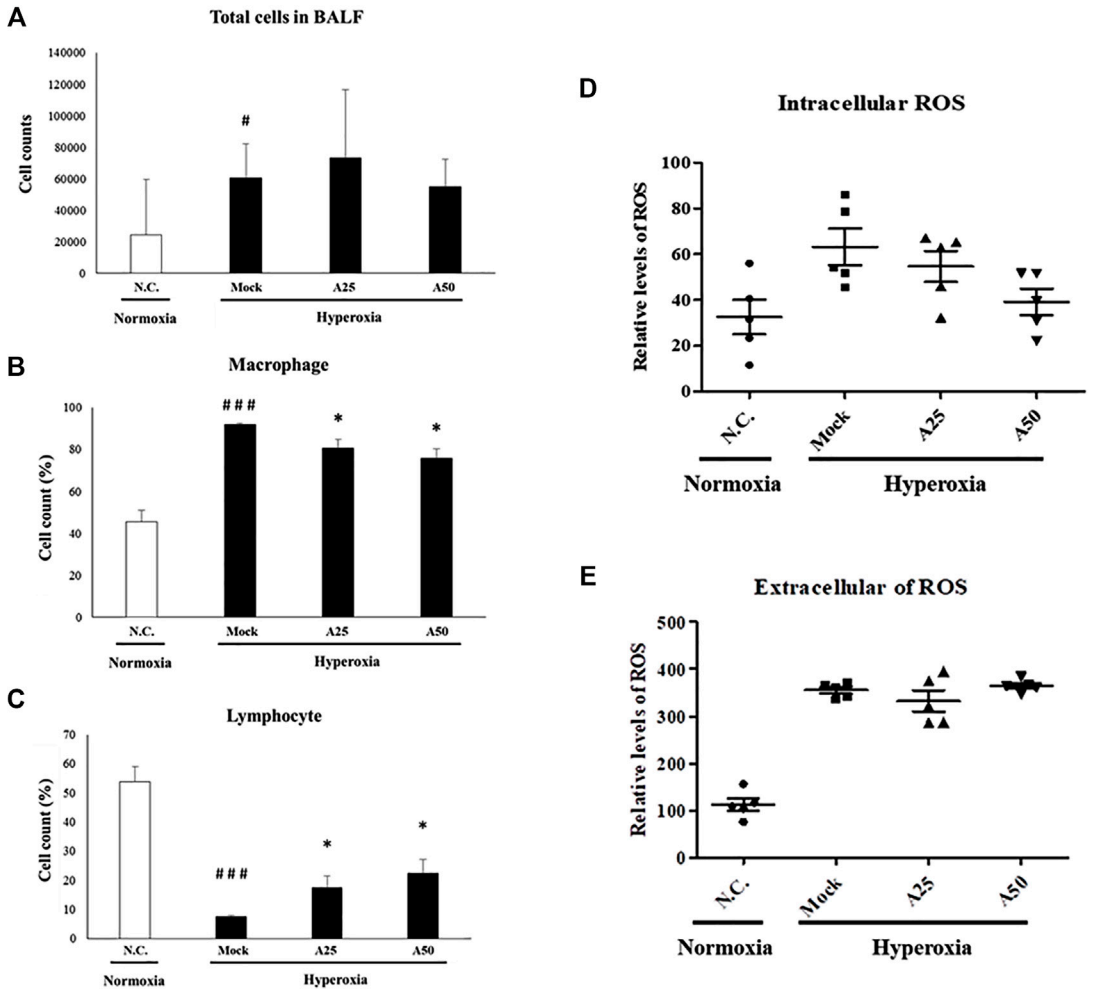

FIGURE 3 | Therapeutic efficacy of aspirin against acute lung injury in mice **(A)** Total cells in the bronchoalveolar lavage fluid (BALF) from NF-κB-luciferase$^{+/+}$ transgenic mice exposed to hyperoxia **(B)** The percentage of macrophages among total cells **(C)** The percentage of lymphocytes among total cells **(D)** The generation of intracellular reactive oxygen species (ROS) in bronchoalveolar lavage fluid (BALF) from NF-κB-luciferase$^{+/+}$ transgenic mice exposed to hyperoxia **(E)** The generation of extracellular ROS in bronchoalveolar lavage fluid (BALF) from NF-κB-luciferase$^{+/+}$ transgenic mice exposed to hyperoxia. The values are reported as the means ± SEM (n = 6 mice per group). $^{\#}p < 0.05$ and $^{\#\#\#}p < 0.001$ compared with the N.C. group; $^{*}p < 0.05$ compared with the Mock group. N.C, treatment with PBS at 0, 24, and 48 h and exposure to normoxia; Mock, treatment with PBS at 0, 24, and 48 h and exposure to hyperoxia for 72 h; A25, treatment with 25 μg/g aspirin at 0, 24, and 48 h and exposure to hyperoxia for 72 h; A50, treatment with 50 μg/g aspirin at 0, 24, and 48 h and exposure to hyperoxia for 72 h.

decrease in the expression of the NF-κB protein compared with the mock group (**Figure 5** and **Supplementary Figure S2**). Moderate expression heme oxygenase-1 (HO-1) exerts a protective effect on various organs by modulating tissue responses to injuries, including lung injury associated with hyperoxia (Pereira et al., 2018). In the present study, hyperoxia significantly increased the HO-1 protein expression level compared with that in the negative control group. However, treatment with 25 μg/g aspirin reversed the hyperoxia-induced increase in HO-1 expression. eNOS is involved in endothelial cell proliferation, and Nrp-1 is related to cell growth. Hyperoxia reduced the expression of the eNOS and Nrp-1 proteins. However, posttreatment with 25 or 50 μg/g aspirin resulted in a significant increase in the expression of the Nrp-1 protein compared with that in the mock group (**Figure 4**). Additionally, a significant dose-dependent effect on Nrp-1 expression was observed.

Therapeutic Efficacy of Aspirin Against Hyperoxia-Induced Inflammation in the Lung Tissue

Hyperoxia activates the transcription factor NF-κB, which induces inflammation through the ubiquitination or proteasomal degradation of IκBα and the translocation of activated NF-κB from the cytoplasm to the nucleus (**Figure 5**). Oxidative stress activates the p-ERK, p-p38 and NF-κB signaling pathways, which converge and result in the expression of survival and stress response proteins and ultimately lead to inflammation. Posttreatment with 25 μg/g aspirin decreased the

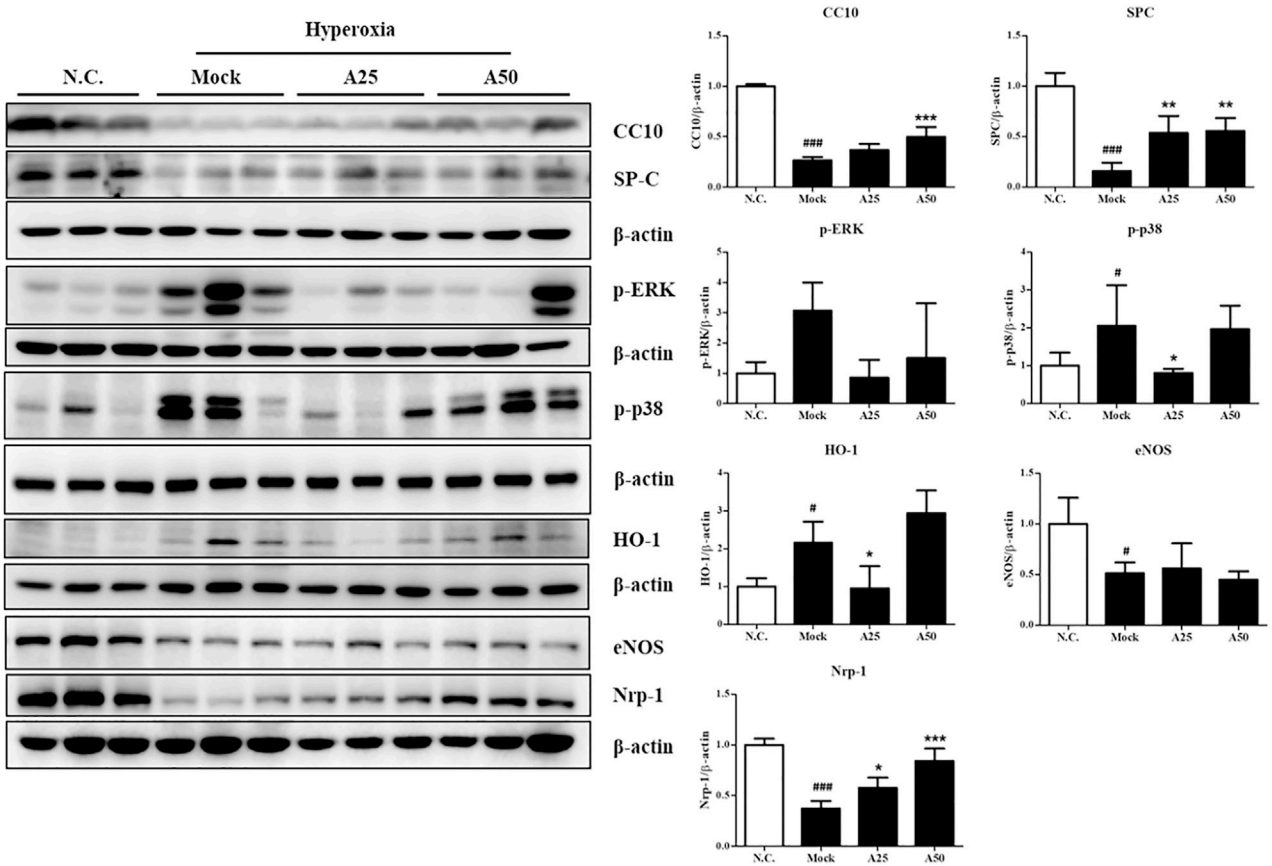

FIGURE 4 | Therapeutic efficacy of aspirin in improving survival and ameliorating the stress response in the lung tissue of NF-κB-luciferase$^{+/+}$ transgenic mice exposed to hyperoxia. The bands were quantified relative to *β*-actin bands using ImageJ software. The values are reported as the means ± SEM (n = 6 mice per group). $^{\#}p < 0.05$, $^{\#\#}p < 0.01$, and $^{\#\#\#}p < 0.001$ compared with the N.C. group; $^{*}p < 0.05$, $^{**}p < 0.01$, and $^{***}p < 0.001$ compared with the Mock group. N.C, treatment with PBS at 0, 24, and 48 h and exposure to normoxia; Mock, treatment with PBS at 0, 24, and 48 h and exposure to hyperoxia for 72 h; A25, treatment with 25 μg/g aspirin at 0, 24, and 48 h and exposure to hyperoxia for 72 h; A50, treatment with 50 μg/g aspirin at 0, 24, and 48 h and exposure to hyperoxia for 72 h.

phosphorylation of p38. However, both doses of aspirin significantly decreased nuclear levels of the NF-κB protein and increased the expression of the IκBα protein compared with the mock group (**Figure 5**). The levels of the inflammatory signaling proteins TNF-α, IL-1β and IL-4 were markedly increased in the mock group compared with the negative control group (**Figure 5**). Posttreatment with 25 or 50 μg/g aspirin significantly reduced proinflammatory protein levels (i.e., TNF-α, IL-1β and IL-4). Therefore, posttreatment with 25 or 50 μg/g aspirin reduced the expression of proinflammatory proteins, minimizing inflammation and improving ALI.

Effect of Aspirin on Platelet-Derived Mediators and Pulmonary Fibrosis Induced by Hyperoxia

The most abundant protein released from platelets is CXCL4 (Mussbacher et al., 2021). CXCL4 is a platelet-derived chemokine and molecular mediator of fibrotic lung injury. It is a key chemokine that is initially secreted by activated platelets (Silva-Cardoso et al., 2020). Compared with the negative control group, CXCL4 expression increased in the alveoli (**Figure 6A**) and bronchi (**Figure 6B**) of the mock group. Simultaneously, posttreatment with 25 or 50 μg/g aspirin significantly reduced the CXCL4 protein level; however, aspirin treatment did not alter the protein levels in blood vessels (**Figure 6C**). CC10, a sensitive marker of lung injury, is primarily secreted by Clara cells. Compared with the negative control group, CC10 levels in the mock group were decreased. However, posttreatment with 25 or 50 μg/g aspirin restored the level of the CC10 protein (**Figure 7**). The Western blot results confirmed that CC10 expression was reduced following hyperoxia exposure but rescued after treatment with 50 μg/g aspirin (**Figure 4**). Therefore, hyperoxia causes lung injury in alveoli, but aspirin attenuates this damage.

DISCUSSION

ALI and ARDS are common disorders that affect approximately 200,000 people each year in the United States (Rubenfeld et al., 2005). The incidence of

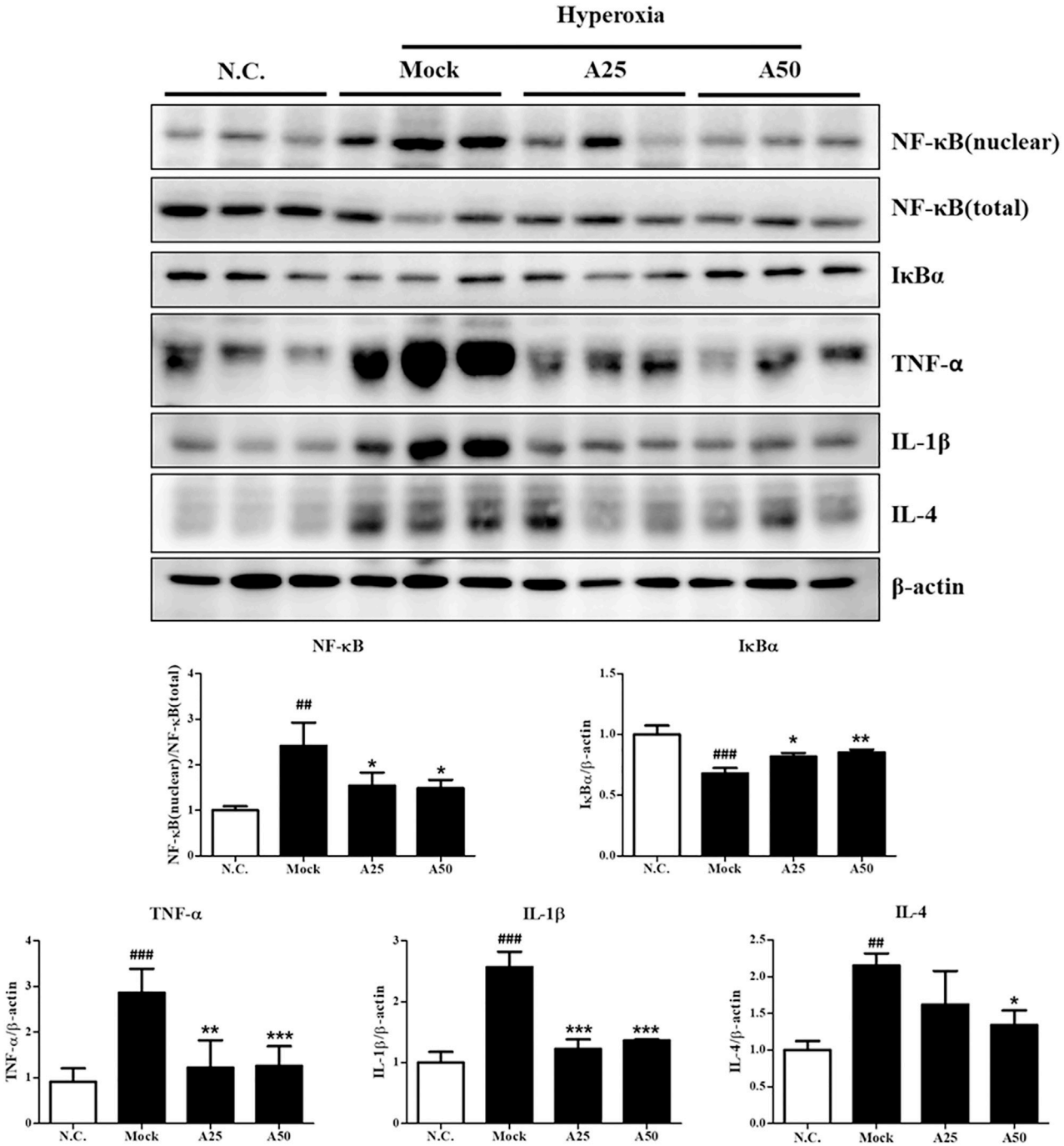

FIGURE 5 | Therapeutic efficacy of aspirin in inhibiting hyperoxia-induced inflammation in the lung tissue of NF-κB-luciferase$^{+/+}$ transgenic mice. The bands were quantified relative to *β*-actin bands using ImageJ software. The values are reported as the means ± SEM (n = 6 mice per group). $^{\#}p < 0.05$, $^{\#\#}p < 0.01$, and $^{\#\#\#}p < 0.001$ compared with the N.C. group; $^{*}p < 0.05$ and $^{**}p < 0.05$ compared with the Mock group. N.C, treatment with PBS at 0, 24, and 48 h and exposure to normoxia; Mock, treatment with PBS at 0, 24, and 48 h and exposure to hyperoxia for 72 h; A25, treatment with 25 μg/g aspirin at 0, 24, and 48 h and exposure to hyperoxia for 72 h; A50, treatment with 50 μg/g aspirin at 0, 24, and 48 h and exposure to hyperoxia for 72 h.

ARDS ranges from 1.5 to 79 cases per 100,000 in European countries (Confalonieri et al., 2017). Because of coronavirus disease 2019 (COVID-19), approximately 33% of hospitalized patients with COVID-19 develop ARDS, and the mortality rate of patients with COVID-19-associated ARDS is 45% (Tzotzos et al., 2020). In human studies, the results of aspirin treatment have been inconsistent because of heterogeneity in the performance, course, and outcome of patients who meet the

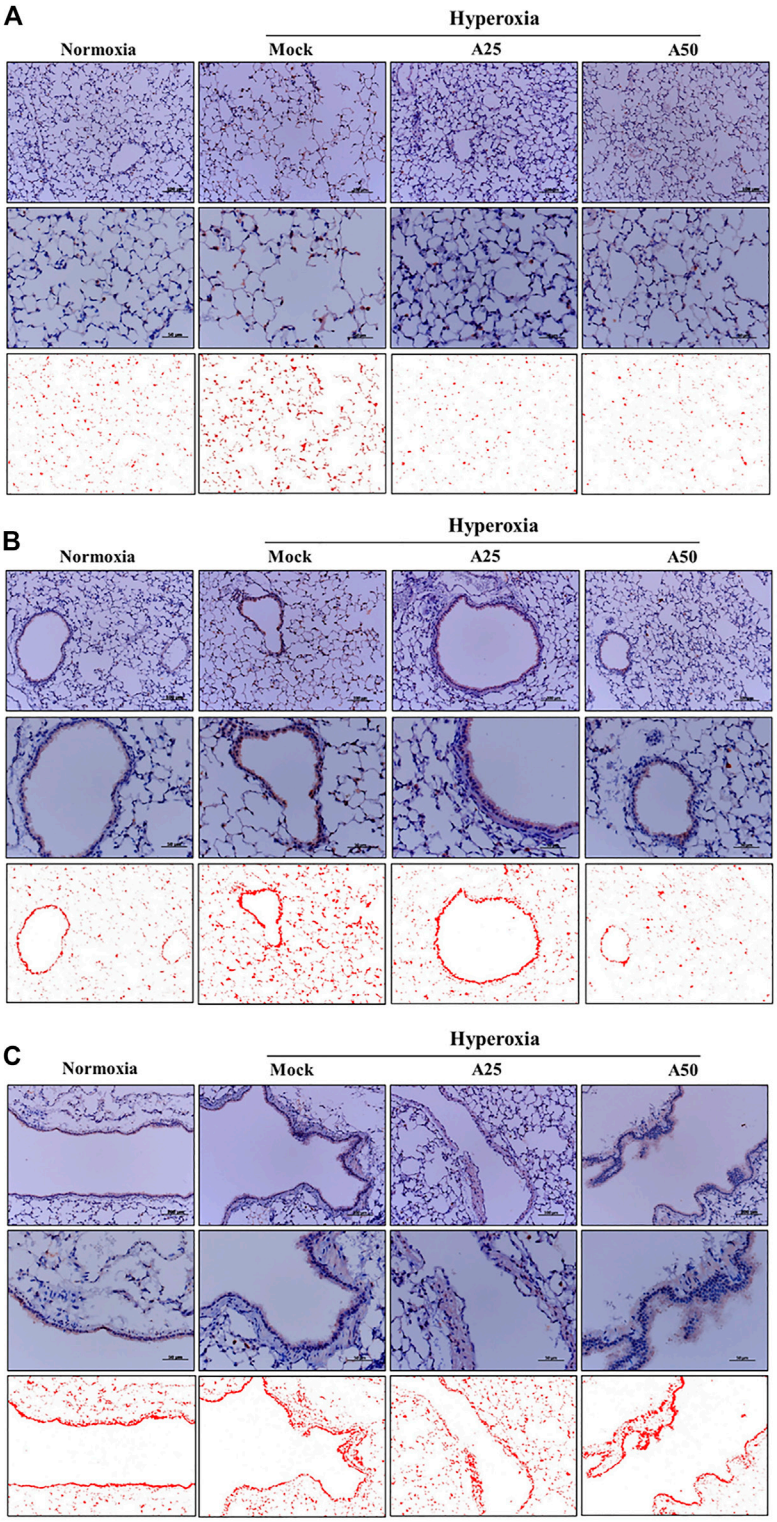

FIGURE 6 | Therapeutic efficacy of aspirin in altering levels of the CXCL4 protein induced by hyperoxia in NF-κB-luciferase$^{+/+}$ transgenic mice, as detected using immunohistochemical (IHC) staining **(A)** Images of alveoli; scale bars for the upper panel represent 200 μm and middle panel represent 50 μm **(B)** Images of bronchi; scale bars for the upper panel represent 200 μm and middle panel represent 50 μm **(C)** Images of blood vessels. Scale bars for the upper panel represent 200 μm and middle panel represent 50 μm. DAB-specific threshold selection (red selection) was performed using ImageJ software. NF-κB-luciferase$^{+/+}$ transgenic mice were assigned to four groups (n = 6 mice per group): Mock group, treatment with PBS at 0, 24 and 48 h, and exposure to hyperoxia for 72 h. A25 group, treatment with 25 μg/g aspirin at 0, 24 and 48 h, and exposure to hyperoxia for 72 h. A50 group: treatment with 50 μg/g aspirin at 0, 24 and 48 h, and exposure to hyperoxia for 72 h.

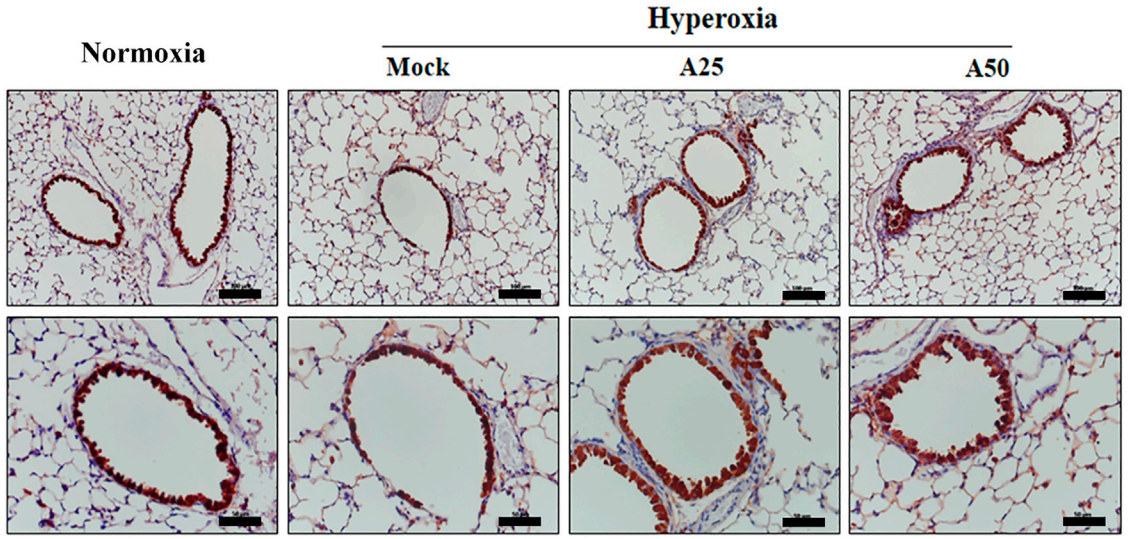

FIGURE 7 | Immunohistochemical staining indicating the therapeutic efficacy of aspirin at altering levels of the CC10 protein in NF-κB-luciferase$^{+/+}$ transgenic mice exposed to hyperoxia. Scale bars for the upper panel represent 200 μm and lower panel represent 50 μm. NF-κB-luciferase$^{+/+}$ transgenic mice were assigned to four groups (n = 6 mice per group): Mock group, treatment with PBS at 0, 24, and 48 h and exposure to hyperoxia for 72 h; A25 group, treatment with 25 μg/g aspirin at 0, 24, and 48 h and exposure to hyperoxia for 72 h; A50 group, treatment with 50 μg/g aspirin at 0, 24, and 48 h and exposure to hyperoxia for 72 h.

clinical definition of ARDS. Hamid et al. (Hamid et al., 2017) reported that both low-dose and high-dose aspirin inhibit pulmonary neutrophil inflammation in bronchoalveolar lavage fluid. Even after adjustment for the propensity of prehospital aspirin use, prehospital aspirin use is independently associated with a reduced ARDS risk (Chen et al., 2015) and is related to a reduced risk of mortality for patients in intensive care units. However, Kor et al. (Kor et al., 2016) found that aspirin use did not reduce the ARDS risk at 7 days after hospitalization compared with the placebo. However, the mechanism and efficacy of aspirin in the treatment of ALI caused by hyperoxia are unclear. Hyperoxia exposure is widely used as an experimental model for ARDS (Reddy et al., 2009).

Oxidant- or toxicant-mediated abnormal tissue repair and inflammation lead to the occurrence and development of various lung diseases (Reddy et al., 2009). A relatively short exposure time of hyperoxia (48–72 h) produces ALI, which is used as a model to study the mechanisms that control lung injury, repair, and inflammation (Reddy et al., 2009). Acute exposure to hyperoxia (72 h) reportedly induces inflammation and damage to the lungs, leading to impaired respiratory function, and prolonged exposure (96–120 h) results in rodent death (Hamid et al., 2017). However, prolonged exposure to hyperoxia (65% O_2) may aggravate lung symptoms and cause ALI (Ware and Herridge, 2013). Therefore, we established hyperoxia (FiO_2 > 95%)-induced ALI in NF-κB-luciferase$^{+/+}$ transgenic mice as a model to evaluate the therapeutic efficacy of aspirin in lung injury.

After mice were exposed to hyperoxia for 72 h, luciferase signals were elevated compared with those in the negative control group; however, in the A25 and A50 groups, luciferase signals were decreased compared with the group treated only with hyperoxia. Therefore, posttreatment with aspirin reduced the hyperoxia-induced increase in NF-κB expression. In addition, after hyperoxia, lungs exhibited pulmonary edema, alveolar infiltration, a greater number of macrophages, and a lower number of lymphocytes compared with the negative control group. Song et al. (Song et al., 2020) also indicated that as ARDS severity increases, lymphocyte counts decrease. However, the groups posttreated with 25 or 50 μg/g aspirin exhibited less pulmonary edema and alveolar infiltration, a lower number of macrophages, and a greater number of lymphocytes than the group exposed to hyperoxia alone. As shown in our previous study (Chen C. M. et al., 2020), the group pretreated with aspirin for 3 days after hyperoxia exhibited an obvious decrease in hyperoxia-induced macrophages. Wahn and Hammerschmidt (Wahn and Hammerschmidt, 2001) suggested that aspirin reduces the severity of edema and vascular permeability in individuals with ALI caused by oxidative stress. ROS play a vital role in physiological and pathophysiological processes, but high ROS levels are considered toxic and cause cell damage and death (Valko et al., 2007). Hyperoxia produces a large amount of extracellular and intracellular ROS, and posttreatment with 50 μg/g aspirin significantly reduced intracellular ROS production. Increases in exogenous ROS (i.e., free radicals produced by hyperoxia) levels were not reversed by the aspirin posttreatment. However, endogenous ROS are produced by mitochondria, and mitochondria are also targets of ROS. In addition, our previous study (Chen C. M. et al., 2020) indicated that pretreatment with aspirin (12.5 μg/g or 100 μg/g) obviously reduced ROS production.

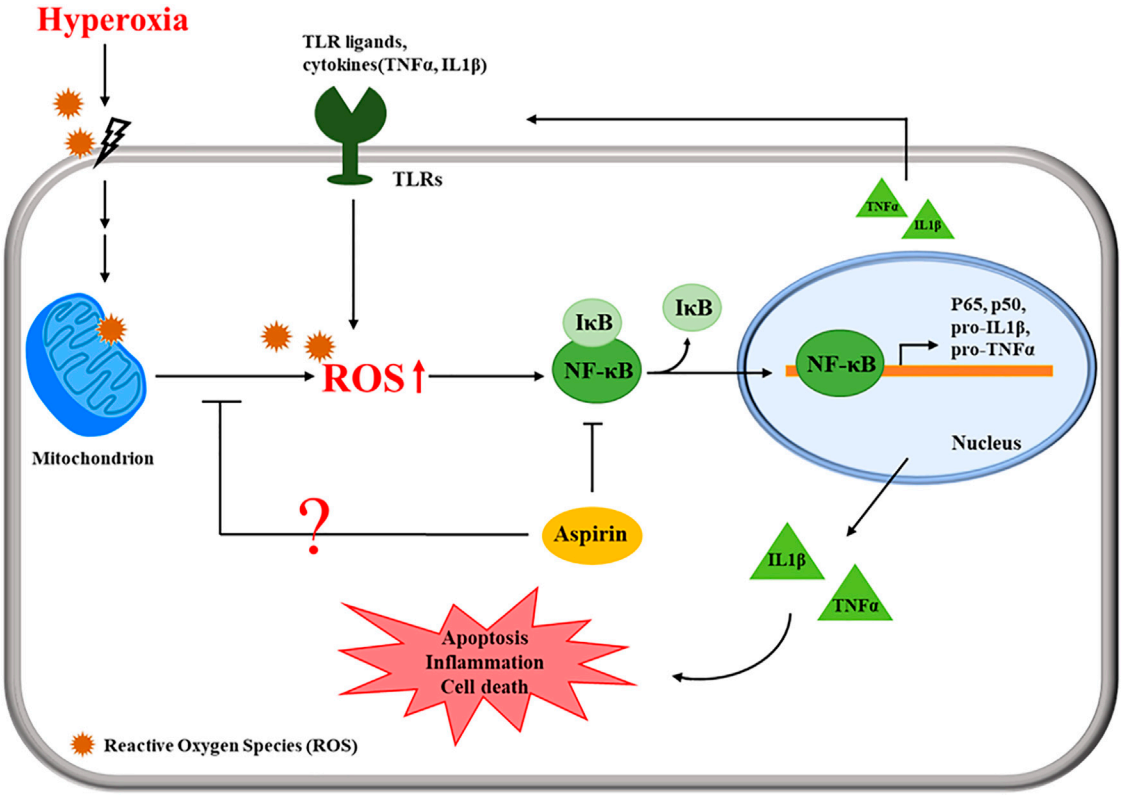

FIGURE 8 | Schematic of the pathway by which the aspirin posttreatment regulates hyperoxia-induced acute respiratory distress syndrome (ARDS) by suppressing pulmonary inflammation via NF-κB signaling.

According to Cox et al. (Cox et al., 2015), aspirin-induced resolvin D1 expression significantly inhibits oxygen-induced pulmonary edema, permeability and inflammation and therefore is an effective treatment for damage induced by prolonged hyperoxia exposure.

Alveolar macrophages secrete cytokines such as IL-1, IL-6, IL-8, IL-10 and TNF-α that act locally to stimulate chemotaxis and activate neutrophils. An imbalance between proinflammatory and anti-inflammatory mediators is observed in ARDS (Ware and Herridge, 2013). In the current study, hyperoxia significantly increased p-ERK, nuclear translocation of NF-κB p65, TNF-α, IL-1β, and IL-4 levels, and reduced IκBα levels. However, posttreatment with aspirin significantly reduced NF-κB p65, TNF-α, IL-1β, and IL-4 levels and increased IκBα levels in the lung tissues of NF-κB-luciferase$^{+/+}$ transgenic mice. Based on these results, aspirin modulates NF-κB p65, IκBα, TNF-α, IL-1β, and IL-4, all of which reduce the inflammatory response. A previous study showed that anti-inflammatory factors, e.g., IL-10 and IL-4, play vital roles in protecting the lung from lipopolysaccharide (LPS)-induced ALI (Cox et al., 2015). In addition, IL-4 inhibits the transcriptional activity of NF-κB and IL-1, IL-6, and TNF-α expression (Huang et al., 2019). As shown in our previous study, pretreatment with aspirin obviously decreases the hyperoxia-induced increase in p-AKT, NF-κB, IL-6, and TNF-α protein levels (Chen C. M. et al., 2020). Wang et al. (Wang et al., 2011) documented that aspirin obviously decreases the nuclear translocation of NF-κB p65 and the degradation of its inhibitor IκB, p-ERK, and p38 MAPK in LPS-activated microglia. Liu et al. (Liu et al., 2019) also reported that aspirin reduces levels of oxygen free radicals (ROS and nitric oxide) and inflammatory cytokines (IL-1β, IL-6, and TNF-α) in LPS-induced nucleus pulposus cells. Aspirin may prevent or treat ARDS by reducing the activation and recruitment of neutrophils to the lung, the expression of TNF-α in pulmonary vascular macrophages, the plasma thromboxane B2 level, and the sequestration of platelets in the lung (Chen et al., 2003; Looney et al., 2009; Eickmeier et al., 2013; Tuinman et al., 2013; Huang et al., 2019). In patients who took 300 mg of aspirin the day before surgery, delayed postoperative neutrophil apoptosis was significantly preserved after surgery, indicating that aspirin promotes the resolution of persistent inflammation (Bates et al., 2004).

The present study revealed that posttreatment with aspirin exerted significant anti-inflammatory effects. Hyperoxia reduced the CC10 protein level; however, aspirin posttreatment obviously increased CC10 protein levels. CC10 is the main protein secreted by Clara cells. Because of its anti-inflammatory properties, CC10 is considered to exert a protective effect on the lungs (Bolton et al., 2008). Tokita et al. (Tokita et al., 2014) indicated that CC10 reduces LPS-induced mucus secretion in airway cells, partially due to the inhibition of NF-κB phosphorylation. Lopez et al. (Lopez et al., 2020) revealed that rhCC10 significantly reduces ARDS progression and lung dysfunction caused by smoke inhalation injury. Therefore, posttreatment with aspirin might increase CC10 expression to

inhibit anti-inflammation in models of hyperoxia-induced ALI and systemic oxidative stress. The chemokine CXCL4 is released from activated platelets during platelet aggregation. According to Bdeir et al. (Bdeir et al., 2017), CXCL4 contributes to the development of ALI by increasing inflammation and pulmonary vascular permeability. Exposure to hyperoxia increased CXCL4 expression, causing serious inflammation in alveoli and bronchi, but the aspirin treatment ameliorated this phenomenon. However, no significant differences in blood vessels were observed among the normal control, mock, A25 and A50 groups because CXCL4 is derived from platelets. The proposed pathway by which the aspirin posttreatment regulates ALI is shown in **Figure 8**. Cells sense the exposure to hyperoxia and activate a series of cellular responses to oxidative stress. The increase in NF-κB activity is essential for inflammatory responses. NF-κB plays a critical role in regulating the survival and activating the transcription of cytokines or additional inflammatory mediators. The secretion of cytokines, such as TNF-α and IL-1β, promotes the activation of NF-κB. However, our results indicated that posttreatment with aspirin rescues lung injury by attenuating the inflammatory response.

CONCLUSION

In the present study, treatment of NF-κB-luciferase$^{+/+}$ transgenic mice exposed to 95% hyperoxia for 72 h with aspirin at 0, 24, and 72 h reduced macrophages infiltration, ROS production, NF-κB activation, and lung edema compared with hyperoxia exposure alone. Furthermore, posttreatment with aspirin significantly reduced p-ERK, p-p38, TNF-α, IL-1β, and IL-4 levels, and increased IκBα levels in the lung tissues of NF-κB-luciferase$^{+/+}$ transgenic mice. Therefore, we concluded that the anti-inflammatory effect of aspirin on hyperoxia-induced ALI and its therapeutic effect on inhibiting ROS-induced damage are mediated by the NF-κB signaling pathway.

DATA AVAILABILITY STATEMENT

The original contributions presented in the study are included in the article/**Supplementary Material** further inquiries can be directed to the corresponding authors.

ETHICS STATEMENT

The animal study was reviewed and approved by the Institutional Animal Care and Utilization Committee (IACUC) of National Chung Hsing University, Taichung, Taiwan (Approval No: IACUC-102-77).

AUTHOR CONTRIBUTIONS

Data curation: C-HW, C-CY, H-EH, P-YL, and Y-TT; Formal analysis: C-HW, C-CY, and Y-TT; Funding acquisition: C-MC and WC; Methodology: C-MC, C-HW, H-EH, and WC; Project administration: Y-TT; Resources: C-MC and WC; Software: Y-TT; Supervision: C-MC; and Writing–original draft: C-HW, LW, and Y-TT All authors have read and agreed to the published version of the manuscript.

FUNDING

This work was supported in part by grants MOST-108-2313-B-005-039-MY3 and MOST-104-2314-B-705-005 from the Ministry of Science and Technology of Taiwan and grant from Chiayi Christian Hospital, Chiayi, Taiwan. And also supported by the Higher Education Sprout Project from the Ministry of Education (MOE-110-S-0023-A) in Taiwan.

ACKNOWLEDGMENTS

We thank our colleague, Dr. Gary Ro-Lin Chang, in the Molecular Embryology and DNA Methylation Laboratory, National Chung Hsing University, for his participation in discussions and assistance with resolving technical issues.

SUPPLEMENTARY MATERIAL

The Supplementary Material for this article can be found online at: https://www.frontiersin.org/articles/10.3389/fphar.2021.793107/full#supplementary-material

REFERENCES

al-Mehdi, A., Shuman, H., and Fisher, A. B. (1994). Fluorescence Microtopography of Oxidative Stress in Lung Ischemia-Reperfusion. *Lab. Invest.* 70, 579–587.

Antithrombotic Trialists, C. (2002). Collaborative Meta-Analysis of Randomised Trials of Antiplatelet Therapy for Prevention of Death, Myocardial Infarction, and Stroke in High Risk Patients. *BMJ* 324, 71–86. doi:10.1136/bmj.324.7329.71

Babior, B. M., Takeuchi, C., Ruedi, J., Gutierrez, A., and Wentworth, P., Jr. (2003). Investigating Antibody-Catalyzed Ozone Generation by Human Neutrophils. *Proc. Natl. Acad. Sci. U S A.* 100, 3031–3034. doi:10.1073/pnas.0530251100

Bates, J. J., Watson, R. W., Glynn, C. M., O'Neill, A. J., Fitzpatrick, J. M., and Buggy, D. J. (2004). Aspirin Preserves Neutrophil Apoptosis after Cardiopulmonary Bypass. *Shock* 21, 495–499. doi:10.1097/01.shk.0000126146.94237.92

Bdeir, K., Gollomp, K., Stasiak, M., Mei, J., Papiewska-Pajak, I., Zhao, G., et al. (2017). Platelet-specific Chemokines Contribute to the Pathogenesis of Acute Lung Injury. *Am. J. Respir. Cel Mol. Biol.* 56, 261–270. doi:10.1165/rcmb.2015-0245OC

Bolton, S. J., Pinnion, K., Marshall, C. V., Wilson, E., Barker, J. E., Oreffo, V., et al. (2008). Changes in Clara Cell 10 kDa Protein (CC10)-Positive Cell Distribution in Acute Lung Injury Following Repeated Lipopolysaccharide challenge in the Rat. *Toxicol. Pathol.* 36, 440–448. doi:10.1177/0192623308315357

Boyle, A. J., Di Gangi, S., Hamid, U. I., Mottram, L. J., McNamee, L., White, G., et al. (2015). Aspirin Therapy in Patients with Acute Respiratory Distress Syndrome (ARDS) Is Associated with Reduced Intensive Care Unit Mortality: a Prospective Analysis. *Crit. Care* 19, 109. doi:10.1186/s13054-015-0846-4

Boyle, A. J., Mac Sweeney, R., and McAuley, D. F. (2013). Pharmacological Treatments in ARDS; a State-Of-The-Art Update. *BMC Med.* 11, 166. doi:10.1186/1741-7015-11-166

Boyle, A. J., McNamee, J. J., and McAuley, D. F. (2014). Biological Therapies in the Acute Respiratory Distress Syndrome. *Expert Opin. Biol. Ther.* 14, 969–981. doi:10.1517/14712598.2014.905536

Chen, C. M., Tung, Y. T., Wei, C. H., Lee, P. Y., and Chen, W. (2020). Anti-Inflammatory and Reactive Oxygen Species Suppression through Aspirin Pretreatment to Treat Hyperoxia-Induced Acute Lung Injury in NF-Kb-Luciferase Inducible Transgenic Mice. *Antioxidants (Basel)* 9, 429. doi:10.3390/antiox9050429

Chen, H. L., Lan, Y. W., Tu, M. Y., Tung, Y. T., Chan, M. N., Wu, H. S., et al. (2021). Kefir Peptides Exhibit Antidepressant-like Activity in Mice through the BDNF/TrkB Pathway. *J. Dairy Sci.* 104, 6415–6430. doi:10.3168/jds.2020-19222

Chen, W., Janz, D. R., Bastarache, J. A., May, A. K., O'Neal, H. R., Jr., Bernard, G. R., et al. (2015). Prehospital Aspirin Use Is Associated with Reduced Risk of Acute Respiratory Distress Syndrome in Critically Ill Patients: a Propensity-Adjusted Analysis. *Crit. Care Med.* 43, 801–807. doi:10.1097/CCM.0000000000000789

Chen, Y.-H., Chen, H.-L., Fan, H.-C., Tung, Y.-T., Kuo, C.-W., Tu, M.-Y., et al. (2020). Anti-inflammatory, Antioxidant, and Antifibrotic Effects of Kefir Peptides on Salt-Induced Renal Vascular Damage and Dysfunction in Aged Stroke-Prone Spontaneously Hypertensive Rats. *Antioxidants* 9, 790. doi:10.3390/antiox9090790

Chen, Z. T., Li, S. L., Cai, E. Q., Wu, W. L., Jin, J. S., and Zhu, B. (2003). LPS Induces Pulmonary Intravascular Macrophages Producing Inflammatory Mediators via Activating NF-kappaB. *J. Cel Biochem.* 89, 1206–1214. doi:10.1002/jcb.10590

Confalonieri, M., Salton, F., and Fabiano, F. (2017). Acute Respiratory Distress Syndrome. *Eur. Respir. Rev.* 26, 144. doi:10.1183/16000617.0116-2016

Cox, R., Jr., Phillips, O., Fukumoto, J., Fukumoto, I., Parthasarathy, P. T., Arias, S., et al. (2015). Enhanced Resolution of Hyperoxic Acute Lung Injury as a Result of Aspirin Triggered Resolvin D1 Treatment. *Am. J. Respir. Cel Mol. Biol.* 53, 422–435. doi:10.1165/rcmb.2014-0339OC

Eickmeier, O., Seki, H., Haworth, O., Hilberath, J. N., Gao, F., Uddin, M., et al. (2013). Aspirin-triggered Resolvin D1 Reduces Mucosal Inflammation and Promotes Resolution in a Murine Model of Acute Lung Injury. *Mucosal Immunol.* 6, 256–266. doi:10.1038/mi.2012.66

Fitzgerald, M., Millar, J., Blackwood, B., Davies, A., Brett, S. J., McAuley, D. F., et al. (2014). Extracorporeal Carbon Dioxide Removal for Patients with Acute Respiratory Failure Secondary to the Acute Respiratory Distress Syndrome: a Systematic Review. *Crit. Care* 18, 222. doi:10.1186/cc13875

Gao, R., and Li, X. (2010). Risk Assessment and Aspirin Use in Asian and Western Populations. *Vasc. Health Risk Manag.* 6, 943–956. doi:10.2147/VHRM.S9400

Guérin, C., Reignier, J., Richard, J. C., Beuret, P., Gacouin, A., Boulain, T., et al. (2013). Prone Positioning in Severe Acute Respiratory Distress Syndrome. *N. Engl. J. Med.* 368, 2159–2168. doi:10.1056/NEJMoa1214103

Hamid, U., Krasnodembskaya, A., Fitzgerald, M., Shyamsundar, M., Kissenpfennig, A., Scott, C., et al. (2017). Aspirin Reduces Lipopolysaccharide-Induced Pulmonary Inflammation in Human Models of ARDS. *Thorax* 72, 971–980. doi:10.1136/thoraxjnl-2016-208571

Ho, T. Y., Chen, Y. S., and Hsiang, C. Y. (2007). Noninvasive Nuclear Factor-kappaB Bioluminescence Imaging for the Assessment of Host-Biomaterial Interaction in Transgenic Mice. *Biomaterials* 28, 4370–4377. doi:10.1016/j.biomaterials.2007.07.005

Hsiang, C. Y., Chen, Y. S., and Ho, T. Y. (2009). Nuclear Factor-kappaB Bioluminescence Imaging-Guided Transcriptomic Analysis for the Assessment of Host-Biomaterial Interaction *In Vivo*. *Biomaterials* 30, 3042–3049. doi:10.1016/j.biomaterials.2009.02.016

Huang, X. L., Wei, X. C., Guo, L. Q., Zhao, L., Chen, X. H., Cui, Y. D., et al. (2019). The Therapeutic Effects of Jaceosidin on Lipopolysaccharide-Induced Acute Lung Injury in Mice. *J. Pharmacol. Sci.* 140, 228–235. doi:10.1016/j.jphs.2019.07.004

Kiefmann, R., Heckel, K., Schenkat, S., Dörger, M., Wesierska-Gadek, J., and Goetz, A. E. (2004). Platelet-endothelial Cell Interaction in Pulmonary Micro-circulation: the Role of PARS. *Thromb. Haemost.* 91, 761–770. doi:10.1160/TH03-11-0685

Kor, D. J., Carter, R. E., Park, P. K., Festic, E., Banner-Goodspeed, V. M., Hinds, R., et al. (2016). Effect of Aspirin on Development of ARDS in At-Risk Patients Presenting to the Emergency Department: The LIPS-A Randomized Clinical Trial. *JAMA* 315, 2406–2414. doi:10.1001/jama.2016.6330

Liu, Y., Lin, J., Wu, X., Guo, X., Sun, H., Yu, B., et al. (2019). Aspirin-mediated Attenuation of Intervertebral Disc Degeneration by Ameliorating Reactive Oxygen Species *In Vivo* and *In Vitro*. *Oxid. Med. Cel Longev.* 2019, 7189854. doi:10.1155/2019/7189854

Looney, M. R., Nguyen, J. X., Hu, Y., Van Ziffle, J. A., Lowell, C. A., and Matthay, M. A. (2009). Platelet Depletion and Aspirin Treatment Protect Mice in a Two-Event Model of Transfusion-Related Acute Lung Injury. *J. Clin. Invest.* 119, 3450–3461. doi:10.1172/JCI38432

Lopez, E., Fujiwara, O., Nelson, C., Winn, M. E., Clayton, R. S., Cox, R. A., et al. (2020). Club Cell Protein, CC10, Attenuates Acute Respiratory Distress Syndrome Induced by Smoke Inhalation. *Shock* 53, 317–326. doi:10.1097/SHK.0000000000001365

Matthay, M. A., Zemans, R. L., Zimmerman, G. A., Arabi, Y. M., Beitler, J. R., Mercat, A., et al. (2019). Acute Respiratory Distress Syndrome. *Nat. Rev. Dis. Primers* 5, 18. doi:10.1038/s41572-019-0069-0

Matthew, E., Kutcher, L., and Dedman, J. (2003). Protection of Lungs from Hyperoxic Injury: Gene Expression Analysis of Cyclosporin A Therapy. *Physiol. Genomics* 14, 129–138. doi:10.1152/physiolgenomics.00130.2002

Mussbacher, M., Brunnthaler, L., Panhuber, A., Starlinger, P., and Assinger, A. (2021). Till Death Do Us Part-The Multifaceted Role of Platelets in Liver Diseases. *Int. J. Mol. Sci.* 22, 3113. doi:10.3390/ijms22063113

Oba, Y., and Salzman, G. A. (2000). Ventilation with Lower Tidal Volumes as Compared with Traditional Tidal Volumes for Acute Lung Injury. *N. Engl. J. Med.* 343, 813–814.

Ortiz-Muñoz, G., Mallavia, B., Bins, A., Headley, M., Krummel, M. F., and Looney, M. R. (2014). Aspirin-triggered 15-Epi-Lipoxin A4 Regulates Neutrophil-Platelet Aggregation and Attenuates Acute Lung Injury in Mice. *Blood* 124, 2625–2634. doi:10.1182/blood-2014-03-562876

Pereira, M. L. M., Marinho, C. R. F., and Epiphanio, S. (2018). Could Heme Oxygenase-1 Be a New Target for Therapeutic Intervention in Malaria-Associated Acute Lung Injury/acute Respiratory Distress Syndrome? *Front. Cel. Infect. Microbiol.* 8, 161. doi:10.3389/fcimb.2018.00161

Reddy, N. M., Kleeberger, S. R., Kensler, T. W., Yamamoto, M., Hassoun, P. M., and Reddy, S. P. (2009). Disruption of Nrf2 Impairs the Resolution of Hyperoxia-Induced Acute Lung Injury and Inflammation in Mice. *J. Immunol.* 182, 7264–7271. doi:10.4049/jimmunol.0804248

Rubenfeld, G. D., Caldwell, E., Peabody, E., Weaver, J., Martin, D. P., Neff, M., et al. (2005). Incidence and Outcomes of Acute Lung Injury. *N. Engl. J. Med.* 353, 1685–1693. doi:10.1056/NEJMoa050333

Silva-Cardoso, S. C., Tao, W., Angiolilli, C., Lopes, A. P., Bekker, C. P. J., Devaprasad, A., et al. (2020). CXCL4 Links Inflammation and Fibrosis by Reprogramming Monocyte-Derived Dendritic Cells *In Vitro*. *Front. Immunol.* 11, 2149. doi:10.3389/fimmu.2020.02149

Song, M., Liu, Y., Lu, Z., Luo, H., Peng, H., and Chen, P. (2020). Prognostic Factors for ARDS: Clinical, Physiological and Atypical Immunodeficiency. *BMC Pulm. Med.* 20, 102. doi:10.1186/s12890-020-1131-0

Tokita, E., Tanabe, T., Asano, K., Suzaki, H., and Rubin, B. K. (2014). Club Cell 10-kDa Protein Attenuates Airway Mucus Hypersecretion and Inflammation. *Eur. Respir. J.* 44, 1002–1010. doi:10.1183/09031936.00080913

Tuinman, P. R., Müller, M. C., Jongsma, G., Hegeman, M. A., and Juffermans, N. P. (2013). High-dose Acetylsalicylic Acid Is superior to Low-Dose as Well as to Clopidogrel in Preventing Lipopolysaccharide-Induced Lung Injury in Mice. *Shock* 40, 334–338. doi:10.1097/SHK.0b013e3182a384f0

Tung, Y. T., Chen, H. L., Lai, C. W., Shen, C. J., Lai, Y. W., and Chen, C. M. (2011). Curcumin Reduces Pulmonary Tumorigenesis in Vascular Endothelial Growth Factor (VEGF)-overexpressing Transgenic Mice. *Mol. Nutr. Food Res.* 55, 1036–1043. doi:10.1002/mnfr.201000654

Tzotzos, S. J., Fischer, B., Fischer, H., and Zeitlinger, M. (2020). Incidence of ARDS and Outcomes in Hospitalized Patients with COVID-19: a Global Literature Survey. *Crit. Care* 24, 516. doi:10.1186/s13054-020-03240-7

Valko, M., Leibfritz, D., Moncol, J., Cronin, M. T., Mazur, M., and Telser, J. (2007). Free Radicals and Antioxidants in normal Physiological Functions and Human Disease. *Int. J. Biochem. Cel Biol.* 39, 44–84. doi:10.1016/j.biocel.2006.07.001

Wahn, H., and Hammerschmidt, S. (2001). Influence of Cyclooxygenase and Lipoxygenase Inhibitors on Oxidative Stress-Induced Lung Injury. *Crit. Care Med.* 29, 802–807. doi:10.1097/00003246-200104000-00025

Wang, Y. P., Wu, Y., Li, L. Y., Zheng, J., Liu, R. G., Zhou, J. P., et al. (2011). Aspirin-triggered Lipoxin A4 Attenuates LPS-Induced Pro-inflammatory Responses by Inhibiting Activation of NF-Kb and MAPKs in BV-2 Microglial Cells. *J. Neuroinflammation* 8, 95. doi:10.1186/1742-2094-8-95

Ware, L. B., and Herridge, M. (2013). Acute Lung Injury. *Semin. Respir. Crit. Care Med.* 34, 439–440. doi:10.1055/s-0033-1351163

Yadav, H., and Kor, D. J. (2015). Platelets in the Pathogenesis of Acute Respiratory Distress Syndrome. *Am. J. Physiol. Lung Cel. Mol. Physiol.* 309, L915–L923. doi:10.1152/ajplung.00266.2015

Yen, C. C., Chang, W. H., Tung, M. C., Chen, H. L., Liu, H. C., Liao, C. H., et al. (2020). Lactoferrin Protects Hyperoxia-Induced Lung and Kidney Systemic Inflammation in an *In Vivo* Imaging Model of NF-κB/Luciferase Transgenic Mice. *Mol. Imaging Biol.* 22, 526–538. doi:10.1007/s11307-019-01390-x

Yen, C. C., Lai, Y. W., Chen, H. L., Lai, C. W., Lin, C. Y., Chen, W., et al. (2011). Aerosolized Human Extracellular Superoxide Dismutase Prevents Hyperoxia-Induced Lung Injury. *PLoS One* 6, e26870. doi:10.1371/journal.pone.0026870

Zarbock, A., and Ley, K. (2009). The Role of Platelets in Acute Lung Injury (ALI). *Front. Biosci. (Landmark Ed.* 14, 150–158. doi:10.2741/3236

Zarbock, A., Singbartl, K., and Ley, K. (2006). Complete Reversal of Acid-Induced Acute Lung Injury by Blocking of Platelet-Neutrophil Aggregation. *J. Clin. Invest.* 116, 3211–3219. doi:10.1172/JCI29499

Conflict of Interest: The authors declare that the research was conducted in the absence of any commercial or financial relationships that could be construed as a potential conflict of interest.

Publisher's Note: All claims expressed in this article are solely those of the authors and do not necessarily represent those of their affiliated organizations, or those of the publisher, the editors and the reviewers. Any product that may be evaluated in this article, or claim that may be made by its manufacturer, is not guaranteed or endorsed by the publisher.

frontiers in Pharmacology

ORIGINAL RESEARCH
published: 17 January 2022
doi: 10.3389/fphar.2021.774859

Evaluation of Rhomboid Intercostal Block in Video-Assisted Thoracic Surgery: Comparing Three Concentrations of Ropivacaine

Wei Deng[1,2], *Chen-Wei Jiang*[3], *Ke-jian Qian*[1,2] *and Fen Liu*[1,2]*

[1]*Department of Critical Medicine, The First Affiliated Hospital of Nanchang University, Nanchang, China,* [2]*Medical Innovation Center, First Affiliated Hospital of Nanchang University, Nanchang, China,* [3]*Department of Anesthesiology and Pain Medicine, The Affiliated Hospital of Jiaxing University, Jiaxing, China*

Background: Ultrasound-guided rhombic intercostal block (RIB) is a novel regional block that provides analgesia for patients who have received video-assisted thoracoscopic surgery (VATS). The anesthetic characteristics of ultrasound-guided RIB with different concentrations of ropivacaine are not known. This research primarily hypothesizes that ultrasound-guided RIB, given in combination with the same volume of different concentrations of ropivacaine, would improve the whole quality of recovery-40 (QoR-40) among patients with VATS.

Approaches: This double-blinded, single-center, prospective, and controlled trial randomized 100 patients undergoing VATS to receive RIB. One hundred patients who have received elective VATS and satisfied inclusion standards were fallen into four groups randomly: control group with no RIB and $R_{0.2\%}$, $R_{0.3\%}$, and $R_{0.4\%}$; they underwent common anesthesia plus the RIB with ropivacaine at 0.2%, 0.3%, and 0.4% in a volume of 30 ml.

Outcomes: Groups $R_{0.2\%}$, $R_{0.3\%}$, and $R_{0.4\%}$ displayed great diversities in the overall QoR-40 scores and QoR-40 dimensions (in addition to psychological support) by comparing with the control group (Group C) ($p < 0.001$ for all contrasts). Groups $R_{0.3\%}$ and $R_{0.4\%}$ displayed great diversities in the overall QoR-40 scores and QoR-40 dimensions (in addition to psychological support) by comparing with the $R_{0.2\%}$ group ($p < 0.001$ for all contrasts). The overall QoR-40 scores and QoR-40 dimensions [physical comfort ($p = 0.585$)] did not vary greatly between Groups $R_{0.3\%}$ and $R_{0.4\%}$ ($p > 0.05$ for all contrasts). Groups $R_{0.2\%}$, $R_{0.3\%}$, and $R_{0.4\%}$ showed significant differences in numerical rating scales (NRS) score region under the curve (AUC) at rest and on movement in 48 h when compared with the Group C ($p < 0.001$ for all contrasts). Groups $R_{0.3\%}$ and $R_{0.4\%}$ displayed great diversities in NRS score AUC at rest and on movement in 48 h when compared with the $R_{0.2\%}$ group ($p < 0.001$ for all contrasts). The NRS mark AUC at rest and, on movement in 48 h, did not vary greatly between the Group $R_{0.3\%}$ and $R_{0.4\%}$ ($p > 0.05$ for all contrasts).

OPEN ACCESS

Edited by:
Irfan Rahman,
University of Rochester, United States

Reviewed by:
Jianfeng Xie,
Southeast University, China
Aiguo Li,
Affiliated Hospital of Guilin Medical University, China
Jian Lu,
Second Hospital of Jiaxing, China

***Correspondence:**
Fen Liu
liufen9934@163.com

Specialty section:
This article was submitted to Respiratory Pharmacology, a section of the journal Frontiers in Pharmacology

Received: *13 September 2021*
Accepted: *25 November 2021*
Published: *17 January 2022*

Citation:
Deng W, Jiang C-W, Qian K-j and Liu F (2022) Evaluation of Rhomboid Intercostal Block in Video-Assisted Thoracic Surgery: Comparing Three Concentrations of Ropivacaine. Front. Pharmacol. 12:774859. doi: 10.3389/fphar.2021.774859

Conclusion: In this study it was found that a dose of 0.3% ropivacaine is the best concentration for RIB for patients undergoing VATS. Through growing ropivacaine concentration, the analgesia of the RIB was not improved greatly.

Clinicaltrials.gov Registration: https://clinicaltrials.gov/, identifier ChiCTR2100046254.

Keywords: rhomboid intercostal blocky, quality of recovery, video-assisted thoracoscopic surgery, anesthesia, analgesic

INTRODUCTION

Post-video-helped thoracoscopic surgery (VATS) pain is a serious and ongoing widespread concern (Jung et al., 2016; Rodriguez-Aldrete et al., 2016; Umari et al., 2018). Moderate to severe pain after VATS is associated with longer hospital stays, readmissions, low patient satisfaction, increased costs, decreased quality of life, and development of chronic pain (Bendixen et al., 2016; Wang et al., 2017; Sun et al., 2020). A variety of analgesic methods have been used to reduce the intensity of acute pain after VATS, including intravenous opioids, local anesthetic drug infiltration, intercostal nerve blocks, paravertebral blocks, and thoracic epidural blocks (Piccioni et al., 2018; Umari et al., 2018; Martin and Mehran, 2019; Bai et al., 2020; Dastan et al., 2020; Taketa et al., 2020). Opioids alone appear to be effective in controlling persistent pain but not episodic pain associated with cough and movement (Hah et al., 2019; Nobel et al., 2019). This would require higher plasma levels of these drugs, which would cause the resulting side effects of sedation and hypoventilation (Umari et al., 2018), weak analgesic effect of local anesthetic infiltration, and intercostal nerve block with short analgesic duration (Kaushal et al., 2019; Sheets et al., 2020). Aravertebral blocks and thoracic epidurals can cause total spinal anesthesia and parasympathetic symptoms, leading to hypotension, bradycardia, and even cardiac arrest (Yeung et al., 2016; Taketa et al., 2020).

The rhomboid intercostal block (RIB) is a novel kind of plane block illustrated by Elsharkawy et al. (2016) recently. They found that local anesthetic spreads across the interfascial plane between the intercostal muscles, penetrates deeply into the anterior serratus muscle, and extends through the rhomboid intercostal plane to the erector spinae; this fascial block has the most significant advantage, as it covers both dorsal rami and lateral cutaneous branches of the thoracic nerves (Altıparmak et al., 2019). Recent studies have shown that RIB can provide good analgesia after VATS and that its analgesic effect is also good compared to other nerve blocks (Adderley and Mullins, 1987; Ince et al., 2020; Deng et al., 2021a; Deng et al., 2021b; Jiang et al., 2021). However, the analgesic effects of different concentrations of RIB blockade after VATS have not been reported in clinical randomized controlled trials, and in order to enable patients to receive both adequate analgesia and reduce unnecessary adverse effects of local anesthetics, we compared the analgesic effect of different concentrations of ropivacaine RIB block after VATS. The experimental study by Deng et al. (2020) used 0.2%, 0.3%, and 0.4% concentrations of ropivacaine for thoracic nerve block and were safe and effective. However, the safety of using higher concentrations of 0.5% and 0.75% ropivacaine for thoracic nerve blocks remains controversial, so 0.2%, 0.3%, and 0.4% ropivacaine were chosen for RIB blocks for the safety of patients in this experiment.

As reported in previous studies, the quality of recovery-40 (QoR-40) provides a broad and valid evaluation on patients' recovery quality after anesthesia and surgery, which can appropriately reflect the quality of postoperative recovery in a scope of clinical and study situations (Myles et al., 2000; Kim et al., 2018). Up to now, the analgesic effects of different concentrations of ropivacaine RIB after VATS were not evaluated by prospective researches with QoR-40.

In consideration of the gaps in scientific literature, this research primary aimed to compare the analgesic roles of 0.2, 0.3, and 0.4% ropivacaine after VATS by QOR-40 scores after 24 h. The secondary aim was to compare the need for 0.2, 0.3, and 0.4% ropivacaine RIB for the region under the receiver operating characteristic curve (AUC) of numerical rating scale (NRS) pain marks, postoperative opioid consumption, and rescue analgesia after VATS.

APPROACHES

Participants and Research Design

The research was a prospective, single-center, and randomized-controlled trial. This study was ethically approved by the Ethics Committee of the Affiliated Hospital of Jiaxing University (LS2021-KY-061), Jiaxing, China on April 16, 2021. The following principles summarized in the Declaration of Helsinki were performed. The registration of research protocol was made in the Chinese Clinical Trial Register (ChiCTR2100046254, links to registration documents: https://www.chictr.org.cn/edit.aspx?pid=126397&htm=4). The Chinese Clinical Trial was registered on May 12, 2021 (May 12, 2021), and patients were enrolled on May 14, 2021 (May 14, 2021). All patients who were screened and met the eligibility standards were invited to take part in the trial, and patients enrolled provided written informed consent. Patients were required to give consent on arrival at the operating room or if they were hospitalized at the night before the surgery. Inclusion standards were American Society of Anesthesiologists (ASA) grades 1–3, age 18–80 years, patients receiving general anesthesia for unilateral VATS, and no contraindications to peripheral regional anesthetic block. Exclusion standards were contraindication to local anesthesia, pre-existing infection at the block site, pre-existing chronic pain or cognitive dysfunction, and history of opioid abuse that would

prevent patients from accurately participating in postoperative quality of recovery and analgesia assessment.

Anesthesia Application

All patients were monitored in the operating room (OR) using standard ECG, non-invasive blood pressure, peripheral oxygen saturation, and dual frequency index (BIS). First, heart rate and mean arterial pressure (MAP) were measured as baseline (minute 0). After placing the 22-gage intravenous (IV) line, a 15 ml/kg/h isotonic saline IV infusion was performed among all patients under the same general anesthesia. Pre-oxygenation was employed to induce anesthesia for 3 min, and the intravenous injection of midazolam (0.05 mg/kg), sufentanil (0.5 μg/kg), propofol (2–3 mg/kg), and rocuronium (0.6 mg/kg) was made. The end-tidal carbon dioxide extent of 35–40 mmHg was kept with a double-lumen endotracheal catheter adopted for positive-pressure ventilation, and a fiber-optic bronchoscope was used to determine the correct location. During operation, the anesthesia maintenance regimen was propofol (50–150 $\mu g\,kg^{-1}\,min^{-1}$) and remifentanil ($0.1\,\mu g^{-1}\,kg^{-1}\,min^{-1}$). An anesthesiologist was employed to titrate the minimum alveolar concentration of sevoflurane, and the BIS value of between 40 and 60 was kept. Volume control ventilation was applied with the coefficients below: tidal volume, 6–8 ml/kg; respiratory rate, 12–20 beats/min; and 2 L gas with 70% oxygen and 30% air.

During anesthesia, the intravenous administration of 0.1 μg/kg sufentanil was made when the heart rate or blood pressure was 20% higher than the basic value; the administration of 0.5 mg atropine was made when the heart rate was <50 beats/min, and the intravenous injection of ringer's lactate solution of 250 ml or ephedrine of 0.1 $mg\,kg^{-1}$ was made when the blood pressure was lower than 20% of the elementary value.

The administration of granisetron 3 mg was made 30 min before the surgery, so as to stop postoperative nausea and vomiting. All patients were sent to the postanesthesia care unit (PACU) after surgery. The administration of atropine of 0.01 mg/kg and neostigmine of $0.05\,mg\,kg^{-1}$ was made to reverse the muscle relaxation role of rocuronium as required. The patients were sent to the surgery ward when they met the PACU discharging standard.

Surgical Procedures

In patients with one trochlear port, a single 3.0–4.0 cm incision was made in the fourth or fifth intercostal space of the anterior axillary line and a trochal port was inserted on the chest wall; then, the surgery procedure was performed *via* the trochal port. A thoracic drainage tube was inserted through the incision before the skin of the fourth or fifth intercostal segments was closed.

Patient Grouping and Randomization

Eligible patients were recruited by surgeons and research nurses. Patients were grouped into four, namely, group control (Group C), group $R_{0.2\%}$, $R_{0.3\%}$, and $R_{0.4\%}$, according to the ratio of 1:1:1:1 randomly. Random numbers were produced on computer and kept in sealed opaque envelopes. After the final part of the trial was randomized, the principal investigator (who would not receive any surgery) decided the four surgeons who would perform the surgery to balance the number of VATS steps for every surgeon. The main investigator or research nurse informed the surgeon of patient assignment the day before surgery and the operating room team on the day of surgery. After induction of anesthesia, RIB was done by an anesthesiologist who has experience in more than 30 cases of RIB independently. The researcher responsible for the 48-h postoperative follow-up was blind to the randomization group. In addition, during the preoperative follow-up, patients were instructed on how to apply a patient-stipulated intravenous analgesia (PCA) device for pain management and how to assess pain at rest and on movement applying the NRS scale.

Application of Block Intervention

After induction of anesthesia, RIB was conducted according to the past description (Elsharkawy et al., 2016). A high-frequency linear ultrasonic probe (LOGIQ e ultrasound system, Deutschland GmbH and Co. KG, Solingen, Germany) was used. The medial placement of oblique sagittal plane was made on the medial margin of the scapula. Ultrasound identified trapezius, intercostal, rhomboid, pleura, and lung markers. Under aseptic conditions, the insertion of an 80-mm gauge 21 needle was conducted at the ultrasonic section T5–6. In the group $R_{0.2\%}$, the injection of a dose of 30 ml of 0.2% ropivacaine was performed in the fascial plane between the rhomboid and intercostal muscles; in the group $R_{0.3\%}$, the injection of a dose of 30 ml 0.3% ropivacaine was performed in the fascial plane between the rhomboid and intercostal muscles; and in the group $R_{0.4\%}$, the injection of a single dose of 30 ml 0.4% ropivacaine was performed in the fascial plane between the rhomboid and intercostal muscles. The diffusion of local anesthetic fluid under rhomboid muscle was observed by ultrasound.

Analgesic Protocol and Assessment of Pain and Sensorial Block

In the PACU, all patients underwent patient-stipulated intravenous analgesia (PCIA): 150 μg sufentanil with a total of 150 ml, loading dose of 2 ml, background dose of 2 ml, and locking time of 15 min. Another blinded anesthesiologist made pain evaluation, about 30 min after being blocked with the 11-point NRS, ranging from 0 (no pain) to 10 (worst pain imaginable). In the surgical ward, the postoperative assessment of patients was made again at 0.5, 1, 3, 6, 12, 18, 24, 36, and 48 h. In case of the NRS mark of >3, the physician pressed the analgesia pump once and evaluate pain after 15 min. If the NRS mark was >3 continuously, the physician pressed the analgesia pump again. Rescue analgesia was made on basis of the anesthesiologist's estimate with parecoxib sodium of 40 mg.

Outcome Methods

This research held the main results of the overall QoR-40 scores 24 h after surgery between the four groups. There were a total of 40 questions for the assessment of five rehabilitation areas in this questionnaire: 12 items about physical comfort, 9 items about emotional state, 5 items about physical independence, 7 item

about psychological support, and 7 item about pain (Kim et al., 2018). The secondary result methods were AUC of the NRS for pain at rest and on movement over 48 h, time of first postoperative analgesic request, postoperative 48-h opioid dosage, and satisfaction mark of patients (1–10, where 10 is the highest). Except these methods, dosage of propofol and remifentanil, PACU duration, postoperative nausea and vomiting (PONV), and total number of patients with a postoperative complication were put into record.

Sample Size

The Power Exploration and Sample Size (PASS) 15.0 program (NCSS, LLC., Kaysville, UT, United States) was adopted to calculate the sample size of this research. Based on past researches, the 10-point diversities in QoR-40 marks between the group $R_{0.2\%}$ and group $R_{0.4\%}$ was considered clinically important (Myles et al., 2018; Altıparmak et al., 2020). On the basis of our preliminary research on 20 patients, the QoR-40 mark of group $R_{0.2\%}$ was 164.7 ± 5.5, and the QoR-40 mark of the group $R_{0.4\%}$ was 170.3 ± 5.9. Assuming α error = 0.05 (two-tailed), β error = 0.1 with a power of 0.90, at least 23 participants were required per group, considering the 20% dropout rate (on basis of a preliminary research); while increasing the sample scale, the research finally included 29 patients in every group.

Statistical Exploration

SPSS version 25.0 (IBM Corp., Armonk, NY, United States) was adopted for data analysis. For every patient, the time interval with the NRS score was multiplied to calculate their AUC of NRS pain marks both on movement and at rest with GraphPad Prism version 7 (GraphPad Software Inc., San Diego, CA, United States). Continuous data were examined and tested for distribution with the Shapiro–Wilk test. One-way analysis of variance was adopted to explore normally distributed data for the comparison of group-wise diversities in the result coefficients [BMI, age, operation time, anesthesia time, remifentanil dosage, propofol dosage, preoperative QoR-40 mark, QoR-40 mark, physical comfort, emotional state, psychological support, physical independence, pain, the NRS mark curve (AUC) for pain at rest and on movement, time to first postoperative analgesic request, PACU duration, postoperative 48-h total amount of opioids, satisfaction score of patients, and parecoxib sodium for injections]. Normally distributed data are shown as mean ± standard deviation. The diversities among male/female, ASAI/II/III, total number of patients with a postoperative complication, operation procedure, and surgical incision (left chest/right chest) were compared with the chi-square test. Operation procedure and PONV scores were analyzed using Kruskal–Wallis test, and a 5-point numerical scale (0 = no symptom, 1 = scarcely, 2 = usually, 3 = most of the time, 4 = all the time) was adopted to assess PONV. p-values <0.05 were regarded significant for the test outcomes displayed.

RESULTS

The flowchart for reporting trials of the consolidated standards is shown in **Figure 1**. One hundred thirty patients were initially enrolled, out of which 10 patients did not satisfy the inclusion standards, four patients rejected to take part in, and 116 patients were eventually categorized into four groups. Five patients in the Group C were excluded due to uncompleted QoR-40 scores and PCA failure. Three patients in the group $R_{0.2\%}$ were excluded due to uncompleted QoR-40 scores. Four patients in the group $R_{0.3\%}$ were excluded because of uncompleted QoR-40 scores and PCA failure. Four patients in the group $R_{0.4\%}$ were excluded due to failure to complete QoR-40 scores and PCA failure. Therefore, 24 patients in the Group C, 26 patients in the group $R_{0.2\%}$, 25 patients in the group $R_{0.3\%}$, and 25 patients in the group $R_{0.4\%}$ were analyzed.

No diversities were observed in the baseline features between the groups (**Table 1**). QOR-40 scores are shown in **Table 2**. A great diversity was found between the mean global QoR-40 marks of the groups. Scores of all QoR-40 dimensions (except psychological support) varied statistically among four groups. Groups $R_{0.2\%}$, $R_{0.3\%}$, and $R_{0.4\%}$ displayed great diversities in the overall QoR-40 scores and QoR-40 dimensions (except psychological support) when compared with the Group C (p < 0.001 for all contrasts). Group $R_{0.3\%}$ and $R_{0.4\%}$ displayed great diversities in the overall QoR-40 scores and QoR-40 dimensions (except psychological support) when compared to the $R_{0.2\%}$ group (p < 0.001for all comparisons). The global QoR-40 scores (p = 0.054) and QoR-40 dimensions [physical comfort (p = 0.585), emotional status (p = 0.101), physical independence (p = 0.731), pain (p = 0.306)] did not vary greatly between the groups $R_{0.3\%}$ and $R_{0.4\%}$.

The difference in NRS score AUC at rest and on movement in 48 h was statistically significant in both groups (**Table 3**). Groups $R_{0.2\%}$, $R_{0.3\%}$, and $R_{0.4\%}$ displayed great diversities in NRS score AUC at rest and on movement in 48 h when compared with the Group C (p < 0.001 for all contrasts). Group $R_{0.3\%}$ and $R_{0.4\%}$ displayed great diversities in NRS score AUC at rest and on movement in 48 h when compared with the $R_{0.2\%}$ group (p < 0.001 for all contrasts). The NRS score AUC at rest and on movement in 48 h did not vary greatly between the Group $R_{0.3\%}$ and $R_{0.4\%}$ (p > 0.05 for all contrasts).

Time of first postoperative analgesic request, postoperative 48-h total amount of opioids, parecoxib sodium for injections, and satisfaction score of patients in the groups $R_{0.2\%}$, $R_{0.3\%}$, and $R_{0.4\%}$ displayed great diversities when compared with the group C (p < 0.001 for all contrasts) (**Figures 2A–D**), and time to first postoperative analgesic request, postoperative 48-h total amount of opioids, parecoxib sodium for injections, and satisfaction score of patients in the $R_{0.3\%}$ and $R_{0.4\%}$ also displayed great diversities when compared with Group $R_{0.2\%}$, (p < 0.001 for all contrasts) (**Figures 2A–D**). The time to first postoperative analgesic request (p = 0.5), postoperative 48-h total amount of opioids (p = 0.526), parecoxib sodium for injections (p = 0.750), and satisfaction score of patients (p = 0.671) did not vary greatly between the groups $R_{0.3\%}$ and $R_{0.4\%}$.

Groups $R_{0.2\%}$, $R_{0.3\%}$, and $R_{0.4\%}$ displayed great diversities in the dose of propofol and remifentanil applied and recovery room duration when compared to the Group C (p < 0.001 for all contrasts) (**Table 4**). Groups $R_{0.3\%}$ and $R_{0.4\%}$ displayed great diversities in the dose of propofol and remifentanil applied and recovery room duration when compared to the $R_{0.2\%}$ group (p <

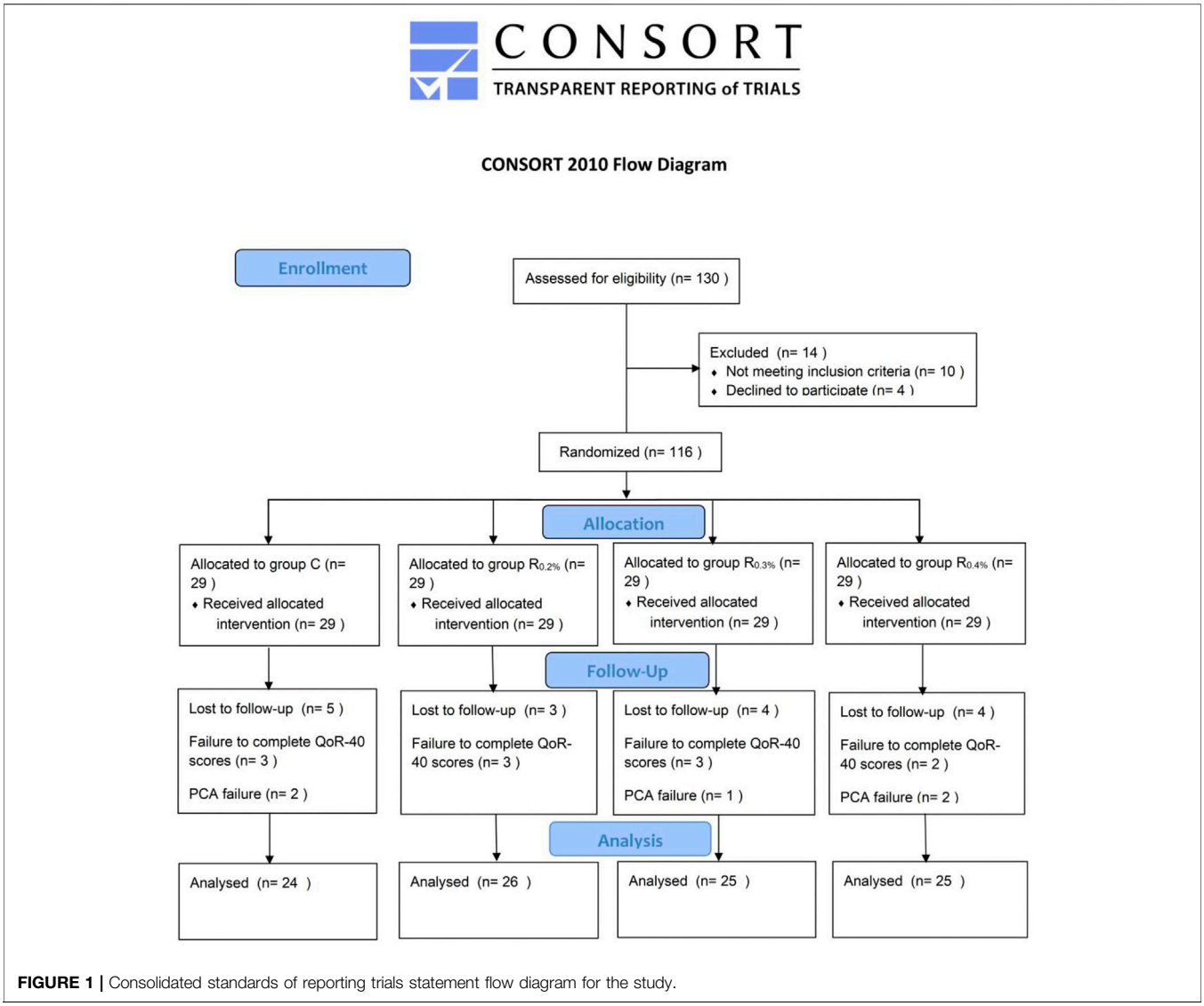

FIGURE 1 | Consolidated standards of reporting trials statement flow diagram for the study.

TABLE 1 | Descriptive variable characteristics of patients in four groups ($\bar{x}$ ± SD).

	Group C	Group $R_{0.2\%}$	Group $R_{0.3\%}$	Group $R_{0.4\%}$	*p* value
Sample size, n	24	26	25	25	
Age (years)	70.0 ± 4.7	66.6 ± 5.2	67.1 ± 5.1	68.3 ± 4.7	0.604*
Gender (male/female)	12/12	14/12	14/11	14/11	0.972#
BMI (kg/m^2)	23.2 ± 3.4	24.1 ± 3.4	23.2 ± 2.6	22.7 ± 2.1	0.295*
Procedure duration (min)	109.1 ± 28.8	104.5 ± 21.7	105.9 ± 25.5	105.8 ± 26.0	0.608*
Duration of anesthesia (min)	130.6 ± 40.7	126.0 ± 23.2	127.2 ± 37.0	125.8 ± 30.2	0.062*
ASA class I/II/III	2/18/4	3/19/4	2/20/3	3/19/3	0.994#
Surgical incision (left/right)	8/16	8/18	10/15	10/15	0.866#
Pre-QoR-40 score	182.4 ± 4.7	181.6 ± 3.9	181.3 ± 3.3	181.8 ± 3.8	0.804*
Operation procedure					0.996**
Wedge resection	15 (63%)	17 (65%)	14 (56%)	16 (64%)	—
Bullectomy	7 (29%)	8 (31%)	9 (36%)	8 (32%)	—
Lobectomy	2 (8%)	1 (4%)	2 (8%)	1 (4%)	—

*Statistical tests: *p value is obtained with one-way analysis of variance. #p value is obtained with Pearson's $\chi 2$ test. **p value is obtained with Kruskal-Wallis test.*

TABLE 2 | Global and dimension QoR-40 questionnaire score at 24th hour after operation in four groups ($\bar{x}$ ±SD).

	Group C	Group $R_{0.2\%}$	Group $R_{0.3\%}$	Group $R_{0.4\%}$	*p* value
Sample size, n	24	26	*25*	25	
Global QoR-40 score	151.7 ± 3.8	164.3 ± 3.8	172.8 ± 3.4	174.6 ± 2.4	<0.001*
Physical comfort	43.8 ± 2.9	49.5 ± 1.9	50.7 ± 1.8	51.0 ± 1.5	<0.001*
Emotional status	34.3 ± 2.1	37.2 ± 1.5	38.9 ± 1.9	39.8 ± 1.7	<0.001*
Physical independence	19.8 ± 1.7	20.4 ± 2.3	21.6 ± 1.1	21.8 ± 1.1	<0.001*
Psychological support	29.9 ± 1.3	30.2 ± 1.4	30.4 ± 1.4	30.5 ± 1.3	0.440*
Pain	23.9 ± 1.6	27.1 ± 1.7	31.2 ± 1.1	31.6 ± 1.0	<0.001*

*Statistical tests: Statistical tests: *p value is obtained with one-way analysis of variance.*

TABLE 3 | The AUC pain NRS vs time at rest and on movement of four groups ($\bar{x}$ ± SD).

	Group C	Group $R_{0.2\%}$	Group $R_{0.3\%}$	Group $R_{0.4\%}$	*p* value
Sample size, n	24	26	*25*	*25*	
AUC pain NRS vs. time (at rest)					
0–6 h postoperatively	7.2 ± 1.4	4.9 ± 1.4	3.1 ± 1.6	2.4 ± 1.5	<0.001*
0–12 h postoperatively	23.4 ± 3.0	17.4 ± 2.3	12.9 ± 2.4	11.4 ± 2.9	<0.001*
0–24 h postoperatively	59.7 ± 5.2	45.8 ± 5.0	32.6 ± 4.7	29.8 ± 5.8	<0.001*
0–48 h postoperatively	116.9 ± 8.5	94.2 ± 8.0	70.4 ± 8.1	64.4 ± 10.3	<0.001*
AUC pain NRS vs. time (on movement)					
0–6 h postoperatively	17.3 ± 2.1	11.1 ± 1.4	8.8 ± 1.5	7.9 ± 1.4	<0.001*
0–12 h postoperatively	55.2 ± 3.5	40.3 ± 4.3	31.5 ± 2.7	29.9 ± 3.1	<0.001*
0–24 h postoperatively	119.9 ± 6.0	95.7 ± 7.4	74.5 ± 4.8	71.6 ± 5.4	<0.001*
0–48 h postoperatively	211.9 ± 11.6	170.7 ± 11.4	136.6 ± 7.5	129.7 ± 8.9	<0.001*

*Statistical tests: *p value is obtained with one-way analysis of variance.*

0.001 for all comparisons). The dose of propofol ($p = 0.562$) and remifentanil ($p = 0.498$) used and recovery room duration ($p = 0.664$) did not vary greatly between the groups $R_{0.3\%}$ and $R_{0.4\%}$. No great diversities were shown in PONV scores ($p = 0.851$ for all contrasts) and total number of patients with a postoperative complication ($p = 0.924$ for all contrasts) among the four groups (**Table 5**).

DISCUSSION

This is the first randomized, double-blind clinical trial that compared different concentrations of ropivacaine RIB block in VATS with the patient-centered result method, QoR-40. A clinically meaningful improvement was shown in QoR at 24 h for patients who underwent 0.3% ropivacaine RIB in comparison with a 0.2% ropivacaine RIB. Furthermore, 0.3% ropivacaine RIB had a smaller burden of pain over time (AUC of NRS) at rest and on movement and less total amount of opioids. The highest concentration of ropivacaine (0.4%) did not show a great merit in terms of postoperative analgesia applying the RIB.

A current international movement uses more patient-centered results in assessing the effectiveness of anesthetic interventions. While lower pain marks are significant, patients may not consider it an excellent recovery experience with other debilitating side effects. The QoR-40 scores are internationally recognized as a valid method to assess patients' quality of recovery after surgery (Kim et al., 2018).

To the best of our ability to review the literature, this trial is the first to assess the effectiveness of various concentrations of ropivacaine RIB in postoperative analgesia in thoracic surgery using QoR-40. Deng et al. (2020) found that 0.3% ropivacaine was the best concentration for pectoral nerve block type II (PECS II block) among patients who have received modified radical mastectomy (MRM) for breast cancer and that a 0.3% concentration provided effective analgesia for MRM for 48 h. Increasing the concentration of ropivacaine did not significantly enhance the analgesic effect of the PECS II block. Su et al. (2015) found that in ultrasound-guided regional anesthesia, growing the concentration of ropivacaine at the same volume led to a progressive growth in analgesia, and 0.4% ropivacaine was not superior to 0.3% ropivacaine in terms of analgesia. At the same time, increasing the blood concentration of ropivacaine may increase the risk of neurotoxicity. Some investigators have applied *in vivo* or *ex vivo* animal models to study the neurotoxicity of local anesthetics, and both showed a concentration-dependent effect on the degree of nerve damage, with higher concentrations resulting in more severe damage. However, it remains to be further studied clinically as to which concentrations are also associated with which adverse effects. In the present experiment, no serious adverse reactions were observed with RIB blockade at 0.2%, 0.3%, and 0.4% concentrations of ropivacaine (Brull et al., 2007).

Our findings, by comparing the QoR-40 scores of 0.2%, 0.3%, and 0.4% ropivacaine RIB, were similar to theirs, but their assessed result was confined to pain severity and time to postoperative opioid demands. Our study showed that improvement of QoR-40 scores after VATS by RIB with

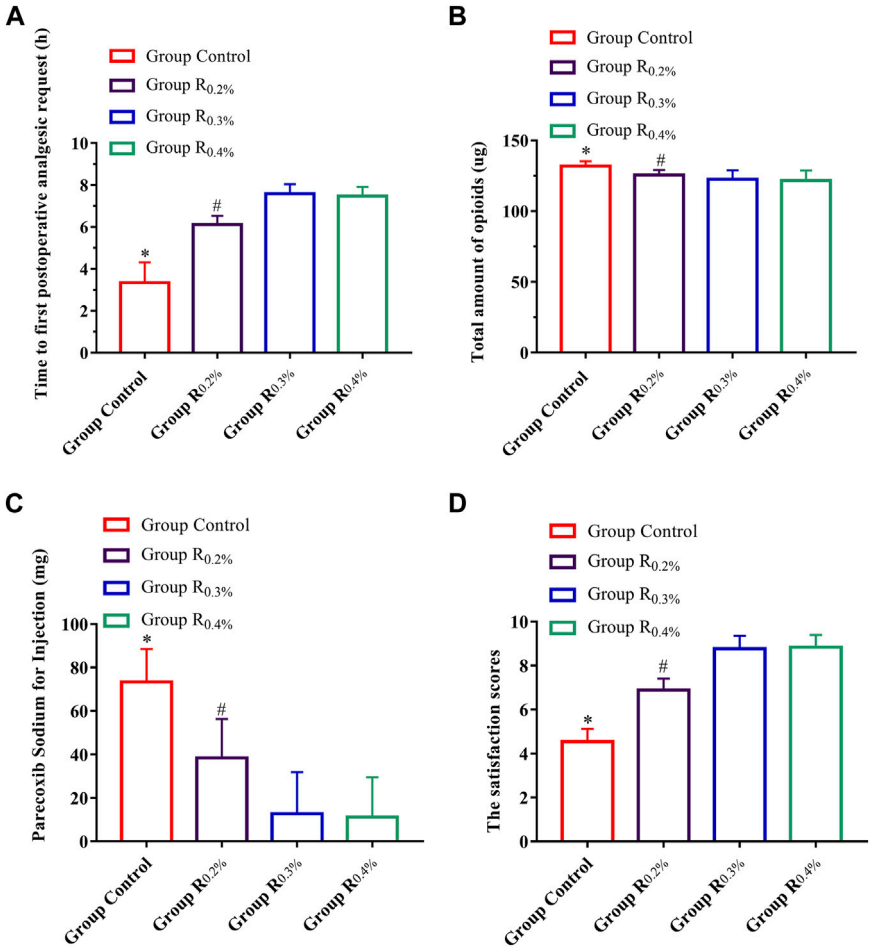

FIGURE 2 | (A). Time to first postoperative analgesic request, **(B)**. Postoperative 48-h total amount of opioids, **(C)**. Parecoxib sodium for injections, **(D)**. Satisfaction score of patients.*$p < 0.05$ compared with $R_{0.2\%}$, $R_{0.3\%}$, and $R_{0.4\%}$ groups, #$p < 0.05$ compared with $R_{0.3\%}$ and $R_{0.4\%}$ groups.

TABLE 4 | Intraoperative anesthetic dosage, postoperative analgesic, and recovery of four groups ($\bar{x}$ ± SD).

	Group C	Group $R_{0.2\%}$	Group $R_{0.3\%}$	Group $R_{0.4\%}$	*p*-value
Sample size, n	24	26	*25*	25	
Remifentanil (μg)	463.8 ± 77.2	415.4 ± 52.8	353.6 ± 64.9	341.2 ± 61.8	<0.001*
Propofol (mg)	477.9 ± 78	421.9 ± 59.7	341.2 ± 74.9	329.2 ± 78.0	<0.001*
PACU duration (min)	22.4 ± 5.0	18.2 ± 2.5	15.6 ± 1.3	15.3 ± 1.3	<0.001*
PONV scores, n (%)					0.851**
0	12	15	17	18	
1	4	7	8	7	
2	5	3	0	0	
3	2	1	0	0	
4	1	0	0	0	

PONV was assessed using a 5-point numerical scale (0 = no symptom, 1 = scarcely, 2 = usually, 3 = most of the time, 4 = all the time).

*p *value is obtained with one-way analysis of variance.*

#p *value is obtained with Pearson's* χ^2 *test.*

**p *PONV scores were analyzed using Kruskal–Wallis test*

ropivacaine relied on the concentration of ropivacaine; 0.2% ropivacaine did not improve QoR-40 scores after VATS, and 0.3% ropivacaine RIB improved QoR-40 scores significantly after VATS in patients, but when the concentration of ropivacaine was increased to 0.4% VATS, there was no great change in QoR-40 scores in patients after surgery.

TABLE 5 | Postoperative complications in four groups ($\bar{x}$ ± SD).

	Group C	Group $R_{0.2\%}$	Group $R_{0.3\%}$	Group $R_{0.4\%}$	*p*-value
Sample size, n	24	26	25	25	
Total number of patients with a postoperative complication	3	2	2	2	0.924[#]
Postoperative pneumonia	0	1	1	1	
Surgical site infection	0	0	0	0	
Recurrent pneumothorax/air leak requiring further intervention	1	0	0	0	
Arrhythmia	1	0	0	0	
Bleeding requiring transfusion	1	1	1	2	
Unplanned ICU admission	0	0	0	0	
Acute kidney injury	0	0	0	0	

Statistical tests: [#]p value is obtained with Pearson's χ^2 test.

Most of the existing methods focus on minimizing the loss of sample pairs. However, in many applications, the number of intra- and interclass sample pairs may be highly unbalanced, which may lead to deteriorating or suboptimal performance, and for such unbalanced distribution problems, AUC can be considered as a more meaningful performance metric (Huo et al., 2018). Therefore, in this study, we used AUC to count NRS scores over 48 h. Then, we found that the AUC of NRS in 48 h was significantly improved with 0.3% ropivacaine as compared to 0.2% ropivacaine; however, no great change was found in the AUC of NRS when it was increased to 0.4%. In addition, time of first postoperative analgesic request, recovery time, postoperative 48-h opioid dosage, and satisfaction score of patients can also be proved. At 0.2% ropivacaine RIB, the patient's time to first postoperative analgesic request is short, postoperative 48-h opioid dosage is large, the injection amount of parecoxib sodium is large, and the patient satisfaction is also low. When the ropivacaine concentration grew to 0.3%, there was a significant improvement, but when the ropivacaine concentration grew to 0.4%, there was no significant change.

It is also important to note that in this trial, when comparing the AUC of NRS scores at 0–48 h between the four groups, in order to compensate for the true number of patients in Group C, Group $R_{0.3\%}$, and Group $R_{0.4\%}$, we used the mean of the NRS in each group to replace the number of patients missing, with two patients missing in Group C and one patient each in Group $R_{0.3\%}$ and Group $R_{0.4\%}$.

Our study has some restrictions. First, a sham block was not given to the control group due to the ethical considerations of making an injection with no administration of a therapeutic drug. Second, no concentration gradient was used to decrease the number of groups and false-negative outcomes from various comparisons; ropivacaine studies at higher concentrations were not performed. Third, there was no measurement of plasma ropivacaine levels at various concentrations; although past studies have not reported any RIB-related adverse reactions, pharmacokinetic studies were not performed.

CONCLUSION

In this study, it was found that a dose of 0.3% ropivacaine is the best concentration for the RIB for patients who have received VATS. Through increasing ropivacaine concentration, the analgesia of the RIB was not improved greatly.

DATA AVAILABILITY STATEMENT

The raw data supporting the conclusion of this article will be made available by the authors, without undue reservation.

AUTHOR CONTRIBUTIONS

WD contributed to the study design, data collection, and recruitment of study patients after randomization. FL contributed to the statistical analysis, data collection, and recruitment of study patients after randomization. C-WJ recruited study patients after randomization. K-JQ drafted the manuscript and gave final approval of the version to be published. All the authors reviewed the final manuscript.

REFERENCES

Adderley, R. J., and Mullins, G. C. (1987). When to Extubate the Croup Patient: the "leak" Test. *Can. J. Anaesth.* 34 (3 (Pt 1)), 304–306. doi:10.1007/BF03015171

Altıparmak, B., Korkmaz Toker, M., Uysal, A. I., Dere, Ö., and Uğur, B. (2020). Evaluation of Ultrasound-Guided Rhomboid Intercostal Nerve Block for Postoperative Analgesia in Breast Cancer Surgery: a Prospective, Randomized Controlled Trial. *Reg. Anesth. Pain Med.* 45 (4), 277–282. doi:10.1136/rapm-2019-101114

Altıparmak, B., Korkmaz Toker, M., Uysal, A. İ., Turan, M., and Gümüş Demirbilek, S. (2019). The Usage of Single-Shot Ultrasound Guided Rhomboid Intercostal Block for Analgesia after Thoracotomy: Clinical Experience in Two Patients. *J. Clin. Anesth.* 56, 98–99. doi:10.1016/j.jclinane.2019.01.032

Bai, J. W., An, D., Perlas, A., and Chan, V. (2020). Adjuncts to Local Anesthetic Wound Infiltration for Postoperative Analgesia: a Systematic Review. *Reg. Anesth. Pain Med.* 45 (8), 645–655. doi:10.1136/rapm-2020-101593

Bendixen, M., Jørgensen, O. D., Kronborg, C., Andersen, C., and Licht, P. B. (2016). Postoperative Pain and Quality of Life after Lobectomy via Video-Assisted Thoracoscopic Surgery or Anterolateral Thoracotomy for Early Stage Lung Cancer: a Randomised Controlled Trial. *Lancet Oncol.* 17 (6), 836–844. doi:10.1016/S1470-2045(16)00173-X

Brull, R., Mccartney, C. J., Chan, V. W., and El-Beheiry, H. (2007). Neurological Complications after Regional Anesthesia: Contemporary Estimates of Risk. *Anesth. Analg* 104, 965–974. doi:10.1213/01.ane.0000258740.17193.ec

Dastan, F., Langari, Z. M., Salamzadeh, J., Khalili, A., Aqajani, S., and Jahangirifard, A. (2020). A Comparative Study of the Analgesic Effects of Intravenous Ketorolac, Paracetamol, and Morphine in Patients Undergoing Video-Assisted Thoracoscopic Surgery: A Double-Blind, Active-Controlled, Randomized Clinical Trial. *Ann. Card. Anaesth.* 23 (2), 177–182. doi:10.4103/aca.ACA_239_18

Deng, W., Fu, D., and He, L. (2020). Evaluation of Pectoral Nerve Block in Modified Radical Mastectomy: Comparison of Three Concentrations of Ropivacaine. *Clin. Interv. Aging* 15, 937–944. doi:10.2147/CIA.S251613

Deng, W., Hou, X. M., Zhou, X. Y., and Zhou, Q. H. (2021). Rhomboid Intercostal Block Combined with Sub-serratus Plane Block versus Rhomboid Intercostal Block for Postoperative Analgesia after Video-Assisted Thoracoscopic Surgery: a Prospective Randomized-Controlled Trial. *BMC Pulm. Med.* 21 (1), 68. doi:10.1186/s12890-021-01432-7

Deng, W., Liu, F., Jiang, W. C., Sun, Y., Shi, G. P., and Zhou, Q. H. (2021). Continuous Rhomboid Intercostal Nerve Block for Thoracoscopic Postoperative Analgesia. *Ann. Thorac. Surg.*, S0003-4975(21)01299-6 doi:10.1016/j.athoracsur.2021.06.068

Elsharkawy, H., Saifullah, T., Kolli, S., and Drake, R. (2016). Rhomboid Intercostal Block. *Anaesthesia* 71 (7), 856–857. doi:10.1111/anae.13498

Hah, J. M., Cramer, E., Hilmoe, H., Schmidt, P., McCue, R., Trafton, J., et al. (2019). Factors Associated with Acute Pain Estimation, Postoperative Pain Resolution, Opioid Cessation, and Recovery: Secondary Analysis of a Randomized Clinical Trial. *JAMA Netw. Open* 2 (3), e190168. doi:10.1001/jamanetworkopen.2019.0168

Huo, J., Gao, Y., Shi, Y., and Yin, H. (2018). Cross-Modal Metric Learning for AUC Optimization. *IEEE Trans. Neural Netw. Learn. Syst.* 29 (10), 4844–4856. doi:10.1109/TNNLS.2017.2769128

Ince, I., Naldan, M. E., Ozmen, O., and Aydin, Y. (2020). Ultrasound Guided Rhomboid Intercostal Plane Block for a 7-Year-Old Boy for Postoperative Thoracotomy Pain. *J. Clin. Anesth.* 60, 85–86. doi:10.1016/j.jclinane.2019.08.045

Jiang, C. W., Liu, F., Zhou, Q., and Deng, W. (2021). Comparison of Rhomboid Intercostal Nerve Block, Erector Spinae Plane Block and Serratus Plane Block on Analgesia for Modified Radical Mastectomy: A Prospective Randomised Controlled Trial. *Int. J. Clin. Pract.* 75, e14539. doi:10.1111/ijcp.14539

Jung, J., Park, S. Y., and Haam, S. (2016). Efficacy of Subpleural Continuous Infusion of Local Anesthetics after Thoracoscopic Pulmonary Resection for Primary Lung Cancer Compared to Intravenous Patient-Controlled Analgesia. *J. Thorac. Dis.* 8 (7), 1814–1819. doi:10.21037/jtd.2016.06.16

Kaushal, B., Chauhan, S., Saini, K., Bhoi, D., Bisoi, A. K., Sangdup, T., et al. (2019). Comparison of the Efficacy of Ultrasound-Guided Serratus Anterior Plane Block, Pectoral Nerves II Block, and Intercostal Nerve Block for the Management of Postoperative Thoracotomy Pain after Pediatric Cardiac Surgery. *J. Cardiothorac. Vasc. Anesth.* 33 (2), 418–425. doi:10.1053/j.jvca.2018.08.209

Kim, D. H., Oh, Y. J., Lee, J. G., Ha, D., Chang, Y. J., and Kwak, H. J. (2018). Efficacy of Ultrasound-Guided Serratus Plane Block on Postoperative Quality of Recovery and Analgesia after Video-Assisted Thoracic Surgery: A Randomized, Triple-Blind, Placebo-Controlled Study. *Anesth. Analg* 126 (4), 1353–1361. doi:10.1213/ANE.0000000000002779

Martin, L. W., and Mehran, R. J. (2019). Intercostal Nerve Blockade for Thoracic Surgery with Liposomal Bupivacaine: the Devil Is in the Details. *J. Thorac. Dis.* 11 (Suppl. 9), S1202–S1205. doi:10.21037/jtd.2019.03.62

Myles, P. S., Boney, O., Botti, M., Cyna, A. M., Gan, T. J., Jensen, M. P., et al. (2018). Systematic Review and Consensus Definitions for the Standardised Endpoints in Perioperative Medicine (StEP) Initiative: Patient comfort. *Br. J. Anaesth.* 120 (4), 705–711. doi:10.1016/j.bja.2017.12.037

Myles, P. S., Weitkamp, B., Melick, K. J., and Hensen, S. (2000). Validity and Reliability of a Postoperative Quality of Recovery Score: the QoR-40. *Br. J. Anaesth.* 84 (1), 11–15. doi:10.1093/oxfordjournals.bja.a013366

Nobel, T. B., Adusumilli, P. S., and Molena, D. (2019). Opioid Use and Abuse Following Video-Assisted Thoracic Surgery (VATS) or Thoracotomy Lung Cancer Surgery. *Transl Lung Cancer Res.* 8 (Suppl. 4), S373–S377. doi:10.21037/tlcr.2019.05.14

Piccioni, F., Segat, M., Falini, S., Umari, M., Putina, O., Cavaliere, L., et al. (2018). Enhanced Recovery Pathways in Thoracic Surgery from Italian VATS Group: Perioperative Analgesia Protocols. *J. Thorac. Dis.* 10 (Suppl. 4), S555–S563. doi:10.21037/jtd.2017.12.86

Rodriguez-Aldrete, D., Candiotti, K. A., Janakiraman, R., and Rodriguez-Blanco, Y. F. (2016). Trends and New Evidence in the Management of Acute and Chronic Post-Thoracotomy Pain-An Overview of the Literature from 2005 to 2015. *J. Cardiothorac. Vasc. Anesth.* 30 (3), 762–772. doi:10.1053/j.jvca.2015.07.029

Sheets, N. W., Davis, J. W., Dirks, R. C., Pang, A. W., Kwok, A. M., Wolfe, M. M., et al. (2020). Intercostal Nerve Block with Liposomal Bupivacaine vs Epidural Analgesia for the Treatment of Traumatic Rib Fracture. *J. Am. Coll. Surg.* 231 (1), 150–154. doi:10.1016/j.jamcollsurg.2019.12.044

Su, Y., Zhang, Z., Zhang, Y., Li, H., and Shi, W. (2015). Efficacy of Ropivacaine by the Concentration of 0.25%, 0.5%, and 0.75% on Surgical Performance, Postoperative Analgesia, and Patient's Satisfaction in Inguinal Hernioplasty: a Randomized Controlled Trial. *Patient Prefer Adherence* 9, 1375–1379. doi:10.2147/PPA.S93276

Sun, K., Liu, D., Chen, J., Yu, S., Bai, Y., Chen, C., et al. (2020). Moderate-severe Postoperative Pain in Patients Undergoing Video-Assisted Thoracoscopic Surgery: A Retrospective Study. *Sci. Rep.* 10 (1), 795. doi:10.1038/s41598-020-57620-8

Taketa, Y., Irisawa, Y., and Fujitani, T. (2020). Comparison of Ultrasound-Guided Erector Spinae Plane Block and Thoracic Paravertebral Block for Postoperative Analgesia after Video-Assisted Thoracic Surgery: a Randomized Controlled Non-inferiority Clinical Trial. *Reg. Anesth. Pain Med.* 45 (1), 10–15. doi:10.1136/rapm-2019-100827

Umari, M., Carpanese, V., Moro, V., Baldo, G., Addesa, S., Lena, E., et al. (2018). Postoperative Analgesia after Pulmonary Resection with a Focus on Video-Assisted Thoracoscopic Surgery. *Eur. J. Cardiothorac. Surg.* 53 (5), 932–938. doi:10.1093/ejcts/ezx413

Wang, H., Li, S., Liang, N., Liu, W., Liu, H., and Liu, H. (2017). Postoperative Pain Experiences in Chinese Adult Patients after Thoracotomy and Video-Assisted Thoracic Surgery. *J. Clin. Nurs.* 26 (17-18), 2744–2754. doi:10.1111/jocn.13789

Yeung, J. H., Gates, S., Naidu, B. V., Wilson, M. J., and Gao Smith, F. (2016). Paravertebral Block versus Thoracic Epidural for Patients Undergoing Thoracotomy. *Cochrane Database Syst. Rev.* 2, CD009121. doi:10.1002/14651858.CD009121.pub2

Conflict of Interest: The authors declare that the research was conducted in the absence of any commercial or financial relationships that could be construed as a potential conflict of interest.

Publisher's Note: All claims expressed in this article are solely those of the authors and do not necessarily represent those of their affiliated organizations, or those of the publisher, the editors, and the reviewers. Any product that may be evaluated in this article, or claim that may be made by its manufacturer, is not guaranteed or endorsed by the publisher.

frontiers in Pharmacology

ORIGINAL RESEARCH
published: 22 February 2022
doi: 10.3389/fphar.2022.835848

House Dust Mite Aeroallergen Suppresses Leukocyte Phagocytosis and Netosis Initiated by Pneumococcal Lung Infection

*Angelica Papanicolaou[1], Hao Wang[1], Jonathan McQualter[1], Christian Aloe[1], Stavros Selemidis[1], Catherine Satzke[2,3,4], Ross Vlahos[1] and Steven Bozinovski[1]**

[1]School of Health and Biomedical Sciences, RMIT University, Bundoora, VIC, Australia, [2]Translational Microbiology Group, Murdoch Children's Research Institute, Parkville, VIC, Australia, [3]Department of Paediatrics, The University of Melbourne, Parkville, VIC, Australia, [4]Department of Microbiology and Immunology, The Peter Doherty Institute for Infection and Immunity, The University of Melbourne, Melbourne, VIC, Australia

OPEN ACCESS

Edited by:
Irfan Rahman, University of Rochester, United States

Reviewed by:
Xingbin Ai, Massachusetts General Hospital and Harvard Medical School, United States
Brian Gregory George Oliver, University of Technology Sydney, Australia

***Correspondence:**
Steven Bozinovski
steven.bozinovski@rmit.edu.au

Specialty section:
This article was submitted to Respiratory Pharmacology, a section of the journal Frontiers in Pharmacology

Received: *15 December 2021*
Accepted: *09 February 2022*
Published: *22 February 2022*

Citation:
Papanicolaou A, Wang H, McQualter J, Aloe C, Selemidis S, Satzke C, Vlahos R and Bozinovski S (2022) House Dust Mite Aeroallergen Suppresses Leukocyte Phagocytosis and Netosis Initiated by Pneumococcal Lung Infection. Front. Pharmacol. 13:835848. doi: 10.3389/fphar.2022.835848

Asthmatics are highly susceptible to developing lower respiratory tract infections caused by *Streptococcus pneumoniae* (SPN, the pneumococcus). It has recently emerged that underlying allergic airway disease creates a lung microenvironment that is defective in controlling pneumococcal lung infections. In the present study, we examined how house dust mite (HDM) aeroallergen exposure altered immunity to acute pneumococcal lung infection. Alveolar macrophage (AM) isolated from HDM-exposed mice expressed alternatively activated macrophage (AAM) markers including YM1, FIZZ1, IL-10, and ARG-1. *In vivo*, prior HDM exposure resulted in accumulation of AAMs in the lungs and 2-log higher bacterial titres in the bronchoalveolar (BAL) fluid of SPN-infected mice (Day 2). Acute pneumococcal infection further increased the expression of IL-10 and ARG1 in the lungs of HDM-exposed mice. Moreover, prior HDM exposure attenuated neutrophil extracellular traps (NETs) formation in the lungs and dsDNA levels in the BAL fluid of SPN-infected mice. In addition, HDM-SPN infected animals had significantly increased BAL fluid cellularity driven by an influx of macrophages/monocytes, neutrophils, and eosinophils. Increased lung inflammation and mucus production was also evident in HDM-sensitised mice following acute pneumococcal infection, which was associated with exacerbated airway hyperresponsiveness. Of note, PCV13 vaccination modestly reduced pneumococcal titres in the BAL fluid of HDM-exposed animals and did not prevent BAL inflammation. Our findings provide new insights on the relationship between pneumococcal lung infections and allergic airways disease, where defective AM phagocytosis and NETosis are implicated in increased susceptibility to pneumococcal infection.

Keywords: asthma, house dust mite, *Streptococcus pneumoniae*, phagocytosis, NEtosis

INTRODUCTION

Asthma is a chronic airway inflammatory disease characterised by pathological airway remodelling that leads to variable and reversible airflow obstruction. A major consequence of chronic asthma and its related immunopathology is that asthmatics can be particularly vulnerable to respiratory infections, which can trigger potentially life-threatening acute exacerbations. Asthmatics have a heightened risk of developing pneumonia caused by *Streptococcus pneumoniae* (SPN, the pneumococcus) (Juhn et al., 2008; Castro-Rodriguez et al., 2020), which is a leading cause of community acquired pneumonia (CAP). The risk of hospitalisation by pneumonia is 2–4 times higher in asthmatics, where severe asthmatics are at even greater risk (Ekbom et al., 2019). This could be due to increased pneumococcal oropharyngeal carriage in both adults and children with asthma (Jounio et al., 2010; Esposito et al., 2016), as the pneumococcus usually infects the lungs by escaping from the upper respiratory tract (Bogaert et al., 2004). The risk of developing asthma is also significantly increased in children that are colonised with pathogenic bacteria including SPN in the upper airways as neonates (Bisgaard et al., 2007). Hence, asthmatics are regarded as a high-risk group where pneumococcal disease can be more severe. Protection of such "high-risk" asthmatics through vaccination continues to be an important priority, although it is unclear as to whether the efficacy of SPN vaccines is compromised in asthmatics (Sheikh et al., 2002).

Whilst SPN vaccines are central to reducing the risk of acquiring SPN and developing pneumonia, they may offer limited protection once SPN infects the lungs of asthmatics where the relationship between asthma and S. *pneumoniae* is complex. Alveolar macrophages (AMs) are the first cellular defence to bacterial pathogens entering the lungs (Franke-Ullmann et al., 1996) where they coordinate operational phagocytosis, which is essential for the removal of pathogenic microorganisms. AMs isolated from adults with severe asthma, phagocytose bacterial pathogens such as *H. influenzae* and *S. aureus* at a reduced capacity (Liang et al., 2014). A similar phenomenon is also observed in children with severe asthma (Fitzpatrick et al., 2008). Type-2 immune cytokines such as IL-4 and IL-13 can also drive the emergence of alternatively activated macrophage (AAM) phenotypes, which express a distinct set of genes that may compromise pathogen control (Varin et al., 2010; Abdelaziz et al., 2020). In addition to AM-mediated pathogen control, neutrophils play a pivotal role in clearing remaining pneumococci within the alveolar spaces. Neutrophil-mediated clearance of SPN involves both the killing of phagocytosed bacteria with stored serine proteases like neutrophil elastase and cathepsin G (Standish and Weiser, 2009), and the formation of neutrophil extracellular traps (NETs) (Mori et al., 2012); a process called NETosis. NETs are found in bronchial biopsies from patients with allergic asthma (Dworski et al., 2011), and their *ex vivo* formation is inversely correlated to lung function (Pham et al., 2017).

How phagocytic cells deal with SPN infections within the allergic airways is still being defined at a cellular and molecular level and there is conflicting data. For example, reduced TLR2 expression in lung phagocytic cells of house dust mite (HDM)-sensitised mice resulted in a failure to effectively clear SPN due to reduced neutrophil migration into the lungs (Habibzay et al., 2012). Contrastingly, in an OVA-model of allergic disease, there was a similar reduction in neutrophil migration in response to acute SPN infection; however, this was associated with an improvement in bacterial clearance due to expansion of a distinct SiglecF^{low} macrophage population (Sanfilippo et al., 2015). In this study, we examined whether acute pneumococcal lung infection altered the phenotype and function of AMs following HDM exposure. We also evaluated the formation of NETs following SPN infection of HDM-sensitised mice and assessed whether the pneumococcal conjugate vaccine (PCV13) restores dysfunctional bacterial clearance in HDM-sensitised mice.

METHODS AND MATERIALS

Mice and Experimental Asthma Exacerbation Model

Specific pathogen-free 6-week-old female BALB/C mice were purchased from the Animal Resources Centre (Western Australia). All mice were housed under normal 12-h day/night cycle at 22°C with free access to food and water. All animal experiments were approved by the Animals Ethics Committee of RMIT University (AEC #1805) and conducted in compliance with the National Health and Medical Research Council of Australia guidelines for experimental animal use and care. Mice were lightly anaesthetised in an induction chamber filled with 4% isoflurane in oxygen and 25 μg of HDM ([D. Pteronyssinus], Stellergenes Greer, United States) in 35 μL of saline was intranasally administered into the nostrils. In total, mice were exposed to HDM aeroallergen three times per week for 3 weeks. Vehicle exposed mice were treated in the same manner receiving 35 μL of saline alone. Twenty-four hours after the last HDM challenge, mice were inoculated with 10^6 CFU *S. pneumoniae* (strain EF3030, serotype 19F), in 35 ml saline delivered by intranasal delivery under light anaesthesia. A separate cohort of mice were vaccinated with the pneumococcal conjugate vaccine (Prevnar 13 [PCV13], Pfizer, United States), where the vaccine was diluted 1:10 with saline prior to administration. Mice received PCV13 via intraperitoneal injection (100 μL per mouse) 1 week prior to initiation of the HDM protocol and a second booster shot was delivered 2 weeks later, as previously described (Ohori et al., 2020).

Isolation of Alveolar Macrophages by Flow Cytometry and Phagocytosis Assay

Mice were killed by an overdose of sodium pentobarbital (240 mg/kg, Virbac, Australia) and lung lobes from saline or HDM challenged mice were dissected and finely minced in a petri dish. Lung cells were dissociated in 4 ml of Liberase™ (Sigma-Aldrich, United States) at 37°C. Following removal of residual tissue debris and erythrocytes, single cell suspensions were

stained with an antibody cocktail including Anti-CD45-FITC, Anti-F4/80-APC, Anti-CD11b-eFluor450, and anti-CD11c-PE-Cy7 (Thermo Fisher Scientific, United States). Alveolar macrophages were sorted using the FACSAria™ Fusion (BD Biosciences, United States) under a strict gating strategy. Briefly, dead cells, cellular debris, and cell doublets were excluded using PI viability dye, side scatter (SSC), and forward scatter (FCS) gates. From this population of live singlets, haemopoietic cells were selected based on high $CD45^{+}$ expression. All F4/80- cells were then excluded from the analysis, and alveolar macrophages were differentiated based upon $CD11c^{high}$ and $CD11b^{low}$ expression. Freshly isolated alveolar macrophages were used for mRNA extraction.

Lung Function, and Assessment of BAL and Lung Inflammation

Mice were anesthetised by ketamine (125 mg/kg) and xylazine (25 mg/kg), after which tracheotomy was performed by inserting an 18G canular into the trachea. Airway reactivity in response to increased doses of methacholine (MCh) was measured *in vivo* with the Flexivent FX1 (SCIREQ® Montreal, QC, Canada) as previously described (Wang et al., 2019). Mice were subsequently killed by an overdose of sodium pentobarbital (240 mg/kg, Virbac, Australia) and lungs were then lavaged using the same cannula with a total volume of 1.3 ml PBS to retrieve the bronchoalveolar (BAL) fluid, as previously described (Wang et al., 2017; Wang et al., 2019; Wang et al., 2021). The total number of viable BAL cells was determined by acridine orange/ethidium bromide viability staining and a hemocytometer chamber. BAL cytospins were prepared by centrifugation using the Cytopsin 3 (Thermo Shandon, United States) at 400 x g for 10 min. Cytospins were air dried, stained using the Kwik-Diff Kit® stain (Thermo Fischer Scientific, United States) procedure and cover slipped, as per the manufacturer's instructions. Differential cell counts were determined based on standard morphological features observed under microscopy with a minimum of 300 cells per slide enumerated. Representative images of macrophages were taken using brightfield microscopy (BX60 microscope, Olympus, Japan).

Following BAL, the left lung lobe was removed and fixed in 10% neutral buffered formalin for histological processing. In order to assess lung inflammation, H&E-stained slides were blindly scored by two assessors for peribronchiolitis and alveolitis, where lung lobe sections were scored based on a scale of 1–5: 0, healthy lungs i.e. no inflammation; 1, very mild; 2, mild; 3, moderate; 4, severe; 5, extremely severe changes, as previously described (Wang et al., 2021). Alcian blue-periodic acid-Schiff (AB-PAS)-stained slides were also analysed to evaluate presence of goblet cell hyperplasia. Slides were captured using a whole slide scanner and analysed using the Olympus CellSens software (V1.18, Olympus, Japan). The mucus positive area fraction (%) within the airways was calculated for four small airways (100–400 μm in diameter) per section using a standardised hue, saturation and value threshold consistent across all samples.

Bacterial Enumeration in Nasal Tissue and Lungs

Nasal tissue was dissected and placed in 1 ml of Dulbecco's Modified Eagle Medium ([DMEM], Gibco™, Thermo Fischer Scientific, United States) prior to homogenisation using the T18 digital ULTRA-TURRAX® (IKA, Germany). Pneumococcal loads were determined by viable count using BAL fluid and homogenised nasal tissue, which was serially diluted 10-fold in PBS. 15 μL of each dilution was pipetted onto horse blood agar (HBA) + 5% gentamycin (5 μg/ml) plates (Media Preparation Unit, The University of Melbourne, Australia) in triplicate. Following overnight incubation, the highest dilution with countable colonies was enumerated and the number of viable pneumococci was expressed as CFU/mL.

Immunohistochemistry for NETs and dsDNA Determination

Unstained lung tissue slides were rehydrated and incubated in antigen retrieval buffer (Tris-EDTA Buffer, 10 mM Tris, 1 mM EDTA, 0.05% Tween 20, pH 9.0). Slides were permeabilised in PBS 0.5% Triton X-100 and blocked (5% horse serum + 5% BSA + 300 mM Glycine in PBS-Tween 0.05%). Slides were then incubated with goat anti-mouse MPO (R&D Systems, United States) and rabbit anti-mouse citrullinated histone H3 (Abcam, United Kingdom) for 2 h, washed and incubated with the secondary antibodies Alexa Fluor 568 donkey anti-rabbit IgG and Alex Fluor 488 donkey anti-goat IgG. Slides were washed three times in PBS-Tween and coverslips were mounted using Fluoroshield™ with DAPI histology mounting medium (Sigma-Aldrich, United States). The mean overlapping histone-MPO area fraction (%), depicted by the yellow staining regions, was determined using a whole slide scanner and the Olympus CellSens software (V1.18, Olympus, Japan). The concentration of dsDNA in the BAL fluid was measured using the Quant-iT™ PicoGreen™ Assay Kit (Thermo Fischer Scientific, United States) as per the manufacturer's instructions.

RTqPCR Analysis of Isolated Alveolar Macrophages and Lung Tissue

Frozen lung tissue was ground to a fine powder using a mortar and pestle. RNA from isolated alveolar macrophages or lung tissue were purified using the RNeasy mini kit as per manufacturers instruction (Qiagen, GMH Germany). The NanoDrop200 (Thermo Fischer Scientific, United States) was used to determine the concentration and purity of extracted RNA and the High-Capacity RNA to cDNA kit (Thermo Fischer Scientific, United States) was used to generate complementary DNA (cDNA). RT-qPCR was performed using the QuantStudio 7 system (Thermo Fischer Scientific, United States), TaqMan primers and the Taqman Fast Advanced Master Mix, as per manufacturer's instructions. The relative expression of each gene was normalised against the housekeeping gene glyceraldehyde phosphate dehydrogenase (GAPDH) and determined using

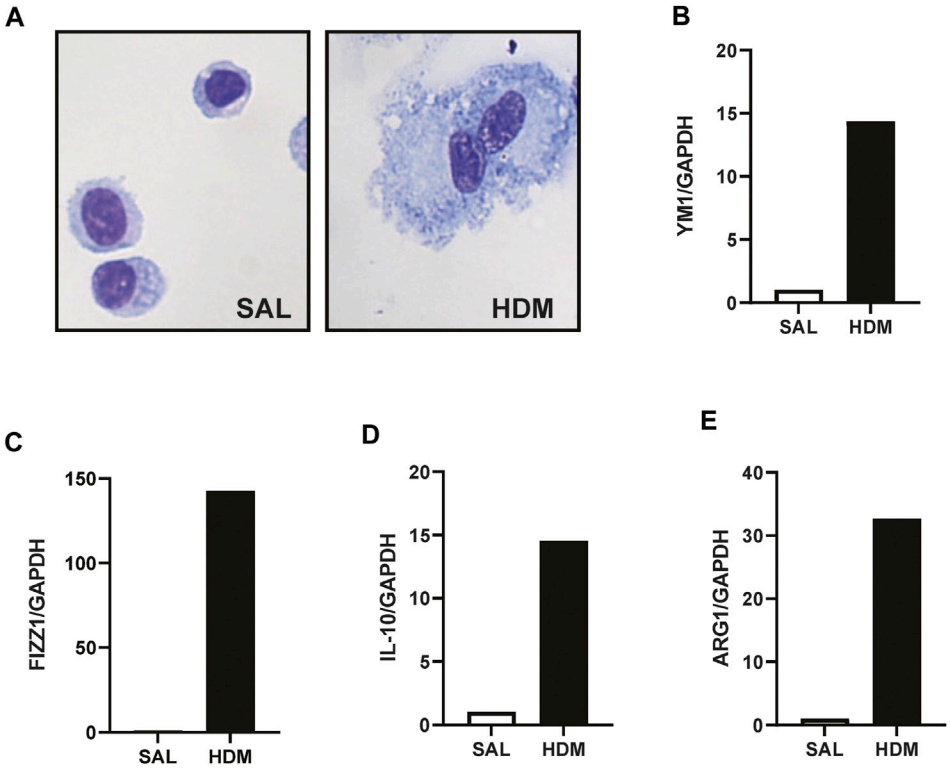

FIGURE 1 | HDM aeroallergen alters the phenotype of lung macrophages. **(A)** Alveolar macrophages were isolated by FACS sorting from the lungs of mice exposed to saline (SAL) or house dust mite (HDM) aeroallergen over 3 weeks and images of representative cytospins were taken. **(B–E)** The expression of alternative activation markers including YM-1, FIZZ1, IL-10, and ARG1 were analysed by RTqPCR using Taqman primers. Data was generated using pooled alveolar macrophages from n = 5–10 mice per treatment group. Data are presented as mean ± SEM.

the ΔΔCt value method, as previously described (Wang et al., 2018; Wang et al., 2019).

RESULTS

HDM Aeroallergen Compromised Clearance of SPN in the Lungs

AMs were isolated using a cell sorting procedure from mice exposed to HDM aeroallergen or saline for 3 weeks. Freshly isolated AMs from control (saline) mice maintained a stereotypical AM morphology, whereas AMs isolated from HDM-exposed mice displayed an enlarged and highly vacuolated morphology (**Figure 1A**). The change in morphology was associated with a marked increase in the expression of the two alternatively activated macrophage (AAM) markers, YM1, and FIZZ1 (**Figures 1B, C**). In addition, IL-10 and ARG1 expression was markedly increased in HDM-exposed AMs (**Figures 1D, E**). To determine whether prior HDM exposure impacted pneumococcal clearance *in vivo*, HDM-sensitised mice were acutely infected with SPN and bacterial titres were evaluated 48 h following SPN inoculation as summarised in **Figure 2A**. Pneumococcal loads remained consistent between HDM and VEH-exposed mice in the nasal tissue (**Figure 2B**); however, SPN titres in the BAL fluid were over 3-log higher in HDM-exposed mice compared to VEH-exposed mice (**Figure 2C**). We next assessed whether an AAM population had emerged *in vivo* as seen in the isolated AM population, where the common AAM markers (FIZZ1, YM1, ARG1, and IL-10) were measured in lung *via* RT-qPCR. HDM sensitisation increased the expression of all four AAM markers and of note, combined HDM exposure and acute SPN infection (HDM-SPN) lead to a further increase in the relative expression of IL-10 and ARG1 compared to HDM alone-exposed mice (**Figures 2D–G**).

Since pneumococcal lung infection promotes the migration of neutrophils into the airspaces to assist with pathogen removal, BAL neutrophils were analysed in our model. There was a significant increase in the number of BAL neutrophils in response to acute pneumococcal infection and the numbers were not significantly altered by prior HDM exposure (**Figure 3A**). The levels of dsDNA in the BAL fluid were also measured as a marker for the release of NETs, where dsDNA levels were significantly increased in mice infected with SPN (**Figure 3B**). Of importance, there was a marked reduction in dsDNA levels in the BAL fluid in mice exposed to HDM prior to SPN infection relative to SPN-infected mice. Complementing these findings, lung sections were co-stained for citrullinated histone H3 (red) and MPO

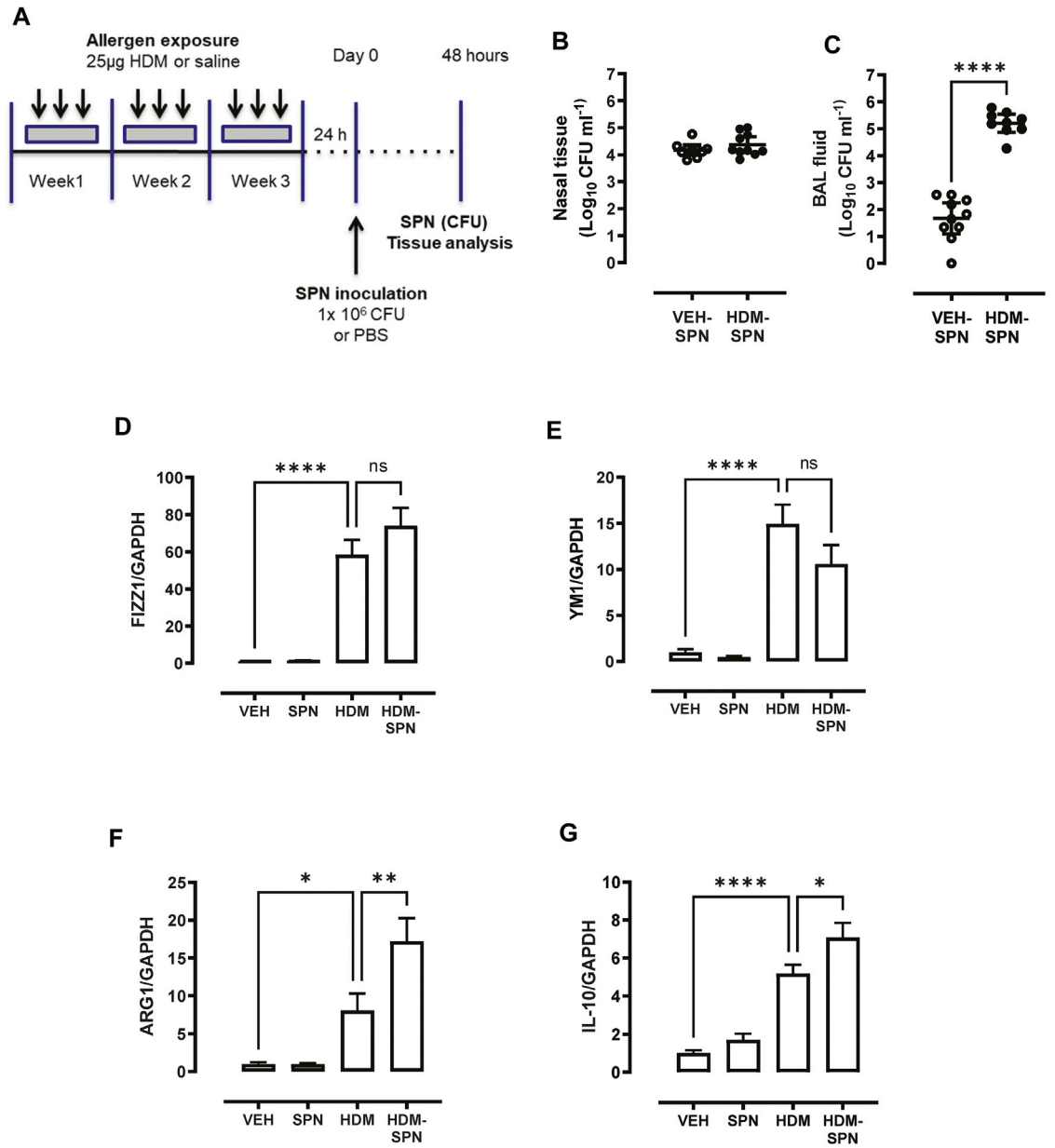

FIGURE 2 | HDM suppresses bacterial clearance and increases IL10/ARG1 expression in SPN-infected mice. **(A)** Mice were sensitized to HDM over three 3 weeks and subsequently infected with SPN *via* intranasal inoculation, and outcomes were assessed 2 days later. Pneumococcal load in the **(B)** nasal tissue and **(C)** BAL fluid was determined. **(D–G)** Expression of the alternative activation markers FIZZ1, YM1, ARG1, and IL-10 in lung tissue was analysed by RTqPCR using Taqman primers. n = 7–10 mice per group. RT-qPCR data are presented as mean ± SEM and statistical comparisons were determined using one-way ANOVA at $^{*}p < 0.05$, $^{**}p < 0.01$, $^{****}p < 0.0001$, followed by Tukey's *post hoc* test. SPN titres are presented as the geometric mean ± 95% confidence interval (CI) and statistical comparisons were determined using the Mann-Whitney U test at $^{****}p < 0.0001$.

(green), two key components of NETs. Overlapping yellow regions were used to define regions of NETs, which were observed in the lungs of SPN-infected mice, as presented in **Figure 3C**. The quantification of co-stained regions displayed a mean area fraction of 0.11% in SPN-infected mice, compared to just 0.045% in SPN-infected animals previously exposed to HDM, although this difference fell short of significance (**Figure 3D**).

Increased Pneumococcal Load Worsened Inflammation and Airway Hyper-Responsiveness

In addition to the influx of neutrophils, differential cell counting revealed that acute pneumococcal infection in HDM-exposed mice significantly increased the total number of BAL macrophages, whereas HDM or SPN alone did not alter

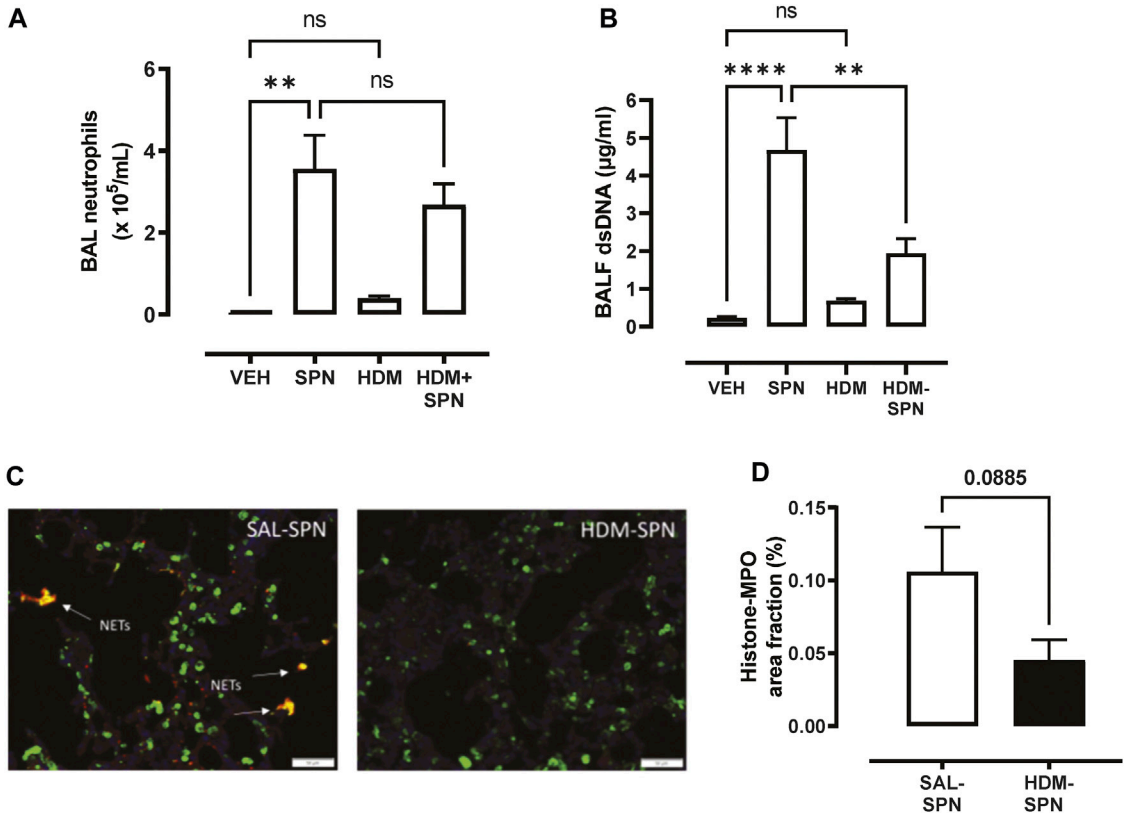

FIGURE 3 | Netosis markers are reduced in HDM-exposed mice infected with SPN. **(A)** BAL neutrophil numbers were enumerated on BAL cytospots. **(B)** The levels of dsDNA were quantified in the BAL fluid. **(C)** NET staining was performed on lung sections and identified yellow regions of H3 and MPO co-staining that is representative of NET formation. **(D)** The area of co-staining was quantified on a slide scanner using cell sense software in SAL and HDM treated mice infected with SPN. n = 6–10 mice per group. Data are presented as mean ± SEM and statistical comparisons were determined using one-way ANOVA for more than two groups, or Students *t-test* for two groups at $^{**}p < 0.01$, $^{****}p < 0.001$, followed by Tukey's *post hoc* test.

BAL macrophage numbers (**Figure 4A**). In addition, eosinophilic inflammation induced by HDM exposure was further increased by concurrent acute pneumococcal infection in HDM-exposed mice (**Figure 4B**). To interrogate the molecular mechanisms that are driving this distinct BAL inflammatory profile in HDM-SPN mice, a panel of immunoregulatory genes were measured in the lungs by RTqPCR. As expected, the classic type-2 cytokines IL4, IL5, and IL-13 were increased in the lungs of HDM-exposed mice (**Figures 4C–E**), and pneumococcal infection did not alter their respective levels. In contrast, the expression of the CCL2 (MCP1) and CCL3 (MIP1a) chemokines were not increased by HDM or SPN alone; however the combination of HDM and SPN significantly increased their levels (**Figures 4F, G**). The expression of CCL11 (eotaxin-1) was increased in HDM-exposed mice and levels were not further altered with SPN infection (**Figure 4H**).

We next investigated whether there were any noticeable histological changes to the airways and parenchyma. To determine the level of peribronchiolitis and alveolitis, whole-lung sections stained with H&E (**Figure 5A**) were blindly scored. SPN infection or HDM exposure alone resulted in increased peribronchiolar (**Figure 5B**) and alveolar inflammation (**Figure 5C**). The combined HDM-SPN exposure specifically led to a significant increase in peribronchiolitis when compared to the HDM alone group. Mucus production around the small airways (<200 µm) was also investigated via AB-PAS staining of the whole lung, where mucus positive cells were rarely observed within the airways of VEH or SPN treated mice (**Figure 6A**). HDM exposure resulted in a mean mucus staining airway wall area fraction of 25.77% that significantly increased to 36.35% with combined acute SPN infection (**Figure 6B**). Lung function parameters were also measured, and dose response analysis revealed that at the maximum nebulised dose of methacholine (100 mg/ml), total resistance (Rrs) peaked in HDM-SPN animals (**Figure 6C**). Comparison of maximal responses revealed that SPN did not significantly increase Rrs, whereas HDM alone increased Rrs, and the combination of HDM and SPN caused a further significant rise in Rrs (**Figure 6D**).

We next determined whether prior HDM exposure impacted pneumococcal clearance in PCV13 vaccinated mice by evaluating bacterial titres during the acute phase of infection as summarised in **Figure 7A**. Pneumococcal loads were high in the nasal tissue with slightly higher bacterial titres in the nasal tissue of PCV13-vaccinated compared to unvaccinated mice (**Figure 7B**). While

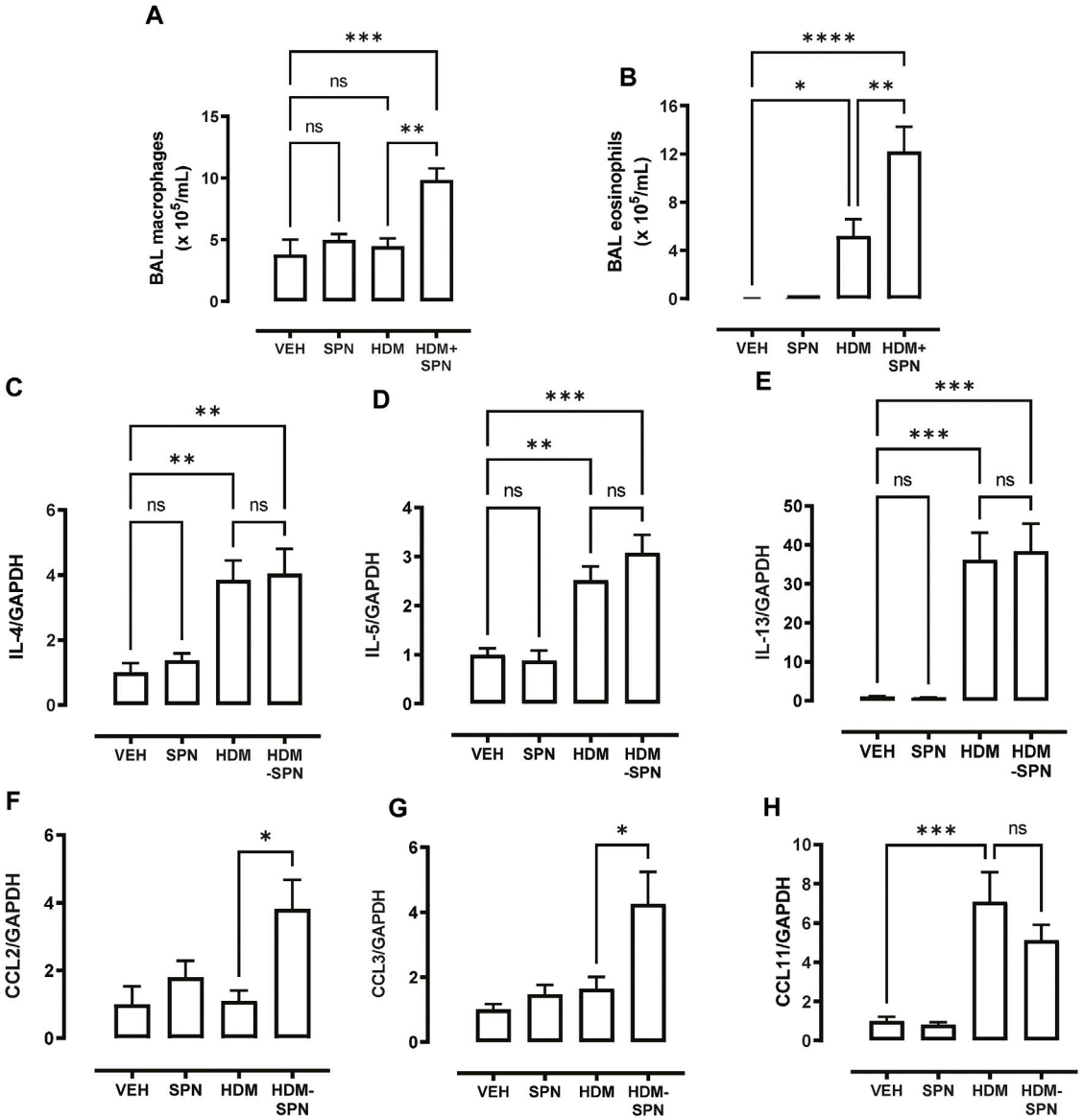

FIGURE 4 | CCL2 and CCL3 are associated with increased BAL macrophages and eosinophils. **(A)** BAL macrophage and **(B)** BAL eosinophil numbers were enumerated on BAL cytospots. **(C–E)** Expression of the TH2 markers including IL4, IL5, and IL13 were analysed by RTqPCR using Taqman primers. **(F–H)** Expression of CCL chemokines including CCL2, CCL3, and CCL11 were analysed by RTqPCR using Taqman primers. $n = 6–10$ mice per group. Data are presented as mean ± SEM and statistical comparisons were determined using one-way ANOVA at $^*p < 0.05$, $^{**}p < 0.01$, $^{***}p < 0.005$, followed by Tukey's *post hoc* test.

PCV-13 did not alter SPN loads in the BAL fluid of VEH-exposed animals, vaccination lead to a significant decrease in pneumococcal CFU in the HDM-exposed group compared to HDM-unvaccinated mice (**Figure 7C**). Immune cell infiltration in the BAL compartment was next assessed where differential cell counting revealed that macrophage/monocyte infiltration remained significantly higher in PCV13-vaccinated HDM-SPN mice (**Figure 7D**). A significant increase in the total number of neutrophils was observed in the PCV13-SPN group compared to VEH (**Figure 7E**); however, this did not differ to PCV13-HDM-SPN animals. In addition, HDM exposure alone also resulted in significant BAL eosinophilia in PCV13-vaccinated animals and numbers were significantly higher in vaccinated HDM-SPN animals compared to vaccinated HDM-exposed animals (**Figure 7F**). Hence, the BAL inflammatory profile in vaccinated mice is very similar to unvaccinated mice.

DISCUSSION

Our results confirm that animals with a HDM-driven allergic airway phenotype are inadequate at clearing pneumococci from the lower airways, as observed previously (Habibzay et al., 2012). To the best of our knowledge, our study describes for the first time

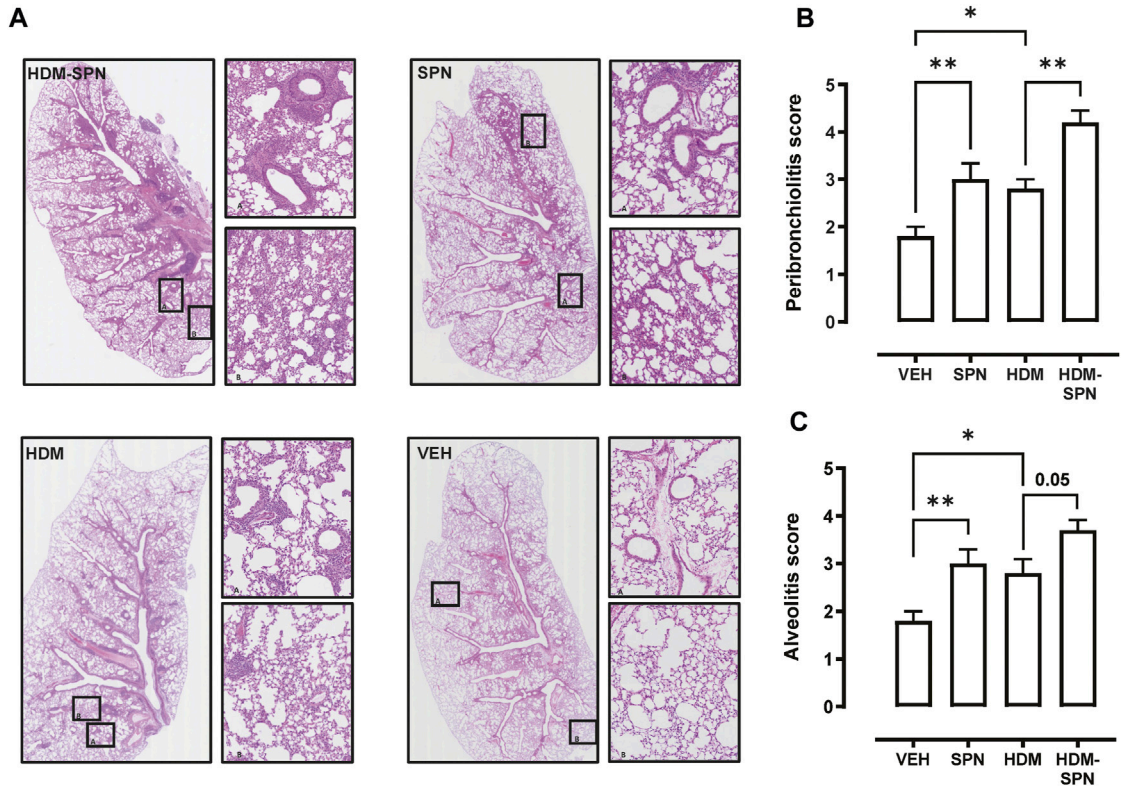

FIGURE 5 | Lung inflammation and injury is increased in HDM-SPN infected mice. **(A)** Lungs were processed for histology and slides were stained with H&E, and whole lung lobes were captured using the VS120 slide scanner. The level of **(B)** peribronchial inflammation and **(C)** alveolitis was blindly scored by two observers. n = 7–10 mice per group. Data are presented as mean ± SEM and statistical comparisons were determined using one-way ANOVA at $^{*}p < 0.05$, $^{**}p < 0.01$, followed by Tukey's *post hoc* test.

how specific facets of macrophage and neutrophil anti-pneumococcal immunity are altered following aeroallergen exposure. We also show that prior PCV13 vaccination modestly accelerates pneumococcal clearance in HDM-exposed animals. Our study demonstrates that during the acute phase of infection, SPN lung titres are over 2-log higher in HDM-exposed mice despite the presence of nearly double the number of BAL macrophages/monocytes in the airways. AMs must engulf and internalise SPN (Franke-Ullmann et al., 1996) before using protease- and nitric-oxide dependant apoptotic pathways for bacterial removal (Marriott et al., 2004; Marriott et al., 2006). A similar phenomenon has been observed in AMs isolated from adults with severe asthma in response to *H. influenzae* and *S. aureus* (Liang et al., 2014). Consequently, a reduction in the phagocytic capacity could contribute towards bacterial outgrowth in the lower airways and may in part underpin why asthmatics have a heightened risk of developing pneumococcal pneumonia (Jounio et al., 2010; Castro-Rodriguez et al., 2020).

Pneumococcal infection in mice results in the robust recruitment of monocytes at day 2 post infection under the direction of the CCL2 chemokine, which enhances the killing of pneumococcus (Winter et al., 2007; Anthony et al., 2020). This recruitment is necessary to replenish local macrophage pools because SPN can induce apoptosis of resident macrophages to enhance pneumococcal killing (Aberdein et al., 2013). It has been reported that approximately 60% of alveolar macrophages are replaced by monocyte derived CD11b+ exudative macrophages following pneumococcal lung infection (Taut et al., 2008). The A limitation of our study is that we did not differentiate between resident alveolar macrophages, monocytes and monocyte derived exudative macrophages. As we have investigated the outcomes at Day 2 post infection, there will be a significant pool of monocyte derived macrophages in the lungs. Our findings suggest that this recruited pool is defective in bacterial clearance as pneumococcal load was 4-log higher in HDM-SPN infected mice compared to SPN-infected mice. Future studies should isolate the individual macrophage populations and investigate their relative capacity to ingest and kill SPN in order to establish whether this defect is shared or restricted across discrete macrophage subsets. In addition, female mice were used in this study as the prevalence of asthma is higher in females then males after puberty. Future studies should investigate whether defective pneumococcal clearance is also seen in male mice exposed to HDM aeroallergen.

Th2 immune cytokine, such as IL-4, IL-5, and IL-13 drive the emergence of AAMs. It was evident from our observations that HDM exposure generated a dominant AAM phenotype, as shown by the increased expression of typical AAM markers ARG1, YM1,

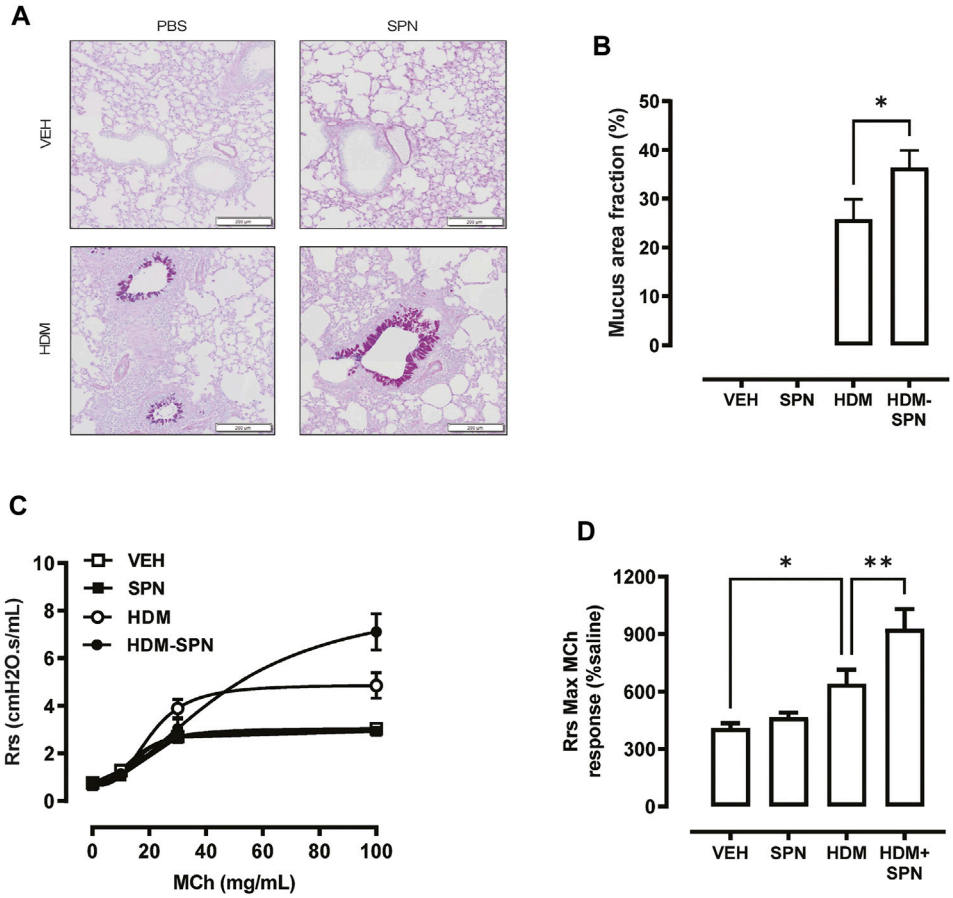

FIGURE 6 | Mice sensitised with HDM and infected with SPN display increased airways hyper-reactivity. **(A)** Lungs were processed for histology and slides were stained with AB-PAS, and whole lung lobes were captured using the VS120 slide scanner. **(B)** The area of mucous staining within the airways was blindly evaluated using Cell Sense software. Lung function in response to increasing concentrations of methacholine was performed, where **(C)** total resistance (Rrs) was presented as a dose response and **(D)** maximal Rrs responses at 100 mg/ml MCh were compared across the different groups. $n = 8–10$ mice per group. Data are presented as mean ± SEM and statistical comparisons were determined using one-way ANOVA at $^{*}p < 0.05$, $^{**}p < 0.01$, followed by Tukey's *post hoc* test.

IL-10, and FIZZ1 in the lung tissue and from isolated AMs. The polarisation of AAMs with IL-4 impairs the non-opsonic phagocytic uptake of *N. meningitidis*, which was associated with a defect in phagosome formation (Varin et al., 2010). We demonstrate that combined HDM exposure and SPN infection significantly increases the expression of ARG1 and IL-10 in murine lungs. IL-13-induced ARG1 expression in murine lungs has been shown to attenuate pneumococcal killing (Knippenberg et al., 2015). The upregulation of arginase depletes arginine and supresses iNOS protein expression, in turn decreasing NO production (El-Gayar et al., 2003). Since iNOS and NO production is important for reducing pneumococcal viability in macrophage-mediated phagocytosis, their suppression by increased arginase may result in loss of bacterial clearance. In addition, the bacterial virulence factor pneumolysin (PLY) increases the expression of arginase, which promotes endothelial barrier dysfunction by reducing nitric oxide generation (Lucas et al., 2012).

A fine balance between attenuating excessive inflammation without compromising bacterial clearance must exist. This especially applies to the role of IL-10 during anti-pneumococcal immune responses. Mice deficient of IL-10 display severe lung histopathology, sustained neutrophil infiltration and increased mortality following SPN infection [258]. Interestingly, pneumococcal titres in the lungs were significantly decreased in IL-$10^{-/-}$ mice compared to WT (Peñaloza et al., 2015). Conversely, others have found that IL-10 diminishes pneumococcal clearance in the lungs and promotes bacterial spread (Peñaloza et al., 2015). Therefore, it is plausible that in our study increased IL-10 expression could contribute towards diminished SPN clearance in the airways. On the other hand, IL-10 plays an important role in reducing airway inflammation in OVA-induced asthma as IL-10 deficient mice display greater peribronchiolar inflammation consisting of lymphocytes, macrophages and eosinophils (Tournoy et al., 2000). Considering the multifaceted role IL-10 plays in infection and in allergy, a greater understanding of IL-10 during asthma exacerbations is needed.

We propose that mediators released in the allergic environment drive an alternately activated macrophage

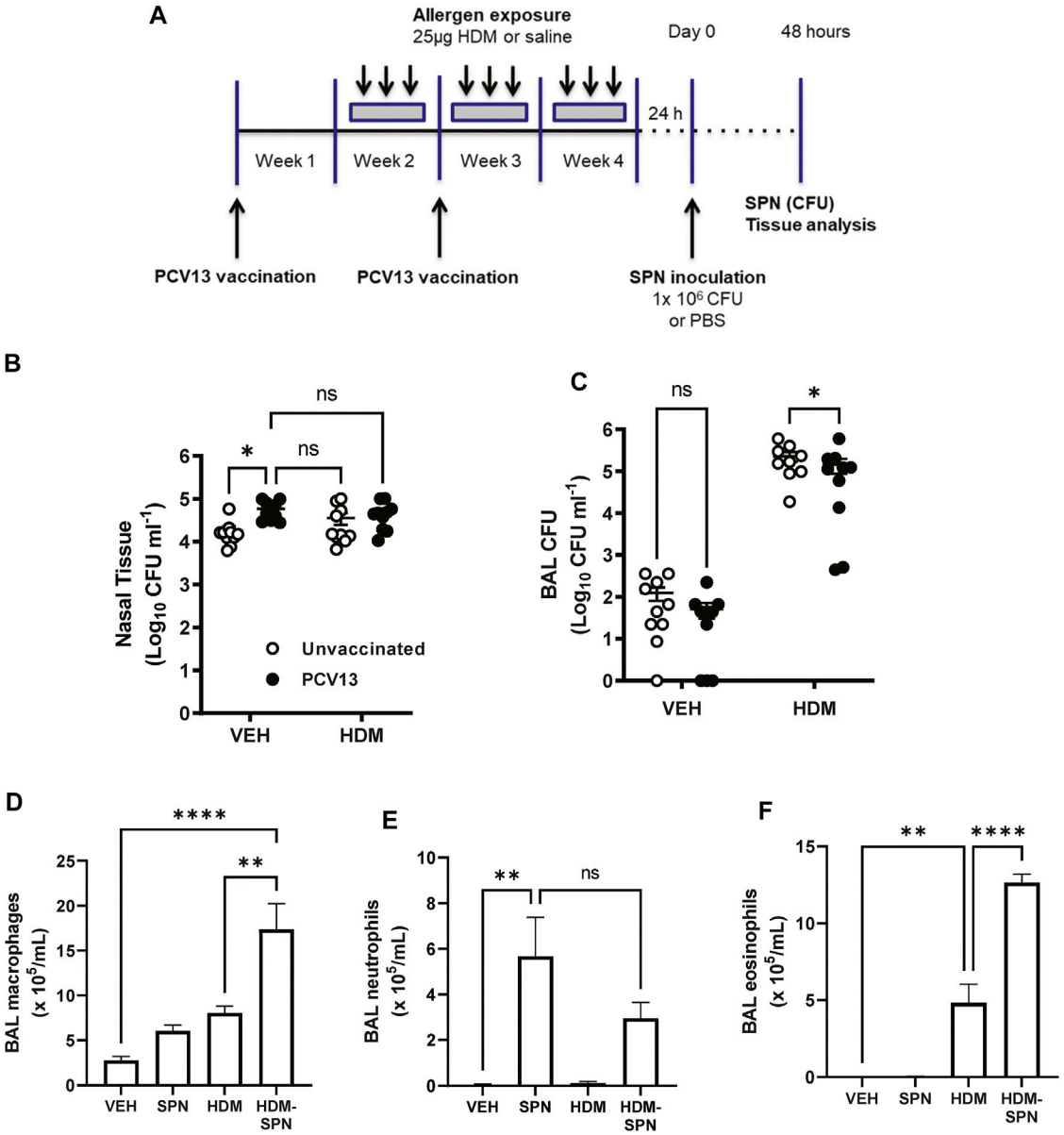

FIGURE 7 | SPN lung clearance is improved in PCV13-vaccinated and HDM-exposed mice. **(A)** Mice were vaccinated with PCV13 at weeks 1 and 2, sensitized to HDM over three 3 weeks and subsequently infected with SPN *via* intranasal inoculation. Outcomes were assessed 2 days later. Pneumococcal load in the **(B)** nasal tissue and **(C)** BAL fluid was determined. **(D)** BAL macrophage, **(E)** BAL neutrophils, and **(F)** BAL eosinophil numbers were enumerated on BAL cytospots. $n = 4$-5 mice per group. SPN titres are presented as the geometric mean ± 95% confidence interval (CI) and statistical comparisons were determined using a mixed-effects model with Sidak's *post hoc test* at $^{*}p < 0.05$. BAL inflammatory cell numbers are presented as mean ± SEM and statistical comparisons were determined using one-way ANOVA at $^{**}p < 0.01$, $^{****}p < 0.0001$, followed by Tukey's *post hoc* test.

phenotype that is defective in pneumococcal clearance and killing. Whilst therapies such as corticosteroids can reduce allergic type-2 inflammation, they can also potentially suppress bacterial clearance. Hence, our pre-clinical model can be used to screen for novel therapies that improve bacterial clearance in the allergic lung environment. Another novel finding from our study is that HDM exposure attenuates the release of NETs in response to acute pneumococcal infection. Neutrophil-mediated removal of SPN involves both the killing of phagocytosed bacteria with stored serine proteases (El-Gayar et al., 2003) and the formation of NETs (Mori et al., 2012). As their name suggests, NETs form net-like structures that trap and kill pathogens (Brinkmann et al., 2004). In addition to neutrophils, eosinophils also produce extracellular traps. To highlight the presence of NETs, we co-stained lung sections with MPO and histone H3, and specifically measured the overlap of these two markers. There was also a significant reduction in dsDNA in the BAL fluid. The reduction in NETosis in HDM-SPN mice was not due to a decrease in the

number of infiltrating neutrophils, as similar number of neutrophils were recruited to the airways in HDM-SPN and SPN groups. Key modulators of NETosis are still being defined. However, it has been highlighted that anti-inflammatory cytokines can inhibit the formation of NETs (Vorobjeva and Chernyak, 2020). Increased IL-10 production by dendritic cells disrupts the formation of NETs; a mechanism employed by HIV-1 to avoid NET-mediated clearance (Saitoh et al., 2012). Therefore, it is possible that increased IL-10 expression in HDM-exposed animals could limit NETosis in our model and enable SPN to evade NET-dependant anti-bacterial responses. SPN can also express a surface endonuclease allowing the bacterium to escape NETosis by breaking down DNA structures (Beiter et al., 2006). It is possible by virtue of the increased number of pneumococci in the lower airways of HDM-exposed mice (via impaired alveolar macrophage phagocytosis), that endonuclease expression is higher allowing for NET degradation.

The present study shows that acute SPN infection exacerbates airway hyperresponsiveness in HDM-exposed mice, which was associated with increased airway inflammation and mucus production. In addition, we showed that CCL2 expression in the lungs is significantly greater in HDM-SPN mice and is likely to drive the recruitment of monocytes to the airways in our model. While eotaxin-1 expression was not markedly higher in combined HDM-SPN animals, increased CCL3 expression may promote the recruitment of eosinophils in murine lungs. Interestingly, administration of the pneumococcal conjugate vaccine (PCV7) can supress type-2 inflammation in OVA-sensitised mice via increasing the induction of suppressive T-regulatory (Treg) cells (Thorburn et al., 2010). We investigated whether pneumococcal vaccination also improved bacterial clearance in HDM-exposed mice, as to the best of knowledge, this has not been described before. It was evident from our study that prior PCV13 vaccination modestly accelerated pneumococcal clearance in HDM-exposed mice, however as the reduction in bacterial load was small, BAL inflammation was still evident.

In this study, we specifically investigated the clearance of SPN during the early phase of infection (2 days post infection), where neutrophils and monocytes are recruited into the airways and play a major role in phagocytosing and killing pneumococcus. The significance of this early innate response is exemplified by the finding that CXCR2 knockout mice that recruit significantly fewer neutrophils and exudative macrophages during pneumococcal infection, display a major defect in bacterial clearance (Herbold et al., 2010). Our data suggests that this early innate response required to eradicate bacteria is defective in HDM-exposed mice. A limitation of our study is that we did not evaluate bacterial BAL titres at later timepoints following vaccination and pneumococcal infection (e.g., Day 3, 4, and 6), as it is plausible that vaccinated mice clear bacteria more effectively at the later timepoints. Furthermore, we did not evaluate antibody titres generated against PCV13 and/or pneumococcus. Future studies should investigate whether antibodies titres against PCV13 are altered in HDM-exposed mice and whether this impacts bacterial clearance at later timepoints. Nonetheless, our findings emphasise that there is a need to develop novel therapies that decrease type-2 and neutrophilic inflammation whilst improving phagocytosis and clearance of respiratory pathogens such as pneumococcus, and our pre-clinical model can be used to screen for such therapeutics.

In summary, we have shown that HDM-exposure reduces pneumococcal-specific AM-mediated phagocytosis and the formation of NETs; a phenomenon which may underpin the observed increase in SPN titres in HDM-exposed animals. We have also demonstrated PCV13-vaccination can enhance pneumococcal clearance in HDM-exposed mice. Our findings provide exciting new insights into the relationship between pneumococcal lung infections and allergic airways disease. The scope of this defect in asthma is accentuated by the fact that there is also a complex interplay between respiratory pathogens and asthma, where respiratory viruses such as rhinovirus can impair the phagocytic clearance of bacteria by human alveolar macrophages (Oliver et al., 2008). Future research should continue to focus on developing therapies that reduce bacterial loads and immunopathology in the background of allergic airways disease, and the pre-clinical model described in this study can contribute to progressing this strategy.

DATA AVAILABILITY STATEMENT

The original contributions presented in the study are included in the article/Supplementary Material, further inquiries can be directed to the corresponding author.

ETHICS STATEMENT

The animal study was reviewed and approved by the RMIT University Animal Ethics Committee.

AUTHOR CONTRIBUTIONS

AP, HW, and SB conceived and planned the experiments. AP, HW, SB, CA, and JM carried out the experiments. RV, CS, and SS contributed to the interpretation of the results and supervision of students. SB acquired funding to support this project. AP and SB took the lead in writing the manuscript. All authors provided critical feedback and helped shape the research, analysis and manuscript.

REFERENCES

Abdelaziz, M. H., Abdelwahab, S. F., Wan, J., Cai, W., Huixuan, W., Jianjun, C., et al. (2020). Alternatively Activated Macrophages; a Double-Edged Sword in Allergic Asthma. *J. Transl Med.* 18 (1), 58. doi:10.1186/s12967-020-02251-w

Aberdein, J. D., Cole, J., Bewley, M. A., Marriott, H. M., and Dockrell, D. H. (2013). Alveolar Macrophages in Pulmonary Host Defence the Unrecognized Role of Apoptosis as a Mechanism of Intracellular Bacterial Killing. *Clin. Exp. Immunol.* 174 (2), 193–202. doi:10.1111/cei.12170

Anthony, D., Papanicolaou, A., Wang, H., Seow, H. J., To, E. E., Yatmaz, S., et al. (2020). Excessive Reactive Oxygen Species Inhibit IL-17A+ γδ T Cells and Innate Cellular Responses to Bacterial Lung Infection. *Antioxid. Redox Signal.* 32 (13), 943–956. doi:10.1089/ars.2018.7716

Beiter, K., Wartha, F., Albiger, B., Normark, S., Zychlinsky, A., and Henriques-Normark, B. (2006). An Endonuclease Allows Streptococcus Pneumoniae to Escape from Neutrophil Extracellular Traps. *Curr. Biol.* 16 (4), 401–407. doi:10.1016/j.cub.2006.01.056

Bisgaard, H., Hermansen, M. N., Buchvald, F., Loland, L., Halkjaer, L. B., Bønnelykke, K., et al. (2007). Childhood Asthma after Bacterial Colonization of the Airway in Neonates. *N. Engl. J. Med.* 357 (15), 1487–1495. doi:10.1056/NEJMoa052632

Bogaert, D., De Groot, R., and Hermans, P. W. (2004). Streptococcus Pneumoniae Colonisation: the Key to Pneumococcal Disease. *Lancet Infect. Dis.* 4 (3), 144–154. doi:10.1016/S1473-3099(04)00938-7

Brinkmann, V., Reichard, U., Goosmann, C., Fauler, B., Uhlemann, Y., Weiss, D. S., et al. (2004). Neutrophil Extracellular Traps Kill Bacteria. *Science* 303 (5663), 1532–1535. doi:10.1126/science.1092385

Castro-Rodriguez, J. A., Abarca, K., and Forno, E. (2020). Asthma and the Risk of Invasive Pneumococcal Disease: A Meta-Analysis. *Pediatrics* 145 (1). doi:10.1542/peds.2019-1200

Dworski, R., Simon, H. U., Hoskins, A., and Yousefi, S. (2011). Eosinophil and Neutrophil Extracellular DNA Traps in Human Allergic Asthmatic Airways. *J. Allergy Clin. Immunol.* 127 (5), 1260–1266. doi:10.1016/j.jaci.2010.12.1103

Ekbom, E., Quint, J., Schöler, L., Malinovschi, A., Franklin, K., Holm, M., et al. (2019). Asthma and Treatment with Inhaled Corticosteroids: Associations with Hospitalisations with Pneumonia. *BMC Pulm. Med.* 19 (1), 254. doi:10.1186/s12890-019-1025-1

El-Gayar, S., Thüring-Nahler, H., Pfeilschifter, J., Röllinghoff, M., and Bogdan, C. (2003). Translational Control of Inducible Nitric Oxide Synthase by IL-13 and Arginine Availability in Inflammatory Macrophages. *J. Immunol.* 171 (9), 4561–4568. doi:10.4049/jimmunol.171.9.4561

Esposito, S., Terranova, L., Patria, M. F., Marseglia, G. L., Miraglia del Giudice, M., Bodini, A., et al. (2016). Streptococcus Pneumoniae Colonisation in Children and Adolescents with Asthma: Impact of the Heptavalent Pneumococcal Conjugate Vaccine and Evaluation of Potential Effect of Thirteen-Valent Pneumococcal Conjugate Vaccine. *BMC Infect. Dis.* 16, 12. doi:10.1186/s12879-016-1335-3

Fitzpatrick, A. M., Holguin, F., Teague, W. G., and Brown, L. A. (2008). Alveolar Macrophage Phagocytosis Is Impaired in Children with Poorly Controlled Asthma. *J. Allergy Clin. Immunol.* 121 (6), 1372–1383. 8 e1. doi:10.1016/j.jaci.2008.03.008

Franke-Ullmann, G., Pförtner, C., Walter, P., Steinmüller, C., Lohmann-Matthes, M. L., and Kobzik, L. (1996). Characterization of Murine Lung Interstitial Macrophages in Comparison with Alveolar Macrophages *In Vitro*. *J. Immunol.* 157 (7), 3097–3104.

Habibzay, M., Saldana, J. I., Goulding, J., Lloyd, C. M., and Hussell, T. (2012). Altered Regulation of Toll-like Receptor Responses Impairs Antibacterial Immunity in the Allergic Lung. *Mucosal Immunol.* 5 (5), 524–534. doi:10.1038/mi.2012.28

Herbold, W., Maus, R., Hahn, I., Ding, N., Srivastava, M., Christman, J. W., et al. (2010). Importance of CXC Chemokine Receptor 2 in Alveolar Neutrophil and Exudate Macrophage Recruitment in Response to Pneumococcal Lung Infection. *Infect. Immun.* 78 (6), 2620–2630. doi:10.1128/IAI.01169-09

Jounio, U., Juvonen, R., Bloigu, A., Silvennoinen-Kassinen, S., Kaijalainen, T., Kauma, H., et al. (2010). Pneumococcal Carriage Is More Common in Asthmatic Than in Non-asthmatic Young Men. *Clin. Respir. J.* 4 (4), 222–229. doi:10.1111/j.1752-699X.2009.00179.x

Juhn, Y. J., Kita, H., Yawn, B. P., Boyce, T. G., Yoo, K. H., McGree, M. E., et al. (2008). Increased Risk of Serious Pneumococcal Disease in Patients with Asthma. *J. Allergy Clin. Immunol.* 122 (4), 719–723. doi:10.1016/j.jaci.2008.07.029

Knippenberg, S., Brumshagen, C., Aschenbrenner, F., Welte, T., and Maus, U. A. (2015). Arginase 1 Activity Worsens Lung-Protective Immunity against Streptococcus Pneumoniae Infection. *Eur. J. Immunol.* 45 (6), 1716–1726. doi:10.1002/eji.201445419

Liang, Z., Zhang, Q., Thomas, C. M., Chana, K. K., Gibeon, D., Barnes, P. J., et al. (2014). Impaired Macrophage Phagocytosis of Bacteria in Severe Asthma. *Respir. Res.* 15, 72. doi:10.1186/1465-9921-15-72

Lucas, R., Yang, G., Gorshkov, B. A., Zemskov, E. A., Sridhar, S., Umapathy, N. S., et al. (2012). Protein Kinase C-α and Arginase I Mediate Pneumolysin-Induced Pulmonary Endothelial Hyperpermeability. *Am. J. Respir. Cell Mol Biol* 47 (4), 445–453. doi:10.1165/rcmb.2011-0332OC

Marriott, H. M., Ali, F., Read, R. C., Mitchell, T. J., Whyte, M. K., and Dockrell, D. H. (2004). Nitric Oxide Levels Regulate Macrophage Commitment to Apoptosis or Necrosis during Pneumococcal Infection. *FASEB J.* 18 (10), 1126–1128. doi:10.1096/fj.03-1450fje

Marriott, H. M., Hellewell, P. G., Cross, S. S., Ince, P. G., Whyte, M. K., and Dockrell, D. H. (2006). Decreased Alveolar Macrophage Apoptosis Is Associated with Increased Pulmonary Inflammation in a Murine Model of Pneumococcal Pneumonia. *J. Immunol.* 177 (9), 6480–6488. doi:10.4049/jimmunol.177.9.6480

Mori, Y., Yamaguchi, M., Terao, Y., Hamada, S., Ooshima, T., and Kawabata, S. (2012). α-Enolase of Streptococcus Pneumoniae Induces Formation of Neutrophil Extracellular Traps. *J. Biol. Chem.* 287 (13), 10472–10481. doi:10.1074/jbc.M111.280321

Ohori, J., Iuchi, H., Maseda, Y., and Kurono, Y. (2020). Phosphorylcholine Intranasal Immunization with a 13-valent Pneumococcal Conjugate Vaccine Can Boost Immune Response against Streptococcus Pneumoniae. *Vaccine* 38 (3), 699–704. doi:10.1016/j.vaccine.2019.10.043

Oliver, B. G., Lim, S., Wark, P., Laza-Stanca, V., King, N., Black, J. L., et al. (2008). Rhinovirus Exposure Impairs Immune Responses to Bacterial Products in Human Alveolar Macrophages. *Thorax* 63 (6), 519–525. doi:10.1136/thx.2007.081752

Peñaloza, H. F., Nieto, P. A., Muñoz-Durango, N., Salazar-Echegarai, F. J., Torres, J., Parga, M. J., et al. (2015). Interleukin-10 Plays a Key Role in the Modulation of Neutrophils Recruitment and Lung Inflammation during Infection by Streptococcus Pneumoniae. *Immunology* 146 (1), 100–112. doi:10.1111/imm.12486

Pham, D. L., Ban, G. Y., Kim, S. H., Shin, Y. S., Ye, Y. M., Chwae, Y. J., et al. (2017). Neutrophil Autophagy and Extracellular DNA Traps Contribute to Airway Inflammation in Severe Asthma. *Clin. Exp. Allergy* 47 (1), 57–70. doi:10.1111/cea.12859

Saitoh, T., Komano, J., Saitoh, Y., Misawa, T., Takahama, M., Kozaki, T., et al. (2012). Neutrophil Extracellular Traps Mediate a Host Defense Response to Human Immunodeficiency Virus-1. *Cell Host Microbe* 12 (1), 109–116. doi:10.1016/j.chom.2012.05.015

Sanfilippo, A. M., Furuya, Y., Roberts, S., Salmon, S. L., and Metzger, D. W. (2015). Allergic Lung Inflammation Reduces Tissue Invasion and Enhances Survival from Pulmonary Pneumococcal Infection in Mice, Which Correlates with Increased Expression of Transforming Growth Factor β1 and SiglecF(low) Alveolar Macrophages. *Infect. Immun.* 83 (7), 2976–2983. doi:10.1128/IAI.00142-15

Sheikh, A., Alves, B., and Dhami, S. (2002). Pneumococcal Vaccine for Asthma. *Cochrane Database Syst. Rev.* 1, CD002165. doi:10.1002/14651858.CD002165

Standish, A. J., and Weiser, J. N. (2009). Human Neutrophils Kill Streptococcus Pneumoniae via Serine Proteases. *J. Immunol.* 183 (4), 2602–2609. doi:10.4049/jimmunol.0900688

Taut, K., Winter, C., Briles, D. E., Paton, J. C., Christman, J. W., Maus, R., et al. (2008). Macrophage Turnover Kinetics in the Lungs of Mice Infected with Streptococcus Pneumoniae. *Am. J. Respir. Cell Mol Biol* 38 (1), 105–113. doi:10.1165/rcmb.2007-0132OC

Thorburn, A. N., O'Sullivan, B. J., Thomas, R., Kumar, R. K., Foster, P. S., Gibson, P. G., et al. (2010). Pneumococcal Conjugate Vaccine-Induced Regulatory T Cells Suppress the Development of Allergic Airways Disease. *Thorax* 65 (12), 1053–1060. doi:10.1136/thx.2009.131508

Tournoy, K. G., Kips, J. C., and Pauwels, R. A. (2000). Endogenous Interleukin-10 Suppresses Allergen-Induced Airway Inflammation and Nonspecific Airway Responsiveness. *Clin. Exp. Allergy* 30 (6), 775–783. doi:10.1046/j.1365-2222.2000.00838.x

Varin, A., Mukhopadhyay, S., Herbein, G., and Gordon, S. (2010). Alternative Activation of Macrophages by IL-4 Impairs Phagocytosis of Pathogens but Potentiates Microbial-Induced Signalling and Cytokine Secretion. *Blood* 115 (2), 353–362. doi:10.1182/blood-2009-08-236711

Vorobjeva, N. V., and Chernyak, B. V. (2020). NETosis: Molecular Mechanisms, Role in Physiology and Pathology. *Biochemistry (Mosc)* 85 (10), 1178–1190. doi:10.1134/S0006297920100065

Wang, H., Aloe, C., McQualter, J., Papanicolaou, A., Vlahos, R., Wilson, N., et al. (2021). G-CSFR Antagonism Reduces Mucosal Injury and Airways Fibrosis in a Virus-dependent Model of Severe Asthma. *Br. J. Pharmacol.* 178 (8), 1869–1885. doi:10.1111/bph.15415

Wang, H., Anthony, D., Yatmaz, S., Wijburg, O., Satzke, C., Levy, B., et al. (2017). Aspirin-triggered Resolvin D1 Reduces Pneumococcal Lung Infection and Inflammation in a Viral and Bacterial Coinfection Pneumonia Model. *Clin. Sci. (Lond)* 131 (18), 2347–2362. doi:10.1042/CS20171006

Wang, H., Blackall, M., Sominsky, L., Spencer, S. J., Vlahos, R., Churchill, M., et al. (2018). Increased Hypothalamic Microglial Activation after Viral-Induced Pneumococcal Lung Infection Is Associated with Excess Serum Amyloid A Production. *J. Neuroinflammation* 15 (1), 200. doi:10.1186/s12974-018-1234-1

Wang, H., FitzPatrick, M., Wilson, N. J., Anthony, D., Reading, P. C., Satzke, C., et al. (2019). CSF3R/CD114 Mediates Infection-dependent Transition to Severe Asthma. *J. Allergy Clin. Immunol.* 143 (2), 785–e6. doi:10.1016/j.jaci.2018.10.001

Winter, C., Taut, K., Srivastava, M., Länger, F., Mack, M., Briles, D. E., et al. (2007). Lung-specific Overexpression of CC Chemokine Ligand (CCL) 2 Enhances the Host Defense to Streptococcus Pneumoniae Infection in Mice: Role of the CCL2-CCR2 axis. *J. Immunol.* 178 (9), 5828–5838. doi:10.4049/jimmunol.178.9.5828

Conflict of Interest: CS is Lead Investigator on a Merck Investigator Studies Program grant funded by MSD on pneumococcal pneumonia and is an Investigator on a clinical research collaboration with Pfizer on PCV13.

The remaining authors declare that the research was conducted in the absence of any commercial or financial relationships that could be construed as a potential conflict of interest.

Publisher's Note: All claims expressed in this article are solely those of the authors and do not necessarily represent those of their affiliated organizations, or those of the publisher, the editors and the reviewers. Any product that may be evaluated in this article, or claim that may be made by its manufacturer, is not guaranteed or endorsed by the publisher.

frontiers in Pharmacology

ORIGINAL RESEARCH
published: 14 March 2022
doi: 10.3389/fphar.2022.762840

Mitochondrial Protein *Akap*1 Deletion Exacerbates Endoplasmic Reticulum Stress in Mice Exposed to Hyperoxia

Sahebgowda Sidramagowda Patil[1], *Ramani Soundararajan*[1], *Jutaro Fukumoto*[1], *Mason Breitzig*[1,2], *Helena Hernández-Cuervo*[1,3], *Matthew Alleyn*[1], *Muling Lin*[1], *Venkata Ramireddy Narala*[4], *Richard Lockey*[1], *Narasaiah Kolliputi*[1,3]* and *Lakshmi Galam*[1]*

[1]University of South Florida, Division of Allergy and Immunology, Department of Internal Medicine, College of Medicine, Tampa, FL, United States, [2]Washington University in St. Louis, Brown School, St. Louis, MO, United States, [3]University of South Florida, Department of Molecular Medicine, College of Medicine, Tampa, FL, United States, [4]Department of Zoology, Yogi Vemana University, Kadapa, India

OPEN ACCESS

Edited by:
Irfan Rahman,
University of Rochester, United States

Reviewed by:
Sekhar P. Reddy,
University of Illinois at Chicago, United States
Sreerama Shetty,
University of Texas at Tyler, United States

***Correspondence:**
Narasaiah Kolliputi
nkollipu@usf.edu
Lakshmi Galam
lgalam@usf.edu

Specialty section:
This article was submitted to Respiratory Pharmacology, a section of the journal Frontiers in Pharmacology

Received: 23 August 2021
Accepted: 27 January 2022
Published: 14 March 2022

Citation:
Sidramagowda Patil S, Soundararajan R, Fukumoto J, Breitzig M, Hernández-Cuervo H, Alleyn M, Lin M, Narala VR, Lockey R, Kolliputi N and Galam L (2022) Mitochondrial Protein Akap1 Deletion Exacerbates Endoplasmic Reticulum Stress in Mice Exposed to Hyperoxia. Front. Pharmacol. 13:762840. doi: 10.3389/fphar.2022.762840

Acute lung injury (ALI) and its severe manifestation, acute respiratory distress syndrome (ARDS), are treated with high concentrations of supplementary oxygen. However, prolonged exposure to high oxygen concentrations stimulates the production of reactive oxygen species (ROS), which damages the mitochondria and accumulates misfolded proteins in the endoplasmic reticulum (ER). The mitochondrial protein A-kinase anchoring protein 1 (*Akap1*) is critical for mitochondrial homeostasis. It is known that *Akap1* deficiency results in heart damage, neuronal development impairment, and mitochondrial malfunction in preclinical studies. Our laboratory recently revealed that deleting *Akap1* increases the severity of hyperoxia-induced ALI in mice. To assess the role of *Akap1* deletion in ER stress in lung injury, wild-type and *Akap1*$^{-/-}$ mice were exposed to hyperoxia for 48 h. This study indicates that *Akap1*$^{-/-}$ mice exposed to hyperoxia undergo ER stress, which is associated with an increased expression of BiP, JNK phosphorylation, eIF2α phosphorylation, ER stress-induced cell death, and autophagy. This work demonstrates that deleting *Akap1* results in increased ER stress in the lungs of mice and that hyperoxia exacerbates ER stress-related consequences.

Keywords: ALI, ARDS, ROS, ER stress, Akap1

INTRODUCTION

The most common treatment for human acute respiratory distress syndrome is supplemental oxygen (Kallet and Matthay, 2013). However, prolonged exposure to high concentrations of supplementary oxygen leads to increased production of reactive oxygen species (ROS). This prolonged exposure induces hyperoxic acute lung injury in rodent models (Galam et al., 2015), leading to death (Kwak et al., 2006; Kallet and Matthay, 2013). This hyperoxia-induced stress (Fukumoto et al., 2013) can cause protein misfolding in the ER and trigger unfolded protein response (UPR) (Gewandter et al., 2009). The endoplasmic reticulum (ER) possesses receptors to alleviate stress by activation of PERK (protein kinase-like ER kinase), activation of transcription factor 6 (ATF6), and inositol requiring

Abbreviations: AK, Akap1; AV, alveoli; HO, hyperoxia; KO, knockout; NO, normoxia; PB, peribronchial; Wt, wild type.

enzyme 1 (IRE1α) (Gewandter et al., 2009). The binding immunoglobulin protein (BiP) also promotes proper folding of proteins (Sano and Reed, 2013). ER stress leads to C-junction N-terminal kinase (JNK) phosphorylation, eukaryotic initiation factor (eIF2α) phosphorylation, ER stress-induced cell death, and autophagy (Sano and Reed, 2013; Lee et al., 2015; Hoffman et al., 2016; Cnop et al., 2017). The rodent hyperoxia model mimics the clinical presentation of ALI by augmenting oxidative stress (Kallet and Matthay, 2013) and exacerbating respiratory failure through ER stress, events for which there are no viable treatments (Gewandter et al., 2009). Therefore, investigating the pathways and mechanisms of acute lung injury in rodents caused by hyperoxia is crucial to finding an effective treatment for acute lung injury in humans. Likewise, the mechanistic role of mitochondrial proteins in hyperoxia-induced ALI needs clarification.

Mitochondria play an essential role in oxidative metabolism, ROS generation, cell cycle progression, and other key biological pathways (McBride et al., 2006; Nagar et al., 2018). Mitochondrial integrity is affected by hyperoxia as it enhances ROS production and thus the levels of lipid peroxidation byproducts, including the reactive aldehyde 4-hydroxy-2-nonenal (4-HNE) (Kolliputi and Waxman, 2009a; Galam et al., 2015; Breitzig et al., 2016; Narala et al., 2018). The resultant mitochondrial disturbances are associated with ER stress due to cross talk between mitochondria and the ER (Malhotra and Kaufman, 2011; van Vliet and Agostinis, 2018; Chu et al., 2019). ER stress is also associated with neurodegenerative diseases, ophthalmological disorders, cancer, inflammation, and metabolic diseases (Sano and Reed, 2013). The cross-link between mitochondria and the ER suggests that targeting ER stress can offer novel insights into the treatment of acute lung injury.

Within mitochondria, *Akap1*, a scaffolding protein, plays an important role in PKA regulation, cAMP signaling, and maintenance of mitochondrial homeostasis (Carlucci et al., 2008a; Merrill and Strack, 2014). *Akap*1 is abundantly expressed in the liver, heart, brain, kidney, and skeletal muscles and has three isoforms: AKAP121 (mouse), AKAP149 (human), and AKAP84 (alternative splicing) (Merrill and Strack, 2014). The downregulation of *Akap1* causes mitochondrial damage, cardiac dysfunction, lung injury, and neuronal death (Perrino et al., 2010; Merrill and Strack, 2014; Narala et al., 2018). *Akap1* deletion is associated with autophagy, mitophagy, and apoptosis in murine studies (Merrill and Strack, 2014; Narala et al., 2018). The significance of *Akap1* has been extensively studied in hypoxia-induced cardiac disease. Our laboratory has studied the role of *Akap1* in hyperoxic lung injury. However, the role of *Akap1* concerning ER stress during hyperoxia is unknown. It is hypothesized that *Akap1* deletion will exacerbate ER stress associated with hyperoxia.

MATERIALS AND METHODS

Mice

All animal procedures were approved by the Institutional Animal Care and Use Committee of the University of South Florida. Dr. Stanley McKnight (University of Washington) generated the *Akap1*$^{-/-}$ mice (Newhall et al., 2006) and donated them to Dr. Stefan Strack (The University of Iowa). The *Akap1*$^{-/-}$ mice were generously donated by Dr. Stefan Strack. All the mice aged 7–9 weeks were accommodated in individually ventilated cages and maintained under similar conditions of a dark–light cycle, humidity (60 ± 5%), and temperature (22 ± 1°C). The mice were fed a regular diet *ad libitum*.

Genotyping

The *Akap1* genotype was determined by PCR, and primers were used according to a previous study (Flippo et al., 2018).

In Vivo Hyperoxia Exposure

Wild-type (*Wt*) and *Akap1*$^{-/-}$ mice were kept in cages within an airtight hyperoxia cabinet (75 × 50 × 50 cm) and exposed to 100% oxygen for 48 h in a specific pathogen-free environment. The oxygen concentration was measured by using a proOx p100 sensor (Biospherix, New York, NY) as described previously (Kolliputi and Waxman, 2009a).

Quantitative Real-Time PCR

Wt and *Akap1*$^{-/-}$ mice lungs were collected after normoxia and hyperoxia (48 h) exposure. Total RNA was extracted from the lungs by using RNeasy kit (Qiagen, Hilden, Germany) and reverse-transcribed by using the iScript cDNA synthesis kit (Biorad Laboratories, Hercules, CA) and 1 ug of total RNA was used. qRT-PCR was performed for PERK, IRE1α, and ATF6 by using the SsoFast EvaGreen Supermix kit as per the manufacturer's instructions (Bio-Rad). The primer sequences for PERK (Saito et al., 2011), IRE1α (Tsuru et al., 2016), ATF6α (Egawa et al., 2011), and 18s (Chen et al., 2009) were obtained from previous studies; and 18s was used as an internal calibrator. The experiment was performed using the Bio-Rad CFX96 real-time system (C1000 Thermal Cycler) as per the manufacturer's guidelines. A relative fold change was analyzed by CFX Manager software (Bio-Rad) based on the ΔΔCT method. The sequences of the primers are as follows.

PERK forward: **5′- TCTTGGTTGGGTCTGATGAAT -3**'.
PERK reverse: **5′- GATGTTCTTGCTGTAGTGGGGG -3**'.
Ire1α forward: **5′-GCCGAAGTTCAGATGGAATC-3**'.
Ire1α reverse: **5′-ATCAGCAAAGGCCGATGA-3**'.
Atf6α forward: **5′-TTATCAGCATACAGCCTGCG-3**'.
Atf6α reverse: **5′- CTTGGGACTTTGAGCCTCTG-3**'.
18s forward primer: **5′-GGCCCTGTAATTGGAATGAGTC-3**'.
18s reverse primer: **5′-CCAAGATCCAACTACGAGCTT-3**'.

Western Blotting

Wild-type (*Wt*) and *Akap1*$^{-/-}$ mice following normoxia and hyperoxia (48 h) exposure were euthanized, and the lungs were collected, snap-frozen, and stored in liquid nitrogen. The lungs were pulverized and lysed in lysis buffer (20 mM Tris–HCl, pH 7.4, 150 mM NaCl, and 0.5%, Triton X-100), and the supernatant was collected by centrifugation at 21,000 rpm for 15 min at 4°C. The amount of protein was assessed by using the BCA assay kit (Pierce, Rockford, Waltham, MA), and equal amounts of protein (5 μg) were separated by using the SDS-PAGE, followed by transfer onto PVDF membranes. The membranes were blocked in 5% BSA and washed with TBST, followed by incubation with specific primary and secondary

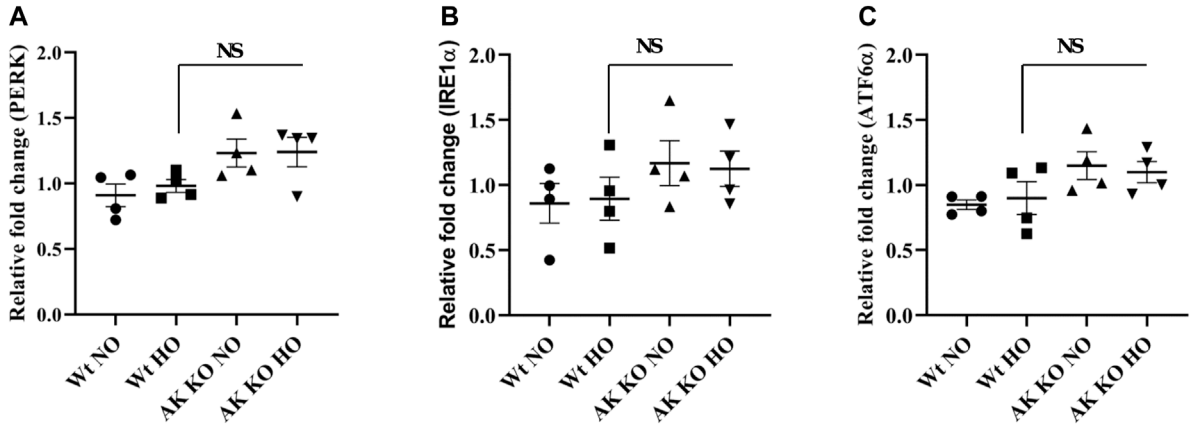

FIGURE 1 | Effect of *Akap1* genetic deletion on ER stress-related receptor transcripts: *Wt* and *Akap1* mice were exposed to normoxia and hyperoxia for 48 h. After hyperoxia, the mice were euthanized, and total RNA was isolated from the lungs and subjected to qRT-PCR analysis and quantified using the ΔΔCt method. Relative fold change in **(A)** PERK, **(B)** IRE1α, and **(C)** ATF6α is shown. Data are expressed as mean ± SEM ($n = 4$ mice per group). NS, not significant; NO, normoxia; HO, hyperoxia; AK, *Akap1*; KO: Knockout.

antibodies, respectively. The primary antibodies used were BiP, JNK, *p*-JNK, eIF2α, *p*-eIF2α, Atg12, Beclin-1, CHOP (C/EBP homologous protein), Lc3b, β-actin (Cell Signaling Technology, Danvers, MA), and Erp57 (Stressgen, Farmingdale, NY), and the secondary antibodies used were anti-rabbit and anti-mouse conjugated to HRP (Jackson ImmunoResearch, West Grove, PA). The proteins were visualized by using Kwik quant ECL solution (Kindle Biosciences, Greenwich, CT) and quantified by using ImageJ (NIH, Bethesda, MD). The ratio of protein to its loading control (β-actin) was recorded. A master mix was prepared by diluting lung lysates to get a protein concentration of 1 μg/μl. From this master mix, equal amount of protein (5 μg) was separated on SDS-PAGE and probed with anti-β-Actin HRP conjugated antibody. The same set of β-Actin control image is shown in multiple figures as it represents identical set of lung lysates used for western blot analyses.

Immunohistochemistry

After euthanizing the mice, the left lung was fixed in 4% paraformaldehyde; immunohistochemistry (IHC) was performed on paraffin-embedded lung tissue sections. In brief, the paraffin-embedded lung sections were deparaffinized with xylene, and the tissue sections were subjected to heat-induced antigen retrieval in a Tris buffer (10 mM Tris–HCl buffer at pH 9). Furthermore, endogenous peroxidase activity was quenched by incubating the sections in 3% hydrogen peroxide for 20 min, and the tissue sections were blocked with 10% goat serum for 20 min. The sections were incubated with specific primary antibodies (BiP, *p*-JNK, Erp57, and Lc3b) overnight at 4°C. The following day, the sections were probed with goat anti-rabbit antibodies (HRP-conjugated). Finally, detection of protein was carried out by using the Immpact VIP peroxidase substrate kit (Vector Laboratories, Burlingame, CA) (Fukumoto et al., 2019). The sections were imaged by using a microscope (Olympus BX43, Tokyo, Japan), attached to an Olympus DP21. The images were processed using Adobe Photoshop ver C56.

Statistical Analysis

The data are represented as mean ± S.E.M. Statistical analysis was carried out using GraphPad Prism (ver 10, San Diego, CA). Comparisons of multiple groups utilized one-way ANOVA, followed by Tukey's post hoc test, for normally distributed data, and $p < 0.05$ was considered statistically significant.

RESULTS

Genotyping and Expression of *Akap*1 Mice

The genotyping was confirmed by PCR. The agarose gel shows the *Wt* band (600 bp) and the *Akap*1 KO band (400 bp) (**Supplementary Figure S1**). The basal protein levels of *Akap1* were previously demonstrated by Western blot (Narala et al., 2018).

Effect of *Akap1* Deletion on ER Stress Receptor Transcripts After Hyperoxia

Wt and *Akap1*$^{-/-}$ mice were exposed to normoxia and hyperoxia as described in earlier studies to investigate the impact of *Akap1* deletion on ER stress receptors (Kolliputi and Waxman, 2009b; Kolliputi et al., 2010). The lung samples were subjected to qRT-PCR analysis in *Akap1*$^{-/-}$ versus *Wt* mice under normoxia, and the data show a 1.35-, 1.36-, and 1.35-fold increase in PERK, IRE1α, and ATF6α, respectively (**Figures 1A–C**) However, no significant increase was observed under hyperoxia exposure, suggesting that *Akap1*$^{-/-}$ may cause slight upregulation of unfolded protein response (UPR) at the transcript level under normoxia.

Akap1 Deletion Enhances BiP Levels After Hyperoxia

Wt and *Akap1*$^{-/-}$ mice were exposed to hyperoxia or kept in normoxia to evaluate the interaction between *Akap1* deletion and BiP. A significant increase of 3.28-fold occurred in the BiP

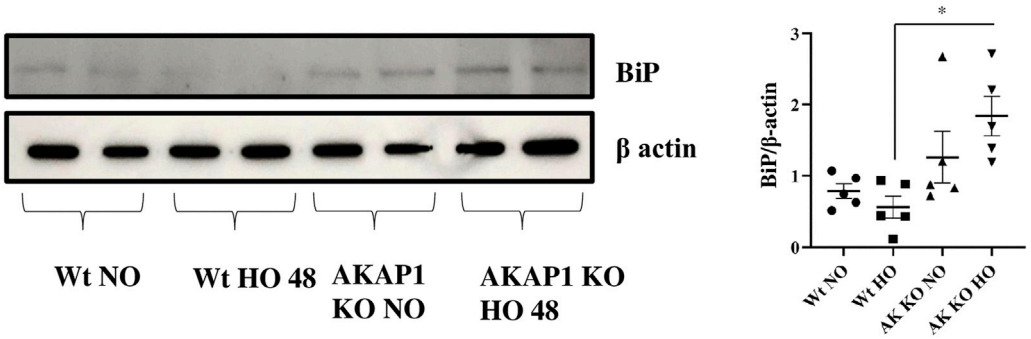

FIGURE 2 | *Akap1* genetic deletion activates BiP after hyperoxic exposure: *Wt* and *Akap1* mice were exposed to normoxia and hyperoxia for 48 h. After hyperoxia, the mice were killed, and protein from the lungs was extracted and subjected to Western blot analysis to evaluate the expression of BiP, and β-actin was used as a loading control. Densitometry analysis of protein was carried out, and fold change was calculated after normalizing to β-Actin. Data are shown as mean ± S.E.M (*p < 0.05) (n = 5 mice per group), NO, normoxia; HO, hyperoxia; AK, *Akap1*; KO: Knockout.

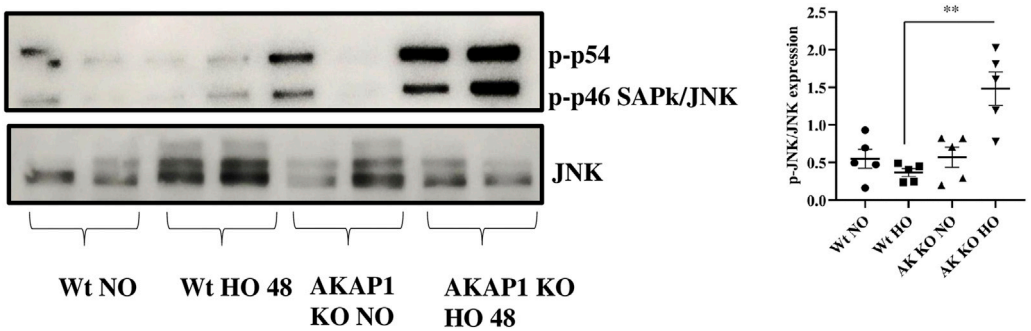

FIGURE 3 | *Akap1* genetic deletion activates JNK after hyperoxic exposure: *Wt* and *Akap1* mice were exposed to normoxia and hyperoxia for 48 h. After hyperoxia, the mice were killed, and protein from the lungs was extracted and subjected to Western blot analysis to evaluate the expression of JNK and *p*-JNK. Densitometry analysis was carried out, and after normalization with β-actin, the results were expressed in fold change. Data are shown as mean ± S.E.M (**p < 0.01) (n = 5 mice per group), NO, normoxia; HO, hyperoxia; AK, *Akap1*; KO: Knockout.

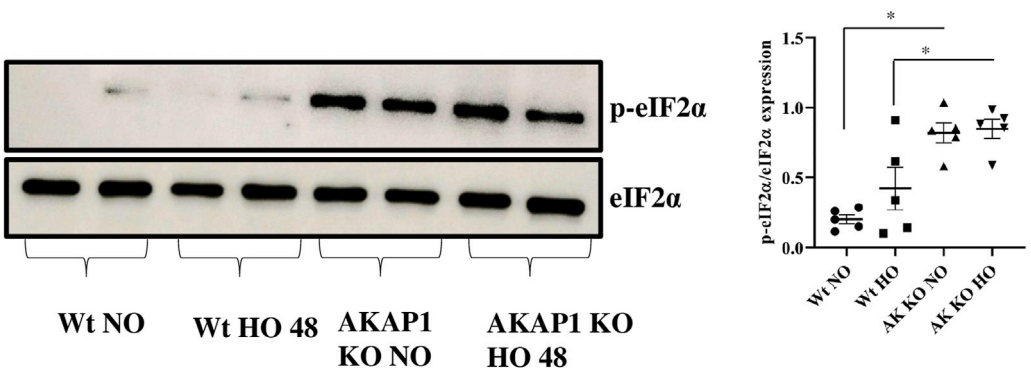

FIGURE 4 | *Akap1* genetic deletion causes phosphorylation of eukaryotic initiation factor (eIF2α): *Wt* and *Akap1* mice were exposed to normoxia and hyperoxia for 48 h. After hyperoxia, the mice were killed, and protein was extracted from the lungs and subjected to Western blot analysis. Following densitometry analysis and normalization with β-actin, the ratio of *p*-eIF2α to eIF2α protein levels was evaluated. Results are expressed in fold change. Data are shown as mean ± SEM (*p < 0.05) (n = 5 mice per group). NO, normoxia; HO, hyperoxia; AK, *Akap1*; KO: Knockout.

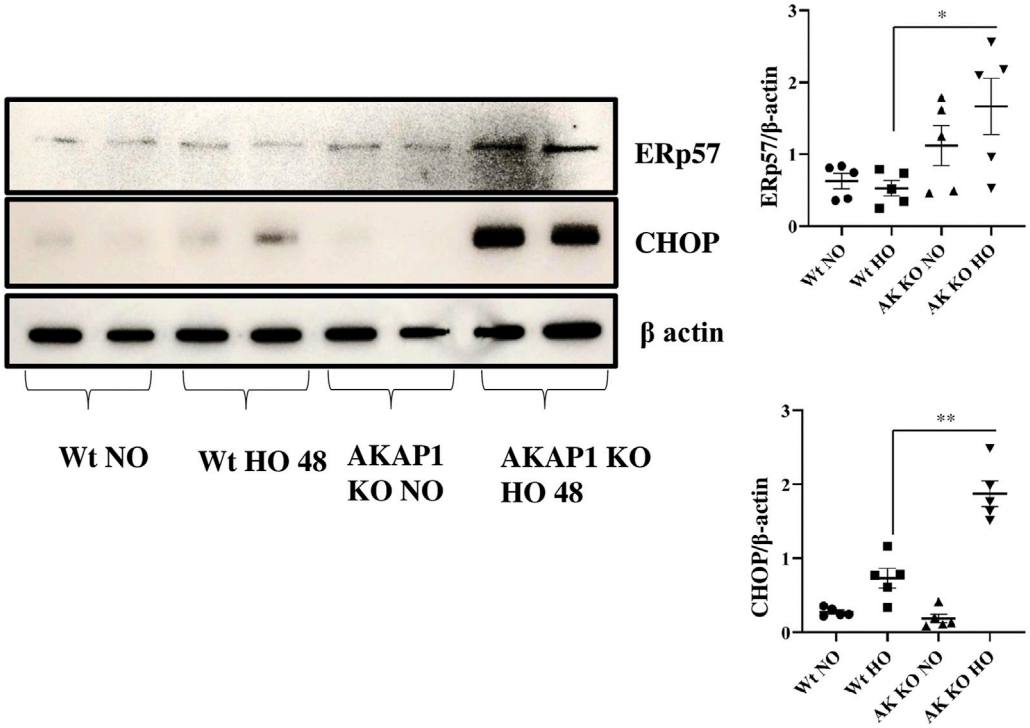

FIGURE 5 | *Akap1* genetic deletion enhances ER stress-induced cell death after hyperoxic exposure: *Wt* and *Akap1* mice were exposed to normoxia and hyperoxia for 48 h. After hyperoxia, the mice were killed, and protein was extracted from the lungs and subjected to Western blot analysis to evaluate the expression of CHOP and Erp57. β-actin was used as a loading control. Densitometry analysis of CHOP and Erp57 protein was followed by normalization to β-actin. Data are expressed as mean ± SEM (*$p < 0.05$, **$p < 0.005$) ($n = 5$ mice per group). NO, normoxia; HO, hyperoxia; AK, *Akap1*; KO: Knockout.

expression (**Figure 2**) in *Akap1*$^{-/-}$ versus *Wt* mice exposed to hyperoxia in the lung lysates subjected to Western blot analysis. There was a non-significant 1.61- and 2.25-fold increase in BiP expression in *Akap1*$^{-/-}$ mice under normoxia versus *Wt* normoxia and *Wt* hyperoxia, respectively. Enhanced BiP signals in the lung samples as evaluated by IHC were observed in the alveolar and peribronchial regions in *Akap1*$^{-/-}$ versus *Wt* mice exposed to hyperoxia (**Supplementary Figures S2A,B**).

Akap1 Deletion Activates JNK After Hyperoxia

Wt and *Akap1*$^{-/-}$ mice were exposed to normoxia or hyperoxia to investigate the relationship between *Akap1* deletion and JNK. The immunoblot analysis showed a 4.1-fold significant increase in the expression of the *p*-JNK (**Figure 3**) in *Akap1*$^{-/-}$ versus *Wt* mice exposed to hyperoxia. There was no difference under normoxia between *Wt* and *Akap1*$^{-/-}$ mice. The expression of *p*-JNK was evaluated by IHC in the lung samples. Increased *p*-JNK signals (**Supplementary Figure.S3**) were observed in the peribronchial region of *Akap1*$^{-/-}$ versus *Wt* mice exposed to hyperoxia.

Akap1 Deletion Causes Phosphorylation of Eukaryotic Initiation Factor

Wt and *Akap1*$^{-/-}$ mice were exposed to normoxia or hyperoxia to investigate the interaction between *Akap1* deletion and eIF2α. Immunoblot results showed a 4-fold significant increase in the expression of *p*-eIF2α (**Figure 4**) in *Akap1*$^{-/-}$ versus *Wt* mice in normoxia and a 2-fold significant increase in *Akap1*$^{-/-}$ versus *Wt* following hyperoxia.

Akap1 Deletion Causes ER Stress-Induced Cell Death After Hyperoxia

Wt and *Akap1*$^{-/-}$ mice were exposed to normoxia or hyperoxia to investigate the connection between *Akap1* deletion and ER stress-induced cell death. Western blot analysis indicated that there were significant increases in the expression of ERp57 (3.13-fold) and CHOP (2.56-fold) (**Figure 5**) in *Akap1*$^{-/-}$ versus *Wt* mice exposed to hyperoxia for 48 h. Furthermore, mouse lung tissue samples were subjected to IHC to confirm ER stress-induced cell death. ERp57 signals (**Supplementary Figures S4A,B**) were more abundant in the alveolar and peribronchial regions of *Akap1*$^{-/-}$ versus *Wt* mice exposed to hyperoxia for 48 h.

Akap1 Deletion Causes Autophagy After Hyperoxia

The protein autophagy-related gene 12 (ATG12) plays a key role in the formation of the autophagosome (Otomo et al., 2013), and the Beclin-1 and Lc3b proteins induce autophagy (Wirawan et al., 2012; Satyavarapu et al., 2018; Vega-Rubín-de-Celis, 2019). *Wt* and *Akap1*$^{-/-}$ mice were exposed to normoxia or hyperoxia to

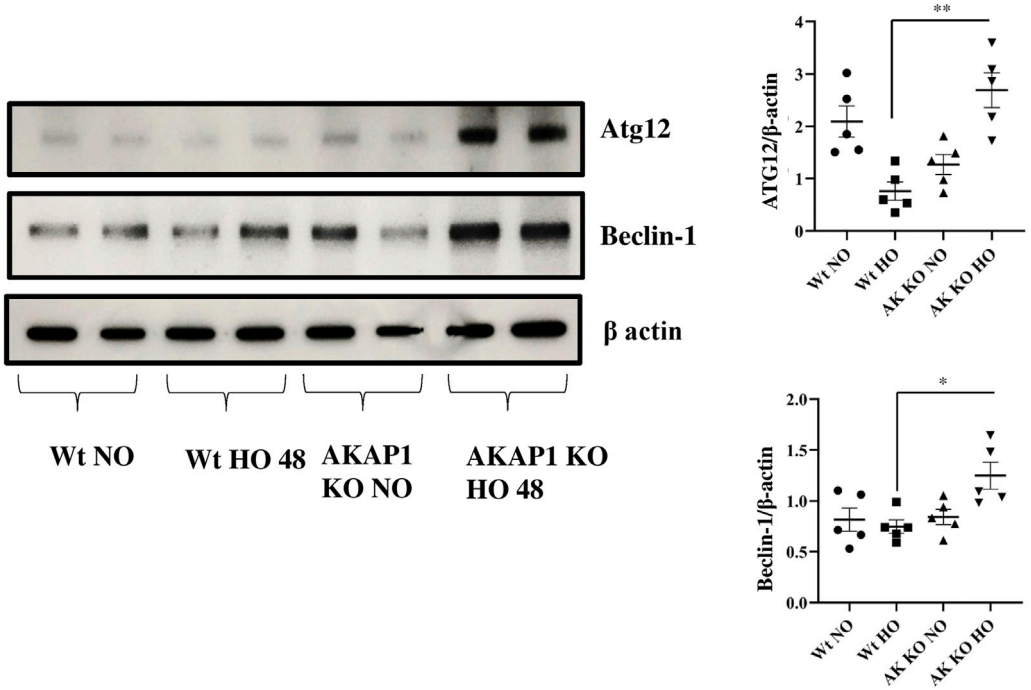

FIGURE 6 | *Akap1* genetic deletion enhances autophagy after hyperoxic exposure: *Wt* and *Akap1* mice were exposed to normoxia and hyperoxia for 48 h. After hyperoxia, the mice were killed, and protein was extracted from the lungs and subjected to Western blot analysis to evaluate the protein expression of Atg12 and Beclin-1. β-actin was used as a loading control. Densitometry analysis of Atg12 and Beclin-1 was followed by normalization with β-actin. Data are shown as mean ± S.E.M (*p < 0.05, **p < 0.01) (n = 5 mice per group). NO, normoxia; HO, hyperoxia; AK, *Akap1*; KO: Knockout.

investigate the effect of *Akap1* deletion on autophagy. Immunoblot results indicate a significant 3.42- and 1.67-fold increase in the expression of ATG12 and Beclin-1 (**Figure 6**), respectively, in *Akap1*$^{-/-}$ versus *Wt* mice exposed to hyperoxia for 48 h. Mouse tissue samples were subjected to IHC analysis to investigate the effects on autophagy. The Lc3b (**Supplementary Figures S5A,B**) was highly expressed in the alveolar and peribronchial regions of *Akap1*$^{-/-}$ versus *Wt* mice exposed to hyperoxia for 48 h.

DISCUSSION

These studies indicate that *Akap1* genetic deletion exacerbates ER stress associated with hyperoxia. *Akap1* deletion results in the following: 1) partial activation of the ER stress receptors under normoxia, 2) BiP activation after hyperoxic exposure, 3) JNK phosphorylation following hyperoxic exposure, 4) phosphorylation of eukaryotic initiation factor, 5) an increase in ER stress-induced cell death, and 6) increased autophagy.

The ER plays an important role in the homeostasis of cells by regulating lipid synthesis, protein secretion, calcium homeostasis, and protein folding (Szegezdi et al., 2006). Disturbance in the homeostasis of the ER triggers UPR by activating the ER receptors PERK, IRE1α, and ATF6 (Malhotra and Kaufman, 2007). In this study, *Akap1* deletion shows a minimal increase in UPR receptor proteins versus *Wt* mice under normoxia. In this study, the mice were exposed to hyperoxia for 48 h which did not seem to affect the ER stress receptors (**Figures 1A–C**). This corroborates with another study which showed that hyperoxia does not impact ER receptors in *Wt* mice exposed to hyperoxia for 64 h (Gewandter et al., 2009). A short period of hyperoxia exposure (3–6 h) may be required to observe the effect of hyperoxia on ER stress receptor transcripts.

BiP is a hallmark of ER stress response and UPR (Ron and Walter, 2007). The consistent protein aggregation from ER stress causes a transition from pro-survival to pro-apoptotic/ER stress-induced cell death (Lu et al., 2015). Increased BiP levels were found in *Akap1*$^{-/-}$ versus *Wt* mice exposed to normoxia and hyperoxia, indicating that *Akap1*$^{-/-}$ mice are susceptible to ER stress and that hyperoxia exacerbates this stress by causing the aggregation of misfolded proteins (Lu et al., 2015). BiP expression can be increased in cancer, drug-resistant cancer cells, and dormant cancer cells (Li et al., 2011).

PKA protects cells from ER stress and *Akap*1 regulates PKA (Gewandter et al., 2009; Aguileta et al., 2016). The presence of PKA negatively regulates the JNK protein (Zeitlin et al., 2011). JNK, as with oxidative stress, environmental stress, and the presence of pro-inflammatory cytokines, is phosphorylated under stress conditions (Yamasaki et al., 2017). Our data indicate that *Akap1* deletion depletes PKA levels and elevates the phosphorylation of JNK. Hyperoxia treatment also augments *p*-JNK levels, in agreement with our previous studies (Kolliputi and Waxman, 2009b; Galam et al., 2016). Additionally, hydrogen

peroxide treatment also activates JNK for initiating apoptosis (Kolliputi and Waxman, 2009b; Wei et al., 2010). JNK phosphorylation can occur during mitochondrial dysfunction, atherosclerosis, and metabolic diseases (Sano and Reed, 2013).

Prolonged hyperoxia exposure cause UPR and can induce eIF2α phosphorylation under stress conditions (Konsavage et al., 2012; Lu et al., 2015). The eIF2α phosphorylation also inhibits protein translation to induce endoplasmic stress-associated degradation (ERAD) (Ohno, 2014). *Akap1* is predominantly a mitochondrial protein. The shorter form of *Akap1* (N0) is known to target mitochondria, while the longer form (N1) targets the ER (Konsavage et al., 2010). It is plausible that the ER effects due to the *Akap1* deletion may be attributed to the N1 form. As previously observed, deletion of *Akap1* alters the size and structure of mitochondria (Schiattarella et al., 2016; Narala et al., 2018; Schiattarella et al., 2018). eIF2α phosphorylation is seen in Parkinson's disease and Alzheimer's disease (Sano and Reed, 2013; Ohno, 2014). These results suggest that *Akap1* deletion leads to eIF2α phosphorylation under normoxic and hyperoxic conditions. Further studies are required to evaluate the interaction between *Akap1* and eIF2α phosphorylation in human cell lines.

CHOP is expressed during ER stress and can lead to apoptosis (Xu et al., 2009; Hoffman et al., 2016). This protein is usually present at low levels but is upregulated and activated by eIF2α phosphorylation during ER stress, which causes DNA damage and growth arrest (Oyadomari and Mori, 2004; Xu et al., 2009; Hoffman et al., 2016). The protein, ERp57, is also expressed during ER stress and causes apoptosis (Xu et al., 2009; Hoffman et al., 2016). The data show an increase in ER stress-induced cell death markers, CHOP and ERp57, in $Akap1^{-/-}$ versus *Wt* mice exposed to hyperoxia. CHOP expression was seen in viral infection, neurodegenerative disease, atherosclerosis, metabolic disease, inflammation, and ophthalmology disease (Sano and Reed, 2013). The $Akap1^{-/-}$ mice under normoxia have increased expression of eIF2α phosphorylation but do not undergo CHOP mediated cell death. $Akap1^{-/-}$ mice under normoxia display enhanced ERp57 expression. It is possible that $Akap1^{-/-}$ mice may suffer ERp57-mediated cell death *via* the NFκB or STAT3 pathway (Liu et al., 2019). A wide array of evidence shows that ERp57 dysregulation occurs in melanoma, laryngeal cancer, and leukemia (Liu et al., 2019). ERp57 deletion causes a decrease in inflammatory cells, epidermal growth factor, periostin, and increased airway resistance (Hoffman et al., 2016).

ER stress leads to cellular degradation, apoptosis, inflammation, autophagy, mitophagy, and protein degradation (Senft and Ronai, 2015). The protein ATG12 plays a role in autophagy initiation and causes mitochondrial apoptosis (Rubinstein et al., 2011), while Beclin-1 is a regulator of autophagy, and LC3b is a marker of autophagy (Meyer et al., 2013). The data suggest that *Akap1* deletion induces autophagy compared to *Wt* mice exposed to hyperoxia. The expression of ATG12 in *Wt* mice is higher than that of $Akap1^{-/-}$ mice under normoxia. This suggests that certain cells undergo the formation of autophagosomes to maintain mitochondrial homeostasis due to damaged mitochondria (Radoshevich et al., 2010). Also, $Lc3b^{-/-}$ mice demonstrate decreased caspase activity (Sauler et al., 2015). Cho et al., 2009 found that Beclin-1 links apoptosis to autophagy in HELA cells mediated by caspases (Cho et al., 2009). Autophagy is also associated with neurodegenerative disease and cancer promotion, suggesting the impact of $Akap1^{-/-}$ on autophagy (Sano and Reed, 2013).

These findings suggest that *Akap1* has a crucial role in the lung in the setting of hyperoxic exposure. *Akap1*-knockout mice exposed to hyperoxia show activation of BiP, JNK phosphorylation, ER stress-induced cell death, autophagy, and eIF2α phosphorylation (even under normoxia). Therefore, *Akap1* is a potential therapeutic target in ALI for patients who require supplemental oxygen.

DATA AVAILABILITY STATEMENT

The raw data supporting the conclusions of this article will be made available by the authors, without undue reservation.

ETHICS STATEMENT

The animal study was reviewed and approved by the University of South Florida.

AUTHOR CONTRIBUTIONS

Concept and experimental design: SSP, LG, JF, RS, and MB; experiments performed: SSP, JF, HH-C, RS, and ML; figure preparations and data analyzed: SSP, JF, RS, VRN, and MA; manuscript revision and proofreading: NK, RS, VRN, MA, LG, RL, MB, HH-C, and MA; and final approval of the manuscript: LG and NK.

FUNDING

LG is supported by the AHA National Scientist Development Grant 17SDG32780002 and NK is supported by the National Institutes of Health R01 HL105932.

SUPPLEMENTARY MATERIAL

The Supplementary Material for this article can be found online at: https://www.frontiersin.org/articles/10.3389/fphar.2022.762840/full#supplementary-material

REFERENCES

Aguileta, M. A., Rojas-Rivera, D., Goossens, V., Estornes, Y., Van Isterdael, G., Vandenabeele, P., et al. (2016). A siRNA Screen Reveals the Prosurvival Effect of Protein Kinase A Activation in Conditions of Unresolved Endoplasmic Reticulum Stress. *Cell Death Differ.* 23, 1670–1680. doi:10.1038/cdd.2016.59

Breitzig, M., Bhimineni, C., Lockey, R., and Kolliputi, N. (2016). 4-Hydroxy-2-nonenal: a Critical Target in Oxidative Stress? *Am. J. Physiol. Cell Physiol.* 311, C537–C543. doi:10.1152/ajpcell.00101.2016

Carlucci, A., Adornetto, A., Scorziello, A., Viggiano, D., Foca, M., Cuomo, O., et al. (2008). Proteolysis of AKAP121 Regulates Mitochondrial Activity during Cellular Hypoxia and Brain Ischaemia. *EMBO J.* 27, 1073–1084. doi:10.1038/emboj.2008.33

Carlucci, A., Lignitto, L., and Feliciello, A. (2008). Control of Mitochondria Dynamics and Oxidative Metabolism by cAMP, AKAPs and the Proteasome. *Trends Cell Biol.* 18, 604–613. doi:10.1016/j.tcb.2008.09.006

Chen, C., Wickenheisser, J., Ewens, K. G., Ankener, W., Legro, R. S., Dunaif, A., et al. (2009). PDE8A Genetic Variation, Polycystic Ovary Syndrome and Androgen Levels in Women. *Mol. Hum. Reprod.* 15, 459–469. doi:10.1093/molehr/gap035

Cho, D. H., Jo, Y. K., Hwang, J. J., Lee, Y. M., Roh, S. A., and Kim, J. C. (2009). Caspase-mediated Cleavage of ATG6/Beclin-1 Links Apoptosis to Autophagy in HeLa Cells. *Cancer Lett.* 274, 95–100. doi:10.1016/j.canlet.2008.09.004

Chu, Q., Martinez, T. F., Novak, S. W., Donaldson, C. J., Tan, D., Vaughan, J. M., et al. (2019). Regulation of the ER Stress Response by a Mitochondrial Microprotein. *Nat. Commun.* 10, 4883. doi:10.1038/s41467-019-12816-z

Cnop, M., Toivonen, S., Igoillo-Esteve, M., and Salpea, P. (2017). Endoplasmic Reticulum Stress and eIF2α Phosphorylation: The Achilles Heel of Pancreatic β Cells. *Mol. Metab.* 6, 1024–1039. doi:10.1016/j.molmet.2017.06.001

Egawa, N., Yamamoto, K., Inoue, H., Hikawa, R., Nishi, K., Mori, K., et al. (2011). The Endoplasmic Reticulum Stress Sensor, ATF6α, Protects against Neurotoxin-Induced Dopaminergic Neuronal Death. *J. Biol. Chem.* 286, 7947–7957. doi:10.1074/jbc.M110.156430

Flippo, K. H., Gnanasekaran, A., Perkins, G. A., Ajmal, A., Merrill, R. A., Dickey, A. S., et al. (2018). AKAP1 Protects from Cerebral Ischemic Stroke by Inhibiting Drp1-dependent Mitochondrial Fission. *J. Neurosci.* 38, 8233–8242. doi:10.1523/JNEUROSCI.0649-18.2018

Fukumoto, J., Fukumoto, I., Parthasarathy, P. T., Cox, R., Huynh, B., Ramanathan, G. K., et al. (2013). NLRP3 Deletion Protects from Hyperoxia-Induced Acute Lung Injury. *Am. J. Physiol. Cell Physiol.* 305, C182–C189. doi:10.1152/ajpcell.00086.2013

Fukumoto, J., Leung, J., Cox, R., Czachor, A., Parthasarathy, P. T., Lagishetty, V., et al. (2019). Oxidative Stress Induces Club Cell Proliferation and Pulmonary Fibrosis in Atp8b1 Mutant Mice. *Aging (Albany NY)* 11, 209–229. doi:10.18632/aging.101742

Galam, L., Failla, A., Soundararajan, R., Lockey, R. F., and Kolliputi, N. (2015). 4-hydroxynonenal Regulates Mitochondrial Function in Human Small Airway Epithelial Cells. *Oncotarget* 6, 41508–41521. doi:10.18632/oncotarget.6131

Galam, L., Soundararajan, R., Breitzig, M., Rajan, A., Yeruva, R. R., Czachor, A., et al. (2016). SOCS-1 Rescues IL-1β-mediated Suppression of Epithelial Sodium Channel in Mouse Lung Epithelial Cells via ASK-1. *Oncotarget* 7, 29081–29091. doi:10.18632/oncotarget.8543

Gewandter, J. S., Staversky, R. J., and O'Reilly, M. A. (2009). Hyperoxia Augments ER-Stress-Induced Cell Death Independent of BiP Loss. *Free Radic. Biol. Med.* 47, 1742–1752. doi:10.1016/j.freeradbiomed.2009.09.022

Hoffman, S. M., Chapman, D. G., Lahue, K. G., Cahoon, J. M., Rattu, G. K., Daphtary, N., et al. (2016). Protein Disulfide Isomerase-Endoplasmic Reticulum Resident Protein 57 Regulates Allergen-Induced Airways Inflammation, Fibrosis, and Hyperresponsiveness. *J. Allergy Clin. Immunol.* 137, 822–e7. doi:10.1016/j.jaci.2015.08.018

Kallet, R. H., and Matthay, M. A. (2013). Hyperoxic Acute Lung Injury. *Respir. Care* 58, 123–141. doi:10.4187/respcare.01963

Kolliputi, N., Shaik, R. S., and Waxman, A. B. (2010). The Inflammasome Mediates Hyperoxia-Induced Alveolar Cell Permeability. *J. Immunol.* 184, 5819–5826. doi:10.4049/jimmunol.0902766

Kolliputi, N., and Waxman, A. B. (2009). IL-6 Cytoprotection in Hyperoxic Acute Lung Injury Occurs via PI3K/Akt-Mediated Bax Phosphorylation. *Am. J. Physiol. Lung Cell Mol. Physiol.* 297, L6–L16. doi:10.1152/ajplung.90381.2008

Kolliputi, N., and Waxman, A. B. (2009). IL-6 Cytoprotection in Hyperoxic Acute Lung Injury Occurs via Suppressor of Cytokine Signaling-1-Induced Apoptosis Signal-Regulating Kinase-1 Degradation. *Am. J. Respir. Cell Mol. Biol.* 40, 314–324. doi:10.1165/rcmb.2007-0287OC

Konsavage, W., Zhang, L., Vary, T., and Shenberger, J. S. (2010). Hyperoxia Inhibits Protein Synthesis and Increases eIF2α Phosphorylation in the Newborn Rat Lung. *Am. J. Physiol. Lung Cell Mol. Physiol.* 298, L678–L686. doi:10.1152/ajplung.00262.2009

Konsavage, W. M., Zhang, L., Wu, Y., and Shenberger, J. S. (2012). Hyperoxia-induced Activation of the Integrated Stress Response in the Newborn Rat Lung. *Am. J. Physiol. Lung Cell Mol. Physiol.* 302, L27–L35. doi:10.1152/ajplung.00174.2011

Kwak, D. J., Kwak, S. D., and Gauda, E. B. (2006). The Effect of Hyperoxia on Reactive Oxygen Species (ROS) in Rat Petrosal Ganglion Neurons during Development Using Organotypic Slices. *Pediatr. Res.* 60, 371–376. doi:10.1203/01.pdr.0000239817.39407.61

Lee, W. S., Yoo, W. H., and Chae, H. J. (2015). ER Stress and Autophagy. *Curr. Mol. Med.* 15, 735–745. doi:10.2174/1566524015666150921105453

Li, X., Zhang, K., and Li, Z. (2011). Unfolded Protein Response in Cancer: the Physician's Perspective. *J. Hematol. Oncol.* 4, 8. doi:10.1186/1756-8722-4-8

Liu, Y., Wang, J. X., Nie, Z. Y., Wen, Y., Jia, X. J., Zhang, L. N., et al. (2019). Upregulation of ERp57 Promotes clear Cell Renal Cell Carcinoma Progression by Initiating a STAT3/ILF3 Feedback Loop. *J. Exp. Clin. Cancer Res.* 38, 439. doi:10.1186/s13046-019-1453-z

Lu, H. Y., Zhang, J., Wang, Q. X., Tang, W., and Zhang, L. J. (2015). Activation of the Endoplasmic Reticulum Stress Pathway Involving CHOP in the Lungs of Rats with Hyperoxia-induced B-ronchopulmonary D-ysplasia. *Mol. Med. Rep.* 12, 4494–4500. doi:10.3892/mmr.2015.3979

Malhotra, J. D., and Kaufman, R. J. (2011). ER Stress and its Functional Link to Mitochondria: Role in Cell Survival and Death. *Cold Spring Harb. Perspect. Biol.* 3, a004424. doi:10.1101/cshperspect.a004424

Malhotra, J. D., and Kaufman, R. J. (2007). The Endoplasmic Reticulum and the Unfolded Protein Response. *Semin. Cell Dev. Biol.* 18, 716–731. doi:10.1016/j.semcdb.2007.09.003

McBride, H. M., Neuspiel, M., and Wasiak, S. (2006). Mitochondria: More Than Just a Powerhouse. *Curr. Biol.* 16, R551–R560. doi:10.1016/j.cub.2006.06.054

Merrill, R. A., and Strack, S. (2014). Mitochondria: a Kinase Anchoring Protein 1, a Signaling Platform for Mitochondrial Form and Function. *Int. J. Biochem. Cell Biol.* 48, 92–96. doi:10.1016/j.biocel.2013.12.012

Meyer, G., Czompa, A., Reboul, C., Csepanyi, E., Czegledi, A., Bak, I., et al. (2013). The Cellular Autophagy Markers Beclin-1 and LC3B-II Are Increased during Reperfusion in Fibrillated Mouse Hearts. *Curr. Pharm. Des.* 19, 6912–6918. doi:10.2174/13816128193931127122510

Nagar, H., Piao, S., and Kim, C. S. (2018). Role of Mitochondrial Oxidative Stress in Sepsis. *Acute Crit. Care* 33, 65–72. doi:10.4266/acc.2018.00157

Narala, V. R., Fukumoto, J., Hernández-Cuervo, H., Patil, S. S., Krishnamurthy, S., Breitzig, M., et al. (2018). Akap1 Genetic Deletion Increases the Severity of Hyperoxia-Induced Acute Lung Injury in Mice. *Am. J. Physiol. Lung Cell Mol. Physiol.* 314, L860–L870. doi:10.1152/ajplung.00365.2017

Newhall, K. J., Criniti, A. R., Cheah, C. S., Smith, K. C., Kafer, K. E., Burkart, A. D., et al. (2006). Dynamic Anchoring of PKA Is Essential during Oocyte Maturation. *Curr. Biol.* 16, 321–327. doi:10.1016/j.cub.2005.12.031

Ohno, M. (2014). Roles of eIF2α Kinases in the Pathogenesis of Alzheimer's Disease. *Front. Mol. Neurosci.* 7, 22. doi:10.3389/fnmol.2014.00022

Otomo, C., Metlagel, Z., Takaesu, G., and Otomo, T. (2013). Structure of the Human ATG12~ATG5 Conjugate Required for LC3 Lipidation in Autophagy. *Nat. Struct. Mol. Biol.* 20, 59–66. doi:10.1038/nsmb.2431

Oyadomari, S., and Mori, M. (2004). Roles of CHOP/GADD153 in Endoplasmic Reticulum Stress. *Cell Death Differ* 11, 381–389. doi:10.1038/sj.cdd.4401373

Perrino, C., Feliciello, A., Schiattarella, G. G., Esposito, G., Guerriero, R., Zaccaro, L., et al. (2010). AKAP121 Downregulation Impairs Protective cAMP Signals, Promotes Mitochondrial Dysfunction, and Increases Oxidative Stress. *Cardiovasc. Res.* 88, 101–110. doi:10.1093/cvr/cvq155

Radoshevich, L., Murrow, L., Chen, N., Fernandez, E., Roy, S., Fung, C., et al. (2010). ATG12 Conjugation to ATG3 Regulates Mitochondrial Homeostasis and Cell Death. *Cell* 142, 590–600. doi:10.1016/j.cell.2010.07.018

Ron, D., and Walter, P. (2007). Signal Integration in the Endoplasmic Reticulum Unfolded Protein Response. *Nat. Rev. Mol. Cell Biol.* 8, 519–529. doi:10.1038/nrm2199

Rubinstein, A. D., Eisenstein, M., Ber, Y., Bialik, S., and Kimchi, A. (2011). The Autophagy Protein Atg12 Associates with Antiapoptotic Bcl-2 Family Members to Promote Mitochondrial Apoptosis. *Mol. Cell* 44, 698–709. doi:10.1016/j.molcel.2011.10.014

Saito, A., Ochiai, K., Kondo, S., Tsumagari, K., Murakami, T., Cavener, D. R., et al. (2011). Endoplasmic Reticulum Stress Response Mediated by the PERK-eIF2(alpha)-ATF4 Pathway Is Involved in Osteoblast Differentiation Induced by BMP2. *J. Biol. Chem.* 286, 4809–4818. doi:10.1074/jbc.M110.152900

Sano, R., and Reed, J. C. (2013). ER Stress-Induced Cell Death Mechanisms. *Biochim. Biophys. Acta* 1833, 3460–3470. doi:10.1016/j.bbamcr.2013.06.028

Satyavarapu, E. M., Das, R., Mandal, C., Mukhopadhyay, A., and Mandal, C. (2018). Autophagy-independent Induction of LC3B through Oxidative Stress Reveals its Non-canonical Role in Anoikis of Ovarian Cancer Cells. *Cell Death Dis.* 9, 934. doi:10.1038/s41419-018-0989-8

Sauler, M., Zhang, Y., Min, J. N., Leng, L., Shan, P., Roberts, S., et al. (2015). Endothelial CD74 Mediates Macrophage Migration Inhibitory Factor protection in Hyperoxic Lung Injury. *FASEB J.* 29, 1940–1949. doi:10.1096/fj.14-260299

Schiattarella, G. G., Cattaneo, F., Carrizzo, A., Paolillo, R., Boccella, N., Ambrosio, M., et al. (2018). Akap1 Regulates Vascular Function and Endothelial Cells Behavior. *Hypertension* 71, 507–517. doi:10.1161/HYPERTENSIONAHA.117.10185

Schiattarella, G. G., Cattaneo, F., Pironti, G., Magliulo, F., Carotenuto, G., Pirozzi, M., et al. (2016). Akap1 Deficiency Promotes Mitochondrial Aberrations and Exacerbates Cardiac Injury Following Permanent Coronary Ligation via Enhanced Mitophagy and Apoptosis. *PloS One* 11, e0154076. doi:10.1371/journal.pone.0154076

Senft, D., and Ronai, Z. A. (2015). UPR, Autophagy, and Mitochondria Crosstalk Underlies the ER Stress Response. *Trends Biochem. Sci.* 40, 141–148. doi:10.1016/j.tibs.2015.01.002

Szegezdi, E., Logue, S. E., Gorman, A. M., and Samali, A. (2006). Mediators of Endoplasmic Reticulum Stress-Induced Apoptosis. *EMBO Rep.* 7, 880–885. doi:10.1038/sj.embor.7400779

Tsuru, A., Imai, Y., Saito, M., and Kohno, K. (2016). Novel Mechanism of Enhancing IRE1α-XBP1 Signalling via the PERK-ATF4 Pathway. *Sci. Rep.* 6, 24217. doi:10.1038/srep24217

van Vliet, A. R., and Agostinis, P. (2018). Mitochondria-Associated Membranes and ER Stress. *Curr. Top. Microbiol. Immunol.* 414, 73–102. doi:10.1007/82_2017_2

Vega-Rubín-de-Celis, S. (2019). The Role of Beclin 1-Dependent Autophagy in Cancer. *Biology (Basel)* 9. doi:10.3390/biology9010004

Wei, H., Li, Z., Hu, S., Chen, X., and Cong, X. (2010). Apoptosis of Mesenchymal Stem Cells Induced by Hydrogen Peroxide Concerns Both Endoplasmic Reticulum Stress and Mitochondrial Death Pathway through Regulation of Caspases, P38 and JNK. *J. Cell Biochem.* 111, 967–978. doi:10.1002/jcb.22785

Wirawan, E., Lippens, S., Vanden Berghe, T., Romagnoli, A., Fimia, G. M., Piacentini, M., et al. (2012). Beclin1: a Role in Membrane Dynamics and beyond. *Autophagy* 8, 6–17. doi:10.4161/auto.8.1.16645

Xu, D., Perez, R. E., Rezaiekhaligh, M. H., Bourdi, M., and Truog, W. E. (2009). Knockdown of ERp57 Increases BiP/GRP78 Induction and Protects against Hyperoxia and Tunicamycin-Induced Apoptosis. *Am. J. Physiol. Lung Cell Mol. Physiol.* 297, L44–L51. doi:10.1152/ajplung.90626.2008

Yamasaki, T., Deki-Arima, N., Kaneko, A., Miyamura, N., Iwatsuki, M., Matsuoka, M., et al. (2017). Age-dependent Motor Dysfunction Due to Neuron-specific Disruption of Stress-Activated Protein Kinase MKK7. *Sci. Rep.* 7, 7348. doi:10.1038/s41598-017-07845-x

Zeitlin, R., Patel, S., Burgess, S., Arendash, G. W., and Echeverria, V. (2011). Caffeine Induces Beneficial Changes in PKA Signaling and JNK and ERK Activities in the Striatum and Cortex of Alzheimer's Transgenic Mice. *Brain Res.* 1417, 127–136. doi:10.1016/j.brainres.2011.08.036

Conflict of Interest: The authors declare that the research was conducted in the absence of any commercial or financial relationships that could be construed as a potential conflict of interest.

Publisher's Note: All claims expressed in this article are solely those of the authors and do not necessarily represent those of their affiliated organizations, or those of the publisher, the editors, and the reviewers. Any product that may be evaluated in this article, or claim that may be made by its manufacturer, is not guaranteed or endorsed by the publisher.

frontiers in Pharmacology

ORIGINAL RESEARCH
published: 18 March 2022
doi: 10.3389/fphar.2022.767705

Chemerin Regulates the Proliferation and Migration of Pulmonary Arterial Smooth Muscle Cells *via* the ERK1/2 Signaling Pathway

*Linqian Peng[1,2†], Yunwei Chen[1,2†], Yan Li[1,2], Panpan Feng[1], Yan Zheng[1,2], Yongjie Dong[1,2], Yunjing Yang[1], Ruiyu Wang[1,2], Ailing Li[1], Jianghong Yan[2], Feifei Shang[2], Ping Tang[1], Dewei Chen[3], Yuqi Gao[3] and Wei Huang[1]**

[1]Department of Cardiology, The First Affiliated Hospital of Chongqing Medical University, Chongqing, China, [2]Institute of Life Science, Chongqing Medical University, Chongqing, China, [3]Institute of Medicine and Equipment for High Altitude Region, College of High Altitude Military Medicine, Army Medical University, Chongqing, China

OPEN ACCESS

Edited by:
Irfan Rahman, University of Rochester, United States

Reviewed by:
Haiyang Tang, University of Arizona, United States
Laurence Dewachter, Université libre de Bruxelles, Belgium

***Correspondence:**
Wei Huang
weihuangcq@gmail.com

[†]These authors have contributed equally to this work

Specialty section:
This article was submitted to Respiratory Pharmacology, a section of the journal Frontiers in Pharmacology

Received: *31 August 2021*
Accepted: *21 February 2022*
Published: *18 March 2022*

Citation:
Peng L, Chen Y, Li Y, Feng P, Zheng Y, Dong Y, Yang Y, Wang R, Li A, Yan J, Shang F, Tang P, Chen D, Gao Y and Huang W (2022) Chemerin Regulates the Proliferation and Migration of Pulmonary Arterial Smooth Muscle Cells via the ERK1/2 Signaling Pathway. Front. Pharmacol. 13:767705. doi: 10.3389/fphar.2022.767705

Pulmonary arterial hypertension (PAH) is an incurable disease with high mortality. Chemerin has been found to be associated with pulmonary hypertension (PH). However, the specific role of chemerin in mediating PH development remains unclear. This study aimed to elucidate the regulatory effects and the underlying mechanism of chemerin on PH and to investigate the expression levels of chemerin protein in plasma in PAH patients. *In vivo*, two animal models of PH were established in rats by monocrotaline (MCT) injection and hypoxia. We found that the expression levels of chemerin and its receptor, chemokine-like receptor 1 (CMKLR1), were significantly upregulated in the lungs of PH rats. Primary cultured pulmonary arterial smooth muscle cells [(PASMCs) (isolated from pulmonary arteries of normal healthy rats)] were exposed to hypoxia or treated with recombinant human chemerin, we found that CMKLR1 expression was upregulated in PASMCs in response to hypoxia or chemerin stimulation, whereas the exogenous chemerin significantly promoted the migration and proliferation of PASMCs. Notably, the regulatory effects of chemerin on PASMCs were blunted by PD98059 (a selective ERK1/2 inhibitor). Using enzyme linked immunosorbent assay (ELISA), we found that the protein level of chemerin was also markedly increased in plasma from idiopathic pulmonary arterial hypertension (IPAH) patients compared to that from healthy controls. Moreover, the diagnostic value of chemerin expression in IPAH patients was determined through receiver operating characteristic (ROC) curve analysis and the result revealed that area under ROC curve (AUC) for plasma chemerin was 0.949. Taken together, these results suggest that chemerin exacerbates PH progression by promoting the proliferation and migration of PASMCs via the ERK1/2 signaling pathway, and chemerin is associated with pulmonary hypertension.

Keywords: chemerin, chemokine-like receptor 1, pulmonary arterial hypertension, pulmonary arterial smooth muscle cells, ERK1/2

INTRODUCTION

As a serious life-threatening disease, pulmonary arterial hypertension (PAH) is characterized by pulmonary vascular remodeling, which often leads to progressive increases in pulmonary arterial pressure (PAP) and pulmonary vascular resistance (PVR), eventually resulting in right heart failure and death (Rich and Rich 2014). The primary pathological signs of pulmonary vascular remodeling include media hypertrophy, intimal proliferation, and adventitial thickening and fibrosis (Tuder 2017). Of note, among them, the proliferation of pulmonary arterial smooth muscle cells (PASMCs) is the main pathological feature of pulmonary vascular remodeling (Morrell et al., 2009). Mechanistically, inappropriate activation of the ERK1/2 signaling pathway plays a crucial role in the regulation of pulmonary vascular remodeling, and suppressing ERK1/2 activation effectively delays PH progression (Yu et al., 2017; Xing et al., 2019; Yang et al., 2021).

Chemerin, which is encoded by retinoic acid receptor responder 2 (RARRES2), is an adipokine secreted by the liver and adipocytes and is closely associated with inflammation, adipocyte growth, angiogenesis, and energy metabolism (Kennedy and Davenport 2018). Chemerin can bind to the following three receptors: chemokine-like receptor 1 (CMKLR1), C-C motif chemokine receptor like 2 (CCRL2) and G protein-coupled receptor 1 (GPR1) (Kennedy and Davenport 2018). Among them, CCRL2 elevates the local concentration of chemerin to promote chemerin binding to GPR1 and CMKLR1 (Zabel et al., 2008). Although GPR1 may be associated with glucose homeostasis, little is known about its specific biological effects (Rourke et al., 2014). In fact, chemerin participates in a variety of biological processes mainly by activating CMKLR1 (Kennedy et al., 2016; Wen et al., 2019). Therefore, the chemerin/CMKLR1 axis plays an important role in tumorigenesis, cardiovascular disease, metabolic syndrome and other conditions (Kunimoto et al., 2015; Weng et al., 2017; Jiang et al., 2018; Shin and Pachynski 2018). Furthermore, a study on systemic hypertension demonstrated that the chemerin/CMKLR1 axis regulated the activation and transduction of ERK1/2 signaling during vascular remodeling (Kunimoto et al., 2015), which has led to interest in exploring the association between chemerin and PH.

A recent study showed that chemerin and its receptor (CMKLR1) could be detected in the pulmonary arterial tissues of rats (Hanthazi et al., 2020). Chemerin-9-induced contraction was enhanced through the upregulation of CMKLR1 in the isolated pulmonary arteries of PH rats (Omori et al., 2020). Recombinant chemerin protein exogenously enhanced the effect of endothelin (ET) on the proliferation and migration of PASMCs (Hanthazi et al., 2020); however, chemerin alone failed to promote the proliferation of PASMCs directly. Accordingly, the specific role of chemerin in mediating PH has not been fully elucidated, and the expression levels of chemerin protein in plasma in PAH patients was not known.

In the present study, we examined alterations in the chemerin/CMKLR1 axis both in monocrotaline (MCT)/hypoxia induced PH rats and in hypoxia-treated PASMCs. Moreover, the effects of chemerin on pulmonary vascular remodeling and the underlying mechanisms in PASMCs were also explored using recombinant chemerin protein. Furthermore, expression levels of chemerin protein in the plasma of idiopathic pulmonary arterial hypertension (IPAH) patients were determined and the diagnostic value of chemerin expression in IPAH patients was estimated using receiver operating characteristic (ROC) curve analysis.

MATERIALS AND METHODS

Study Population

This clinical study was approved by the Ethics Committee of the First Affiliated Hospital of Chongqing Medical University. Written informed consent was obtained from all the participants. In this study, control subjects (n = 21) were recruited from healthy volunteers, and IPAH patients (n = 14) were enrolled at the First Affiliated Hospital of Chongqing Medical University from april 2016 to December 2020. IPAH was diagnosed according to the following criteria: mean pulmonary arterial pressure (mPAP) > 20 mmHg, pulmonary artery wedge pressure (PAWP) ≤ 15 mmHg and PVR ≥3 Wood units measured at rest and at sea level by right heart catheterization (RHC) (Rosenkranz et al., 2019). No etiology or familial history of PAH was identified in IPAH patients. All clinical data and samples were collected during the patient admission at the first visit. Plasma samples were collected as follows: whole blood was collected and centrifuged (3,000 rpm, 10 min), and plasma was collected and stored at −80°C.

Enzyme Linked Immunosorbent Assay

Plasma levels of chemerin were measured using ELISA kit (Ruixin Biotech, Quanzhou, China). Blank control, standard and sample wells were set following the manufacturer's instructions. Then, each well was added with HRP-labeled antibody (100 μL/well) followed by shaking gently. After being incubated at 37°C for 30 min, the reaction plates were rinsed repeatedly with a washing liquor. Next, 100 μL of substrate mixture was added to each well and incubated at 37°C for 15 min. Finally, 50 μL of stop solution was added per well and the absorbance was read at 450 nm wavelength. The plasma concentrations of chemerin were calculated using the standard curve.

Animal Experiments

Specific pathogen-free (SPF) male Sprague-Dawley (SD) rats (n = 20,180–200 g) were purchased from the Experimental Animal Center of Chongqing Medical University (Chongqing, China) and raised in individual ventilated cages (IVCs) in the animal experiment room. All experiments were conducted in accordance with the guidelines of the Ethics Committee of Chongqing Medical University and in compliance with the Guidelines for the Care and Use of Laboratory Animals published by the National Institutes of Health (Bethesda, MD, United States). Twenty SD rats were randomly divided into the control and monocrotaline (MCT, Mengbio, Chongqing, China) groups (n = 10 per group). MCT

(500 mg) was dissolved in anhydrous alcohol (10 ml) and saline (40 ml). Rats in the MCT group were intraperitoneally (i.p.) injected with MCT (55 mg/kg), and the remaining rats were injected with equal volumes of a mixture of alcohol and saline (1:4) as controls. And other twelve rats were randomly divided into the nomoxia and hypoxia groups (n = 6 per group). Rats in the hypoxia group were housed in a closed chamber with 12% oxygen concentration for 4 weeks to induce PH and there was no intervention in the control rats.

Echocardiography

On the 21st day after MCT injection, the rats were anesthetized with 2% pentobarbital sodium (Merck KGaA; 60 mg/kg, i. p.), and the fur on the left chest was removed with depilatory cream. Then, echocardiography was performed with an ultrasound system (IE33, Philip, Holland) to examine right ventricular structure and function.

RHC

Hemodynamic data of rats were measured by RHC. A polyethylene catheter (inner diameter, 0.5 mm; outside diameter, 0.9 mm) filled with heparinized saline was connected to the MP150 multi-channel physiological recorder (BIOPAC Systems, CA, United States). Subsequently, the anesthetized rats were fixed on the operating table and the right external jugular vein was exposed through surgery. Finally, the catheter was inserted into the right ventricle (RV) by cutting a V-shaped incision on the external jugular vein and introduced into pulmonary artery (PA) under the guidance of the pressure waveforms. The right ventricular systolic pressure (RVSP) and mPAP were measured by recorded waveforms of RV and PA, respectively.

Histochemistry

Rat pulmonary tissues were fixed with 4% paraformaldehyde at 4°C, embedded in paraffin, and sectioned at a thickness of 5 μm for hematoxylin-eosin (HE) staining (Servicebio, Wuhan, China). Images of pulmonary arterioles were captured with a microscope (Leica Microsystems DFC550, Germany).

Immunofluorescent Staining

Paraffin section of lung tissue were dewaxed and progressively rehydrated in alcoholic baths. Nonspecific binding sites were blocked with 3% bovine serum albumin (BSA) (Servicebio, Wuhan, China); After overnight incubation with a polyclonal rabbit anti-rat CMKLR1 (Affinity Antibodies, United States) or a polyclonal rabbit anti-rat chemerin (Invitrogen Antibodies, United States) and a polyclonal rabbit anti-rat α-SMA (Boster, Wuhan, China), sections were incubated for 50 min with corresponding secondary fluorescent-labeled antibodies [Goat Anti-Rabbit IgG(H + L)-Cy3, AIFang biological, Changsha, China]. Nuclei were counterstained with 4',6-diamidino-2-phenylindole[(DAPI) (Servicebio, Wuhan, China)]. Images were taken using a fluorescence microscope (Leica Microsystems DFC550, Germany).

Immunohistochemistry Staining

The lung tissue sections were deparaffinized and rehydrated in graduated alcohol. The endogenous peroxidase activity was blocked by incubation with 0.3% hydrogen peroxide at room temperature for 25 min. Then the sections were blocked with 3% bovine serum albumin (BSA) (Servicebio, Wuhan, China) for 30 min and then incubated with a polyclonal rabbit anti-rat α-SMA (Boster Antibodies, Wuhan, China) antibodies overnight, followed by incubation with the secondary antibody [Goat Anti-Rabbit IgG(H + L)-HRP, AIFang biological, Changsha, China] for 50 min. After the colour development through incubation with diaminobenzidine, the sections were counterstained with haematoxylin. The developed tissue sections were imaged under a microscope (Leica Microsystems DFC550, Germany).

Isolation and Identification of PASMCs

Primary PASMCs were obtained from SD rats (6–8 weeks, 180–200 g) as previously described (Tang et al., 2020). Briefly, the lungs were rapidly excised after the rats were anesthetized with 2% pentobarbital sodium (Merck KGaA; 120 mg/kg, i. p.). The pulmonary arteries were isolated from the lungs in phosphate-buffered saline (PBS, HyClone, Utah, United States) and cut along the long axis of the vessel with ophthalmic scissors. Then, the endothelial cells and adventitial fibroblasts were gently removed by rubbing the internal and external surfaces of the pulmonary artery with tweezers. Subsequently, the remaining smooth muscle layer was cut into pieces, transferred to a culture dish with Dulbecco's modified Eagle's medium/nutrient mixture F-12 (DMEM/F-12, HyClone, Utah, United States) containing 20% fetal bovine serum (FBS, PAN-Biotech, Adenbach, Germany), and cultured in a humidified incubator at 37°C with 5% CO_2. The purity of PASMCs was identified by immunofluorescence staining with an α-SMA antibody. Cells at passages 3-6 were used for subsequent experiments.

Quantitative Reverse Transcription PCR

Total RNA was extracted from rat lung tissue with TRIzol reagent (Invitrogen, CA, United States). Then, cDNA was prepared by reverse transcription using the PrimeScript RT reagent kit with gDNA Eraser (TaKaRa, Japan) according to the manufacturer's instructions. Subsequently, real-time quantitative PCR was conducted using SYBR® Premix Ex Taq (TaKaRa, Japan) on an ABI7500 quantitative PCR instrument. PCR primers were designed using NCBI Primer-BLAST and synthesized by Tsingke (Chongqing, China). The sequences of primers used in the present study were as follows: Chemerin, 5′-AGGGCCTCTCTAAAGCAA CGA-3' (Forward), 5′-CAAGCTCTGTCCCGTGTATGT-3' (Reverse); CMKLR1, 5′-TGTGCTTCCTCGGGATCCTA-3' (Forward), 5′-GGTGATGTGGATGGGCAAGA-3' (Reverse); and β-actin, 5′-TCAGGTCATCACTATCGGCAA T-3' (Forward), 5′-ACTGTGTTGGCATAGAGGTCTT-3' (Reverse). The relative mRNA expression was calculated by the $2^{-\triangle\triangle Ct}$ method. β-actin was used as an internal control for normalizing the expression of the target genes.

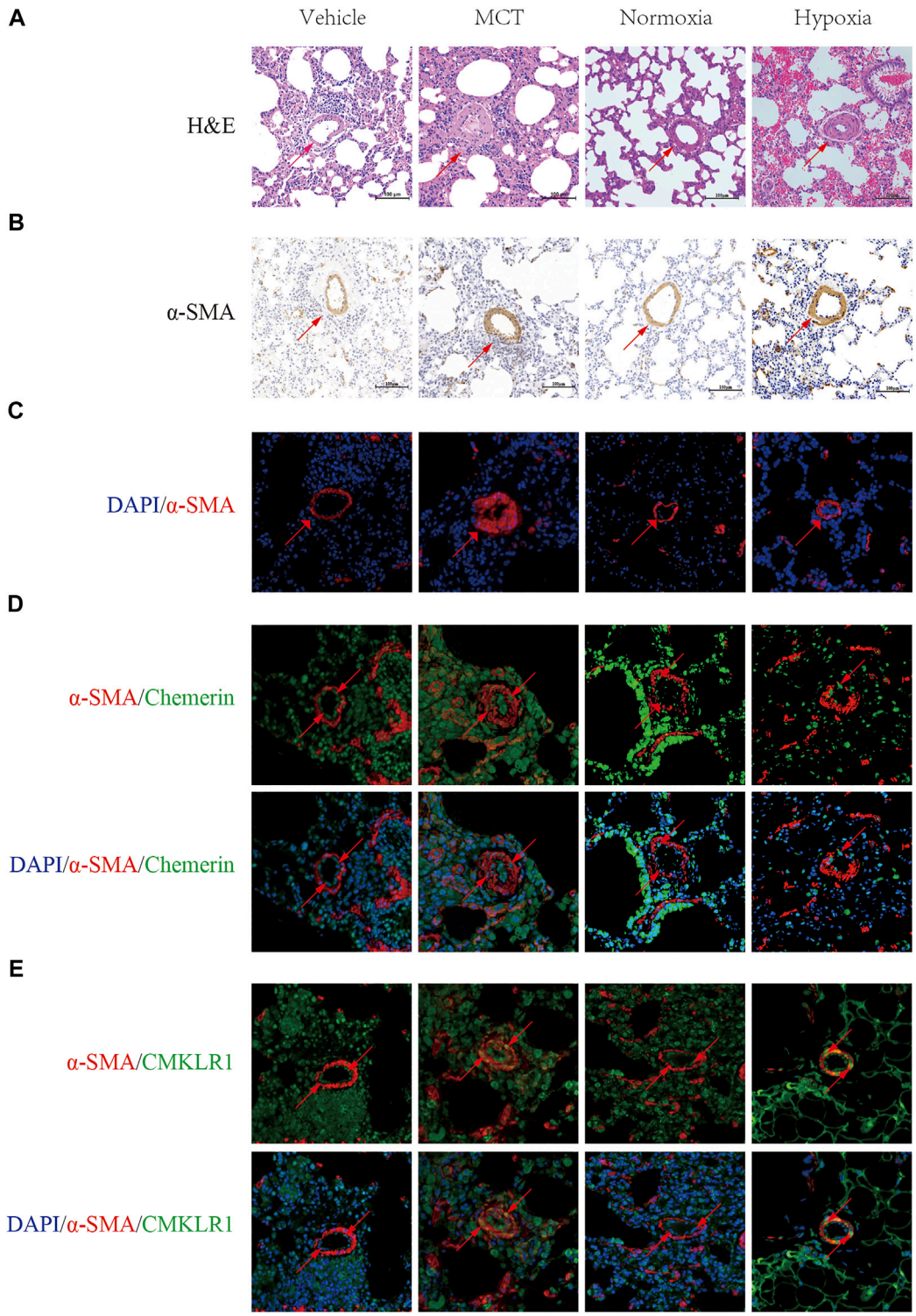

FIGURE 1 | Localization and expression of Chemerin and its receptor CMKLR1 in rat lungs. Characterizing the localization of chemerin and its receptor CMKLR1 expression in rat lung tissues. **(A)** Representative images of H&E-stained lung tissues (original magnification, × 200, scale bars, 100 um). **(B)** Immunohistochemistry staining of pulmonary arteries stained with α-SMA (original magnification, × 200, scale bars, 100 um). **(C)** Immunofluoresce staining of pulmonary arteries stained with α-SMA (red) and DAPI (blue) (original magnification, × 400, scale bars, 50 um). **(D)** Representative immunofluorescence images of chemerin (green), α-SMA (red) and DAPI (blue) in normal and PH rat lung tissues (original magnification, × 400, Scale bars, 50 um). **(E)** Representative immunofluorescence images of CMKLR1(green), α-SMA (red) and DAPI (blue) in normal and PH rat lung tissues (original magnification, × 400, Scale bars, 50 um).

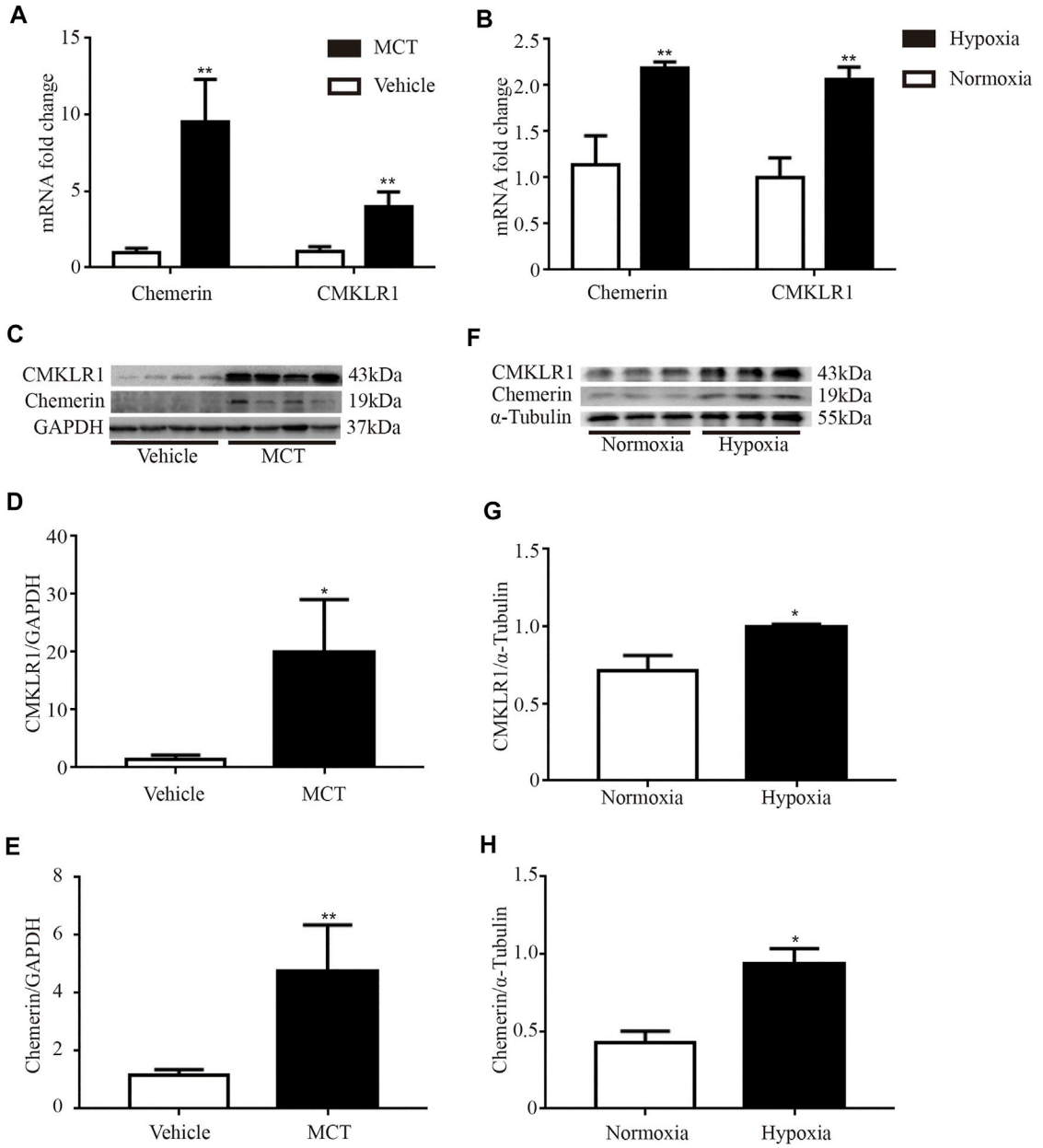

FIGURE 2 | The mRNA and protein expression levels of chemerin and CMKLR1 are upregulated in MCT/hypoxia induced PH rat lungs. The mRNA and protein expression levels of chemerin and CMKLR1 in rat lungs. **(A)** The mRNA expression levels of chemerin and CMKLR1 in MCT group ($n = 4$ per group, $^{**}p < 0.01$ *vs.* control group). **(B)** The mRNA expression levels of chemerin and CMKLR1 in hypoxia group ($n = 3$ in each group, $^{**}p < 0.01$ *vs*. control group). **(C–E)** Western blot analysis of chemerin **(C and E)** and CMKLR1**(C and D)** expressions in the lungs of MCT group ($n = 4$ per group, $^{*}p < 0.05$ *vs*. control group; $^{**}p < 0.01$ *vs*. control group). **(F–H)** Western blot analysis of chemerin **(F and H)** and CMKLR1**(F and G)** expressions in the lungs of hypoxia group ($n = 3$ per group, $^{*}p < 0.05$ *vs*. control group).

Western Blotting

Proteins were extracted from rat pulmonary tissues and PASMCs in RIPA lysis buffer with PMSF on ice. The protein concentration was determined by a BCA protein assay kit (MultiSciences, Hangzhou, China). Protein samples (15–25 μg) were separated by 12% SDS-PAGE and then transferred onto PVDF membranes (Bio-Rad, California, United States). After being blocked with 5% nonfat milk at room temperature for 1.5 h, the membranes were incubated with primary antibodies overnight at 4°C. Then, the membranes were incubated with horseradish peroxidase (HRP)-conjugated secondary antibodies (MultiSciences, Hangzhou, China) at room temperature for 1 h. Immunoreactive bands were visualized using an enhanced ECL kit (Beyotime, Shanghai, China). GAPDH,α-Tubulin or β-actin served as an endogenous control for equal sample loading. The primary antibodies used in this study were as follows: Chemerin (Invitrogen, CA, United States),

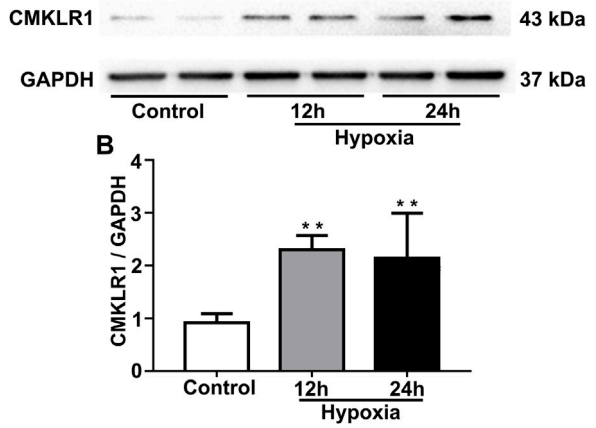

FIGURE 3 | CMKLR1 expression is upregulated in PASMCs under hypoxic conditions. To mimic PH *in vitro*, PASMCs were exposed to hypoxia (2%) for two different durations (12 and 24 h). **(A,B)** Western blot analysis of CMKLR1 expression in the groups. $^{**}p < 0.01$ vs. the control group.

CMKLR1 [(Bauer et al., 2011) (Abcam, Cambridge, UK)], proliferating cell nuclear antigen (PCNA) [(Hu et al., 2019) (Proteintech, Wuhan, China)], p-ERK1/2 (Thr202/Tyr204)[(Karadeniz et al., 2021) (Cell Signaling Technology, Massachusetts, United States)], ERK1/2 [(Karadeniz et al., 2021) (Cell Signaling Technology, Massachusetts, United States)], β-actin [(Zhao et al., 2018) (Proteintech, Wuhan, China)], α-Tubulin [(Zhang et al., 2019) (Proteintech, Wuhan, China)]and GAPDH [(Zhang et al., 2018) (Proteintech, Wuhan, China)].

EdU Staining

A BeyoClick™ EdU-555 Cell Proliferation Kit (Beyotime Bio, Shanghai, China) was used for the cell proliferation assay. The PASMCs were incubated with10 μmol/L EdU for 2 h at 37 °C after treatment. The cells were permeabilized with Enhanced Immunostaining Permeabilization Buffer for 15 min after fixation with 4% formaldehyde for 15 min at room temperature. After three washes with PBS, the cells were incubated with click additive solution for 30 min. PASMC nuclei stained with Hoechst-33,342 were used for the cell counts and examined using fluorescence microscope.

Scratch Wound Healing Assay

PASMCs at 90% confluence were wounded with a 200 μL pipette tip in 6-well plates. Then, the cells were washed three times to remove cell debris, pretreated with or without PD98059 (MCE, New Jersey, United States) for 30 min and cultured with recombinant human chemerin (R&D, Minneapolis, United States) as indicated. Wound closure was observed and photographed at 0 and 12 h with a microscope (Leica Microsystems DFC550, Germany).

Transwell Migration Assay

The Transwell migration assay was performed in 24-well plates with Transwell chambers (8-μm pores; Biofil, Guangzhou, China). Briefly, PASMCs were trypsinized and resuspended in serum-free medium. Subsequently, 1×10^4 cells were added to the upper chamber, while 500 μL of complete medium containing chemerin with or without PD98059 was placed in the lower chamber. After 12 h, the cells that failed to migrate from the upper chamber were removed with cotton swabs. Then, the migrated cells on the lower side of the membrane were photographed after being stained with 1% crystal violet (Mengbio, Chongqing, China).

Statistical Analysis

The results are presented as the mean ± standard error of the mean (SEM), median or percentages. Unpaired t-tests were used for comparisons between two groups. One-way ANOVA followed by the LSD test was used to assess statistical significance among groups. The diagnostic value of plasma chemerin for PAH was evaluated by receiver operating characteristic (ROC) curve analysis. A value of $p < 0.05$ was considered statistically significant.

RESULTS

Chemerin and CMKLR1 Were Upregulated in the Lung Tissues of PH Rats

To evaluate the PH rat model, HE staining showed that the walls of pulmonary arterioles were significantly thickened and that the lumens were obviously narrowed in PH rats (**Figure 1A**). Moreover, Immunohistochemistry and Immunofluorescent staining of pulmonary arteries stained with α-SMA were used to further evaluate the PH model, and indicated that the walls of PH groups' pulmonary arterioles were significantly thickened (**Figures 1B,C**). These data suggested that the PH rat models were successfully established by MCT administration and hypoxia.

Next, to localize and identify chemerin and its receptor CMKLR1, we co-immunostained lung tissues, with either antibody against chemerin and its receptor CMKLR1 together with a smooth muscle-specific marker, the α-smooth muscle actin. In control rat lungs, microscopic analysis revealed a strong staining of chemerin and its receptor CMKLR1 within the intimal layer (**Figures 1D,E**). However, as illustrated in **Figures 1D,E**, chemerin/CMKLR1 was upregulated within the media of PH rat lungs compared to the controls.

Then, the mRNA and protein expression levels of chemerin and CMKLR1 were measured in the rat lungs. As shown in **Figure 2A**, the mRNA levels of chemerin and CMKLR1 in the MCT group were significantly higher than those in the control group (both $p < 0.01$, **Figure 2A**), and these elevations were also verified by Western blot analysis (chemerin, $p < 0.01$, **Figures 2C,E**; CMKLR1, $p < 0.05$, **Figures 2C,D**). We also observed this phenomenon in the hypoxia group (both $p < 0.01$, **Figure 2B**; chemerin, $p < 0.05$, **Figures 2F,H**; CMKLR1, $p < 0.05$, **Figures 2F,G**).

Hypoxia Upregulated CMKLR1 Expression in PASMCs

To mimic PH conditions *in vitro*, PASMCs were exposed to hypoxia (2%) for 12 and 24 h, respectively. As shown in **Figure 3**, the protein level of CMKLR1 was markedly increased in the hypoxia groups compared to the control group (both $p < 0.01$).

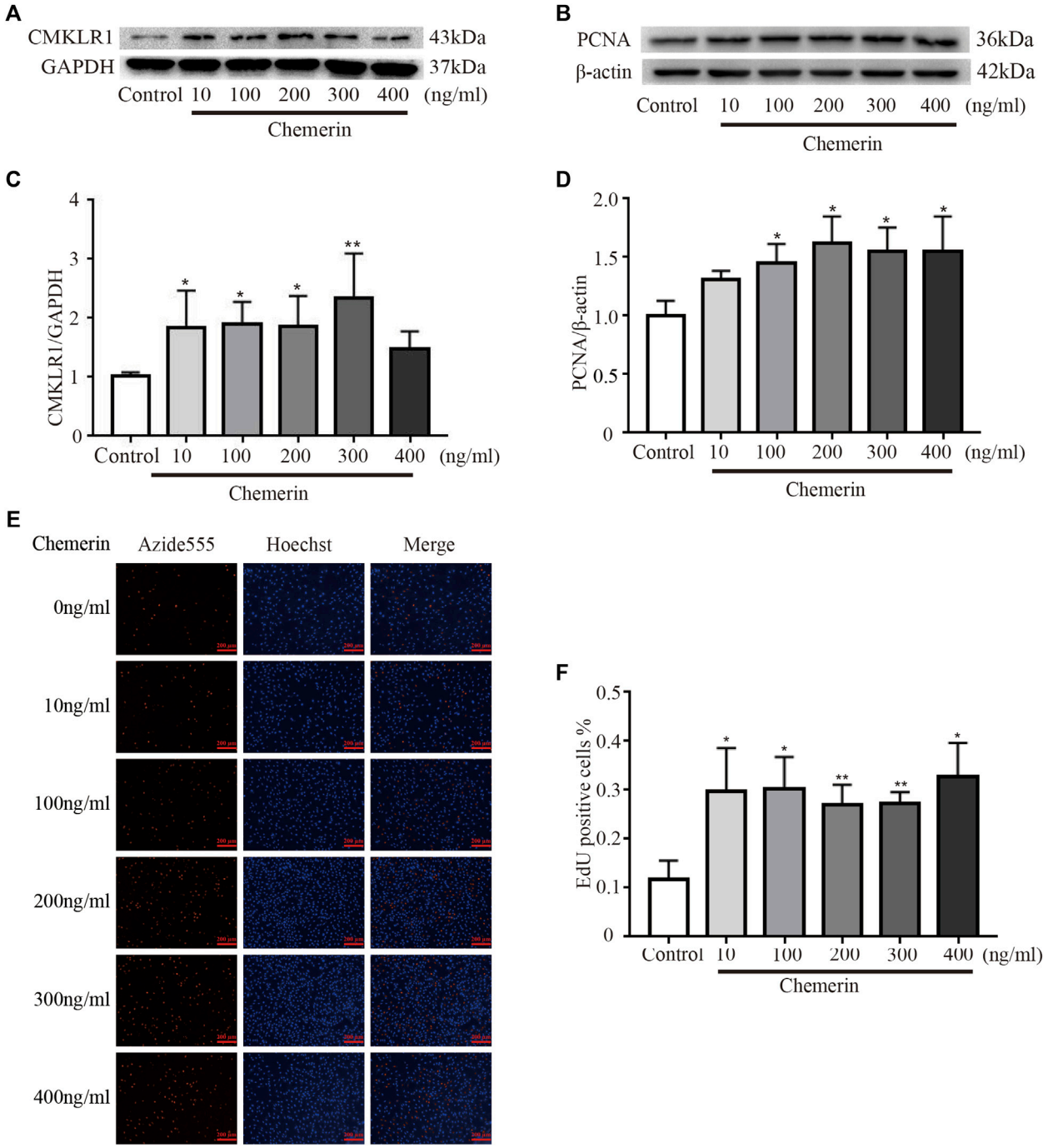

FIGURE 4 | Chemerin/CMKLR1 promotes the proliferation of PASMCs. PASMCs were stimulated with various concentrations of chemerin. **(A–D)** Western blot analysis of the expression of CMKLR1 **(A and C)** and PCNA **(B and D)** in PASMCs after 24 h of treatment. **(E and F)** PASMCs proliferation was measured by an EdU staining assay after 24 h of treatment. (original magnification, ×100, scale bars, 200 μm). *$p < 0.05$ *vs.* the control group; **$p < 0.01$ *vs.* the control group.

Chemerin/CMKLR1 Promoted the Proliferation and Migration of PASMCs

PASMCs were treated with various concentrations of exogenous recombinant chemerin protein. As shown in **Figures 4A,C**, after stimulation for 24 h, the expression of CMKLR1 was significantly increased in the chemerin groups (10–300 ng/ml) compared to the control group (10 ng/ml, 100 ng/ml, and 200 ng/ml, all $p < 0.05$; 300 ng/ml, $p <$

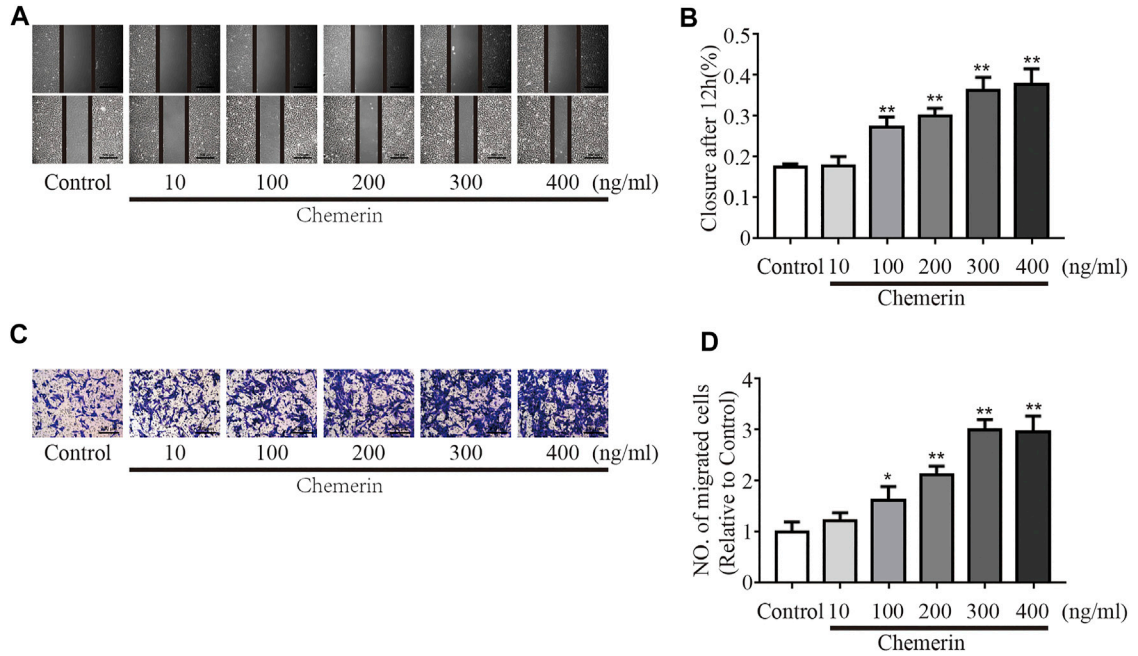

FIGURE 5 | Chemerin/CMKLR1 promotes the migration of PASMCs. PASMCs were stimulated with various concentrations of chemerin. **(A–B)** Images of scratches in PASMCs photographed at 0 and 12 h under different treatment conditions (original magnification, × 50, scale bars, 500 μm). **(C–D)**: Transwell migration assays of PASMCs after different treatments for 12 h (original magnification, × 100, scale bars, 200 μm). *$p < 0.05$ vs. the control group; **$p < 0.01$ vs. the control group.

0.01). Furthermore, as the concentration of chemerin increased, the protein expression of PCNA was gradually upregulated compared to that in the control group (100 ng/ml, 200 ng/ml, 300 ng/ml, and 400 ng/ml, all $p < 0.05$, **Figures 4B,D**). To further elucidate whether the chemerin promotes the proliferation of PASMCs, we conducted the EdU assay. As shown in **Figures 4E,F**, chemerin can significantly promote the proliferation of PASMCs measured by EdU compared to control group (10 ng/ml, 100 ng/ml, 400 ng/ml, all $p < 0.05$, 200 ng/ml, 300 ng/ml, $p < 0.01$).

As shown in **Figures 5A,B**, as the concentration of chemerin increased, the migration distance of PASMCs gradually increased (100 ng/ml, 200 ng/ml, 300 ng/ml, and 400 ng/ml, all $p < 0.01$, **Figures 5A,B**). Consistent with the scratch assay results, the number of migrated cells was similarly increased by chemerin stimulation, as shown in the Transwell migration assay (100 ng/ml, $p < 0.05$; 200 ng/ml, 300 ng/ml, and 400 ng/ml, all $p < 0.01$, **Figures 5C,D**).

Chemerin Mediated PASMCs Proliferation and Migration by Activating the ERK1/2 Signaling Pathway

To investigate the potential mechanism of chemerin-induced phenotypic changes in PASMCs, the key regulatory proteins in the ERK1/2 signaling pathway were analyzed by Western blotting. As shown in **Figures 6A,B**, under exogenous chemerin stimulation, the ERK1/2 signaling pathway was significantly activated, as indicated by the increased p-ERK/ERK ratios in the chemerin group compared with the control group, and the increase was reduced by PD98059 (an inhibitor of ERK1/2 signaling) (*$p < 0.05$ *vs.* control group, &&$p < 0.01$ *vs.* chemerin group). Furthermore, PD98059 pretreatment eliminated the increase in PCNA expression in chemerin-treated PASMCs (*$p < 0.05$ *vs.* control group, &$p < 0.05$ *vs.* chemerin group, **Figures 6C,D**). Similarly, The proliferation promoting effect of chemerin on PASMCs can be decreased by PD98059 (*$p < 0.05$ *vs.* control group, &$p < 0.05$ *vs.* chemerin group, **Figures 6E,F**). In addition, the migration assays showed that chemerin induced sharp increases in the migration distance and number of migrated PASMCs, which were reversed by PD98059 (**$p < 0.01$ vs. control group, &&P < 0.01 *vs.* chemerin group, **Figures 6G,H** and **Figures 6I,J**).

Plasma Chemerin Levels Were Significantly Upregulated in IPAH Patients

The clinical characteristics of all participants were summarized in **Table 1**. The median age of control individuals was 25 years and that of IPAH patients was 31.5 years. The proportion of females was 85.7% in the IPAH group, and 61.9% in the control group. The median mPAP was 53 mmHg, the median PAWP was 7.5 mmHg, the median PVR was 13.06 Wood units, and median cardiac output (CO) was 3.85 L/min in the IPAH group.

ELISA assay result showed that compared to the control group, the plasma level of chemerin was markedly increased

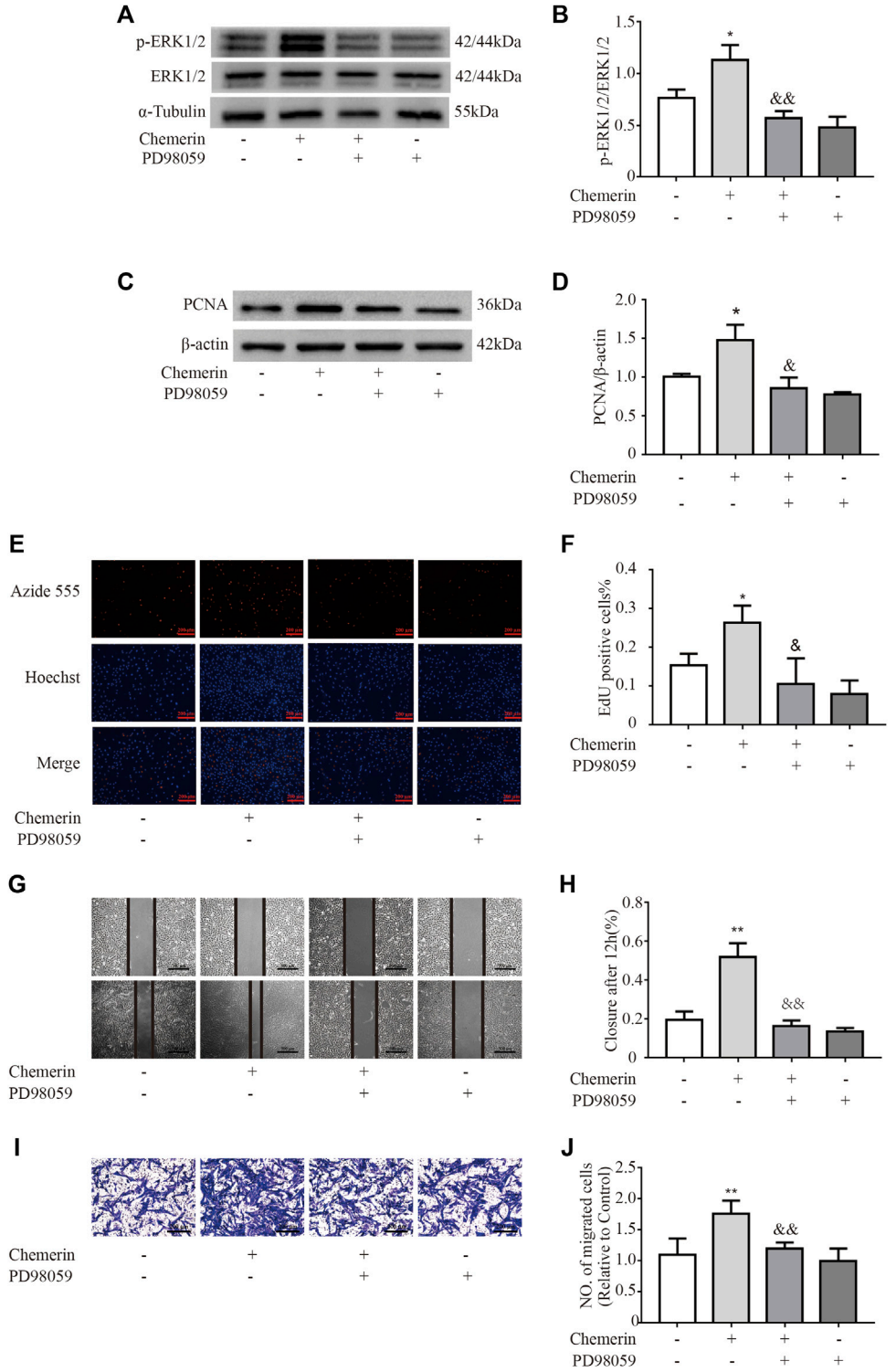

FIGURE 6 | Chemerin induces phenotypic changes in PASMCs *via* the ERK1/2 signaling pathway. PASMCs were pretreated with PD98059 (50 μM) 30 min prior to chemerin treatment (300 ng/ml). **(A and B)** Western blot analysis of p-ERK1/2 and ERK1/2 expression in PASMCs after stimulation by chemerin with or without PD98059 pretreatment for 12 h. **(C and D)** Western blot analysis of PCNA expression in chemerin-treated cells with or without PD98059 pretreatment for 24 h. **(E and F)** PASMC cell proliferation was measured by an EdU staining assay after 24 h of treatment (original magnification, × 100, scale bars, 200 μm). **(G and H)** Images of scratches in PASMCs photographed at 0 and 12 h under different treatment conditions (original magnification, × 50, scale bars, 500 μm). **(I and J)** Transwell migration assays of PASMCs after different treatments for 12 h (original magnification, ×100, scale bars, 200 μm). *$p < 0.05$ vs. the control group; **$p < 0.01$ *vs.* the control group; & $p < 0.05$ *vs*. the chemerin group. && $p < 0.01$ *vs.* the chemerin group.

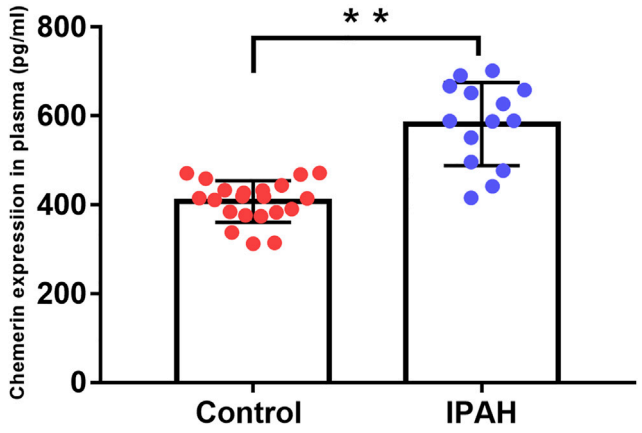

FIGURE 7 | Plasma chemerin levels are increased in IPAH patients. Human plasma chemerin protein levels were measured by ELISA in the control and IPAH groups. Quantitative analysis of chemerin protein expression in the plasma of each group was also performed (control, $n = 21$; IPAH, $n = 14$). $^{**}p < 0.01$ *vs.* the control group.

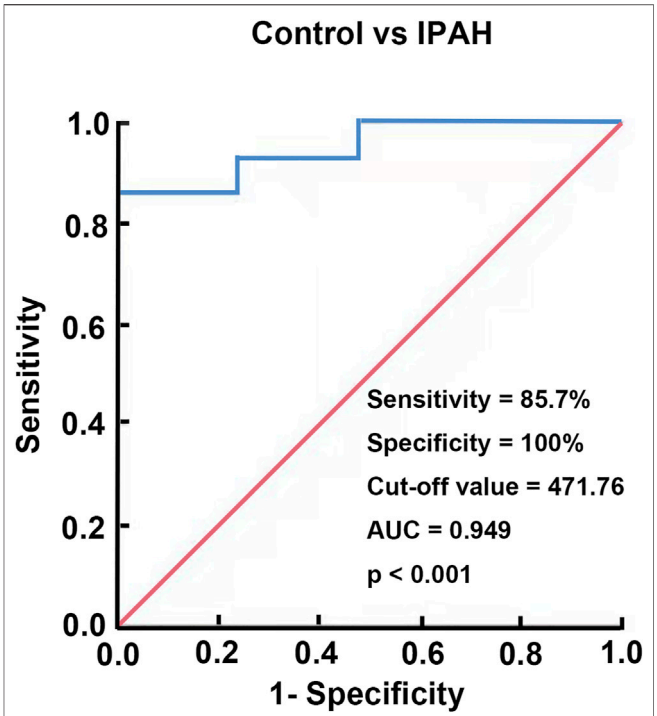

FIGURE 8 | Diagnostic value of chemerin expression in IPAH. A ROC curve of plasma chemerin for discriminating IPAH patients from healthy controls.

in the IPAH group (581.7 ± 24.9 pg/ml *vs.* 407.5 ± 10.23 pg/ml, $p < 0.01$, **Figure 7**).

Diagnostic Value of Chemerin Expression in IPAH

To assess the diagnostic value of plasma chemerin, we generated a ROC curve using the expression data measured by ELISA. As shown in **Figure 8**, the area under the ROC curve (AUC) reached 0.949 [95% confidence interval (CI): 87.3–100%], and plasma chemerin had a satisfactory sensitivity (85.7%) and specificity (100%) at a concentration of 471.76 pg/ml ($p < 0.001$), which indicated considerable diagnostic value for IPAH.

DISCUSSION

The present study revealed that chemerin/CMKLR1 promoted the proliferation and migration of PASMCs via activating the ERK1/2 signaling pathway in PH rats and the plasma level of chemerin was markedly increased in iPAH patients. The main findings are as follows: 1) the expression of chemerin and CMKLR1 was upregulated in the lungs of MCT/hypoxia induced PH rats; 2) CMKLR1 expression was significantly increased in PASMCs under hypoxic conditions; 3) PASMC stimulation with exogenous chemerin promoted cell proliferation and migration via the ERK1/2 signaling pathway; and 4) the expression of chemerin protein was significantly increased in plasma of IPAH patients. Increasing evidence has shown that chemerin is closely associated with cardiovascular diseases; in addition to regulating systemic blood pressure and promoting intimal hyperplasia, chemerin contributes to angiogenesis and vascular remodeling in hypertension (Kunimoto et al., 2015; Xiong et al., 2016; Liu et al., 2019; Wen et al., 2019). Besides, chemerin can enhance vascular responses to vasoconstrictors in the pulmonary artery and reduce acetylcholine-induced pulmonary artery vasodilation partly by nitric oxide (NO) signaling and oxidative stress (Hanthazi et al., 2019). Furthermore, as an active fragment of chemerin, chemerin-9 augmented the contraction of isolated pulmonary arteries from MCT rats at least partially through enhancing CMKLR1 activity in smooth muscle (Omori et al., 2020). In this study, for the first time, we revealed that chemerin was significantly upregulated in the lung tissues of MCT/hypoxia induced PH rats, indicating that chemerin associated with PH.

CMKLR1, as a functional receptor, directly interacts with chemerin, contributing to various biological processes, such as inflammation, immune responses, adipogenesis and angiogenesis (Goralski et al., 2007; Nakamura et al., 2018; Pachynski et al., 2019; Xie et al., 2020). Omori A et al. reported that the protein levels of CMKLR1 were markedly increased in the lungs and PASMCs of MCT-induced PH rats (Omori et al., 2020). Similarly, in the present study, we showed that CMKLR1 was sharply upregulated in the lungs of MCT and hypoxia induced-PH rats and further demonstrated that the expression of CMKLR1 was significantly elevated in isolated PASMCs under hypoxic conditions.

Excessive PASMC proliferation and migration play crucial roles in pulmonary vascular remodeling, thus facilitating PH development (Tuder 2017). A previous study demonstrated

TABLE 1 | Basic demographics of all participants in clinical trials. The mPAP (mean pulmonary arterial pressure), PAWP (pulmonary artery wedge pressure) and PVR (pulmonary vascular resistance) and CO (cardiac output) were measured by the right cardiac catheterization (RHC). The Treatment means that the patient has been treated with targeted drugs for IPAH (idiopathic pulmonary arterial hypertension), before the RHC for the first time at the First Affiliated Hospital of Chongqing Medical University.

Baseline demographics	Participants	
	Control (n = 21)	IPAH (n = 14)
Age (year)		
Mean (SEM)	25.67 (0.78)	29.5 (2.72)
Median (range)	25 (23–36)	31.5 (10–52)
Sex		
Female, % (n)	61.9% (13)	85.7% (12)
Male, % (n)	38.1% (8)	14.3% (2)
mPAP (mmHg)		
Mean (SEM)	_	55.57 (4.20)
Median (range)	_	53 (27–90)
PAWP (mmHg)		
Mean (SEM)	_	7.71 (1.11)
Median (range)	_	7.5 (0–14)
PVR (Woods units)		
Mean (SEM)	_	14.44 (2.77)
Median (range)	_	13.06 (3.62–42)
CO (L/min)		
Mean (SEM)	_	4.26 (0.45)
Median (range)	_	3.85 (1.5–7.2)

https://www.jianguoyun.com/p/DQIvgQQQIJrqCRi2iqYE

that silencing CMKLR1 could alleviate the proliferation of thoracic aortic smooth muscle cells (SMCs) in mice, which was associated with a decrease in p-JNK expression (Liu et al., 2016). Here, we showed that chemerin significantly upregulated CMKLR1 expression in PASMCs even at very low concentrations, indicating that the regulatory effects of chemerin on PASMCs may ultimately be mediated by CMKLR1. However, this finding was different from a recent study, which indicated that chemerin alone did not exert a positive effect on PASMCs proliferation (Hanthazi et al., 2020). These discrepant results may result from different cell treatment conditions and variable cell proliferation protocol. Nevertheless, other than CMKLR1, whether the other receptors of chemerin participate in theses signal transduction needs to be further investigated.

ERK1/2 signaling is a major member of the MAPK family, which is widely involved in many physiological and pathological processes (Tian et al., 2018; Bao et al., 2019; Hu et al., 2020; Zou et al., 2020). It has been demonstrated that the ERK1/2 signaling pathway is significantly activated in a variety of PH animal models, while knockdown of the ERK1/2 gene effectively suppresses pulmonary vascular remodeling, ultimately preventing PH development (Yu et al., 2017). The intrinsic links between chemerin and the ERK1/2 signaling pathway have been verified in a few pathological processes, including systemic hypertension, lipolytic metabolism and insulin resistance (Zhang et al., 2014; Fu et al., 2018; Jiang et al., 2018). Lobato et al. found that chemerin increased the contractile response of the aorta to phenylephrine (PE) and ET-1 by activating ERK1/2 (Lobato et al., 2012). Kunimoto H et al. reported that chemerin stimulated the proliferation and migration of SMCs via oxidative-dependent phosphorylation of ERK1/2 in hypertension (Kunimoto et al., 2015). Similarly, we found that chemerin could activate the ERK1/2 signaling pathway in PASMCs and PD98059 reversed the regulatory effects of chemerin on PASMCs. In addition, a previous study indicated that chemerin expression was elevated through ERK1/2 signaling in human coronary artery endothelial cells in response to hypoxia (Chua et al., 2016). These data suggest that there may be crosstalk between chemerin and ERK1/2 signaling under different pathological conditions.

Evidence from multiple clinical studies suggests that circulating chemerin levels are associated with cardiovascular diseases (Ji et al., 2014; Zhang et al., 2017; Wójcik et al., 2020). On that basis, Zhou X et al. reported that serum chemerin levels could be used to predict the presence of adverse cardiovascular events in patients with chronic heart failure (Zhou et al., 2019). Interestingly, in our clinical study, we also found that chemerin expression was significantly upregulated in the plasma of IPAH patients, which was consistent with the results of the rat experiment mentioned previously. Moreover, ROC curve analysis indicated that plasma chemerin may have a considerable diagnostic value for IPAH as its high sensitivity and specificity with an AUC of 0.949. These data demonstrated that plasma chemerin level is closely related to PAH. However, a study with larger sample size of IPAH patients and long-term follow-up is needed to further confirm the potential association between chemerin plasma levels and PAH outcomes.

In conclusion, our study reveals that the chemerin/CMKLR1 axis promotes PASMC proliferation and migration by activating the ERK1/2 signaling pathway, and chemerin protein levels are increased in the plasma of IPAH patients. The present study provides significant insights intothe development of potential therapies for PH.

DATA AVAILABILITY STATEMENT

The original contributions presented in the study are included in the article/Supplementary Material, further inquiries can be directed to the corresponding author.

ETHICS STATEMENT

The studies involving human participants were reviewed and approved by the Ethics Committee of the First Affiliated Hospital of Chongqing Medical University. Written informed consent to

participate in this study was provided by the participants' legal guardian/next of kin. The animal study was reviewed and approved by the Ethics Committee of Chongqing Medical University.

AUTHOR CONTRIBUTIONS

Participated in research design: LP and YC Conducted experiments: LP, YC, YZ, YD, YY and AL Contributed materials: YD, RW, JY, FS and PT Analyzed and interpreted the data: LP and YC Wrote or contributed to the writing of the manuscript: LP, YC, RW, and WH conducted experiments: YL Contributed materials: DC and YG Analyzed and interpreted the data: PF.

FUNDING

This work was supported by the Chongqing Municipal Health and Health Committee (ZQNYXGDRCGZS2019001, No. 2019ZY3340, and No. 2016HBRC001) and Chongqing Science and Health Joint Medical Research Project (2020MSXM045).

REFERENCES

Bao, G., Pan, W., Huang, J., and Zhou, T. (2019). K-RasG12V/T35S-ERK1/2 Pathway Regulates H2BS14ph through Mst1 to Facilitate the Advancement of Breast Cancer Cells. *Biofactors*. doi:10.1002/biof.1589

Bauer, S., Wanninger, J., Schmidhofer, S., Weigert, J., Neumeier, M., Dorn, C., et al. (2011). Sterol Regulatory Element-Binding Protein 2 (SREBP2) Activation after Excess Triglyceride Storage Induces Chemerin in Hypertrophic Adipocytes. *Endocrinology* 152, 26–35. doi:10.1210/en.2010-1157

Chua, S. K., Shyu, K. G., Lin, Y. F., Lo, H. M., Wang, B. W., Chang, H., et al. (2016). Tumor Necrosis Factor-Alpha and the ERK Pathway Drive Chemerin Expression in Response to Hypoxia in Cultured Human Coronary Artery Endothelial Cells. *PLoS One* 11, e0165613. doi:10.1371/journal.pone.0165613

Fu, Y. Y., Hu, B. H., Chen, K. L., and Li, H. X. (2018). Chemerin Induces Lipolysis through ERK1/2 Pathway in Intramuscular Mature Adipocytes of Dairy Bull Calves. *J. Cel Biochem* 10. doi:10.1002/jcb.2750610.1002/jcb.27506

Goralski, K. B., McCarthy, T. C., Hanniman, E. A., Zabel, B. A., Butcher, E. C., Parlee, S. D., et al. (2007). Chemerin, a Novel Adipokine that Regulates Adipogenesis and Adipocyte Metabolism. *J. Biol. Chem.* 282, 28175–28188. doi:10.1074/jbc.M700793200

Hanthazi, A., Jespers, P., Vegh, G., Degroot, G. N., Springael, J. Y., Lybaert, P., et al. (2019). Chemerin Influences Endothelin- and Serotonin-Induced Pulmonary Artery Vasoconstriction in Rats. *Life Sci.* 231, 116580. doi:10.1016/j.lfs.2019.116580

Hanthazi, A., Jespers, P., Vegh, G., Dubois, C., Hubesch, G., Springael, J. Y., et al. (2020). Chemerin Added to Endothelin-1 Promotes Rat Pulmonary Artery Smooth Muscle Cell Proliferation and Migration. *Front. Physiol.* 11, 926. doi:10.3389/fphys.2020.00926

Hu, A., Huang, J., Li, S., Gao, Y., Wu, L., Deng, J., et al. (2019). Involvement of Stromal Cell-Derived Factor-1α (SDF-1α), Stem Cell Factor (SCF), Fractalkine (FKN) and VEGF in TSG protection against Intimal Hyperplasia in Rat Balloon Injury. *Biomed. Pharmacother.* 110, 887–894. doi:10.1016/j.biopha.2018.12.030

Hu, Y., Fu, J., Liu, X., and Xue, X. (2020). ERK1/2 Signaling Pathway Activated by EGF Promotes Proliferation, Transdifferentiation, and Migration of Cultured Primary Newborn Rat Lung Fibroblasts. *Biomed. Res. Int.* 2020, 7176169. doi:10.1155/2020/7176169

Ji, Q., Lin, Y., Liang, Z., Yu, K., Liu, Y., Fang, Z., et al. (2014). Chemerin Is a Novel Biomarker of Acute Coronary Syndrome but Not of Stable Angina Pectoris. *Cardiovasc. Diabetol.* 13, 145. doi:10.1186/s12933-014-0145-4

Jiang, Y., Liu, P., Jiao, W., Meng, J., and Feng, J. (2018). Gax Suppresses chemerin/CMKLR1-Induced Preadipocyte Biofunctions through the Inhibition of Akt/mTOR and ERK Signaling Pathways. *J. Cel Physiol* 233, 572–586. doi:10.1002/jcp.25918

Karadeniz, F., Oh, J. H., Kim, H. R., Ko, J., and Kong, C. S. (2021). Camellioside A, Isolated from Camellia Japonica Flowers, Attenuates UVA-Induced Production of MMP-1 in HaCaT Keratinocytes via Suppression of MAPK Activation. *Exp. Ther. Med.* 21, 16. doi:10.3892/etm.2020.9448

Kennedy, A. J., and Davenport, A. P. (2018). International Union of Basic and Clinical Pharmacology CIII: Chemerin Receptors CMKLR1 (Chemerin1) and GPR1 (Chemerin2) Nomenclature, Pharmacology, and Function. *Pharmacol. Rev.* 70, 174–196. doi:10.1124/pr.116.013177

Kennedy, A. J., Yang, P., Read, C., Kuc, R. E., Yang, L., Taylor, E. J., et al. (2016). Chemerin Elicits Potent Constrictor Actions via Chemokine-like Receptor 1 (CMKLR1), Not G-Protein-Coupled Receptor 1 (GPR1), in Human and Rat Vasculature. *J. Am. Heart Assoc.* 5. doi:10.1161/jaha.116.004421

Kunimoto, H., Kazama, K., Takai, M., Oda, M., Okada, M., and Yamawaki, H. (2015). Chemerin Promotes the Proliferation and Migration of Vascular Smooth Muscle and Increases Mouse Blood Pressure. *Am. J. Physiol. Heart Circ. Physiol.* 309, H1017–H1028. doi:10.1152/ajpheart.00820.2014

Liu, H., Xiong, W., Luo, Y., Chen, H., He, Y., Cao, Y., et al. (2019). Adipokine Chemerin Stimulates Progression of Atherosclerosis in ApoE-/- Mice. *Biomed. Res. Int.* 2019, 7157865. doi:10.1155/2019/7157865

Liu, H. D., Xiong, W., Liu, Q. Y., Li, J. H., Wu, M. S., Zhang, J., et al. (2016). Role of CMKLR1 on Mouse Vascular Smooth Muscle Cells Proliferation and Related Mechanism. *Zhonghua Xin Xue Guan Bing Za Zhi* 44, 605–609. doi:10.3760/cma.j.issn.0253-3758.2016.07.010

Lobato, N. S., Neves, K. B., Filgueira, F. P., Fortes, Z. B., Carvalho, M. H., Webb, R. C., et al. (2012). The Adipokine Chemerin Augments Vascular Reactivity to Contractile Stimuli via Activation of the MEK-Erk1/2 Pathway. *Life Sci.* 91, 600–606. doi:10.1016/j.lfs.2012.04.013

Morrell, N. W., Adnot, S., Archer, S. L., Dupuis, J., Jones, P. L., MacLean, M. R., et al. (2009). Cellular and Molecular Basis of Pulmonary Arterial Hypertension. *J. Am. Coll. Cardiol.* 54, S20–S31. doi:10.1016/j.jacc.2009.04.018

Nakamura, N., Naruse, K., Kobayashi, Y., Miyabe, M., Saiki, T., Enomoto, A., et al. (2018). Chemerin Promotes Angiogenesis *In Vivo*. *Physiol. Rep.* 6, e13962. doi:10.14814/phy2.13962

Omori, A., Goshima, M., Kakuda, C., Kodama, T., Otani, K., Okada, M., et al. (2020). Chemerin-9-induced Contraction Was Enhanced through the Upregulation of Smooth Muscle Chemokine-like Receptor 1 in Isolated Pulmonary Artery of Pulmonary Arterial Hypertensive Rats. *Pflugers Arch.* 472, 335–342. doi:10.1007/s00424-019-02345-5

Pachynski, R. K., Wang, P., Salazar, N., Zheng, Y., Nease, L., Rosalez, J., et al. (2019). Chemerin Suppresses Breast Cancer Growth by Recruiting Immune Effector Cells into the Tumor Microenvironment. *Front. Immunol.* 10, 983. doi:10.3389/fimmu.2019.00983

Rich, J. D., and Rich, S. (2014). Clinical Diagnosis of Pulmonary Hypertension. *Circulation* 130, 1820–1830. doi:10.1161/circulationaha.114.006971

Rosenkranz, S., Diller, G. P., Dumitrescu, D., Ewert, R., Ghofrani, H. A., Grünig, E., et al. (2019). Hemodynamic Definition of Pulmonary Hypertension: Commentary on the Proposed Change by the 6th World Symposium on Pulmonary Hypertension. *Dtsch Med. Wochenschr* 144, 1367–1372. doi:10.1055/a-0918-3772

Rourke, J. L., Muruganandan, S., Dranse, H. J., McMullen, N. M., and Sinal, C. J. (2014). Gpr1 Is an Active Chemerin Receptor Influencing Glucose Homeostasis in Obese Mice. *J. Endocrinol.* 222, 201–215. doi:10.1530/JOE-14-0069

Shin, W. J., and Pachynski, R. K. (2018). Chemerin Modulation of Tumor Growth: Potential Clinical Applications in Cancer. *Discov. Med.* 26, 31–37.

Tang, M., Wang, R., Feng, P., Dong, Q., Chen, W., Zhao, Y., et al. (2020). Dihydroartemisinin Attenuates Pulmonary Hypertension through Inhibition of Pulmonary Vascular Remodeling in Rats. *J. Cardiovasc. Pharmacol.* 76, 337–348. doi:10.1097/FJC.0000000000000862

Tian, P., Zhu, Y., Zhang, C., Guo, X., Zhang, P., and Xue, H. (2018). Ras-ERK1/2 Signaling Contributes to the Development of Colorectal Cancer via Regulating H3K9ac. *BMC Cancer* 18, 1286. doi:10.1186/s12885-018-5199-3

Tuder, R. M. (2017). Pulmonary Vascular Remodeling in Pulmonary Hypertension. *Cell Tissue Res* 367, 643–649. doi:10.1007/s00441-016-2539-y

Wen, J., Wang, J., Guo, L., Cai, W., Wu, Y., Chen, W., et al. (2019). Chemerin Stimulates Aortic Smooth Muscle Cell Proliferation and Migration via Activation of Autophagy in VSMCs of Metabolic Hypertension Rats. *Am. J. Transl Res.* 11, 1327–1342.

Weng, C., Shen, Z., Li, X., Jiang, W., Peng, L., Yuan, H., et al. (2017). Effects of chemerin/CMKLR1 in Obesity-Induced Hypertension and Potential Mechanism. *Am. J. Transl Res.* 9, 3096–3104.

Wójcik, M., Kozioł-Kozakowska, A., Januś, D., Furtak, A., Małek, A., Sztefko, K., et al. (2020). Circulating Chemerin Level May Be Associated with Early Vascular Pathology in Obese Children without Overt Arterial Hypertension - Preliminary Results. *J. Pediatr. Endocrinol. Metab.* 33, 729–734. doi:10.1515/jpem-2019-0460

Xie, Y., Huang, Y., Ling, X., Qin, H., Wang, M., and Luo, B. (2020). Chemerin/CMKLR1 Axis Promotes Inflammation and Pyroptosis by Activating NLRP3 Inflammasome in Diabetic Cardiomyopathy Rat. *Front. Physiol.* 11, 381. doi:10.3389/fphys.2020.00381

Xing, J., Wang, M., Hong, J., Gao, Y., Liu, Y., Gu, H., et al. (2019). TRPM7 Channel Inhibition Exacerbates Pulmonary Arterial Hypertension through MEK/ERK Pathway. *Aging (Albany NY)* 11, 4050–4065. doi:10.18632/aging.102036

Xiong, W., Luo, Y., Wu, L., Liu, F., Liu, H., Li, J., et al. (2016). Chemerin Stimulates Vascular Smooth Muscle Cell Proliferation and Carotid Neointimal Hyperplasia by Activating Mitogen-Activated Protein Kinase Signaling. *PLoS One* 11, e0165305. doi:10.1371/journal.pone.0165305

Yang, Y., Yin, L., Zhu, M., Song, S., Sun, C., Han, X., et al. (2021). Protective Effects of Dioscin on Vascular Remodeling in Pulmonary Arterial Hypertension via Adjusting GRB2/ERK/PI3K-AKT Signal. *Biomed. Pharmacother.* 133, 111056. doi:10.1016/j.biopha.2020.111056

Yu, M., Liu, X., Wu, H., Ni, W., Chen, S., and Xu, Y. (2017). Small Interfering RNA against ERK1/2 Attenuates Cigarette Smoke-Induced Pulmonary Vascular Remodeling. *Exp. Ther. Med.* 14, 4671–4680. doi:10.3892/etm.2017.5160

Zabel, B. A., Nakae, S., Zúñiga, L., Kim, J. Y., Ohyama, T., Alt, C., et al. (2008). Mast Cell-Expressed Orphan Receptor CCRL2 Binds Chemerin and Is Required for Optimal Induction of IgE-Mediated Passive Cutaneous Anaphylaxis. *J. Exp. Med.* 205, 2207–2220. doi:10.1084/jem.20080300

Zhang, G., Xiao, M., Zhang, L., Zhao, Y., and Yang, Q. (2017). Association of Serum Chemerin Concentrations with the Presence of Atrial Fibrillation. *Ann. Clin. Biochem.* 54, 342–347. doi:10.1177/0004563216664367

Zhang, R., Liu, S., Guo, B., Chang, L., and Li, Y. (2014). Chemerin Induces Insulin Resistance in Rat Cardiomyocytes in Part through the ERK1/2 Signaling Pathway. *Pharmacology* 94, 259–264. doi:10.1159/000369171

Zhang, Y., Lu, Y., Ong'achwa, M. J., Ge, L., Qian, Y., Chen, L., et al. (2018). Resveratrol Inhibits the TGF-B1-Induced Proliferation of Cardiac Fibroblasts and Collagen Secretion by Downregulating miR-17 in Rat. *Biomed. Res. Int.* 2018, 8730593. doi:10.1155/2018/8730593

Zhang, Y., Zhou, F., Bai, M., Liu, Y., Zhang, L., Zhu, Q., et al. (2019). The Pivotal Role of Protein Acetylation in Linking Glucose and Fatty Acid Metabolism to β-cell Function. *Cell Death Dis* 10, 66. doi:10.1038/s41419-019-1349-z

Zhao, G., Li, K., Chen, J., and Li, L. (2018). Protective Effect of Extract of Bletilla Striata on Isoflurane Induced Neuronal Injury by Altering PI3K/Akt Pathway. *Transl Neurosci.* 9, 183–189. doi:10.1515/tnsci-2018-0027

Zhou, X., Tao, Y., Chen, Y., Xu, W., Qian, Z., and Lu, X. (2019). Serum Chemerin as a Novel Prognostic Indicator in Chronic Heart Failure. *J. Am. Heart Assoc.* 8, e012091. doi:10.1161/jaha.119.012091

Zou, M., Zhang, G., Zou, J., Liu, Y., Liu, B., Hu, X., et al. (2020). Inhibition of the ERK1/2-Ubiquitous Calpains Pathway Attenuates Experimental Pulmonary Fibrosis *In Vivo* and *In Vitro*. *Exp. Cel Res* 391, 111886. doi:10.1016/j.yexcr.2020.111886

Conflict of Interest: The authors declare that the research was conducted in the absence of any commercial or financial relationships that could be construed as a potential conflict of interest.

Publisher's Note: All claims expressed in this article are solely those of the authors and do not necessarily represent those of their affiliated organizations, or those of the publisher, the editors and the reviewers. Any product that may be evaluated in this article, or claim that may be made by its manufacturer, is not guaranteed or endorsed by the publisher.

frontiers in Pharmacology

ORIGINAL RESEARCH
published: 28 March 2022
doi: 10.3389/fphar.2022.852029

Standardized Cannabis Smoke Extract Induces Inflammation in Human Lung Fibroblasts

*Noof Aloufi[1,2,3,4], Yoon Namkung[5], Hussein Traboulsi[1,2,5], Emily T. Wilson[1,2,6], Stephane A. Laporte[5,6], Barbara L.F. Kaplan[7], Matthew K. Ross[7], Parameswaran Nair[8], David H. Eidelman[1,2,5] and Carolyn J. Baglole[1,2,3,5,6]**

[1]Meakins-Christie Laboratories, Montreal, QC, Canada, [2]Translational Research in Respiratory Diseases Program at the Research Institute of the McGill University Health Centre, Montreal, QC, Canada, [3]Department of Pathology, McGill University, Montreal, QC, Canada, [4]Department of Medical Laboratory Technology, Applied Medical Science, Taibah University, Medina, Saudi Arabia, [5]Department of Medicine, McGill University, Montreal, QC, Canada, [6]Department of Pharmacology and Therapeutics, McGill University, Montreal, QC, Canada, [7]Department of Comparative Biomedical Sciences, Mississippi State University, Mississippi State, MS, United States, [8]Department of Medicine, McMaster University and St Joseph's Healthcare, Hamilton, ON, Canada

OPEN ACCESS

Edited by:
Irfan Rahman, University of Rochester, United States

Reviewed by:
Jiries Meehan-Atrash, University of Rochester, United States
Alexander Fiske Hoffman, National Institute on Drug Abuse (NIH), United States

***Correspondence:**
Carolyn J. Baglole
Carolyn.baglole@mcgill.ca

Specialty section:
This article was submitted to Respiratory Pharmacology, a section of the journal Frontiers in Pharmacology

Received: *10 January 2022*
Accepted: *25 February 2022*
Published: *28 March 2022*

Citation:
Aloufi N, Namkung Y, Traboulsi H, Wilson ET, Laporte SA, Kaplan BLF, Ross MK, Nair P, Eidelman DH and Baglole CJ (2022) Standardized Cannabis Smoke Extract Induces Inflammation in Human Lung Fibroblasts. Front. Pharmacol. 13:852029. doi: 10.3389/fphar.2022.852029

Cannabis (marijuana) is the most commonly used illicit product in the world and is the second most smoked plant after tobacco. There has been a rapid increase in the number of countries legalizing cannabis for both recreational and medicinal purposes. Smoking cannabis in the form of a joint is the most common mode of cannabis consumption. Combustion of cannabis smoke generates many of the same chemicals as tobacco smoke. Although the impact of tobacco smoke on respiratory health is well-known, the consequence of cannabis smoke on the respiratory system and, in particular, the inflammatory response is unclear. Besides the combustion products present in cannabis smoke, cannabis also contains cannabinoids including Δ^9-tetrahydrocannabinol (Δ^9-THC) and cannabidiol (CBD). These compounds are hydrophobic and not present in aqueous solutions. In order to understand the impact of cannabis smoke on pathological mechanisms associated with adverse respiratory outcomes, the development of *in vitro* surrogates of cannabis smoke exposure is needed. Therefore, we developed a standardized protocol for the generation of cannabis smoke extract (CaSE) to investigate its effect on cellular mechanisms *in vitro*. First, we determined the concentration of Δ^9-THC, one of the major cannabinoids, by ELISA and found that addition of methanol to the cell culture media during generation of the aqueous smoke extract significantly increased the amount of Δ^9-THC. We also observed by LC-MS/MS that CaSE preparation with methanol contains CBD. Using a functional assay in cells for CB1 receptors, the major target of cannabinoids, we found that this CaSE contains Δ^9-THC which activates CB1 receptors. Finally, this standardized preparation of CaSE induces an inflammatory response in human lung fibroblasts. This study provides an optimized protocol for aqueous CaSE preparation containing biologically active cannabinoids that can be used for *in vitro* experimentation of cannabis smoke and its potential impact on various indices of pulmonary health.

Keywords: fibroblast, inflammation, cannabis smoke, thc, cbd, lungs, CB1, BRET

INTRODUCTION

Cannabis has been used for medical purposes for thousands of years (Hillig, 2005; Rana, 2010; Atakan, 2012). Cannabis, commonly referred as marijuana, is a flowering plant belonging to the family *Cannabaceae*. There are three main subspecies of cannabis: *C. sativa*, *C. indica* and *C. ruderalis*, which are differentiated by key physical characteristics and production of cannabinoids (Hillig, 2005; Rana, 2010; Atakan, 2012). Cannabis produces more than 100 cannabinoids (Baron, 2018) that have many effects in the human body, including modulation of mood, memory and the immune response. One of the major cannabinoids is Δ^9-tetrahydrocannabinol (Δ^9-THC), which is responsible for the psychotropic effect of cannabis via activation of cannabinoid-1 (CB1) receptors in the brain (Mersiades et al., 2018). Cannabidiol (CBD), cannabigerol (CBG) and cannabichromene (CBC) are other cannabinoids currently under scientific investigation for their therapeutic potential. Of these, CBD has gained the most interest, particularly as an anti-inflammatory agent that lacks the psychoactive properties of Δ^9-THC (Rajan et al., 2016; Morales et al., 2017).

Δ^9-THC and CBD are produced in the trichomes of the female inflorescence as acidic precursors THCA and CBDA, respectively, that undergo decarboxylation when heated by consumption methods such as smoking (Tahir et al., 2021). According to the World Health Organization (WHO), approximately 15 million people (3% of world population) consume cannabis each year, making this the most widely-used illicit drug in the world. Currently, cannabis is the second most-smoked plant after tobacco (Baron, 2018; Brown, 2020; Campeny et al., 2020; Li et al., 2020), making inhalation of cannabis smoke the most common consumption method (Schuermeyer et al., 2014). Smoking cannabis provides the fastest Δ^9-THC delivery to the body, resulting in rapid onset of psychoactive effects. Like tobacco smoke, cannabis smoke also contains carcinogens [e.g., polycyclic aromatic hydrocarbons (PAHs)] and other toxicants (e.g., carbon monoxide) (Moir et al., 2008; Maertens et al., 2009; Graves et al., 2020). A recent study showed that there are 4,350 and 2,575 compounds in tobacco and cannabis smoke, respectively. Of these, 69 were common in both and are known to have adverse health risks through carcinogenic, mutagenic, or other toxic mechanisms (Graves et al., 2020). Unlike tobacco smoke, where the adverse respiratory effects are well-established (Strzelak et al., 2018), there are significant gaps in our understanding of the impact of cannabis smoke on respiratory health. Based on a limited number of studies, there is evidence that cannabis smoking is associated with inflammation and chronic bronchitis (Yayan and Rasche, 2016; Urban and Hureaux, 2017). Cannabis smoke can also negatively affect physical (e.g., mucociliary clearance) and immunological respiratory defense mechanisms (Chatkin et al., 2017). Regular cannabis use may also increase risk for asthma and accelerate the decline in lung function (Chatkin et al., 2019). However, the net effects of cannabis smoke on respiratory health, and in particular inflammation, remain largely unknown and such findings are often complicated by concurrent tobacco use in human participants. Thus, there is a pressing need to understand the consequences of cannabis smoke on the inflammatory response.

Our understanding of the ill health effects of tobacco smoke were driven in part by preclinical models of exposure. There are now established *in vitro* and *in vivo* models that recapitulate many of the exposure parameters observed in humans. These models have been extensively used to evaluate the mechanistic impact of tobacco smoke exposure (Carp and Janoff, 1978; Aoshiba et al., 2001; Carnevali et al., 2003; Baglole et al., 2006; Damico et al., 2011; Zago et al., 2013; de Souza et al., 2014; Guerrina et al., 2021a; Rico de Souza et al., 2021). Of these, cigarette smoke extract (CSE) is a widely-utilized *in vitro* surrogate for tobacco smoke exposure, and protocols for the generation of CSE are established and readily adaptable by many laboratories (Carp and Janoff, 1978; Martey et al., 2005; Baglole et al., 2006; Baglole et al., 2008b; Bertram et al., 2009; Damico et al., 2011). However, no such standardized protocol for cannabis smoke extract (CaSE) currently exists, greatly limiting investigation into the impact of cannabis smoke on biological and toxicological indices. Therefore, we developed a standardized protocol for the preparation of an aqueous cannabis smoke extract (CaSE) for *in vitro* evaluation. We used a legal cannabis source with a described composition and developed a protocol for standardization that allows for comparison between studies; this CaSE can be prepared and standardized using common laboratory equipment. Importantly, we confirmed that these CaSE preparations contain pharmacologically active Δ^9-THC using a signaling pathway downstream of the CB1 receptor: the Rho small G protein, with a Bioluminescence Resonance Energy Transfer (BRET) assay for this effector (Namkung et al., 2018). Finally, we used CaSE to show that key inflammatory markers are induced in human lung cells, suggesting that cannabis smoke is not harmless. With more countries legalizing cannabis for medical purposes, additional research is needed to better understand the cellular and molecular consequences of cannabis smoke exposure.

MATERIALS AND METHODS

Chemicals

All chemicals were obtained from Sigma (St. Louis, MO) unless otherwise indicated. Coelenterazine 400a was purchased from Nanolight™ Technology. 2-AG, Δ^9-THC and CBD are from Cayman Chemical (Ann Arbor, MI). The sp-hCB1 encoding plasmid (signal peptide human CB1) was a gift from Michel Bouvier, (University of Montreal).

Preparation of Cigarette Smoke Extract (CSE)

Research grade cigarettes (3R4F) with a filter were acquired from the Kentucky Tobacco Research Council (Lexington, KY). Research grade cigarettes (3R4F) contain 0.73 mg of nicotine, 9.4 mg of tar, and 12.0 mg of CO as described by the manufacturer. CSE was produced as previously described by us (Baglole et al., 2008a; Zago et al., 2013; Guerrina et al., 2021a; Guerrina et al., 2021b).

Briefly, CSE was prepared by bubbling smoke from a cigarette through 10 ml of serum-free cell culture medium with the exception that some extracts were prepared with 30% methanol (MeOH). The CSE was then sterile-filtered with a 0.45-μm filter (25-mm Acrodisc; Pall Corp., Ann Arbor, MI). Standardization was done for each CSE preparation by spectrophotometer using an OD_{320} nm of 0.65 to represent 100% CSE as described (Baglole et al., 2006; Zago et al., 2013).

Preparation of Cannabis Smoke Extract

Cannabis was purchased from the *Société québécoise du cannabis* SQDC online store (Quebec, Canada). Whole flower cannabis that was selected for purchase contained varying cannabinoid profiles based on THC/CBD content. Those purchased were as follows: 1) Indica-THC dominant; contains 16–22% THC and 0–0.1% CBD (#688083002311). 2): Sativa-CBD dominant; contains 0.1–2% THC and 13–19% CBD (#694144000219) and 3) Hybrid-Balanced: contains 5–11% THC and 5–11% CBD (#688083002588). Cannabis joints (cigarettes) were hand-rolled by grinding the dried cannabis flower with a plastic grinder and packing the product into classic 1 1/4 size rolling paper (RAW®). Each cannabis cigarette contained 0.5 ± 0.05 g of cannabis. A slim unrefined cellulose filter (RAW®) was added to the end of the joint. Then, CaSE was produced as previously described for CSE (Baglole et al., 2008a; Zago et al., 2013; Guerrina et al., 2021b) where the smoke from the lit cannabis cigarette was bubbled through 10ml of serum-free cell culture Dulbecco's modified Eagle's medium (DMEM) with or without 30% methanol (MeOH) or 30% ethanol (EtOH). CaSE was then filtered using a 0.45-μm filter (25-mm Acrodisc; Pall Corp., Ann Arbor, MI). Because the tar components in tobacco and cannabis are similar (Tashkin, 2013), and chemical species of tobacco tar absorb light at 320 nm (Taylor et al., 2020), we standardized each CaSE preparation as previously described for CSE (Baglole et al., 2008a; Zago et al., 2013; Guerrina et al., 2021a; Guerrina et al., 2021b) to ensure consistency in CaSE preparations between experiments. Similar to CSE preparation described above, an optical density of 0.65 was considered to represent 100% CaSE. Then, the CaSE solution was diluted with serum-free MEM for further analysis. The pH of 2% CaSE and 5% CaSE was 7.3 ± 0.06 and 7.7 ± 0.08, respectively.

Enzyme-Linked Immunosorbent Assay

Δ^9-THC concentration in CaSE was analyzed by a direct competitive THC Forensic ELISA kit (NEOGEN®) according to manufacturer's instructions. The concentration of interleukin-8 (IL-8) in the cell culture supernatant was determined by ELISA (Human IL-8 ELISA Duo Set, R&D Systems, United States) according to the manufacturer's instructions. The absorbance was read at 450 and 570 nm within 15 minutes by infinite TECAN (M200 pro, TECAN, CA).

Cell Culture and Transfection

Human embryonic kidney (HEK) 293 cells were cultured in DMEM supplemented with 10% fetal bovine serum (FBS) and gentamicin (20 μg/ml). Cells were grown at 37°C in 5% CO_2 and 90% humidity. HEK293 cells were seeded at a density of 1×10^6 cells per 100-mm dish and transfected the next day with 3 μg of sp-hCB1 with 120 ng of PKN-RBD-RlucII and 480 ng of rGFP-CAAX using PEI methods as described previously (Boussif et al., 1995; Namkung et al., 2018). Briefly, a total of 6 μg of DNA (adjusted with pcDNA3.1 zeo (+)) in 0.5 ml of PBS was mixed with 12 μl of PEI (25 kDa linear, 1 mg/ml) in 0.5 ml PBS and then incubated for 20 min at RT prior to applying to the cells. After 24 h, cells were detached and seeded onto poly-ornithine-coated 96-well white plates at a density of 25,000 cells per well for the BRET assays, which were performed 48 h after transfection.

Primary human lung fibroblasts (HLFs) were isolated from cancer-free lung tissue by explant procedure as described (Baglole et al., 2005). This study was approved by the Research Ethics Board of St. Joseph's Healthcare Hamilton and informed written consent was obtained from each patient. Experiments were conducted with fibroblasts from three different individuals of the non-smoker group (Normal; M/F = 1/2; age 68 ± 9 years) and within passage six to nine. HLFs were cultured in 10% MEM and treated with THC dominant CaSE for 6 and 24 h.

Rho BRET Assay

BRET assay for detecting Rho activation was performed as previously described (Namkung et al., 2018). Briefly, cells in 96 well plates were washed once with 150 μl/well of Tyrode's buffer (140 mM NaCl, 2.7 mM KCl, 1 mM $CaCl_2$, 12 mM $NaHCO_3$, 5.6 mM D-glucose, 0.5 mM $MgCl_2$, 0.37 mM NaH_2PO_4, 25 mM HEPES, pH 7.4) and left in 80 μl/well of Tyrode's buffer. 2-AG, THC, and CBD were serially diluted in 15% MeOH in Tyrode's buffer. The final concentration of MeOH in the assay is 3.75%. For BRET assay, the cells were loaded with 10 μl of coelenterazine 400a (final concentrations of ~3.5 μM) and then the cells were stimulated with 30 μl of ligands or two-fold diluted CaSE in Tyrode's buffer for 4 min prior to BRET measurement. Thus, final concentrations of CaSE were 12.5% (8-fold dilution of original CaSE). BRET signals were measured using a Synergy2 (BioTek) microplate reader. The filter was set at 410/80 nm and 515/30 nm for detecting the RlucII *Renilla* luciferase (donor) and rGFP (acceptor) light emissions, respectively. The BRET ratio was determined by calculating the ratio of the light emitted by rGFP over the light emitted by the RlucII.

Liquid Chromatography With Tandem Mass Spectrometry

CaSE culture media samples were diluted 1:20 v/v by adding 10 μl to 190 μl of MeOH containing an internal standard CBD-d9 (10 pmol); 10 μl was subsequently analyzed by LC-MS/MS. In some cases, a 1:2 dilution was prepared by mixing 100 μl of CaSE culture medium with 100 μl of methanol containing internal standard CBD-d9 (10 pmol). CBD was chromatographed on a Waters UPLC reversed phase column (100 × 2.1 mm i.d.) using a blend of water and acetonitrile containing 0.1% acetic acid with a flow rate of 0.2 ml/min. The eluate was directed into a Thermo Quantum Access Max triple-quadrupole mass spectrometer and the CBD and CBD-d9 detected by single-reaction monitoring. The peak area for CBD was normalized by the peak area for the internal standard (CBD-d9) and the ratio compared to an

TABLE 1 | Primer sequences used for qRT-PCR analysis.

Gene	Forward Primer Sequence	Reverse Primer Sequence
PTGS2	TCA CAG GCT TCC ATT GAC CAG	CCG AGG CTT TTC TAC CAG A
CXCL8	GAT GTC AGT GCA TAA AGA CAT ACT CCA A	GCT CTC TTC CAT CAG AAA GCT TTA CAA TA
S9	CAG CTT CAT CTT GCC CTC A	CTG CTG ACG CTT GAT GAG AA

external calibration curve for CBD prepared in MeOH. The limit of quantitation for CBD was 10 nM.

Western Blot

HLFs were grown to approximately 70–80% confluence and cultured with serum-free MEM for 18 h before the treatment. Total cellular protein was extracted using RIPA lysis buffer (Thermo Scientific, Rockford) containing Protease Inhibitor Cocktail (PIC, Roche, United States). Ten to 20 μg of protein lysate were subjected to 10% SDS-PAGE gels and transferred onto Immuno-blot PVDF membranes (Bio-Rad Laboratories, Hercules, CA). Then, the membrane was blocked for 1 hour at room temperature in blocking solution (5% w/v of non-fat dry milk in 1x PBS/0.1% Tween-20). The primary antibodies, COX-2 (1:1,000; Cell Signaling Technology, CA) and β-Tubulin (1:50000; Sigma, CA) were added to the membranes and incubated overnight at 4°C or 1 h at room temperature. After several washes, membrane was incubated with secondary antibodies goat anti-rabbit IgG HRP-linked (1:10000, Cell Signaling Technology, CA) or HRP-conjugated horse anti-mouse IgG (1: 10000, Cell Signaling Technology, CA). Detection of protein was done by enhanced chemiluminescence (ECL) and visualized using a ChemiDoc™ MP Imaging System (Bio-Rad, CA). Densitometric analysis was performed using Image Lab™ Software Version 5 (Bio-Rad, CA). Protein expression was normalized to β-tubulin and the data presented as the fold-change relative to the untreated condition.

Quantitative RT-PCR

Using the Aurum™ Total RNA Kit (Bio-Rad, CA), total RNA was isolated according to the manufacturer's instructions. Quantification of RNA was conducted on a Nanodrop 1,000 spectrophotometer. Reverse transcription of RNA was carried out using iScript™ Reverse Transcription Supermix (Bio-Rad, CA). Then, using this cDNA template, mRNA levels of *PTGS2*, *CXCL8* and *S9* were analyzed by quantitative PCR (qPCR) by using 1 μl of cDNA (10 ng/μl) and 0.5 μM primers with SsoFast™ EvaGreen® (Bio-Rad, CA). Sequences of gene-specific primers are listed in **Table 1**. PCR amplification was performed using a CFX96 Real-Time PCR Detection System (Bio-Rad, CA). Thermal cycling was initiated at 95°C for 3 min and followed by 39 cycles denaturation at 95°C for 10 s and annealing at 59°C for 5 s. Gene expression was analyzed using the $\Delta\Delta C_T$ method, and results are presented as fold-change normalized to housekeeping gene (*S9*).

Statistical Analysis

Using GraphPad Prism 6 (v. 6.02; La Jolla, CA), statistical analysis was performed using a one-way analysis of variance (ANOVA) followed by Dunn's multiple comparisons test to assess differences between treatments. Groups of two were analyzed by paired t-test. A two-way analysis of variance (ANOVA), followed by Tukey's multiple comparisons test was used to evaluate differences between groups and conditions of more than two. Results are presented as mean ± standard error of the mean (SEM) or as mean ± standard deviation (SD) of the fold-changes compared to control cells. Experimental readings were done in triplicate and averaged; statistical analysis was therefore done using averaged values from three to five independent experiments unless otherwise indicated. In all cases, a p value <0.05 is considered statistically significant. For **Tables 4**, **5**, the standard THC concentration response curve was obtained from a nonlinear regression curve fitting in GraphPad Prism software. The mean, upper limits, and lower limits of the unknowns were interpolated from the fitted standard curve with a confidential interval of 95%.

RESULTS

Generation of Cannabis Smoke Extract Preparations That Contains Δ^9-THC and CBD

Like tobacco, cannabis smoke contains hundreds of combustion products. However, cannabis also contains cannabinoids that exert biological and pharmacological effects. Standardized preparations of aqueous cigarette smoke extract (CSE) are well-described in the literature and are used to understand the consequences of tobacco exposure (Carnevali et al., 2003; Baglole et al., 2006; Baglole et al., 2008b; Hecht et al., 2014); no such standardized extract for cannabis smoke exists. Moreover, CSE prepared in cell culture media or PBS contains water soluble gas and particle phases of cigarette smoke (Kim et al., 2018). While many of these same compounds would be captured from cannabis smoke, cannabis also contains cannabinoids which are hydrophobic (Huestis, 2007) and unlikely to be present in an aqueous extract suitable for *in vitro* testing. Therefore, we sought to develop a cannabis smoke extract (CaSE) that contains biologically active cannabinoids. First, we utilized a semi-quantitative THC Forensic ELISA kit for which we developed a standard curve using Δ^9-THC to allow for subsequent quantification. The standard curve was first prepared to calculate the relative concentration of Δ^9-THC relative to the absorbance. We diluted Δ^9-THC (in the ELISA buffer) from a starting concentration of 1 mg/ml to an upper limit of 4 μg/ml. The concentration of this Δ^9-THC standard curve therefore ranged from 0 μg/ml (buffer only)- 4 μg/ml

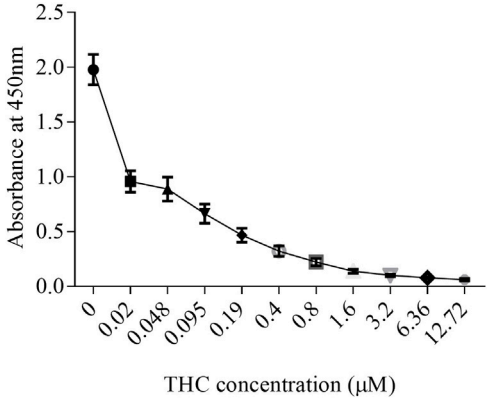

FIGURE 1 | The standard curve for Δ^9-THC. Δ^9-THC was diluted in ELISA buffer from a starting concentration of 1 mg/ml to an upper limit of 4 μg/ml. Then, the concentration of this Δ^9-THC standard curve was ranged from 0 μg/ml (buffer only)- 4 μg/ml (0–12.7 μM). Results are expressed as the mean ± SEM of two to four independent experiments.

(0–12.7 μM) (**Figure 1**) and was used for analysis with all CaSE preparations.

Next, we evaluated Δ^9-THC level by ELISA and CBD level LC-MS/MS in various aqueous CaSE preparations. Given that cannabinoids are hydrophobic, we compared Δ^9-THC levels in CaSE prepared in standard cell culture media with and without MeOH. As additional controls, we also evaluated Δ^9-THC concentrations in CSE prepared from research grade cigarettes. As expected, cell culture media alone with 30% MeOH as well as CSE (with 30% MeOH) contained no Δ^9-THC or CBD (**Table 2**). We also measured Δ^9-THC and CBD concentrations in CaSE prepared from the different strains of cannabis with reported varying amounts of Δ^9-THC and CBD. Δ^9-THC levels in CaSE generated from the Δ^9-THC dominant and THC/CBD balanced strains with 10% MeOH were 0.62 ± 0.2 and 0.36 ± 0.02, respectively, and were therefore similar to the level in CaSE without MeOH. However, in CaSE generated from the Δ^9-THC dominant strain with 30% MeOH, there were significantly higher levels of Δ^9-THC compared to the CaSE without MeOH (THC dominant CaSE; **Table 2**). CBD levels were below the limit of detection by LC-MS/MS. Here, the estimated Δ^9-THC concentration was 6.7 ± 0.29 μM in CaSE prepared in cell culture media with 30% MeOH. Preparation of CaSE from the balanced cannabis strain with 5–10% THC and 5–11% CBD also yielded significant Δ^9-THC levels only when CaSE was prepared in media containing 30% MeOH. Finally, CaSE prepared from the CBD dominant cannabis strain in media with 30% MeOH has less Δ^9-THC compared to CaSE prepared from the other two cannabis strains (**Table 2**). In CaSE generated from the balanced cannabis strain with 5–10% THC and 5–11% CBD, there were higher levels of CBD compared to the CaSE without MeOH (THC/CBD balanced CaSE; **Table 2**). CaSE prepared from the CBD dominant cannabis strain in media with 30% MeOH has higher CBD compared to CaSE prepared from the THC dominant strains. However, CBD levels are similar between CBD dominant and THC/CBD balanced strains (**Table 2**). We also generated CaSE from the Δ^9-THC dominant strain in media with 30% EtOH. We found that the Δ^9-THC level was slightly less in CaSE containing EtOH (5.7 ± 0.35 μM) comparing to CaSE with MeOH (6.7 ± 0.29 μM). These data show that preparation of CaSE in cell culture media with MeOH yields significantly higher concentrations of Δ^9-THC and CBD compared to CaSE prepared without MeOH. Thus, the remainder of experiments were conducted with CaSE prepared in media with 30% MeOH and is refereed to hereafter as CaSE.

Standardization of Cannabis Smoke Extract Using OD_{320}

The tar components in tobacco and cannabis are similar (Tashkin, 2013), and chemical species of tobacco tar absorb light at 320 nm (Taylor et al., 2020). Thus, to ensure consistency in CaSE preparations between experiments, we standardized each CaSE preparation as previously described for CSE (Baglole et al., 2008a; Zago et al., 2013; Guerrina et al., 2021a; Guerrina et al., 2021b). Nine extracts from THC dominant cannabis were prepared and two measurements were taken for fresh extracts and after thawing of the same extracts that had been frozen at −80°C for 16 weeks. The optical density (OD) at 320 was 0.7 ± 0.05 and 0.64 ± 0.05 for fresh and frozen extracts, respectively (**Table 3**). Given that an OD of 0.65 is used to represent 100% CaSE, the percentage of CaSE averaged to be 110% ± 8 and 99% ± 7.7 for fresh and frozen extracts, respectively. We also evaluated Δ^9-THC

TABLE 2 | Estimated concentration of Δ^9-THC and CBD in CaSE.

Extract	THC Absorbance (ELISA)	Δ^9-THC (μM) (ELISA)	CBD (μM) (LC-MS/MS)
Media +30% MeOH	1.662	0	<0.01
CSE+ 30% MeOH	1.398	0	<0.01
THC dominant CaSE	0.29 ± 0.02	0.67 ± 0.05	<0.01
THC dominant CaSE +30% MeOH	0.08 ± 0.002	6.7 ± 0.29*	<0.01
THC/CBD balanced CaSE	0.4538 ± 0.037	0.34 ± 0.05	<0.01
THC/CBD balanced CaSE +30% MeOH	0.087 ± 0.008	5.5 ± 0.46**	10.31 ± 9.125
CBD dominant CaSE+ 30% MeOH	0.16 ± 0.01	1.7 ± 0.4	7.733 ± 2.652

**THC dominant CaSE+30% MeOH was significantly higher (p < 0.03) compared to THC dominant CaSE without MeOH.; **THC/CBD balanced CaSE+30% MeOH was significantly higher (p < 0.008) compared to THC/CBD balanced CaSE without MeOH., Results are expressed as the mean ± SEM, of three to five independent extracts.*

TABLE 3 | Δ^9-THC absorbance (OD_{320}) and estimated concentration by ELISA.

Extract	OD_{320}	Percentage	THC ELISA	Δ^9-THC (μM)
Fresh CaSE	0.7 ± 0.05	110% ± 8	0.06 ± 0.0005	12.4 ± 0.2
Frozen CaSE	0.64 ± 0.05	99% ± 7.7	0.066 ± 0.001	12.2 ± 0.2

Results presented as mean ± SEM, of 9 independent extracts.

content by ELISA. The estimated Δ^9-THC concentration of fresh and frozen extracts was similar and was approximately 12 μM. These data suggest that storage of CaSE extracts up to 16 weeks at −80°C does not affect Δ^9-THC concentration and that an OD_{320} can be used to standardize aqueous CaSE to minimize batch-to-batch variability.

Cannabis Smoke Extract Activates CB1 Receptors

Δ^9-THC has high affinity to CB1 and CB2 receptors (Pertwee, 2010), which are G protein coupled receptors (GPCRs). CB1 couples to not only $G_{i/o}$ but also to the $G_{12/13}$ subfamily and activates the down-stream protein Rho (Inoue et al., 2019; Krishna Kumar et al., 2019; Avet et al., 2020). To determine whether there is sufficient Δ^9-THC in the CaSE preparations to activate CB1, we used a BRET-based Rho biosensor (Namkung et al., 2018). We transiently transfected HEK293 cells with signal-peptide-human CB1 (CB1) along with PKN-RBD-RLucII and rGFP-CAAX (Rho sensor) and stimulated the cells with Δ^9-THC, CBD and 2-arachidonoylglycerol (2-AG), an endogenous CB ligand (**Figure 2**). The BRET signal increased in response to Δ^9-THC and 2-AG but not to CBD (**Figure 2A**). Further, we observed that AM251, a CB1-specific antagonist, abolished the THC- and 2-AG- promoted BRET signals (**Figure 2B**). To verify the specificity of AM251 on CB1-mediated Rho activation, we examined the effect of AM251 on angiotensin II type 1 receptor (AT1R)-mediated Rho activation, which also couple to this pathway (Namkung et al., 2018). AM251 showed no effect on the basal BRET whereas AngII induced a BRET signal in HEK293 cells expressing AT1R along with Rho sensor (**Figure 2C**). These data show that Δ^9-THC- and 2-AG- promoted CB1 activation and signaling to the $G_{12/13}$-Rho pathway.

We next vetted three different extracts prepared from THC dominant or THC/CBD balanced cannabis prepared in media with or without 30% MeOH to verify that these CaSE preparations contained biologically active Δ^9-THC; we utilized

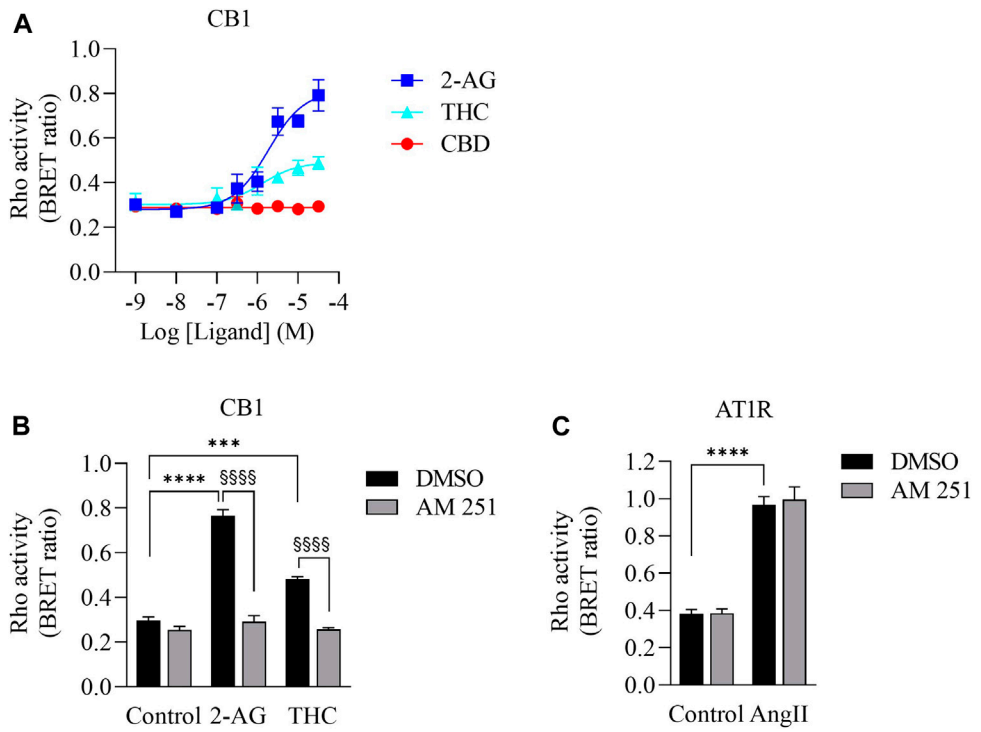

FIGURE 2 | Validation of CB1-mediated Rho activation. **(A)**. Concentration response curves of Rho activation in HEK293 cells expressing CB1, PKN-RBD-RLucII and rGFP-CAAX. Cells were stimulated with either 2-AG (blue square), THC (turquoise triangle) or CBD (red circle). CB1 was activated with 2-AG and Δ^9-THC but not with CBD. Data represent means ± SEM of four independent experiments performed in triplicate. **(B)**. Validation of CB1-mediated Rho activation by CB1 antagonist AM-251. Cells were stimulated with control, 2-AG (10 μM) or Δ^9-THC (THC, 10 μM) in the absence (vehicle, 0.1% DMSO (black bar)) or presence of 10 μM of AM-251 (grey bar). There was an increase in Rho activation in cells exposed to 2-AG (****$p < 0.0001$) and Δ^9-THC (***$p < 0.0002$). AM251 abolished 2-AG- and THC-induced CB1 activation ($^{§§§§}p < 0.0001$). **(C)**. Cells expressing AT1R, PKN-RBD-RLucII and rGFP-CAAX were stimulated with control or with 100 nM of AngII, agonist for AT1R, with 0.1% of DMSO (black bar) or 10 μM of AM-251 (grey bar). There was an increase in AT1R-mediated Rho activation in cells exposed to AngII (****$p < 0.0001$). There was no effect of AM251 on AT1R-mediated Rho activation. Data represent means ± SEM of three independent experiments.

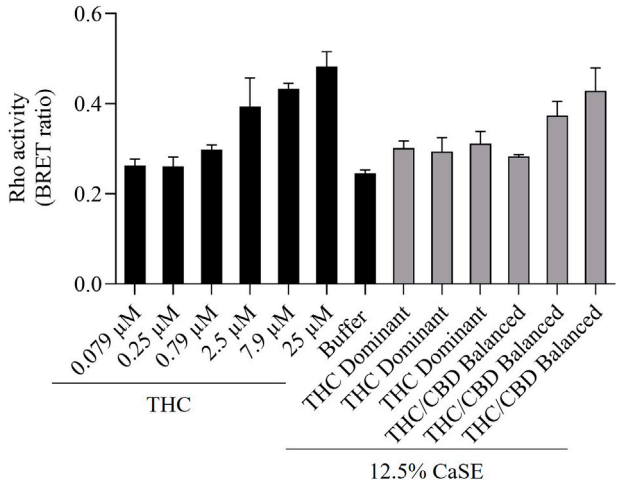

FIGURE 3 | CaSE promotes Rho activation in CB1 expressing cells. HEK293 cells expressing CB1 along with PKN-RBD-RLucII and rGFP-CAAX were stimulated with indicated concentrations of Δ^9-THC in buffer or 8-fold diluted CaSE (15 μl in total 120 μl assay volume, 12.5% CaSE) from Δ^9-THC dominant and THC/CBD balanced strains prepared in media with 30% MeOH. There was an increase in CB1 activation in a concentration-dependent manner by Δ^9-THC. There was an increase in the activation of CB1 in cells treated with CaSE from THC dominant or THC/CBD balanced cannabis. Buffer was 8-fold dilution of 30% MeOH/DMEM with Tyrode's buffer. Data represent means ± SD of triplicate (THC) and duplicate (CaSE) of a representative experiment. Similar results were obtained with 20 μl or 10 μl application of CaSE.

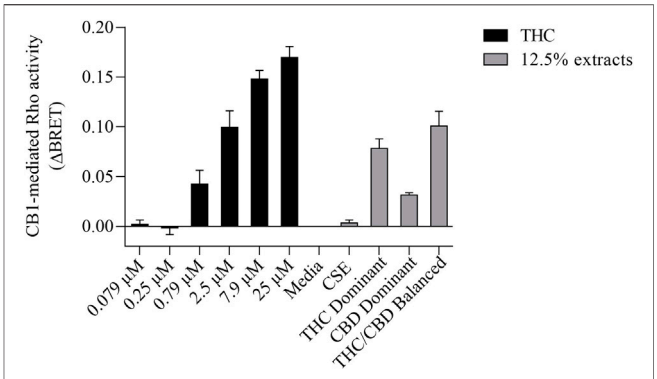

FIGURE 4 | CaSE promotes Rho activation in CB1 expressing cells in comparison to Δ^9-THC. HEK293 cells expressing CB1 along with Rho sensor were stimulated with indicated concentrations of Δ^9-THC in buffer or 8-fold diluted indicated extracts prepared in media with 30% MeOH: Media with only 30% MeOH, CaSE and CSE. There was an increase in CB1 activation in cells exposed to CaSE from THC dominant, THC/CBD balanced and CBD-dominant cannabis, but not Media with MeOH or CSE. Buffer was 8-fold dilution of 30% MeOH/DMEM with Tyrode's buffer. Data were expressed as a ligand-promoted BRET (ΔBRET) by subtracting BRET ratio in control media. Data represent mean ± SEM of three to five independent experiments.

TABLE 4 | Estimation of THC concentrations in 100% CaSE. THC concentrations in CaSE were estimated from interpolation of standard THC concentration response curve in **Figure 3**.

CaSE	THC conc. (μM)	95% CI
THC dominant	5.32	3.47–8.31
THC dominant	4.45	2.77–7.04
THC dominant	6.58	4.43–10.14
THC/CBD balanced	3.23	1.67–5.30
THC/CBD balanced	18.83	12.80–27.10
THC/CBD balanced	47.16	31.88–73.00

TABLE 5 | Estimation of THC concentration in 100% CaSE. THC concentrations in CaSE were estimated from interpolation of standard THC concentration response curve in **Figure 4**.

CaSE	Est. Concentration (μM)	95% CI
THC dominant	13.9	10.0–19.5
THC/CBD balanced	22.1	15.7–30.3
CBD dominant	4.5	3.0–6.7

the same extracts as for the data presented in **Table 2**. First, the activation of CB1 in response to different concentrations of Δ^9-THC (0.3–25 μM) was assessed. There was a concentration-dependent activation of CB1 by Δ^9-THC (**Figure 3**). Furthermore, there was an increase in CB1 activation in cells treated with CaSE from THC dominant or THC/CBD balanced cannabis prepared in media with 30% MeOH (**Figure 3**). Extracts in media without 30% MeOH did not show BRET signals in our assay (data not shown). Based on CB1 activation by Δ^9-THC (**Figure 3**), we extrapolated that CaSE prepared from THC-dominant cannabis activates CB1 in concentrations equivalent to 5–7 μM of Δ^9-THC (**Table 4**). CaSE from THC/CBD balanced cannabis also activates the receptor, which is equivalent to 3–50 μM of Δ^9-THC (**Table 4**).

We then tested whether the receptor itself was affected by the MeOH and evaluated the specificity of the system by adding CSE prepared in media with 30% MeOH; we also included CaSE from all three cannabis strains (see **Table 2**). We found that there was no Rho activation with media containing 30% MeOH or CSE (**Figure 4**). CaSE from THC dominant, THC/CBD balanced, and CBD-dominant cannabis all activated Rho signaling (**Figure 4**), at levels that corresponded approximately to between 4–22 μM of Δ^9-THC present in the extracts (**Table 5**). Thus, CaSE, but not media containing MeOH or CSE, activates the CB1 receptor. Finally, we used the CB1 antagonist AM251 to confirm that CaSE is specific in its ability to activate CB1. AM251 inhibited THC-induced Rho activation. We also found that AM251 significantly inhibits CaSE-induced Rho activation for the CaSE prepared from the THC-dominant and THC/CBD balanced strains (**Figure 5**). Thus, CaSE induces Rho activation through CB1. Taken together, these data show that a standardized preparation of CaSE contains biologically active cannabinoids.

COX-2 and IL-8 Are Increased in HLFs Exposed to Cannabis Smoke Extract

COX-2 and IL-8 are among the proinflammatory mediators that are induced by tobacco smoke (Martey et al., 2004; Li et al., 2007).

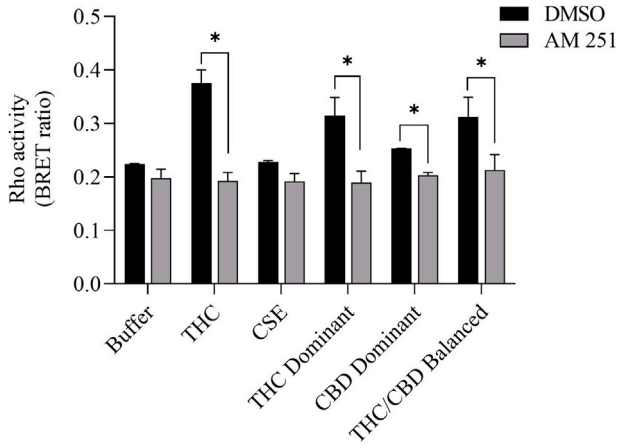

FIGURE 5 | CaSE-induced Rho activation is mediated by CB1. HEK293 cells expressing CB1 and Rho sensor were stimulated with Δ^9-THC (25 μM) or indicated CaSE (12.5%) in the absence (0.1% DMSO, black bar) or presence of AM 251 (10 μM) (grey bar). AM 251 abolished the Δ^9-THC- and CaSE-mediated Rho activation in CaSE prepared from THC dominant and THC/CBD balanced strains (*$p < 0.05$). CSE treatment did not increase Rho activity compared to buffer; AM 251 had no effect. Data represent mean ± SD from two independent experiments.

IL-8 is also elevated in serum from cannabis smokers (Bayazit et al., 2017). To explore whether we could replicate these findings, we characterized the effect of CaSE exposure on the expression of COX-2 and IL-8 at the mRNA and protein levels in primary HLFs. For these experiments, HLFs were treated with either 2% or 5% CaSE that was prepared from THC dominant cannabis. Selection of these concentrations was based on our previous publications with CSE (Baglole et al., 2008a; Guerrina et al., 2021a). These concentrations of CaSE did not affect cell viability (data not shown). The concentration of Δ^9-THC in 2% CaSE was 0.18 ± 0.003 μM and in 5% CaSE was 0.45 ± 0.006 μM (n = 3). The mRNA for *PTGS2* did not increase with 6 h of CaSE (**Figure 6A**). However, there was a significant increase in *PTGS2* mRNA upon exposure to 5% CaSE for 24 h- but not 2% CaSE. Accordingly, there was a significant increase in COX-2 protein with 5% CaSE (**Figure 6B**). There was also a significant increase in *CXCL8* mRNA in response to 5% CaSE for 24 h (**Figure 6C**). At the protein level, IL-8 was also induced upon 5% CaSE treatment for 24 h (**Figure 6D**). These data indicate that a standardized CaSE preparation, containing biologically active cannabinoids, induces an inflammatory response in primary HLFs.

DISCUSSION

Cannabis is the most commonly-smoked plant after tobacco (Baron, 2018; Brown, 2020; Campeny et al., 2020; Li et al., 2020). Recently, the personal use of cannabis has been approved in nine states of the United States as well as in Uruguay and Canada (Campeny et al., 2020). Cannabis smoke is often considered to be harmless compared to tobacco smoke (Sinclair et al., 2013). However, cannabis smoke contains many chemicals (toxicants, irritants, carcinogens, and fine particles) as does tobacco smoke (Moir et al., 2008; Manolis et al., 2019; Graves et al., 2020). The latest report from the Canadian Centre on Substance Use and Addiction (CCSA) highlights the risks of cannabis smoking to the heart and lungs as heavy users of cannabis can potentially develop cardiovascular and respiratory diseases (Canadian Centre on Substance Use and Addiction, 2020). Cannabis smoking is associated with a greater incidence of respiratory symptoms including sore throat, productive cough and shortness of breath (Henderson et al., 1972). These symptoms are likely due to harmful impacts of cannabis smoke on the respiratory system. Indeed, there is evidence of goblet cell hyperplasia, squamous metaplasia and inflammation in tracheobronchial specimens of cannabis smokers compared to non-smokers (Fligiel et al., 1997) as well as airway inflammatory changes in asymptomatic marijuana smokers compared to non-smokers (Roth et al., 1998). This is also supported by *in vivo* studies which showed that exposing mice to cannabis smoke alters the immune cell populations in the airways and lung tissue (Fantauzzi et al., 2021) and induces bronchial hyperreactivity, inflammation, and tissue destruction (Helyes et al., 2017). Thus, cannabis smoke may cause adverse respiratory features, and may increase the risk of developing lung diseases similar to tobacco smoke. However, the number of studies investigating the health effects of cannabis smoke exposure remains limited, and it is not well understood if there is a link between exposure to cannabis smoke and respiratory disease development. Thus, there is a need for experimental models into order to investigate the impact of cannabis smoke on respiratory health.

Despite this need, there are no validated experimental models with which to perform detailed evaluations on the effect of cannabis smoke *in vitro*. We are only aware of one study utilizing a cannabis smoke extract for *in vitro* assessment (Aguiar et al., 2019). However, the cannabis smoke extract in that study was prepared without adding a solvent to capture the cannabinoids in the aqueous solution; the presence of Δ^9-THC or other cannabinoids was also not measured (Aguiar et al., 2019). Based on our results, an aqueous preparation of cannabis smoke-as in the study by Aguiar and colleagues-likely did not contain active cannabinoids. Therefore, we sought to develop a standardized protocol for the preparation of CaSE utilizing a protocol similar to that used in the generation of CSE (Baglole et al., 2008a; Zago et al., 2013; Guerrina et al., 2021a; Guerrina et al., 2021b) but one that contains cannabinoids. To achieve this, we made a modification to the preparation via the addition of MeOH to the cell culture media, as cannabinoids are hydrophobic (Huestis, 2007) and MeOH is a suitable solvent for the isolation of fat-soluble compounds (Rozanc et al., 2021). Thus, the addition of MeOH significantly increased the concentration of Δ^9-THC and CBD in the extract compared to negligible levels in CaSE prepared in culture media alone. One of the advantages of this standardized method is that it can be performed using common laboratory equipment, allowing for easy adaptation. Here, we followed the same standardization method for CSE by measuring the absorbance of CaSE at 320 nm, similar to what we have previously used for CSE (Martey et al., 2004; Baglole et al., 2008a;

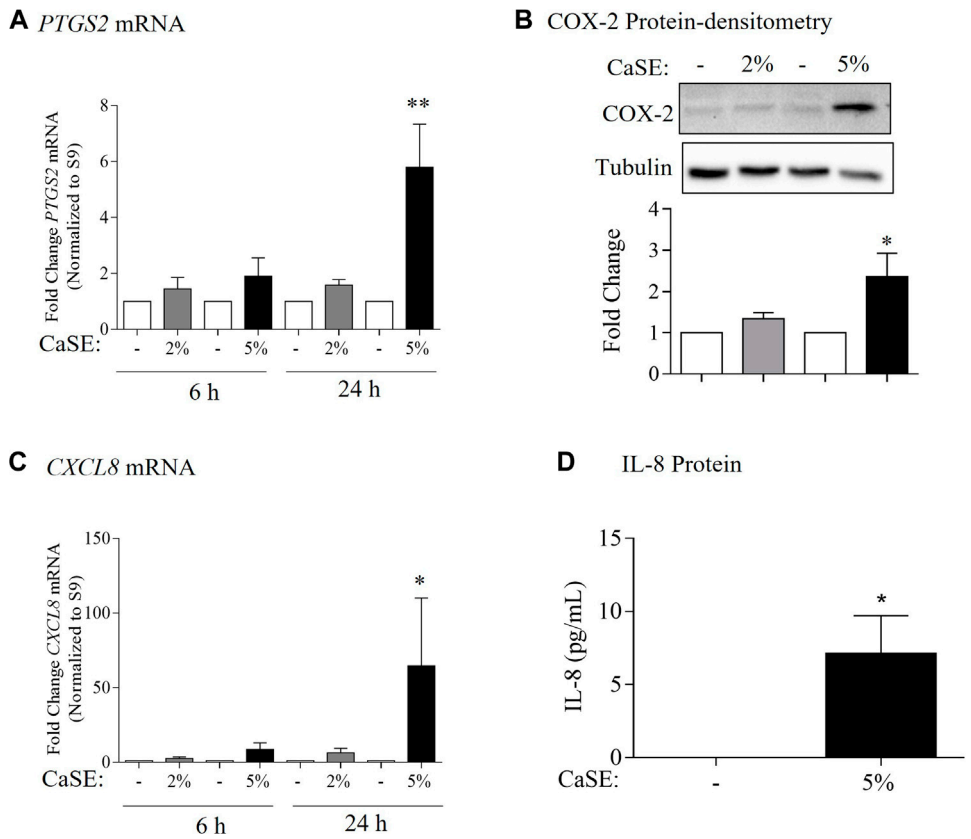

FIGURE 6 | CaSE induces COX-2 and IL-8 expression in human lung fibroblasts. **(A)**. *PTGS2* mRNA: there was a slight increase, but not statistically significant, in *PTGS2* mRNA in HLFs exposed to 2 and 5% CaSE for 6 h and in HLFs exposed to 2% CaSE for 24 h compared to corresponding control. There was significant increase in *PTGS2* mRNA in HLFs exposed to 5% CaSE for 24 h (**$p = 0.009$) compared to corresponding control. Results are expressed as the mean ± SEM of 4 independent experiments of HLFs used from 3 Normal subjects. **(B)**. COX-2 Protein-densitometry: there was significant increase in COX-2 protein levels in HLFs exposed to 5% CaSE for 24 h (*$p = 0.04$) compared to corresponding control. Results are expressed as the mean ± SEM of 3 independent experiments (HLFs used from 3 Normal subjects). **(C)**. *CXCL8* mRNA: there was a slight -but not statistically significant-increase in *CXCL8* mRNA in HLFs exposed to 2 and 5% CaSE for 6 h There was significant increase in *CXCL8* mRNA in HLFs exposed to 5% CaSE for 24 h (*$p = 0.01$) compared to corresponding control. Results are expressed as the mean ± SEM of 4 independent experiments (HLFs used from 3 Normal subjects). **(D)**. IL-8 Protein: there was an increase in IL-8 protein levels in the media from HLFs exposed to 5% CaSE for 24 h compared to corresponding control. Results are expressed as the mean ± SEM of 3 independent experiments (HLFs used from 3 Normal subjects).

Zago et al., 2013; Zago et al., 2014). Because the tar components in tobacco and cannabis are similar (Tashkin, 2013) and the chemical species of tar in tobacco absorb light at 320 nm (Taylor et al., 2020), standardization can be performed via spectroscopy, and confirmation of cannabinoid presence made by a commercial ELISA. One of the limitations of this study is that we measured only Δ^9-THC and CBD levels in CaSE, and thus cannot provide information on the presence or absence of additional cannabinoids or other compounds, including those could also affect the activity of the CB1 receptor. Another limitation that we did not assess whether MeOH affects the solubility of the chemical species found in the tar fraction. Nonetheless, this methodology allows for robust and reliable generation of a cannabis extract that contains biologically-active cannabinoids (Δ^9-THC and CBD) to allow for consistency between experiments and comparison between studies.

The detection of cannabinoids in CaSE is important as cannabinoids carry out a variety of physiological functions by engaging with receptors present in the body, including cannabinoids receptors (CBR) (Reggio, 2010). The first discovered CBRs are CB1 and CB2, which belong to the GPCR superfamily. CB1 is expressed predominantly in the central nervous system (CNS), particularly in the basal ganglia, hippocampus, cortex, and cerebellum; these CB1 receptors mediate the psychoactive effects from Δ^9-THC (Sim-Selley, 2003; Kawamura et al., 2006). Δ^9-THC also binds to CB2 receptors with similar binding affinity (Pertwee, 2010). CB2 receptors are present mainly on the surface of immune and hematopoietic cells (Graham et al., 2010). In the respiratory system, CB1 and CB2 receptors are both expressed on epithelial cells with alveolar type II cells displaying CB1 receptor and lung fibroblasts having CB2 receptor (Kicman et al., 2021). Although lung fibroblasts provide structure and support to the lungs by synthesizing and maintaining an extracellular matrix (ECM) (White, 2015), fibroblast activation also leads to the production of several cytokines and chemokines (Buckley et al., 2001; Davidson et al., 2021). The effects of CSE on

lung fibroblasts is well-described by us and others (Carnevali et al., 2003; Martey et al., 2004; Baglole et al., 2006; Baglole et al., 2008a; Baglole et al., 2008b), making these a relevant lung cell type. Herein, we observed that the CaSE-like CSE-induces an inflammatory response in primary lung fibroblasts, including induction of COX-2 and IL-8 levels by 5% CaSE derived from the THC dominant strain. By our estimation, this preparation contains ~0.45 μM of Δ^9-THC, which is similar to the plasma levels of THC in cannabis smokers (~ 1 μM) (Azorlosa et al., 1992). The ability of 5% CaSE to induce COX-2 and IL-8 expression occurred despite the presence of cannabinoids at physiologically-relevant concentrations. It could be that Δ^9-THC itself induced the inflammatory response; this would be in line with another publication whereby COX-2 is induced by Δ^9-THC in neurons and astroglial cells (Chen et al., 2013). It could also be that the cannabinoids present in the extract could not compensate for products of combustion-which promote an inflammatory response typified by the induction of COX-2 (Martey et al., 2004). Of note is the absence of CBD from extracts prepared from the THC dominant strain. CBD has anti-oxidative and anti-inflammatory properties (Atalay et al., 2019). Comparison of CaSE prepared from different cannabis strains (with varying THC/CBD ratios) may shed light on whether all CaSE preparations have the same inflammatory potential.

In order for Δ^9-THC and CBD to be biologically active, the acidic precursors THCA and CBDA need to undergo decarboxylation, a process that is facilitated by combustion. Our standardized CaSE indeed contained forms of cannabinoids that activated the CB1 receptor. As the CB1 receptor is coupled to $G_{i/o}$ and $G_{12/13}$ subfamilies and activates its down-stream Rho (Inoue et al., 2019; Krishna Kumar et al., 2019; Avet et al., 2020), we transfected cells with CB1 receptors along with Rho sensor to evaluate CB1 receptor activation. Here, it was only with CaSE prepared with MeOH that activated the CB1 receptor, with highest activation in extracts from the THC/CBD balanced strain. This was surprising, given that CBD has relatively low affinity for the CB1 receptor (McPartland et al., 2015) and our result showed that pure CBD does not activate CB1. However, it is still possible that CBD may modulate the activity of the receptor (McPartland et al., 2015) or that CBD and/or other cannabinoids in the extract affects the binding of Δ^9-THC to the CB1 receptor. We also found that the estimated Δ^9-THC concentration in these extracts from the functional assay was 3–50 μM, which is higher than the estimated concentration from the ELISA (~5.5 μM). Nonetheless, the presence of biologically-active cannabinoids in this CaSE preparation further highlights its utility in evaluating the physiological and pathological implications of cannabis smoke.

A limitation of this study is that we did not assess additional signaling mechanisms that may account for the induction of inflammation of CaSE or the ability of CaSE to activate other receptors. For example, Δ^9-THC also binds to the CB2 receptor (Pertwee, 2010) with CB2 activation controlling inflammation and immune functions (Turcotte et al., 2016). Δ^9-THC can also activate the nuclear factor-κB (NF-κB) pathway (Do et al., 2004), a transcription factor that regulates genes involved inflammation, such as COX-2 and IL-8 (Ahn and Aggarwal, 2005). As lung fibroblasts express the CB2 receptor (Kicman et al., 2021), it may be that CaSE induces inflammation via the activation of CB2 receptor and/or NF-κB. However, Δ^9-THC can also activate other GPCRs such as GPR55 (Sharir and Abood, 2010) which is also expressed in the lung (Ryberg et al., 2007). Interestingly, agonist interaction with GPR55 can also activate NF-κB (Henstridge et al., 2010). However, direct regulation of cannabinoids on the activation of GPR55 still needs to be elucidated. Finally, one of the downstream signaling pathways of the CB1 receptor is p38 MAPK (Chen et al., 2013). It is well studied that cigarette smoke can also active p38 MAPK to induce an inflammatory response (Moretto et al., 2012; Marumo et al., 2014). However, nothing is known about the effect of cannabis smoke on this- and other-signaling pathways in pulmonary cells, a deficit in knowledge that can be addressed by utilization of this standardized extract.

In this study, we sought to develop a protocol for the preparation of a cannabis smoke extract that could be used to investigate the effect of cannabis smoke *in vitro*. We successfully captured Δ^9-THC and CBD within an aqueous preparation (CaSE), which allowed us to recapitulate as closely as possible to what smokers are inhaling; this includes cannabinoids and combustion products. Our data also revealed that this CaSE activates CB1 receptors, further highlighting that it contains biologically active cannabinoids. Importantly, this extract can be prepared and standardized using common laboratory equipment. This CaSE can be used for further molecular investigation into the downstream mechanisms of cannabis smoke/cannabinoids that will ultimately improve our understanding about the effect of cannabis smoke on features of lung pathology.

DATA AVAILABILITY STATEMENT

The authors acknowledge that the data presented in this study must be deposited and made publicly available in an acceptable repository, prior to publication.

ETHICS STATEMENT

The studies involving human participants were reviewed and approved by Research Ethics Board of St. Joseph's Healthcare Hamilton. The patients/participants provided their written informed consent to participate in this study.

AUTHOR CONTRIBUTIONS

Data curation and/or analysis: NA, YN, MR; Funding acquisition: CB; Methodology: NA, YN, HT, EW, SL, BK, MR; Resources: PN, SL; Project administration: CB, SL; Supervision: CB, SL; Intellectual contributions: NA, CB, DE, SL, BK, MR; Manuscript writing, review and editing: NA, YN, HT, CB, DE, SL, BK, MR.

FUNDING

This work was supported by the Canadian Institutes for Health Research Project Grants (168836 and 162273) and the Natural Sciences and Engineering Research Council of Canada (NSERC). CB was supported by a salary award from the Fonds de recherche du Quebec-Sante (FRQ-S). NA was supported by a scholarship from Taibah University, Saudi Arabia. HT was supported by a Réseau de recherche en santé réspiratoire du Québec (RSR) Scholarship and a Meakins-Christie Laboratories Collaborative Research Award. SL was supported by the Canadian Institutes of Health Research (PJT-162368 and PJT-173504).

REFERENCES

Aguiar, J. A., Huff, R. D., Tse, W., Stämpfli, M. R., Mcconkey, B. J., Doxey, A. C., et al. (2019). Transcriptomic and Barrier Responses of Human Airway Epithelial Cells Exposed to Cannabis Smoke. *Physiol. Rep.* 7, e14249. doi:10.14814/phy2.14249

Ahn, K. S., and Aggarwal, B. B. (2005). Transcription Factor NF-kappaB: a Sensor for Smoke and Stress Signals. *Ann. N. Y Acad. Sci.* 1056, 218–233. doi:10.1196/annals.1352.026

Aoshiba, K., Tamaoki, J., and Nagai, A. (2001). Acute Cigarette Smoke Exposure Induces Apoptosis of Alveolar Macrophages. *Am. J. Physiol. Lung Cel. Mol. Physiol.* 281, L1392–L1401. doi:10.1152/ajplung.2001.281.6.L1392

Atakan, Z. (2012). Cannabis, a Complex Plant: Different Compounds and Different Effects on Individuals. *Ther. Adv. Psychopharmacol.* 2, 241–254. doi:10.1177/2045125312457586

Atalay, S., Jarocka-Karpowicz, I., and Skrzydlewska, E. (2019). Antioxidative and Anti-inflammatory Properties of Cannabidiol. *Antioxidants (Basel)* 9, 21. doi:10.3390/antiox9010021

Avet, C., Mancini, A., Breton, B., Le Gouill, C., Hauser, A. S., Normand, C., et al. (2020). Selectivity Landscape of 100 Therapeutically Relevant GPCR Profiled by an Effector Translocation-Based BRET Platform. *bioRxiv*. doi:10.1101/2020.04.20.052027

Azorlosa, J. L., Heishman, S. J., Stitzer, M. L., and Mahaffey, J. M. (1992). Marijuana Smoking: Effect of Varying delta 9-Tetrahydrocannabinol Content and Number of Puffs. *J. Pharmacol. Exp. Ther.* 261, 114–122.

Baglole, C. J., Reddy, S. Y., Pollock, S. J., Feldon, S. E., Sime, P. J., Smith, T. J., et al. (2005). Isolation and Phenotypic Characterization of Lung Fibroblasts. *Methods Mol. Med.* 117, 115–127. doi:10.1385/1-59259-940-0:115

Baglole, C. J., Bushinsky, S. M., Garcia, T. M., Kode, A., Rahman, I., Sime, P. J., et al. (2006). Differential Induction of Apoptosis by Cigarette Smoke Extract in Primary Human Lung Fibroblast Strains: Implications for Emphysema. *Am. J. Physiol. Lung Cel Mol Physiol* 291, L19–L29. doi:10.1152/ajplung.00306.2005

Baglole, C. J., Maggirwar, S. B., Gasiewicz, T. A., Thatcher, T. H., Phipps, R. P., and Sime, P. J. (2008a). The Aryl Hydrocarbon Receptor Attenuates Tobacco Smoke-Induced Cyclooxygenase-2 and Prostaglandin Production in Lung Fibroblasts through Regulation of the NF-kappaB Family Member RelB. *J. Biol. Chem.* 283, 28944–28957. doi:10.1074/jbc.M800685200

Baglole, C. J., Sime, P. J., and Phipps, R. P. (2008b). Cigarette Smoke-Induced Expression of Heme Oxygenase-1 in Human Lung Fibroblasts Is Regulated by Intracellular Glutathione. *Am. J. Physiol. Lung Cel Mol. Physiol.* 295, L624–L636. doi:10.1152/ajplung.90215.2008

Baron, E. P. (2018). Medicinal Properties of Cannabinoids, Terpenes, and Flavonoids in Cannabis, and Benefits in Migraine, Headache, and Pain: An Update on Current Evidence and Cannabis Science. *Headache* 58, 1139–1186. doi:10.1111/head.13345

Bayazit, H., Selek, S., Karababa, I. F., Cicek, E., and Aksoy, N. (2017). Evaluation of Oxidant/Antioxidant Status and Cytokine Levels in Patients with Cannabis Use Disorder. *Clin. Psychopharmacol. Neurosci.* 15, 237–242. doi:10.9758/cpn.2017.15.3.237

Bertram, K. M., Baglole, C. J., Phipps, R. P., and Libby, R. T. (2009). Molecular Regulation of Cigarette Smoke Induced-Oxidative Stress in Human Retinal Pigment Epithelial Cells: Implications for Age-Related Macular Degeneration. *Am. J. Physiol. Cel. Physiol.* 297, C1200–C1210. doi:10.1152/ajpcell.00126.2009

Boussif, O., Lezoualc'h, F., Zanta, M. A., Mergny, M. D., Scherman, D., Demeneix, B., et al. (1995). A Versatile Vector for Gene and Oligonucleotide Transfer into Cells in Culture and *In Vivo*: Polyethylenimine. *Proc. Natl. Acad. Sci. U S A.* 92, 7297–7301. doi:10.1073/pnas.92.16.7297

Brown, J. D. (2020). Potential Adverse Drug Events with Tetrahydrocannabinol (THC) Due to Drug-Drug Interactions. *J. Clin. Med.* 9, 919. doi:10.3390/jcm9040919

Buckley, C. D., Pilling, D., Lord, J. M., Akbar, A. N., Scheel-Toellner, D., and Salmon, M. (2001). Fibroblasts Regulate the Switch from Acute Resolving to Chronic Persistent Inflammation. *Trends Immunol.* 22, 199–204. doi:10.1016/s1471-4906(01)01863-4

Campeny, E., Lopez-Pelayo, H., Nutt, D., Blithikioti, C., Oliveras, C., Nuno, L., et al. (2020). The Blind Men and the Elephant: Systematic Review of Systematic Reviews of Cannabis Use Related Health Harms. *Eur. Neuropsychopharmacol.* 33, 1–15. doi:10.1016/j.euroneuro.2020.02.003

Canadian Centre on Substance Use and Addiction (2020). *COVID-19 and Cannabis Smoking and Vaping: Four Things You Should Know*. [Online]. Available at: https://ccsa.ca/covid-19-and-cannabis-smoking-and-vaping-four-things-you-should-know-report (Accessed October, 2021).

Carnevali, S., Petruzzelli, S., Longoni, B., Vanacore, R., Barale, R., Cipollini, M., et al. (2003). Cigarette Smoke Extract Induces Oxidative Stress and Apoptosis in Human Lung Fibroblasts. *Am. J. Physiol. Lung Cel Mol. Physiol.* 284, L955–L963. doi:10.1152/ajplung.00466.2001

Carp, H., and Janoff, A. (1978). Possible Mechanisms of Emphysema in Smokers. *In Vitro* Suppression of Serum Elastase-Inhibitory Capacity by Fresh Cigarette Smoke and its Prevention by Antioxidants. *Am. Rev. Respir. Dis.* 118, 617–621. doi:10.1164/arrd.1978.118.3.617

Chatkin, J. M., Zabert, G., Zabert, I., Chatkin, G., Jiménez-Ruiz, C. A., De Granda-Orive, J. I., et al. (2017). Lung Disease Associated with Marijuana Use. *Arch. Bronconeumol* 53, 510–515. doi:10.1016/j.arbres.2017.03.019

Chatkin, J. M., Zani-Silva, L., Ferreira, I., and Zamel, N. (2019). Cannabis-Associated Asthma and Allergies. *Clin. Rev. Allergy Immunol.* 56, 196–206. doi:10.1007/s12016-017-8644-1

Chen, R., Zhang, J., Fan, N., Teng, Z. Q., Wu, Y., Yang, H., et al. (2013). Δ9-THC-caused Synaptic and Memory Impairments Are Mediated through COX-2 Signaling. *Cell* 155, 1154–1165. doi:10.1016/j.cell.2013.10.042

Damico, R., Simms, T., Kim, B. S., Tekeste, Z., Amankwan, H., Damarla, M., et al. (2011). p53 Mediates Cigarette Smoke-Induced Apoptosis of Pulmonary Endothelial Cells: Inhibitory Effects of Macrophage Migration Inhibitor Factor. *Am. J. Respir. Cel Mol Biol* 44, 323–332. doi:10.1165/rcmb.2009-0379OC

Davidson, S., Coles, M., Thomas, T., Kollias, G., Ludewig, B., Turley, S., et al. (2021). Fibroblasts as Immune Regulators in Infection, Inflammation and Cancer. *Nat. Rev. Immunol.* 21, 704–717. doi:10.1038/s41577-021-00540-z

de Souza, A. R., Zago, M., Eidelman, D. H., Hamid, Q., and Baglole, C. J. (2014). Aryl Hydrocarbon Receptor (AhR) Attenuation of Subchronic Cigarette Smoke-Induced Pulmonary Neutrophilia Is Associated with Retention of Nuclear RelB and Suppression of Intercellular Adhesion Molecule-1 (ICAM-1). *Toxicol. Sci.* 140, 204–223. doi:10.1093/toxsci/kfu068

Do, Y., Mckallip, R. J., Nagarkatti, M., and Nagarkatti, P. S. (2004). Activation through Cannabinoid Receptors 1 and 2 on Dendritic Cells Triggers NF-kappaB-dependent Apoptosis: Novel Role for Endogenous and Exogenous Cannabinoids in Immunoregulation. *J. Immunol.* 173, 2373–2382. doi:10.4049/jimmunol.173.4.2373

Fantauzzi, M. F., Cass, S. P., Mcgrath, J. J. C., Thayaparan, D., Wang, P., Stampfli, M. R., et al. (2021). Development and Validation of a Mouse Model of Contemporary Cannabis Smoke Exposure. *ERJ Open Res.* 7, 00107–02021. doi:10.1183/23120541.00107-2021

Fligiel, S. E., Roth, M. D., Kleerup, E. C., Barsky, S. H., Simmons, M. S., and Tashkin, D. P. (1997). Tracheobronchial Histopathology in Habitual Smokers of Cocaine, Marijuana, And/or Tobacco. *Chest* 112, 319–326. doi:10.1378/chest.112.2.319

Graham, E. S., Angel, C. E., Schwarcz, L. E., Dunbar, P. R., and Glass, M. (2010). Detailed Characterisation of CB2 Receptor Protein Expression in Peripheral

Blood Immune Cells from Healthy Human Volunteers Using Flow Cytometry. *Int. J. Immunopathol. Pharmacol.* 23, 25–34. doi:10.1177/039463201002300103

Graves, B. M., Johnson, T. J., Nishida, R. T., Dias, R. P., Savareear, B., Harynuk, J. J., et al. (2020). Comprehensive Characterization of Mainstream Marijuana and Tobacco Smoke. *Sci. Rep.* 10, 7160. doi:10.1038/s41598-020-63120-6

Guerrina, N., Aloufi, N., Shi, F., Prasade, K., Mehrotra, C., Traboulsi, H., et al. (2021a). The Aryl Hydrocarbon Receptor Reduces LC3II Expression and Controls Endoplasmic Reticulum Stress. *Am. J. Physiol. Lung Cel Mol. Physiol.* 320, L339–L355. doi:10.1152/ajplung.00122.2020

Guerrina, N., Traboulsi, H., Rico De Souza, A., Bossé, Y., Thatcher, T. H., Robichaud, A., et al. (2021b). Aryl Hydrocarbon Receptor Deficiency Causes the Development of Chronic Obstructive Pulmonary Disease through the Integration of Multiple Pathogenic Mechanisms. *FASEB J.* 35, e21376. doi:10.1096/fj.202002350R

Hecht, E., Zago, M., Sarill, M., Rico De Souza, A., Gomez, A., Matthews, J., et al. (2014). Aryl Hydrocarbon Receptor-dependent Regulation of miR-196a Expression Controls Lung Fibroblast Apoptosis but Not Proliferation. *Toxicol. Appl. Pharmacol.* 280, 511–525. doi:10.1016/j.taap.2014.08.023

Helyes, Z., Kemény, Á., Csekő, K., Szőke, É., Elekes, K., Mester, M., et al. (2017). Marijuana Smoke Induces Severe Pulmonary Hyperresponsiveness, Inflammation, and Emphysema in a Predictive Mouse Model Not via CB1 Receptor Activation. *Am. J. Physiol. Lung Cel. Mol. Physiol.* 313, L267–L277. doi:10.1152/ajplung.00354.2016

Henderson, R. L., Tennant, F. S., and Guerry, R. (1972). Respiratory Manifestations of Hashish Smoking. *Arch. Otolaryngol.* 95, 248–251. doi:10.1001/archotol.1972.00770080390012

Henstridge, C. M., Balenga, N. A., Schröder, R., Kargl, J. K., Platzer, W., Martini, L., et al. (2010). GPR55 Ligands Promote Receptor Coupling to Multiple Signalling Pathways. *Br. J. Pharmacol.* 160, 604–614. doi:10.1111/j.1476-5381.2009.00625.x

Hillig, K. W. (2005). Genetic Evidence for Speciation in Cannabis (Cannabaceae). *Genet. Resour. Crop Evol.* 52, 161–180. doi:10.1007/s10722-003-4452-y

Huestis, M. A. (2007). Human Cannabinoid Pharmacokinetics. *Chem. Biodivers* 4, 1770–1804. doi:10.1002/cbdv.200790152

Inoue, A., Raimondi, F., Kadji, F. M. N., Singh, G., Kishi, T., Uwamizu, A., et al. (2019). Illuminating G-Protein-Coupling Selectivity of GPCRs. *Cell* 177, 1933–1947.e25. doi:10.1016/j.cell.2019.04.044

Kawamura, Y., Fukaya, M., Maejima, T., Yoshida, T., Miura, E., Watanabe, M., et al. (2006). The CB1 Cannabinoid Receptor Is the Major Cannabinoid Receptor at Excitatory Presynaptic Sites in the hippocampus and Cerebellum. *J. Neurosci.* 26, 2991–3001. doi:10.1523/JNEUROSCI.4872-05.2006

Kicman, A., Pędzińska-Betiuk, A., and Kozłowska, H. (2021). The Potential of Cannabinoids and Inhibitors of Endocannabinoid Degradation in Respiratory Diseases. *Eur. J. Pharmacol.* 911, 174560. doi:10.1016/j.ejphar.2021.174560

Kim, Y. H., An, Y. J., Jo, S., Lee, S. H., Lee, S. J., Choi, S. J., et al. (2018). Comparison of Volatile Organic Compounds between Cigarette Smoke Condensate (CSC) and Extract (CSE) Samples. *Environ. Health Toxicol.* 33, e2018012–2018010. doi:10.5620/eht.e2018012

Krishna Kumar, K., Shalev-Benami, M., Robertson, M. J., Hu, H., Banister, S. D., Hollingsworth, S. A., et al. (2019). Structure of a Signaling Cannabinoid Receptor 1-G Protein Complex. *Cell* 176, 448–458.e12. doi:10.1016/j.cell.2018.11.040

Li, C. J., Ning, W., Matthay, M. A., Feghali-Bostwick, C. A., and Choi, A. M. (2007). MAPK Pathway Mediates EGR-1-HSP70-dependent Cigarette Smoke-Induced Chemokine Production. *Am. J. Physiol. Lung Cel Mol Physiol.* 292, L1297–L1303. doi:10.1152/ajplung.00194.2006

Li, H., Liu, Y., Tian, D., Tian, L., Ju, X., Qi, L., et al. (2020). Overview of Cannabidiol (CBD) and its Analogues: Structures, Biological Activities, and Neuroprotective Mechanisms in Epilepsy and Alzheimer's Disease. *Eur. J. Med. Chem.* 192, 112163. doi:10.1016/j.ejmech.2020.112163

Maertens, R. M., White, P. A., Rickert, W., Levasseur, G., Douglas, G. R., Bellier, P. V., et al. (2009). The Genotoxicity of Mainstream and Sidestream Marijuana and Tobacco Smoke Condensates. *Chem. Res. Toxicol.* 22, 1406–1414. doi:10.1021/tx9000286

Manolis, T. A., Manolis, A. A., and Manolis, A. S. (2019). Cannabis Associated "High" Cardiovascular Morbidity and Mortality: Marijuana Smoke like Tobacco Smoke? A Déjà Vu/Déjà Vécu Story? *Mrmc* 19, 870–879. doi:10.2174/1389557518666181114113947

Martey, C. A., Pollock, S. J., Turner, C. K., O'reilly, K. M., Baglole, C. J., Phipps, R. P., et al. (2004). Cigarette Smoke Induces Cyclooxygenase-2 and Microsomal Prostaglandin E2 Synthase in Human Lung Fibroblasts: Implications for Lung Inflammation and Cancer. *Am. J. Physiol. Lung Cel Mol Physiol.* 287, L981–L991. doi:10.1152/ajplung.00239.2003

Martey, C. A., Baglole, C. J., Gasiewicz, T. A., Sime, P. J., and Phipps, R. P. (2005). The Aryl Hydrocarbon Receptor Is a Regulator of Cigarette Smoke Induction of the Cyclooxygenase and Prostaglandin Pathways in Human Lung Fibroblasts. *Am. J. Physiol. Lung Cel Mol Physiol.* 289, L391–L399. doi:10.1152/ajplung.00062.2005

Marumo, S., Hoshino, Y., Kiyokawa, H., Tanabe, N., Sato, A., Ogawa, E., et al. (2014). p38 Mitogen-Activated Protein Kinase Determines the Susceptibility to Cigarette Smoke-Induced Emphysema in Mice. *BMC Pulm. Med.* 14, 79. doi:10.1186/1471-2466-14-79

McPartland, J. M., Duncan, M., Di Marzo, V., and Pertwee, R. G. (2015). Are Cannabidiol and Δ(9) -tetrahydrocannabivarin Negative Modulators of the Endocannabinoid System? A Systematic Review. *Br. J. Pharmacol.* 172, 737–753. doi:10.1111/bph.12944

Mersiades, A. J., Tognela, A., Haber, P. S., Stockler, M., Lintzeris, N., Simes, J., et al. (2018). Oral Cannabinoid-Rich THC/CBD Cannabis Extract for Secondary Prevention of Chemotherapy-Induced Nausea and Vomiting: a Study Protocol for a Pilot and Definitive Randomised Double-Blind Placebo-Controlled Trial (CannabisCINV). *BMJ Open* 8, e020745. doi:10.1136/bmjopen-2017-020745

Moir, D., Rickert, W. S., Levasseur, G., Larose, Y., Maertens, R., White, P., et al. (2008). A Comparison of Mainstream and Sidestream Marijuana and Tobacco Cigarette Smoke Produced under Two Machine Smoking Conditions. *Chem. Res. Toxicol.* 21, 494–502. doi:10.1021/tx700275p

Morales, P., Hurst, D. P., and Reggio, P. H. (2017). Molecular Targets of the Phytocannabinoids: A Complex Picture. *Prog. Chem. Org. Nat. Prod.* 103, 103–131. doi:10.1007/978-3-319-45541-9_4

Moretto, N., Bertolini, S., Iadicicco, C., Marchini, G., Kaur, M., Volpi, G., et al. (2012). Cigarette Smoke and its Component Acrolein Augment IL-8/CXCL8 mRNA Stability via P38 MAPK/MK2 Signaling in Human Pulmonary Cells. *Am. J. Physiol. Lung Cel. Mol. Physiol.* 303, L929–L938. doi:10.1152/ajplung.00046.2012

Namkung, Y., Legouill, C., Kumar, S., Cao, Y., Teixeira, L. B., Lukasheva, V., et al. (2018). Functional Selectivity Profiling of the Angiotensin II Type 1 Receptor Using Pathway-wide BRET Signaling Sensors. *Sci. Signal.* 11, eaat1631. doi:10.1126/scisignal.aat1631

Pertwee, R. G. (2010). Receptors and Channels Targeted by Synthetic Cannabinoid Receptor Agonists and Antagonists. *Curr. Med. Chem.* 17, 1360–1381. doi:10.2174/092986710790980050

Rajan, T. S., Giacoppo, S., Iori, R., De Nicola, G. R., Grassi, G., Pollastro, F., et al. (2016). Anti-inflammatory and Antioxidant Effects of a Combination of Cannabidiol and Moringin in LPS-Stimulated Macrophages. *Fitoterapia* 112, 104–115. doi:10.1016/j.fitote.2016.05.008

Rana, A. C. N. (2010). Floral Biology and Pollination Biology of Cannabis Sativa L. *Int. J. Plant Reprod. Biol.* 2, 191–195.

Reggio, P. H. (2010). Endocannabinoid Binding to the Cannabinoid Receptors: what Is Known and what Remains Unknown. *Curr. Med. Chem.* 17, 1468–1486. doi:10.2174/092986710790980005

Rico de Souza, A., Traboulsi, H., Wang, X., Fritz, J. H., Eidelman, D. H., and Baglole, C. J. (2021). The Aryl Hydrocarbon Receptor Attenuates Acute Cigarette Smoke-Induced Airway Neutrophilia Independent of the Dioxin Response Element. *Front. Immunol.* 12, 630427. doi:10.3389/fimmu.2021.630427

Roth, M. D., Arora, A., Barsky, S. H., Kleerup, E. C., Simmons, M., and Tashkin, D. P. (1998). Airway Inflammation in Young Marijuana and Tobacco Smokers. *Am. J. Respir. Crit. Care Med.* 157, 928–937. doi:10.1164/ajrccm.157.3.9701026

Rozanc, J., Kotnik, P., Milojevic, M., Gradisnik, L., Knez Hrncic, M., Knez, Z., et al. (2021). Different Cannabis Sativa Extraction Methods Result in Different

Biological Activities against a Colon Cancer Cell Line and Healthy Colon Cells. *Plants (Basel)* 10, 566. doi:10.3390/plants10030566

Ryberg, E., Larsson, N., Sjögren, S., Hjorth, S., Hermansson, N. O., Leonova, J., et al. (2007). The Orphan Receptor GPR55 Is a Novel Cannabinoid Receptor. *Br. J. Pharmacol.* 152, 1092–1101. doi:10.1038/sj.bjp.0707460

Schuermeyer, J., Salomonsen-Sautel, S., Price, R. K., Balan, S., Thurstone, C., Min, S. J., et al. (2014). Temporal Trends in Marijuana Attitudes, Availability and Use in Colorado Compared to Non-medical Marijuana States: 2003-11. *Drug Alcohol Depend* 140, 145–155. doi:10.1016/j.drugalcdep.2014.04.016

Sharir, H., and Abood, M. E. (2010). Pharmacological Characterization of GPR55, a Putative Cannabinoid Receptor. *Pharmacol. Ther.* 126, 301–313. doi:10.1016/j.pharmthera.2010.02.004

Sim-Selley, L. J. (2003). Regulation of Cannabinoid CB1 Receptors in the central Nervous System by Chronic Cannabinoids. *Crit. Rev. Neurobiol.* 15, 91–119. doi:10.1615/critrevneurobiol.v15.i2.10

Sinclair, C. F., Foushee, H. R., Scarinci, I., and Carroll, W. R. (2013). Perceptions of Harm to Health from Cigarettes, Blunts, and Marijuana Among Young Adult African American Men. *J. Health Care Poor Underserved* 24, 1266–1275. doi:10.1353/hpu.2013.0126

Strzelak, A., Ratajczak, A., Adamiec, A., and Feleszko, W. (2018). Tobacco Smoke Induces and Alters Immune Responses in the Lung Triggering Inflammation, Allergy, Asthma and Other Lung Diseases: A Mechanistic Review. *Int. J. Environ. Res. Public Health* 15, 1033. doi:10.3390/ijerph15051033

Tahir, M. N., Shahbazi, F., Rondeau-Gagné, S., and Trant, J. F. (2021). The Biosynthesis of the Cannabinoids. *J. Cannabis Res.* 3, 7. doi:10.1186/s42238-021-00062-4

Tashkin, D. P. (2013). Effects of Marijuana Smoking on the Lung. *Ann. Am. Thorac. Soc.* 10, 239–247. doi:10.1513/AnnalsATS.201212-127FR

Taylor, M., Santopietro, S., Baxter, A., East, N., Breheny, D., Thorne, D., et al. (2020). *In Vitro* biological Assessment of the Stability of Cigarette Smoke Aqueous Aerosol Extracts. *BMC Res. Notes* 13, 492. doi:10.1186/s13104-020-05337-2

Turcotte, C., Blanchet, M. R., Laviolette, M., and Flamand, N. (2016). The CB2 Receptor and its Role as a Regulator of Inflammation. *Cell Mol Life Sci* 73, 4449–4470. doi:10.1007/s00018-016-2300-4

Urban, T., and Hureaux, J. (2017). Cannabis et poumon. Ce que l'on sait et tout ce que l'on ne sait pas. *Rev. Pneumol Clin.* 73, 283–289. doi:10.1016/j.pneumo.2017.08.013

White, E. S. (2015). Lung Extracellular Matrix and Fibroblast Function. *Ann. Am. Thorac. Soc.* 12 Suppl 1 (Suppl. 1), S30–S33. doi:10.1513/AnnalsATS.201406-240MG

Yayan, J., and Rasche, K. (2016). Damaging Effects of Cannabis Use on the Lungs. *Adv. Exp. Med. Biol.* 952, 31–34. doi:10.1007/5584_2016_71

Zago, M., Sheridan, J. A., Nair, P., Rico De Souza, A., Gallouzi, I. E., Rousseau, S., et al. (2013). Aryl Hydrocarbon Receptor-dependent Retention of Nuclear HuR Suppresses Cigarette Smoke-Induced Cyclooxygenase-2 Expression Independent of DNA-Binding. *PLoS One* 8, e74953. doi:10.1371/journal.pone.0074953

Zago, M., Rico De Souza, A., Hecht, E., Rousseau, S., Hamid, Q., Eidelman, D. H., et al. (2014). The NF-κB Family Member RelB Regulates microRNA miR-146a to Suppress Cigarette Smoke-Induced COX-2 Protein Expression in Lung Fibroblasts. *Toxicol. Lett.* 226, 107–116. doi:10.1016/j.toxlet.2014.01.020

Conflict of Interest: The Rho BRET biosensor has been licensed to Domain Therapeutics for commercialization. It can be obtained for academic research with a standard academic material transfer agreement (MTA) from SL.

The remaining authors declare that the research was conducted in the absence of any commercial or financial relationships that could be construed as a potential conflict of interest.

Publisher's Note: All claims expressed in this article are solely those of the authors and do not necessarily represent those of their affiliated organizations, or those of the publisher, the editors and the reviewers. Any product that may be evaluated in this article, or claim that may be made by its manufacturer, is not guaranteed or endorsed by the publisher.

frontiers | Frontiers in Pharmacology

ORIGINAL RESEARCH
published: 14 June 2022
doi: 10.3389/fphar.2022.794952

Midkine-Notch2 Pathway Mediates Excessive Proliferation of Airway Smooth Muscle Cells in Chronic Obstructive Lung Disease

Tang Deng[1,2], Qifeng Huang[1], Kaiwen Lin[3], Jin Qian[1,2], Qi Li[2], Lihua Li[2], Shuangqin Xu[2], Hongfang Yun[2], Hangfei Wang[2], Xinxin Wu[2], Heng Liu[1,2], Guiyun Jin[1]* and Xiaoran Liu[1,2]**

[1]Department of Interventional radiology and vascular surgery, The First Affiliated Hospital of Hainan Medical University, Hainan Medical University, Haikou, China, [2]Key Laboratory of Emergency and Trauma of Hainan Medical University, Ministry of Education, Key Laboratory of Hainan Trauma and Disaster Rescue, Hainan Medical University, Haikou, China, [3]Hainan Women and Children's Medical Center, Haikou, China

OPEN ACCESS

Edited by:
Hideyuki Takeuchi,
University of Shizuoka, Japan

Reviewed by:
Yongchun Shen,
Sichuan University, China
Antonio Recchiuti,
University of Studies G. d'Annunzio Chieti and Pescara, Italy

***Correspondence:**
Heng Liu
liuheng11b@hubu.edu.cn
Guiyun Jin
13976609625@163.com
Xiaoran Liu
liuxiaoran3192@163.com

Specialty section:
This article was submitted to Respiratory Pharmacology, a section of the journal Frontiers in Pharmacology

Received: 14 October 2021
Accepted: 24 May 2022
Published: 14 June 2022

Citation:
Deng T, Huang Q, Lin K, Qian J, Li Q, Li L, Xu S, Yun H, Wang H, Wu X, Liu H, Jin G and Liu X (2022) Midkine-Notch2 Pathway Mediates Excessive Proliferation of Airway Smooth Muscle Cells in Chronic Obstructive Lung Disease. Front. Pharmacol. 13:794952. doi: 10.3389/fphar.2022.794952

Inflammation-induced proliferation of airway smooth muscle cells (ASMCs) and subsequent airway remodeling is a hallmark of chronic obstructive lung disease (COPD). The role of midkine (MK) in COPD is unclear. In this work, we explored the role of MK-Notch2 signaling in COPD by inhibiting the expression of MK using lentivirus shRNA in ASMCs *in vitro* and instillation of AAV9-MK in the airway of a COPD rat model *in vivo*. The results demonstrated that LPS decreased ASMC migration and proliferation, increased apoptosis and induced the expression of MK and Notch2 signaling molecules. Inhibition of MK exacerbated the changes in migration and proliferation but decreased the expression of MK and Notch2 signaling molecules. Rats treated with smoke fumigation and LPS showed features of COPD. The small airways of COPD rats were remodeled and lung function was significantly reduced. The expressions of TGF-β, ICAM-1, HA, MMP-9, PC-III, and LN in BALF and the expression of MK and Notch2 signaling molecules were significantly increased in the COPD rats compared with controls. Inhibition of MK reversed these changes. In conclusion, the MK-Notch2 pathway plays a key role in airway remodeling induced by ASMC proliferation. Targeting the MK-Notch2 pathway may be a new strategy for improving airway remodeling and preventing progressive decline of pulmonary function in COPD.

Keywords: Midkine-Notch2 pathway, inflammation, chronic obstructive lung disease, ASMC proliferation, airway remodeling

INTRODUCTION

Chronic obstructive pulmonary disease (COPD) is the third leading cause of death in the world, following myocardial infarction and stroke. With the increase in the number of smokers and the aggravation of air pollution, the incidence of COPD is predicted to continue to rise. The estimated annual death toll from COPD in 2050 is approximated at close to 6 million. At present, the number of COPD patients in China has exceeded 100 million, with a male to female ratio of approximately 2:1. The incidence rate among individuals over 60 years old is 27% (Spero et al., 2017; Disease, 2018) COPD is not only detrimental to the health, quality of life and longevity of the individual, but also poses a heavy burden on the family and society (Iheanacho et al., 2020)

Cigarette smoking is the primary cause of COPD. Harmful particles in smoke directly damage bronchial mucosa, cause chronic inflammation in the small airways and stimulate airway smooth muscle cell (ASMC) proliferation, leading to smooth muscle hypertrophy. Chronic inflammation weakens the immune defense of the respiratory system (Ritchie and Wedzicha, 2020). Macrophages that are recruited to the sites of inflammation release proteases that break down the airway epithelial basement membrane. Decomposition of extracellular matrix produces hyaluronic acid (HA), laminin (LN) and type III procollagen (PC-III), which are deposited in the airway to cause airway remodeling. Together, these processes lead to non-reversible airway remodeling and COPD (Hatipoğlu, 2018). Together, airway remodeling is a complex pathological process that consists of multiple factors and components interacting to cause structural changes in the airway resulting in progressive worsening of airflow limitation. Current treatment of airway remodeling is mostly centered on the release of airway smooth muscle spasm, airway dilation, anti-infection, and anti-inflammation. Overproliferation of ASMCs is also an important cause of airway remodeling, and targeted therapy for airway smooth muscle cell proliferation has rarely been reported (Chan et al., 2019).

Midkine (MK) is a novel heparin-binding growth factor discovered by Japanese researchers in the late 1980s (Kadomatsu et al., 1988). MK is a pleiotropic molecule that is involved in functions such as chemotaxis, mitosis, anti-apoptosis activity and carcinogenesis (Muramatsu, 2014; Sato and Sato, 2014). MK is highly expressed in many malignant tumors, including pancreatic cancer and neuroblastoma. Notch2 is one of the receptors for MK in humans (Kosugi et al., 2007). MK activates the Notch2 signaling pathway, up-regulates the downstream target HES1 and promotes tumor cell proliferation while inhibiting tumor cell apoptosis (Kishida et al., 2013) Notch signaling has been found to be upregulated in pulmonary fibrosis, and inhibition of Notch significantly alleviated pulmonary fibrosis. Our preliminary results showed that MK was highly expressed in a rat model of COPD. We speculate that the MK-Notch2 signaling pathway may promote inflammation and excessive proliferation of ASMCs, resulting in airway stenosis and the progressive decline of pulmonary function in patients with COPD. In this work, the role of MK-Notch2 signaling in COPD was explored by inhibiting the expression of MK using lentivirus shRNA in ASMCs *in vitro* and instillation of AAV9-MK in the airway of a COPD rat model *in vivo*. The study aims to provide new ideas for therapeutic strategies that have the potential of slowing down the progressive decline of pulmonary function in patients with COPD.

MATERIALS AND METHODS

Cell Culture

Rat ASMCs (Shanghai Qingqi, China) were cultured, passaged and cryopreserved in a complete high-glucose medium supplemented with 10% fetal bovine serum (FBS) (BI, Israel). Cell experiments were conducted in a high-glucose medium supplemented with 3% FBS. In experiments, the ASMCs were divided into the following six groups: control, non-target shRNA, shRNA 413, control+LPS, non-target+LPS and shRNA 413+LPS. Lentivirus shRNA used to inhibit the expression of MK were designed and purchased from Jikai Gene, Shanghai, China. Successful transfection was observed under fluorescence microscope and verified by western blot and qPCR methods.

Animal Model

Adult male SD rats, weighing 160 ± 10 g, were purchased from Tianqin, Hunan, China and housed in the Drug Safety Evaluation Center of Hainan Medical College. All animal experiments were carried out in accordance with the recommendations of the International guidelines for the care and use of laboratory animals. The experimental protocols were approved by the Animal Ethics Committee of Hainan Medical College. Rat model of COPD was established by exposure to LPS combined with smoking. LPS (200 μL) was instilled via tracheal intubation 10 min after anesthesia with sodium pentobarbital (40 μg/g) injected intraperitoneally. LPS was instilled at day 1, 10, 25, 40, 55, 70, and 85. Rats were exposed to cigarette smoke for 40–45 min each time via a homemade smoking box once in the morning and once in the evening for 100 days. The cigarette used for smoking had a nicotine content of 1.2 mg and tar content of 13 mg per cigarette. A total of 24 rats were divided into 4 groups with 6 rats in each group: control, COPD, COPD+AAV9-non-target and COPD+AAV9-MK. The control group received 300 μL of normal saline (NS) per rat. The COPD group was exposed to combined smoke fumigation and instillation of LPS for 100 days. The COPD group received 300 μL of normal saline (NS) per rat. The COPD + AAV9-non-target rats were instilled with 1.5×10^{11} vg/300 μL AAV9-non-target per rat. The COPD + AAV9-MK rats were instilled with 1.5×10^{11} vg/300 μL AAV9-MK per rat. The rats were sacrificed 21 days after AAV9 instillation. AAV9 were designed and purchased from Jikai Gene, Shanghai, China **Table 1**.

Migration Assay

ASMCs were seeded in a 6-well plate, and the scratch test was performed by scratching the cell monolayer with a 200 μL pipette tip. Cell migration before and after treatment with 300 μg/ml LPS was observed under a light microscope. Images were taken at 0, 24, 48 and 72 h. The rates at which cells repopulate were analyzed by ImageJ software.

Cell Proliferation and Apoptosis Assays

ASMCs were seeded in a 96-well plate and CCK-8 reagent (Dojindo, Japan) was added. They assay was performed according to the manufacturer's instructions. The cell proliferation rate was calculated based on OD values. ASMCs were seeded in a 6-well plate and apoptosis was detected with an apoptosis detection kit (Shanghai Yisheng, China). The ASMCs were digested by EDTA-free trypsin and centrifuged. The supernatant was discarded. The cells were diluted to 3×10^6 cells/ml. Six replicate tubes were divided into 6 groups. For each

TABLE 1 | Gene sequence of AAV9-MK-shRNA.

NO.	5′	STEM	Loop	STEM	3′
Midkine-shRNA (413)-a	ACCGG	CTGAAGAAGGCTCGGTACAAT	TTCAAGAGA	ATTGTACCGAGCCTTCTTCAG	TTTTT
Midkine-shRNA (413)-b	TCTAAAAAA	CTGAAGAAGGCTCGGTACAAT	TCTCTTGAA	ATTGTACCGAGCCTTCTTCAG	C

TABLE 2 | Primer sequences.

Name primer sequence length		
ACTIN	F:GCCTTCCTTCCTGGGTATGG R:TCCGATTCAACTCATACTGC	186 bp
Midkine	F:TTGCTACACCTAGTACCCAAAG R:CTCGATAACAGGTATCAGGGTG	169 bp
HES1	F:GTAGGGGTCAGTGGCTTAGC R:GAGGGTGGGGTAGGCTAAGA	106 bp
Notch2	F:TGCGAGACCAACATCAACGAGTG R:TCAGGCAGAAGCAGAGGTAGGC	128 bp

group, 100 μL of cell solution was added. The cells were centrifuged, and supernatant was discarded, 100 μL of Binding Buffer was added, 5 μL of Annexin V-FITC, 10 μL of PI Staining Solution, and then 400 μL of 1 × Binding Buffer was added. The solution was thoroughly mixed and FACS was used to detect the apoptosis rate of each group.

Pulmonary Function Test

The rats were anesthetized by intraperitoneal injection of sodium pentobarbital (40 μg/g), tracheostomized and connected to a lung function instrument (Shanghai Tawang, China). The FEV mode was used to measure 0.3s FEV/FVC and maximal mid-expiratory flow (MMEF).

ELISA

ELISA kits (Qingdao Baizhou, China) were used to quantify the levels of MK-Notch2 signaling molecules *in vitro*. Intracellular molecules were released from the cells by repeated freeze and thaw cycles. The cells were centrifuged and the supernatant was collected for quantification of MK, HES1, and Notch2 using ELISA. ELISA kits were also used to quantify the levels of inflammatory mediators transforming growth factor-β (TGF-β), intercellular adhesion molecule 1 (ICAM-1), HA, matrix metalloproteinase-9 (MMP-9), PC-III and LN in the bronchoalveolar lavage (BALF) of rats. Experiments and standard curves were performed according to the manufacturer's instructions.

qPCR

The mRNA levels of MK-Notch2 signaling molecules MK, Notch2 and HES1 were semi-quantified with qPCR. RNA extraction, reverse transcription and fluorescence quantification were carried out with kits purchased from Yisheng, Shanghai, China. Primers were designed by Shanghai Shenggong, China; the primer sequences are listed in **Table 2**. The PCR amplification program consisted of 40 cycles. Actin mRNA was used for the normalization of gene expression.

Hematoxylin and Eosin staining

Lung tissue from rats were fixed with 4% formaldehyde, dehydrated and embedded in paraffin. The paraffin blocks were sectioned into thin slices and stained with H&E (Biosharp, China) after deparaffination and rehydration.

Immunofluorescence

Cryosectioned lung tissue was immersed in 4°C acetone and washed with PBS, and the cell membranes were permeabilized with 0.3% Triton X-100 (Biosharp, China). The slides were incubated with antibody against green florescent protein (GFP, 1:500, Abcam, UK) under room temperature and washed with PBS. The cell nuclei were visualized with DAPI (1:2000, Abcam, United Kingdom).

Western Blot

Protein extraction was performed using RIPA lysis buffer (Wuhan Boster, China). Protein samples were separated by electrophoresis and transferred to polyvinylidene difluoride (PVDF) membranes. The membrane was blocked with 5% skimmed milk for 90 min at room temperature. The PVDF membrane was incubated with the primary antibody at 4 °C overnight on a shaker. The membrane was then incubated with secondary antibody at room temperature for 1 h. The membrane was placed into a chemiluminescence machine to visualize the protein bands after washing. ImageJ software was used to analyze band densities. Tubulin was used as a loading control. All antibodies were purchased from Abcam, UK; the antibody dilutions used were as follows: MK 1:1000; Notch2, 1:1000; HES1, 1:500.

Immunohistochemistry

Lung tissue slices were deparaffinized and washed with PBS, immersed in citric acid for antigen retrieval and incubated with 3% H_2O_2. The slices were washed with PBS and blocked with 4% sheep serum before incubation with the primary antibody (same concentrations as for western blot) under room temperature. The slides were stained with DAB, counterstained with hematoxylin and dehydrated with increasing concentrations of alcohol and xylene before sealing.

Data and Statistical Analysis

Results are expressed as mean ± standard deviation (x ± SD). Sample means were compared pairwise using one-way ANOVA. $p < 0.05$ was considered statistically significant. All statistical analysis was carried out by Graphpad software.

RESULTS

IC_{50} of LPS in ASMCs and the Efficacy of Different Lentivirus shRNAs in Silencing MK

The injury of ASCMs was first induced with LPS and the IC_{50} value of LPS was determined. ASMCs were stimulated with increasing

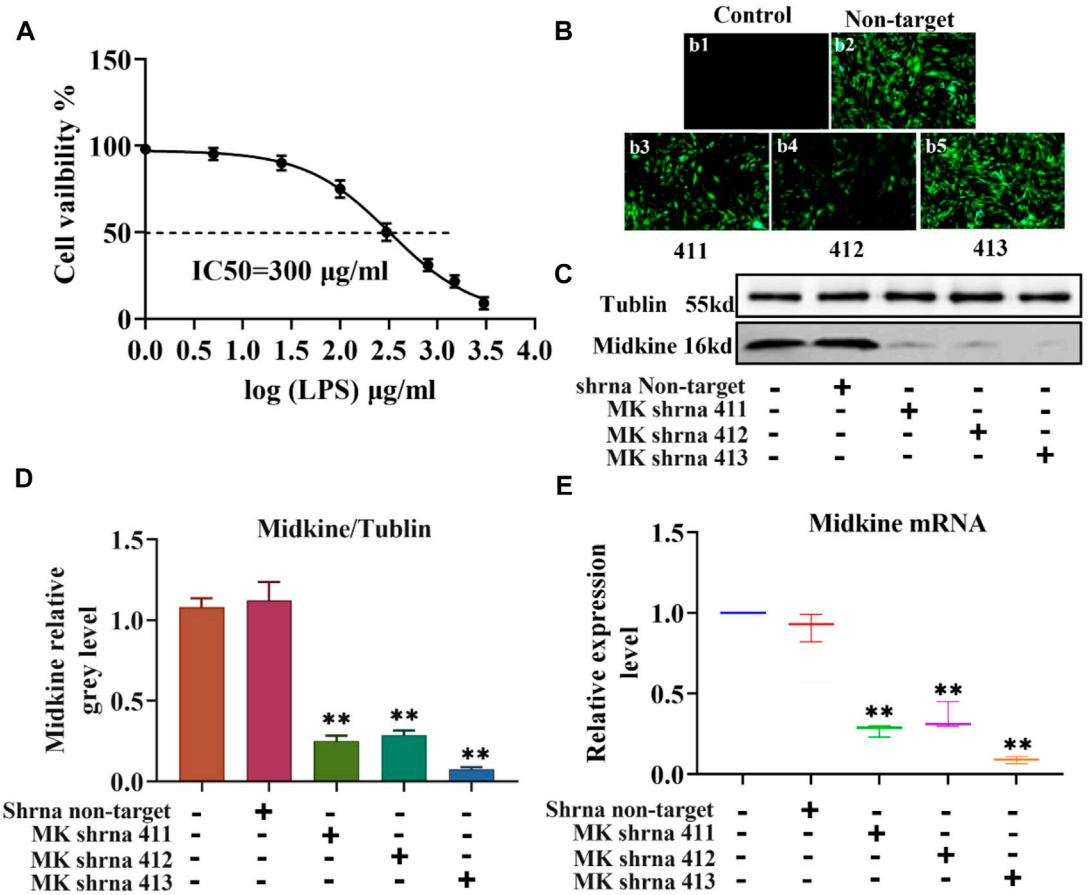

FIGURE 1 | IC_{50} of LPS in ASMCs by LPS and the efficacy of different lentivirus shRNAs in silencing MK. **(A)** Dose-response curves for determining the IC_{50} of LPS in ASMCs. $n = 5$, x±SD. **(B)** The expression of different lentivirus in ASMCs (200x). **(C)** Western blot analysis of ASMCs transfected with the indicated lentivirus. **(D)** Quantification of the MK protein content relative to the tubulin loading control. **(E)** qPCR was performed on ASMCs transfected with the indicated lentivirus; the relative MK mRNA expression levels normalized to the control group are shown. * $p < 0.05$ and ** $p < 0.01$ compared with the control group.

concentrations of LPS (1 μg/ml, 5 μg/ml, 25 μg/ml, 100 μg/ml, 300 μg/ml, 800 μg/ml, 1500 μg/ml and 3000 μg/ml) and the effect of LPS on proliferation was detected using the CCK-8 kit. The results showed that increased concentration of LPS caused decreased cell viability and that the cell viability was close to zero at the highest LPS dose (3000 μg/ml) (**Figure 1A**). The IC_{50}, i.e. the concentration of LPS that inhibits ASMC activity by 50%, was found to be 300 μg/ml. Then, we transfected ASCMs with different lentivirus shRNAs targeting MK and examined the expression of GFP under a fluorescence microscope at 72 h after transfection. There was no expression of GFP in the control group and strong fluorescence expression in the non-target group. Among the different shRNAs targeting MK, shRNA 411, shRNA 412 and shRNA 413 all resulted in different florescence intensities, and shRNA 413 displayed the strongest fluorescence signal (**Figure 1B**). We also performed western blot analysis on ASMCs transfected with lentivirus shRNAs. The expression level of MK mRNA was also quantified with qPCR. While there was no significant difference in MK protein (**Figures 1C,D**) or mRNA expression level (**Figure 1E**) between the non-target shRNA group and the control group, MK protein and mRNA expression levels in the shRNA 411, 412 and 413 groups were all significantly lower than that in the control group. MK levels were the lowest in the shRNA 413 group; the inhibition rate of MK protein was 91 and 93% for MK mRNA.

Cell Migration, Proliferation and Apoptosis of ASMCs Before and After LPS Treatment and Inhibition of MK Expression

Next, we used scratch assay, flow cytometry and CCK-8 to explore the effect of MK on the migration, apoptosis and proliferation of ASMCs. As illustrated in **Figure 2A**, the results of the scratch test showed that there was no significant difference in the scratch healing rate between the non-target shRNA and control groups. The scratch healing rate of the shRNA 413 group (91.66%) was not significantly different from that of control group (91.33%) (**Figure 2B**). The scratch healing rate of control + LPS group (42%) was not significantly different from non-target + LPS group (41.33%), but the rate was significantly lower than that of the control group. The scratch

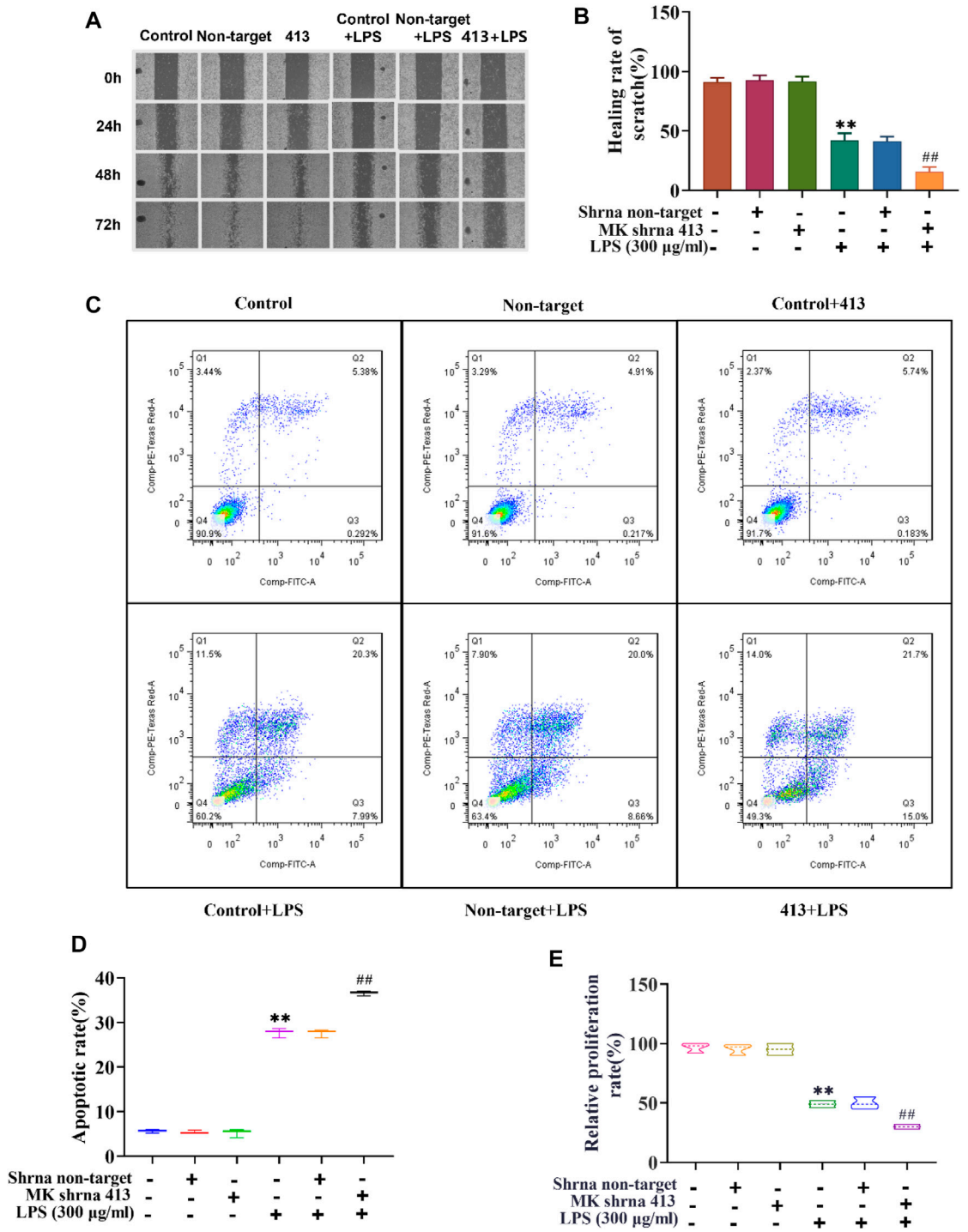

FIGURE 2 | Cell migration, proliferation and apoptosis of ASMCs before and after LPS treatment and inhibition of MK expression. **(A)** Images taken at 0, 24, 48 and 72 h after the cell scratch. **(B)** The scratch healing rate of each group was calculated by ImageJ software after 72 h. **(C)** Flow cytometry analysis of cells in each group. **(D)** The apoptosis rate of each group was determined. **(E)** The cell proliferation rate was detected by CCK-8 assay. $n = 3$, x±3. * $p < 0.05$, ** $p < 0.01$ compared with the control group. # $p < 0.05$, ## $p < 0.01$ compared with control+LPS.

healing rate of the shRNA 413+LPS group (15.66%) was significantly lower than that of the control + LPS group. The apoptosis rate of cells in each group was detected by flow cytometry after 72 h of treatment. The results showed that there was no significant change in apoptosis rate between the non-target (5.13%), control (5.67%) and shRNA 413 groups

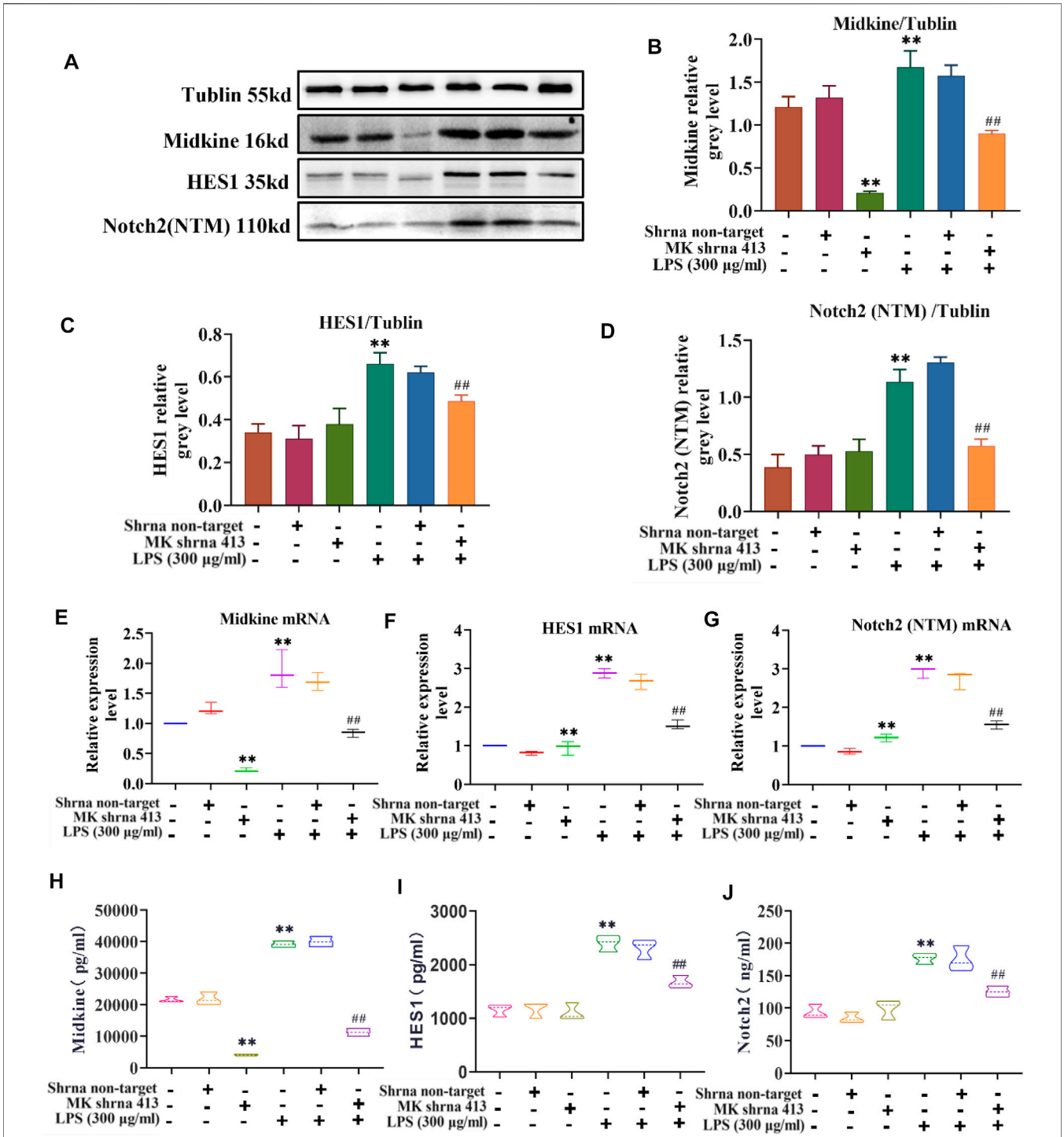

FIGURE 3 | Characterization of the MK-Notch2 signaling pathway *in vitro*. **(A)** Western blot analysis. **(B)** Quantification of MK levels normalized to tubulin. **(C)** Quantification of HES1 levels normalized to tubulin. **(D)** Quantification of Notch2 levels normalized to tubulin. **(E)** The relative expression of MK mRNA. **(F)** The relative expression of HES1 mRNA. **(G)** The relative expression of Notch2 mRNA. **(H)** MK concentration detected by ELISA. **(I)** HES1 concentration detected by ELISA. **(J)** Notch2 concentration detected by ELISA.

(5.92%) (**Figures 2C,D**). The apoptosis rate in the control + LPS group (28.66%) was significantly higher than that in the control group (5.67%). There was no significant difference in the apoptosis rate between the non-target + LPS (28.29%) and control + LPS groups (28.66%). The apoptosis rate in the shRNA 413+LPS group (36.7%) was significantly higher than

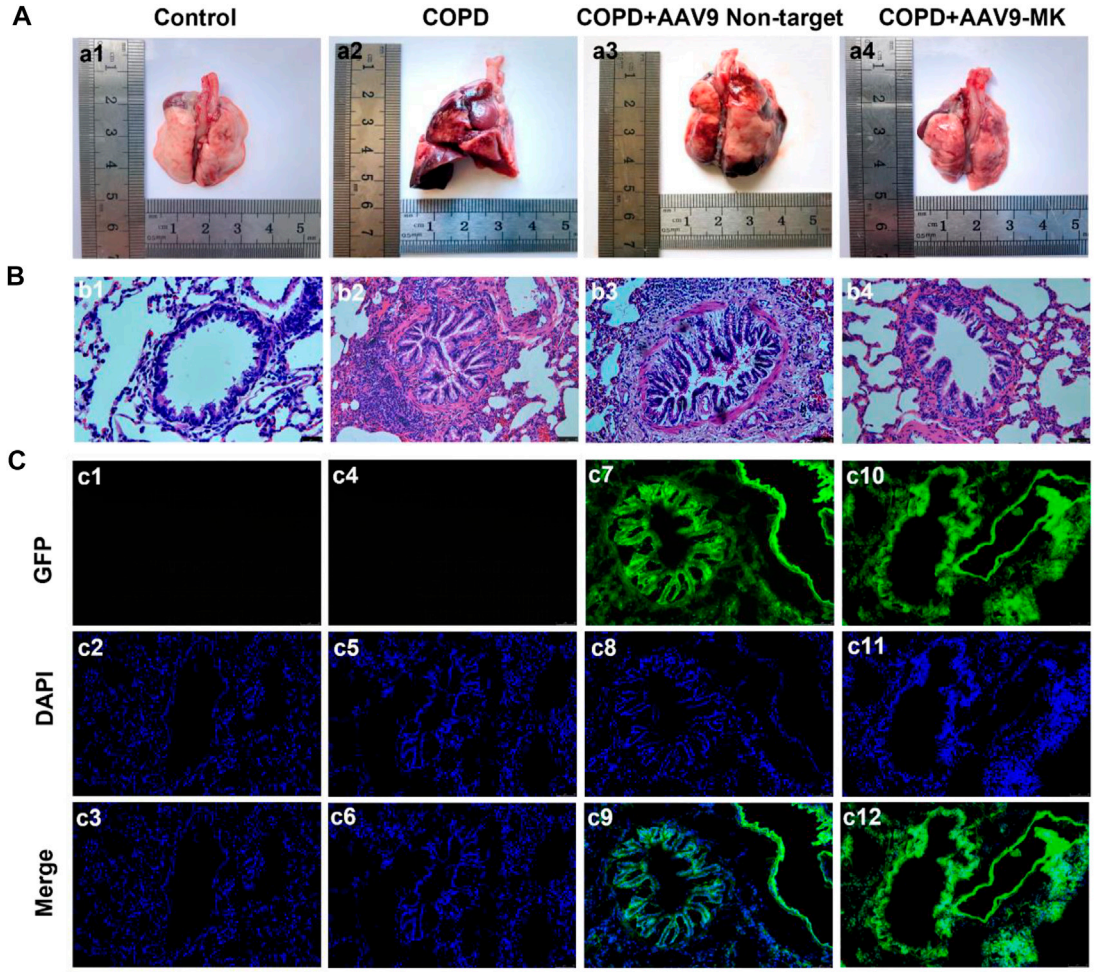

FIGURE 4 | Morphology of lungs of COPD rats with or without inhibition of MK expression and the expression of GFP. **(A1–A4)** Representative photos of lung tissue. **(B1–B4)** H&E staining of lung tissue. **(C1–C12)** Fluorescence microscopy photos under GFP, DAPI and merge (synthesis) mode. Note: GFP expression is green, DAPI is blue (200x).

that in the control + LPS group (28.66%). The proliferation rate of cells in each group was detected by CCK-8 assays after 72 h of treatment. The results showed that the proliferation rate of the non-target group (96.67%) and shRNA 413 group (95%) were not significantly different from that of the control group (95.33%) (**Figure 2E**). The proliferation rate of the control + LPS group (49%) was significantly lower than that of the control group. The proliferation rate of the non-target + LPS group (49.67%) was not significantly different from that of the control + LPS group. The proliferation rate of the shRNA 413+LPS group (30%) was significantly lower than that of the control + LPS group.

Characterization of the MK-Notch2 Signaling Pathway *in vitro*

The relationship between MK and Notch2 signaling pathway in the injury of ASMCs was investigated. As depicted in **Figure 3**, western blot analysis of MK protein, ELISA of MK in cell supernatants and qPCR of MK mRNA expression showed that there was no significant difference in MK protein and mRNA expression between the non-target group and control group. MK was significantly lower in the shRNA 413 group and significantly higher in the control + LPS compared with the control group. MK in the non-target + LPS group was not significantly different from that of the control + LPS group, but MK in the shRNA 413+LPS group was significantly lower than that of the control + LPS group (**Figures 3A,B,E,H**). ELISA of MK from the supernatant of cells showed a similar trend as the qPCR results (**Figure 3H**). The protein and mRNA expression patterns of HES1 and Notch2 were similar. There was no significant difference in HES1 and Notch2 expression between the non-target, shRNA 413 and control groups. HES1 and Notch2 were significantly higher in the control + LPS group than in the control group. HES1 and Notch2 were not significantly different in non-target + LPS group

compared with the control + LPS group. Both HES1 and Notch2 expressions in the shRNA 413+LPS group were significantly lower than those in the control + LPS group (**Figures 3C,D,F,G**). The expressions of HES1 and Notch2 were also detected in the supernatant by ELISA after repeated freeze-thawing and centrifugation (**Figures 3I,J**). The trend of HES1 and Notch2 expression was the same as that observed in qPCR.

Inhibition of MK Expression in COPD Rats Alleviated COPD-Induced Morphological Changes in the Lungs

It was well known that inhibiting the proliferation of ASMCs could improve airway remodeling. Therefore, we would observe the changes in rat lung tissue and airway remodeling by inhibiting the expression of MK in COPD rat model. As shown in **Figure 4a1**, the surface of the lungs from rats in the control group was smooth, pinkish and without edema or nodule. Lungs of rats from the COPD and COPD + AAV9-non-target groups showed clear signs of inflammation and edema, with rough surface and congestion (**Figures 4a2,a3**). The signs of inflammation and edema were alleviated in the COPD + AAV9-MK group (**Figure 4a4**). H&E staining of lung tissue showed that the control group had no inflammatory cell infiltration. The small airway smooth muscle layer and lumen size were normal (**Figure 4b1**). The COPD and COPD + AAV9-non-target groups showed significantly increased small airway smooth muscle cells, airway muscle layer thickening, lumen deformation, stenosis, remodeling and peripheral inflammatory cell infiltration (**Figures 4b2,b3**). In the COPD + AAV9-MK group, the infiltration of inflammatory cells around the small airway was significantly reduced, the small airway smooth muscle cells decreased, the airway muscle layer became thinner, the lumen widened and the airway remodeling improved compared with the COPD + AAV9-non-target group (**Figure 4b4**). Cryosectioned lung tissue showed that the smooth muscle layer and lumen of the small airway in the control group were normal under DAPI mode and no green fluorescence was seen under GFP mode (**Figures 4c1–c3**). In the COPD group, the lumen was deformed, narrowed and remodeled under DAPI mode and no green fluorescence was seen under GFP mode (**Figures 4c4–c6**). In the COPD + AAV9-non-target group, the small airway lumen was deformed and narrowed, and the degree of remodeling was similar to that in COPD group under DAPI mode; green fluorescence was observed under GFP mode (**Figures 4c7–c9**). In the COPD + AAV9-MK group, the airway remodeling was improved and the lumen of small airway was widened; green fluorescence was observed under GFP mode (**Figures 4c10–c12**).

Inhibition of MK Expression in COPD Rats Improves Lung Function and Decreases Inflammatory Mediators in BALF

In COPD rats, the relationship between MK expression, inflammatory mediators in BALF and lung function was further explored. As illustrated in **Figures 5A,B**, the pulmonary function parameters 0.3sFEV/FVC and MMEF were measured using the FEV mode. The results showed that 0.3sFEV/FVC and MMEF in the COPD group were significantly lower than those in control group. There was no significant difference in 0.3sFEV/FVC between the COPD + AAV9-non-target group and COPD group. The COPD + AAV9-MK group had significantly improved 0.3sFEV/FVC and MMEF compared with the COPD group. The levels of TGF-β, ICAM-1, HA, MMP-9, PC-III, and LN were measured in BALF by ELISA (**Figures 5C–H**). The results showed that levels of TGF-β, ICAM-1, HA, MMP-9, PC-III and LN were significantly higher in the COPD group than the control group. These inflammatory mediators were not significantly different between the COPD + AAV9-non-target and COPD group, but were significantly lower in the COPD + AAV9-MK group compared with the COPD group.

Characterization of the MK-Notch2 Signaling Pathway *in vivo*

As depicted in **Figure 6A**, IHC of lung tissue showed that the expression of MK, HES1 and Notch2 was increased in COPD group compared with control. There was no significant difference in MK, HES1 and Notch2 expression between the COPD + AAV9-non-target and COPD group. The expression of MK, HES1 and Notch2 was significantly lower in the COPD + AAV9-MK group than that in the COPD group. A similar expression pattern was seen in the western blot analysis of protein extracted from lung tissue as well as the mRNA expressions of these signaling molecules by qPCR (**Figures 6B–H**).

DISCUSSION

MK is highly expressed in a variety of inflammatory diseases such as rheumatoid arthritis and Crohn's disease (Shindo et al., 2017). MK is chemotactic and promotes the accumulation and infiltration of inflammatory mediators (Inoh et al., 2004; Zhang et al., 2015). MK also stimulates the release of macrophage inflammatory protein (MIP-2), which attracts and recruits macrophages and neutrophils. In the airway, MK-stimulated neutrophil recruitment aggravates the inflammatory response (Sato et al., 2002; Weckbach et al., 2014). Cigarette smoking is the most important risk factor for COPD. Harmful substances in smoke cause ASMC injury and stimulate the repair process, which lead to excessive proliferation of ASMCs. ASMC proliferation is closely related to the occurrence of COPD.

In our study, we induced injury of ASMCs with LPS and investigated the role of MK on proliferation, migration and apoptosis of injured ASMCs by inhibiting MK expression in ASMCs by lentiviral shRNA. Our results showed that inhibition of MK did not cause any changes in cell migration, proliferation and apoptosis in ASMCs that were not treated with LPS. Some studies have shown that the expression of MK is high in the embryo and decreases after birth, and the expression of MK in the kidney, small intestinal epithelium and other parts of the body is very low in healthy adult animals (Kadomatsu and Muramatsu,

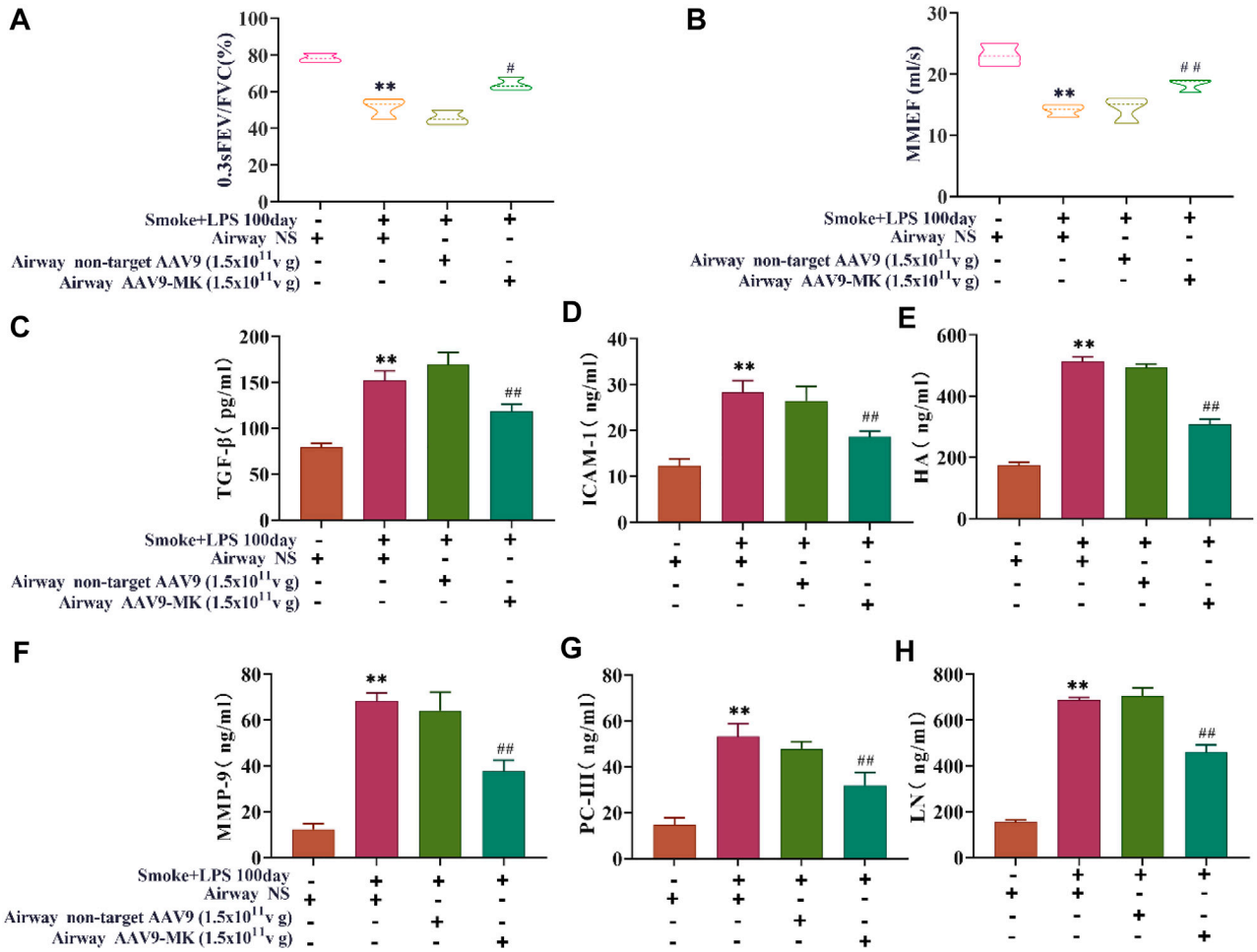

FIGURE 5 | Pulmonary function and inflammatory mediators in BALF. **(A)** Pulmonary function parameter 0.3sFEV/FVC. **(B)** Pulmonary function parameter MMEF. **(C–H)** The concentrations of TGF-β, ICAM-1, HA, MMP-9, PC-III and LN in BALF. $n = 6$, x ± SD. * $p < 0.05$, ** $p < 0.01$ compared with the control group; # $p < 0.05$, ## $p < 0.01$ compared with the COPD group.

2004). Inhibition of MK does not affect normal physiological function in healthy people. This is consistent with our finding that inhibition of MK expression in normal ASMCs had no effect on cell migration, proliferation and apoptosis. However, when the ASMCs were exposed to LPS, the expression of MK began to increase. The cells showed signs of acute injury, with decreased migration and increased apoptosis. When the expression of MK was inhibited in cells treated with LPS, ASMC viability and migration further decreased, and the apoptosis rate was higher. These results support the role of MK in cell proliferation, migration and inhibition of cell apoptosis in response to injury.

Research on COPD has been performed using a wide range of animal models (Wright and Churg, 2010; Polverino et al., 2015). Many animals have been used to establish COPD models, including mice, SD rats, goats, dogs and monkeys. However, rats and mice are considered the best choice because their genome has been sequenced in detail and the relatively low price associated with this model system. There is currently no national or international consensus on the evaluation criteria for COPD models in rats. In a review of the literature, 0.3sFEV/FVC, MMEF, histopathological signs on H&E staining and inflammatory factors in BALF were identified as common criteria (Ghorani et al., 2017). In this study, the COPD rats had a significantly lower 0.3sFEV/FVC and MMEF than control rats, suggesting airflow limitation and pulmonary function decline. The measured inflammatory mediators were all significantly increased in BALF, suggesting chronic inflammation in the airway. H&E staining showed neutrophil infiltration around the airway, airway smooth muscle thickening, deformation and stenosis of airway lumen, suggesting airway remodeling. Taken together, the results show that our rat COPD model reflects the pathophysiological changes of COPD.

Long-term smoke causes chronic airway inflammation in patients with COPD, stimulating airway mucosa to produce TGF-β and MMP-9, which leads to protease/anti-protease imbalance, alveoli destruction, hydrolyzed alveolar elastic fibers, alveolar fusion, and finally emphysema (Vlahos and

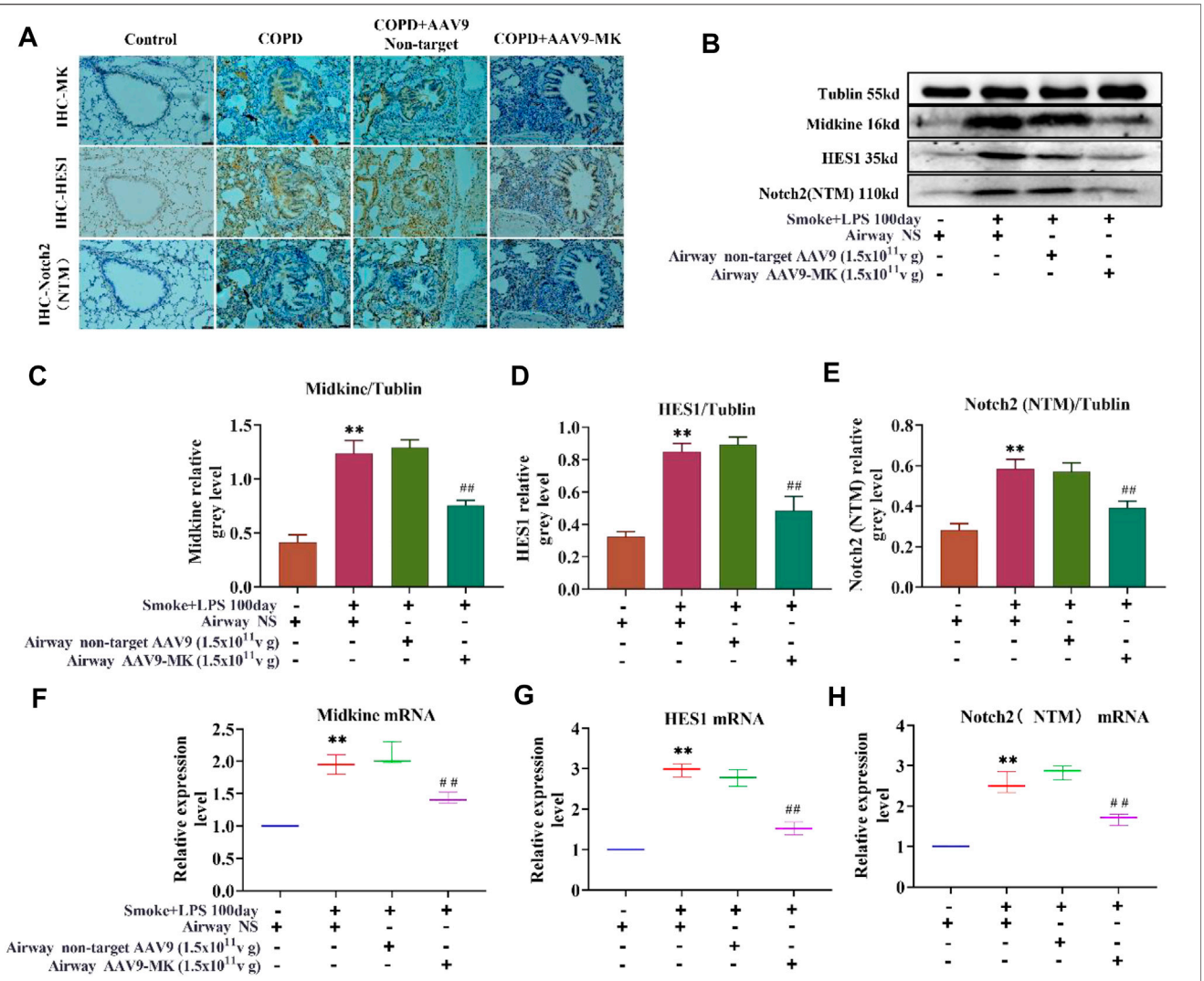

FIGURE 6 | Characterization of the MK-Notch2 signaling pathway *in vivo*. **(A)** IHC of MK, HES1 and Notch2 protein in the lung tissue of the control group by IHC (200x). **(B)** Western blot analysis of MK, HES1 and Notch2 protein. **(C–E)** Quantification of MK, HES1 and Notch2 protein relative to tubulin. **(F–H)** Quantification of the relative expression of MK, HES1 and Notch2 mRNA in the lung tissue. * $p < 0.05$, ** $p < 0.01$ compared with the control group; # $p < 0.05$, ## $p < 0.01$ compared with the COPD group.

Bozinovski, 2014). MMP-9 can directly damage the basement membrane of airway epithelium and cause breakdown of the extracellular matrix (ECM), releasing HA, LN and PC-III (Seemungal et al., 2008). Airway injury activates TGF-β and promotes the secretion of HA, LN and PC-III from the ECM (Mahmood et al., 2017; Di Stefano et al., 2018). HA, LN and PC-III deposit in the airways, leading to accelerated airway stenosis and remodeling (Westergren-Thorsson et al., 2018). Airway injury can also cause upregulated expression of ICAM-1 to promote the adhesion of neutrophils to airway epithelial cells, drive neutrophils to migrate into the airway, and thereby aggravate the inflammatory response (Zimmerman et al., 1994). Chronic airway inflammation accelerates the destruction of lung tissue and leads to airway remodeling, persistent airflow limitation, decreased lung function, and finally COPD. In our *in vivo* experiments, we also found that the expression of TGF-β, ICAM-1, HA, MMP-9, PC-III, and LN in BALF were significantly increased in COPD rats. Decreased pulmonary function and airway remodeling were also seen. Upon inhibition of MK expression in COPD rats with AAV9-MK, the lung function parameters 0.3sFEV/FVC and MMEF both increased, while the inflammatory mediators in BALF and neutrophil infiltration decreased; the airway smooth muscle layer also became thinner and the airway lumen widened. We also saw an improvement of airway remodeling in H&E-stained lung tissue sections. Taken together, the results suggest that MK plays an important role in COPD pathology and targeting the MK-related signaling pathways can reduce the inflammatory reaction, improve airway remodeling and enhance lung function.

MK expression is significantly increased in many malignant tumors, including gastric cancer, pancreatic cancer, lung cancer, breast cancer, colorectal cancer, esophageal cancer, hepatocellular

carcinoma and bladder cancer (Ren and Zhang, 2006; Krzystek-Korpacka et al., 2012; Zhao et al., 2012; Yao et al., 2014; Li et al., 2015; Yuan et al., 2015; Song et al., 2016; Vu Van et al., 2016). MK has been shown to promote tumor cell proliferation and inhibit tumor cell apoptosis. The specific inhibitor of MK APT-1 significantly reduced the volume and weight of neuroblastoma and also reduced the expression of the nuclear transcription factor HES1 in the Notch2 signaling pathway. The HES1 transcription factor promotes downstream cell proliferation and inhibits apoptosis. The Notch2 signaling pathway has also been shown to be involved in the chemotactic inflammatory response (Danahay et al., 2015; Zhang et al., 2017; Carrer et al., 2020). In patients with asthma, inhibiting the Notch signaling pathway in goblet cells reduces inflammation and metaplasia and improves airway remodeling. MK promotes epithelial-mesenchymal transition (EMT), and inhibiting both MK and Notch signaling pathways alleviates pulmonary fibrosis. These studies suggest that the MK-Notch2 signaling pathway plays an important role in cell proliferation, inflammation and remodeling, which is consistent with the results of this study.

In the *in vitro* experiments, LPS was used to establish an acute injury model of ASMCs, and lentivirus shRNA was used to inhibit the expression of MK in ASMCs. We measured changes in MK and Notch2 signaling pathway factors (MK, Notch2 and HES1) and found that the MK-Notch2 signaling pathway in ASMCs was activated following acute injury. Inhibition of MK expression weakened the expression of Notch2 signaling pathway–related factors, as well as decreased ASMC proliferation and migration while increasing apoptosis. These results are consistent with findings from our *in vivo* experiments. In the COPD rat model, both MK and Notch2 signaling pathways were highly expressed. After inhibiting MK by AAV9, the expression of Notch2 signaling pathway factors also decreased. The NTM transmembrane protein is a factor in the Notch2 signaling pathway and is responsible for signal transduction; HES1 is a transcription factor downstream in the Notch2 signaling pathway that promotes cell proliferation and inhibits cell apoptosis. Thus, MK may enhance the signal transduction of the Notch2 signaling pathway through upregulation of the expression of the Notch2 receptor, the transmembrane protein NTM and downstream target HES1, and thereby regulate the cell cycle of AMSCs, promote ASMC proliferation, inhibit apoptosis, and lead to airway narrowing, thereby play a role in the development of COPD.

In summary, our findings showed that inhibiting the expression of MK *in vitro* and *in vivo* reduced the proliferation of ASMCs, decreased pulmonary inflammation and improved lung function and remodeling. Targeting MK, for example, by gene therapy, may be a new strategy to improve airway remodeling and prevent the progressive decline of pulmonary function in COPD.

DATA AVAILABILITY STATEMENT

The original contributions presented in the study are included in the article/supplementary material, further inquiries can be directed to the corresponding authors.

ETHICS STATEMENT

The animal study was reviewed and approved by Hainan Medical University.

AUTHOR CONTRIBUTIONS

All authors listed have made a substantial, direct, and intellectual contribution to the work and approved it for publication.

FUNDING

This work was supported by the National Natural Science Foundation of China (NSFC. 81660011, 81460006, 21961010), Hainan Province Science and Technology Special Fund (ZDYF2021SHFZ219) and Hainan Province Clinical Medical Center (2021).

REFERENCES

Carrer, M., Crosby, J. R., Sun, G., Zhao, C., Damle, S. S., Kuntz, S. G., et al. (2020). Antisense Oligonucleotides Targeting Jagged 1 Reduce House Dust Mite-Induced Goblet Cell Metaplasia in the Adult Murine Lung. *Am. J. Respir. Cell Mol. Biol.* 63, 46–56. doi:10.1165/rcmb.2019-0257OC

Chan, S. M. H., Selemidis, S., Bozinovski, S., and Vlahos, R. (2019). Pathobiological Mechanisms Underlying Metabolic Syndrome (MetS) in Chronic Obstructive Pulmonary Disease (COPD): Clinical Significance and Therapeutic Strategies. *Pharmacol. Ther.* 198, 160–188. doi:10.1016/j.pharmthera.2019.02.013

Danahay, H., Pessotti, A. D., Coote, J., Montgomery, B. E., Xia, D., Wilson, A., et al. (2015). Notch2 Is Required for Inflammatory Cytokine-Driven Goblet Cell Metaplasia in the Lung. *Cell Rep.* 10, 239–252. doi:10.1016/j.celrep.2014.12.017

Di Stefano, A., Sangiorgi, C., Gnemmi, I., Casolari, P., Brun, P., Ricciardolo, F. L. M., et al. (2018). TGF-β Signaling Pathways in Different Compartments of the Lower Airways of Patients with Stable COPD. *Chest* 153, 851–862. doi:10.1016/j.chest.2017.12.017

Disease, G. B. D. (2018). Global, Regional, and National Incidence, Prevalence, and Years Lived with Disability for 354 Diseases and Injuries for 195 Countries and Territories, 1990-2017: a Systematic Analysis for the Global Burden of Disease Study 2017. *Lancet* 392, 1789–1858. doi:10.1016/S0140-6736(18)32279-7

Ghorani, V., Boskabady, M. H., Khazdair, M. R., and Kianmeher, M. (2017). Experimental Animal Models for COPD: a Methodological Review. *Tob. Induc. Dis.* 15, 25. doi:10.1186/s12971-017-0130-2

Hatipoğlu, U. (2018). Chronic Obstructive Pulmonary Disease: More Than Meets the Eye. *Ann. Thorac. Med.* 13, 1–6. Jan-Mar. doi:10.4103/atm.ATM_193_17

Iheanacho, I., Zhang, S., King, D., Rizzo, M., and Ismaila, A. S. (2020). Economic Burden of Chronic Obstructive Pulmonary Disease (COPD): A Systematic Literature Review. *Int. J. Chron. Obstruct. Pulmon. Dis.* 15, 439–460. doi:10.2147/COPD.S234942

Inoh, K., Muramatsu, H., Ochiai, K., Torii, S., and Muramatsu, T. (2004). Midkine, a Heparin-Binding Cytokine, Plays Key Roles in Intraperitoneal Adhesions. *Biochem. Biophys. Res. Commun.* 317, 108–113. doi:10.1016/j.bbrc.2004.03.015

Kadomatsu, K., and Muramatsu, T. (2004). Midkine and Pleiotrophin in Neural Development and Cancer. *Cancer Lett.* 204, 127–143. doi:10.1016/S0304-3835(03)00450-6

Kadomatsu, K., Tomomura, M., and Muramatsu, T. (1988). cDNA Cloning and Sequencing of a New Gene Intensely Expressed in Early Differentiation Stages of Embryonal Carcinoma Cells and in Mid-gestation Period of Mouse Embryogenesis. *Biochem. Biophys. Res. Commun.* 151, 1312–1318. doi:10.1016/s0006-291x(88)80505-9

Kishida, S., Mu, P., Miyakawa, S., Fujiwara, M., Abe, T., Sakamoto, K., et al. (2013). Midkine Promotes Neuroblastoma through Notch2 Signaling. *Cancer Res.* 73, 1318–1327. doi:10.1158/0008-5472.CAN-12-3070

Kosugi, T., Yuzawa, Y., Sato, W., Arata-Kawai, H., Suzuki, N., Kato, N., et al. (2007). Midkine Is Involved in Tubulointerstitial Inflammation Associated with Diabetic Nephropathy. *Lab. Invest.* 87, 903–913. doi:10.1038/labinvest.3700599

Krzystek-Korpacka, M., Diakowska, D., Grabowski, K., and Gamian, A. (2012). Tumor Location Determines Midkine Level and its Association with the Disease Progression in Colorectal Cancer Patients: a Pilot Study. *Int. J. Colorectal Dis.* 27, 1319–1324. doi:10.1007/s00384-012-1476-9

Li, F., Tian, P., Zhang, J., and Kou, C. (2015). The Clinical and Prognostic Significance of Midkine in Breast Cancer Patients. *Tumour Biol.* 36, 9789–9794. doi:10.1007/s13277-015-3710-x

Mahmood, M. Q., Reid, D., Ward, C., Muller, H. K., Knight, D. A., Sohal, S. S., et al. (2017). Transforming Growth Factor (TGF) β1 and Smad Signalling Pathways: A Likely Key to EMT-Associated COPD Pathogenesis. *Respirology* 22, 133–140. doi:10.1111/resp.12882

Muramatsu, T. (2014). Structure and Function of Midkine as the Basis of its Pharmacological Effects. *Br. J. Pharmacol.* 171, 814–826. doi:10.1111/bph.12353

Polverino, F., Doyle-Eisele, M., McDonald, J., Wilder, J. A., Royer, C., Laucho-Contreras, M., et al. (2015). A Novel Nonhuman Primate Model of Cigarette Smoke-Induced Airway Disease. *Am. J. Pathol.* 185, 741–755. doi:10.1016/j.ajpath.2014.11.006

Ren, Y. J., and Zhang, Q. Y. (2006). Expression of Midkine and its Clinical Significance in Esophageal Squamous Cell Carcinoma. *World J. Gastroenterol.* 12, 2006–2010. doi:10.3748/wjg.v12.i13.2006

Ritchie, A. I., and Wedzicha, J. A. (2020). Definition, Causes, Pathogenesis, and Consequences of Chronic Obstructive Pulmonary Disease Exacerbations. *Clin. Chest Med.* 41, 421–438. doi:10.1016/j.ccm.2020.06.007

Sato, W., and Sato, Y. (2014). Midkine in Nephrogenesis, Hypertension and Kidney Diseases. *Br. J. Pharmacol.* 171, 879–887. doi:10.1111/bph.12418

Sato, W., Yuzawa, Y., Kadomatsu, K., Tayasu, T., Muramatsu, H., Muramatsu, T., et al. (2002). Midkine Expression in the Course of Nephrogenesis and its Role in Ischaemic Reperfusion Injury. *Nephrol. Dial. Transpl.* 17 (Suppl. 9), 52–54. doi:10.1093/ndt/17.suppl_9.52

Seemungal, T. A., Wilkinson, T. M., Hurst, J. R., Perera, W. R., Sapsford, R. J., and Wedzicha, J. A. (2008). Long-term Erythromycin Therapy Is Associated with Decreased Chronic Obstructive Pulmonary Disease Exacerbations. *Am. J. Respir. Crit. Care Med.* 178, 1139–1147. doi:10.1164/rccm.200801-145OC

Shindo, E., Nanki, T., Kusunoki, N., Shikano, K., Kawazoe, M., Sato, H., et al. (2017). The Growth Factor Midkine May Play a Pathophysiological Role in Rheumatoid Arthritis. *Mod. Rheumatol.* 27, 54–59. doi:10.1080/14397595.2016.1179860

Song, P., Tang, Q., Feng, X., and Tang, W. (2016). Biomarkers: Evaluation of Clinical Utility in Surveillance and Early Diagnosis for Hepatocellular Carcinoma. *Scand. J. Clin. Lab. Invest. Suppl.* 245, S70–S76. doi:10.1080/00365513.2016.1210328

Spero, K., Bayasi, G., Beaudry, L., Barber, K. R., and Khorfan, F. (2017). Overdiagnosis of COPD in Hospitalized Patients. *Int. J. Chron. Obstruct. Pulmon. Dis.* 12, 2417–2423. doi:10.2147/COPD.S139919

Vlahos, R., and Bozinovski, S. (2014). Role of Alveolar Macrophages in Chronic Obstructive Pulmonary Disease. *Front. Immunol.* 5, 435. doi:10.3389/fimmu.2014.00435

Vu Van, D., Heberling, U., Wirth, M. P., and Fuessel, S. (2016). Validation of the Diagnostic Utility of Urinary Midkine for the Detection of Bladder Cancer. *Oncol. Lett.* 12, 3143–3152. doi:10.3892/ol.2016.5040

Weckbach, L. T., Gola, A., Winkelmann, M., Jakob, S. M., Groesser, L., Borgolte, J., et al. (2014). The Cytokine Midkine Supports Neutrophil Trafficking during Acute Inflammation by Promoting Adhesion via β2 Integrins (CD11/CD18). *Blood* 123, 1887–1896. doi:10.1182/blood-2013-06-510875

Westergren-Thorsson, G., Bagher, M., Andersson-Sjöland, A., Thiman, L., Löfdahl, C. G., Hallgren, O., et al. (2018). VEGF Synthesis Is Induced by Prostacyclin and TGF-β in Distal Lung Fibroblasts from COPD Patients and Control Subjects: Implications for Pulmonary Vascular Remodelling. *Respirology* 23, 68–75. doi:10.1111/resp.13142

Wright, J. L., and Churg, A. (2010). Animal Models of Cigarette Smoke-Induced Chronic Obstructive Pulmonary Disease. *Expert Rev. Respir. Med.* 4, 723–734. doi:10.1586/ers.10.68

Yao, J., Li, W. Y., Li, S. G., Feng, X. S., and Gao, S. G. (2014). Midkine Promotes Perineural Invasion in Human Pancreatic Cancer. *World J. Gastroenterol.* 20, 3018–3024. doi:10.3748/wjg.v20.i11.3018

Yuan, K., Chen, Z., Li, W., Gao, C. E., Li, G., Guo, G., et al. (2015). MDK Protein Overexpression Correlates with the Malignant Status and Prognosis of Non-small Cell Lung Cancer. *Arch. Med. Res.* 46, 635–641. doi:10.1016/j.arcmed.2015.11.006

Zhang, J., Yuan, G., Dong, M., Zhang, T., Hua, G., Zhou, Q., et al. (2017). Notch Signaling Modulates Proliferative Vitreoretinopathy via Regulating Retinal Pigment Epithelial-To-Mesenchymal Transition. *Histochem. Cell Biol.* 147, 367–375. doi:10.1007/s00418-016-1484-x

Zhang, R., Pan, Y., Fanelli, V., Wu, S., Luo, A. A., Islam, D., et al. (2015). Mechanical Stress and the Induction of Lung Fibrosis via the Midkine Signaling Pathway. *Am. J. Respir. Crit. Care Med.* 192, 315–323. doi:10.1164/rccm.201412-2326OC

Zhao, Z. Q., Yang, S., and Lu, H. S. (2012). Expression of Midkine and Vascular Endothelial Growth Factor in Gastric Cancer and the Association of High Levels with Poor Prognosis and Survival. *Mol. Med. Rep.* 5, 415–419. doi:10.3892/mmr.2011.649

Zimmerman, B. J., Holt, J. W., Paulson, J. C., Anderson, D. C., Miyasaka, M., Tamatani, T., et al. (1994). Molecular Determinants of Lipid Mediator-Induced Leukocyte Adherence and Emigration in Rat Mesenteric Venules. *Am. J. Physiol.* 266, H847–H853. doi:10.1152/ajpheart.1994.266.3.H847

Conflict of Interest: The authors declare that the research was conducted in the absence of any commercial or financial relationships that could be construed as a potential conflict of interest.

Publisher's Note: All claims expressed in this article are solely those of the authors and do not necessarily represent those of their affiliated organizations, or those of the publisher, the editors and the reviewers. Any product that may be evaluated in this article, or claim that may be made by its manufacturer, is not guaranteed or endorsed by the publisher.

frontiers | Frontiers in Pharmacology

ORIGINAL RESEARCH
published: 15 July 2022
doi: 10.3389/fphar.2022.801337

Metformin Alleviates LPS-Induced Acute Lung Injury by Regulating the SIRT1/NF-κB/NLRP3 Pathway and Inhibiting Endothelial Cell Pyroptosis

Yunqian Zhang†, *Hui Zhang*†, *Siyuan Li*†, *Kai Huang*, *Lai Jiang** *and Yan Wang**

Department of Anesthesiology and Surgical Intensive Care Unit, Xinhua Hospital Affiliated to Shanghai Jiaotong University School of Medicine, Shanghai, China

OPEN ACCESS

Edited by:
Irfan Rahman,
University of Rochester, United States

Reviewed by:
Yin Cai,
Hong Kong Polytechnic University, Hong Kong SAR, China
Antonio Recchiuti,
University of Studies G.d'Annunzio Chieti and Pescara, Italy

***Correspondence:**
Yan Wang
wangyan@xinhuamed.com.cn
Lai Jiang
jianglai@xinhuamed.com.cn

†*These authors have contributed equally to this work and share first authorship*

Specialty section:
This article was submitted to Respiratory Pharmacology, a section of the journal Frontiers in Pharmacology

Received: *25 October 2021*
Accepted: *13 June 2022*
Published: *15 July 2022*

Citation:
Zhang Y, Zhang H, Li S, Huang K, Jiang L and Wang Y (2022) Metformin Alleviates LPS-Induced Acute Lung Injury by Regulating the SIRT1/NF-κB/NLRP3 Pathway and Inhibiting Endothelial Cell Pyroptosis. Front. Pharmacol. 13:801337. doi: 10.3389/fphar.2022.801337

Acute respiratory distress syndrome (ARDS), a devastating complication of numerous conditions, is often associated with high mortality. It is well known that endothelial cell (EC) damage and inflammation are vital processes in the pathogenesis of ARDS. Nevertheless, the mechanisms of EC damage are largely unknown. In the present study, we investigated the role of pyroptosis in the initiation of ARDS and demonstrated that endothelial pyroptosis might play a pivotal role in the pathophysiology of ARDS. Metformin, an antidiabetic drug, exhibited a protective effect in lipopolysaccharide (LPS)-induced lung injury, and we hypothesized that metformin alleviated LPS-induced lung injury *via* inhibiting ECs pyroptosis. *In vivo*, male ICR mice were intratracheally injected with LPS, and metformin was previously administered intraperitoneally. Morphological properties of lung tissues were detected. We showed that metformin inhibited NLRP3 inflammasome activation and NLRP3-stimulated pyroptosis induction, as shown by decreased levels of cleaved caspase-1, N-terminal fragment of GSDMD, and protein contents of IL-1β in lung tissues of mice exposed to LPS. LPS-induced expression of vascular adhesion molecules was also reduced after the treatment with metformin. *In vitro*, exposure of pulmonary ECs to LPS resulted in increased expression of NLRP3 and pyroptosis-associated indicators. By inhibiting the expression of NLRP3 with NLRP3 inhibitor MCC950, pyroptosis-related markers and vascular adhesion molecules were ameliorated. Moreover, metformin treatment significantly inhibited the NF-κB signaling pathway and increased the expression of sirtuin 1 (SIRT1) both in LPS-stimulated lung tissues and pulmonary ECs. Administration of the selective SIRT1 inhibitor nicotinamide significantly reversed the protective effect of metformin against endothelial pyroptosis and lung injury in LPS-treated ECs and LPS-induced acute lung injury (ALI). Thus, these findings demonstrated that metformin alleviated LPS-induced ALI by inhibiting NF-κB-NLRP3–mediated ECs pyroptosis, possibly by upregulating the expression of SIRT1.

Keywords: ARDS, endothelial pyroptosis, metformin, NLRP3, SIRT1

INTRODUCTION

Acute lung injury (ALI) or acute respiratory distress syndrome (ARDS) is a devastating complication triggered by various factors (Han and Mallampalli, 2015), and it is often associated with high mortality. It is characterized by difficult breathing and low blood oxygen, thereby leading directly to respiratory failure and death in fatal COVID-19 cases (Zhang et al., 2020). ARDS and sepsis share some of the underlying mechanisms, which include inflammatory responses and endothelial damage. Lung vascular endothelium injury is the most important initial cause of ARDS following sepsis, which affects pulmonary homeostasis (Matthay and Zemans, 2011). At present, advances in rescue therapies, including lung-protective ventilation (Amato et al., 2015), prone positioning (Guerin et al., 2013), infusion of neuromuscular blockade (Papazian et al., 2010), and extracorporeal life support (Peek et al., 2009), have improved the outcome of ARDS in recent years. However, there is no specific treatment strategy for ARDS. Therefore, further studies are needed to explore the pathogenesis and treatment modalities of ARDS.

Pyroptosis is a specialized form of cell death, different from apoptosis and necrosis (Shi et al., 2015). Canonical pyroptosis can be activated by inflammasomes (Jia et al., 2019). NLRP3 inflammasome can recognize microbial and endogenous danger signals and trigger innate immune responses. After priming, cytosolic NLRP3 oligomerizes with other proteins of the inflammasome complex, primarily ASC and pro-caspase-1 (Broz, 2019), and pro-caspase-1 is subsequently activated, leading to the cleavage of gasdermin D (GSDMD). After the activation, the N-terminal fragment of GSDMD oligomerizes and forms membrane pores, thereby causing cellular swelling, plasma membrane rupture, and release of cytoplasmic contents. Activation of caspase-1 also cleaves proinflammatory cytokines IL-1β and IL-18 into their functional conformation (Herman and Pasinetti, 2018; Mathur et al., 2018). Lung endothelial cells (ECs) are an important source of IL-1β, and the production of active IL-1β is controlled by the inflammasome. Pyroptosis has been shown to play a requisite role in endotoxemic lung injury, suggesting that inhibiting endothelial pyroptosis may offer an important therapeutic strategy for the treatment of ALI (Cheng et al., 2017).

Metformin is an effective antidiabetic drug which exhibits pulmonary protective effects in diverse ALI models, including ventilator-induced lung injury (Tsaknis et al., 2012), PM 2.5–induced lung injury (Gao et al., 2020), and endotoxemia-induced lung injury (Wu et al., 2018). In addition, metformin decreases the disease severity and mortality in COVID-19 patients (Bramante et al., 2021). Current evidence suggests that metformin alleviates endothelial dysfunction in the vasculature (de Aguiar et al., 2006). Metformin also protects from vascular endothelial dysfunction in type 2 diabetes patients with metabolic syndrome (Nafisa et al., 2018) and women with polycystic ovary syndrome (PCOS) (Heidari et al., 2019). NLRP3 inflammasome activation in lung vascular ECs is associated with different pulmonary disorders (Xiang et al., 2011; Wang et al., 2017; Ito et al., 2020). A previous study has demonstrated that metformin treatment ameliorates the NLRP3 inflammasome-mediated pyroptosis in diabetic periodontitis (Zhou et al., 2020); however, it remains unclear whether metformin reverses pulmonary endothelial dysfunction during the pathogenesis of ARDS.

Sirtuin 1 (SIRT1) is an NAD+ -dependent protein deacetylase that is involved in a wide range of cellular processes, including cellular metabolism and embryogenesis (Wang et al., 2008; Tang et al., 2014). There is emerging evidence that SIRT1 regulates NLRP3 in vascular ECs, thereby inhibiting the inflammatory response (Li et al., 2016; Li et al., 2017; Wang et al., 2017). NF-κB, a proinflammatory gene, activates a variety of genes in the nucleus, including NLRP3. Therefore, the present study investigated the effect of metformin in NLRP3 inflammasome activation-mediated pyroptosis exposed to lipopolysaccharide (LPS) and in LPS-treated lung ECs. Here, we demonstrated that metformin blunted the severity of LPS-induced ARDS and inflammasome activation. We hypothesize that metformin exerts the pulmonary protective role by upregulating the expression of SIRT1, thereby inhibiting NF-κB-NLRP3–triggered ECs pyroptosis. Therefore, we suggest that metformin, a safe and inexpensive antidiabetic drug, may be useful for the treatment of ARDS.

MATERIALS AND METHODS

Animals and Experimental Design

Institute of Cancer Research (ICR) mice (25–30 g) were purchased from Shanghai Sippr-BK laboratory animal Co. Ltd. (Shanghai, China). The mice were acclimated to standard conditions (22 ± 2°C; 12 h light/dark periods) with access to food and water *ad libitum* for 7 days prior to conducting experiments. All animal studies were implemented in accordance with the principles of the Ethical Committee of Xinhua Hospital affiliated with Shanghai Jiao Tong University, School of Medicine. In addition, LPS from *Escherichia coli* O111: B4 (L2630, Sigma-Aldrich, St. Louis, MO, United States, 5 mg/kg) was intratracheally injected *via* a 22-gauge catheter, and the mice were euthanized 9 h later. Metformin (Bristol Myers Squibb, Shanghai, China) was administered intraperitoneally, 50 mg/kg, 30 min prior to the LPS challenge (Park et al., 2012; Vaez et al., 2016). SIRT-1 inhibitor nicotinamide (NAM, 60 mg/kg, Sigma) was given intraperitoneally 1 h before metformin treatment. At the indicated time, the mice were sacrificed, and the left lower lung lobes were removed and fixed in 4% formalin for morphological evaluation. Other lobes were frozen at −80°C for further analysis.

Pulmonary ECs Cells Culture and Treatment

Mouse lung vascular ECs were isolated in accordance with a previously published article (Dong et al., 2015). In brief, ICR mice weighing around 15 g were anesthetized; their lungs were inflated with cold phosphate buffer saline (PBS) to remove blood; peripheral tissues were cut into small pieces. Dulbecco's modified Eagle's medium (DMEM) with 20% fetal bovine serum (FBS) was added as a culture medium. ECs crawled out beneath the lung tissue 60 h later. The adherent cells were grown

in DMEM supplemented with 10% FBS for 3 days after removal of the tissue dices. Mouse lung ECs were characterized by their cobblestone morphology, and factor VIII-related antigen staining and CD31 staining were performed to identify their purity. The cells were exposed to 1 μg/ml LPS with/without pretreatment with metformin (10 mM), MCC950 (10 μM), NAM (1 mM), or SIRT1 siRNA (sc-40987, Santa Cruz). The supernatants were collected and stored at −80°C until assayed.

Monocyte–ECs Adhesion

For activation, HMEC-1 cells (human microvascular endothelial cell-1) were cultured in 24-well plates and incubated with LPS and metformin in the presence or absence of NAM for 24 h. For monocyte–ECs adhesion experiments, assays were performed by adding 5×10^5 THP1 cells (Zhong Qiao Xin Zhou Biotechnology Co., Ltd., Shanghai, China) that were labeled with 2 μM calcein-AM with green fluorescence (Beyotime Biotechnology, China) to 1×10^5 confluent HMEC-1 cells (FuHeng Biology, Shanghai, China) for 2 h (Lin et al., 2018). THP-1 cells that were firmly bound to HMEC-1 were observed with a fluorescence microscope (Olympus, Tokyo, Japan).

Histological Evaluation

Fixed lung specimens were embedded in paraffin, and tissue sections (4 μm) were stained with hematoxylin and eosin (H&E) to detect pathological changes.

Lung Wet-To-Dry Ratio

The extent of lung edema was evaluated by the wet-to-dry (W/D) ratio. The wet weight was measured immediately after the excision of the lung, and the dry weight was recorded after drying in an oven at 60°C for 48 h. The lung W/D ratio was calculated as wet weight/dry weight.

Evans Blue Albumin

An Evans blue dye–labeled albumin mixture (EB, 40 mg/kg, Sigma) was injected into the left jugular vein of each mouse 45 min before the mice were killed. The lungs were perfused with PBS and weighed. The lung tissues were homogenized in PBS and incubated with 2 ml formamide at 60°C overnight. The homogenate was centrifuged for 30 min at 5,000 g. The optical density of the supernatant was observed at 620 nm (A620) spectrophotometrically. Extravasated EB concentrations in the lung homogenate were presented as micrograms of Evans blue dye per gram of tissue.

Immunohistochemistry and Immunofluorescence of Lung Samples

In brief, lung sections (4 μm) were deparaffinized, hydrated, and transferred to citrate buffer (pH = 6.0) for antigen retrieval, followed by cooling for 20 min. Endogenous peroxidase activity was blocked by H_2O_2, and incubation with normal goat serum was performed to reduce nonspecific binding. The lung sections were incubated with primary antibodies specific for F4/80 (a macrophage marker) and myeloperoxidase (MPO, a neutrophil marker). NLRP3 and caspase-1 activation in pulmonary endothelium was detected by immunofluorescence co-staining with the endothelial marker CD31 in accordance with standard protocols. The sections were imaged through an Olympus fluorescence microscope.

Immunofluorescence Staining of Endothelial Cells

After the treatments, endothelial cells were fixed with 4% paraformaldehyde for 10–20°min, permeabilized with 0.3% Triton X-100 in PBS-Tween, and blocked with 5% BSA for 30°min, followed by incubation with primary antibody against NLRP3 (1:200, ABclonal) or CD31 (1:200, Servicebio) at 4°C overnight. FITC-conjugated or CY3-conjugated secondary antibodies were used for immunodetection. After washing three times, nuclei were stained with 4′,6-diamidino-2-phenylindole (DAPI, Beyotime) for 5 min. Then, the cells were observed, and images were captured under a fluorescence microscope (Olympus).

TUNEL Assay

DNA fragmentation of endothelial cells was measured by TdT-mediated dUTP nick-end labeling (TUNEL) staining in line with the manufacturer's protocol (Beyotime). In brief, endothelial cells were fixed and permeabilized, as described earlier. After rinsing with PBS, the cells were incubated with a one-step TUNEL reaction mixture for 1 h at 37°C in a humidified chamber in the dark. Finally, nuclei were counterstained with DAPI (Beyotime). Images were observed, and photographs were taken under a fluorescence microscope (Olympus).

Western Blot Analysis

Lung samples and cell lysates were prepared in cold RIPA buffer containing a protease inhibitor cocktail (Sigma). Equal amounts of proteins (40 μg) were separated by SDS-PAGE and then transferred to PVDF membranes. The membranes were blocked with 5% nonfat milk and incubated with the following primary antibodies: anti-NLRP3 (1:1,000, Cell Signaling Technology, CST, Inc., United States), anti-caspase-1 (1:1,000, ABclonal), anti-GSDMD (1:500, Abcam, Cambridge, MA, United States), anti-SIRT1 (1:1,000, CST), anti-NF-κB p65 (1:1,000, CST), anti-phosphorylated (p)-NF-κB p65 (1:1,000, CST), anti-IκB-α (1:1,000, CST), anti-Acetyl-NF-κB p65 (Lys310) (1:500, CST), anti-PCNA (D3H8P) (1:500, CST), anti-ICAM-1 (1:1,000, Servicebio), and anti-VCAM-1 (1:1,000, Servicebio) overnight at 4°C. After that, the membranes were incubated with HRP-conjugated secondary antibody for 1–2 h. The blots were detected with an enhanced chemiluminescence (ECL) system (Thermo Fisher Scientific). The protein band intensity was normalized to β-actin (1:3,000, Sigma) and expressed as a ratio of the control.

Nuclear and Cytoplasmic Protein Extraction

The nuclear and cytoplasmic protein extraction was conducted by following the manufacturer's instructions of the commercial kit (P0028, Beyotime).

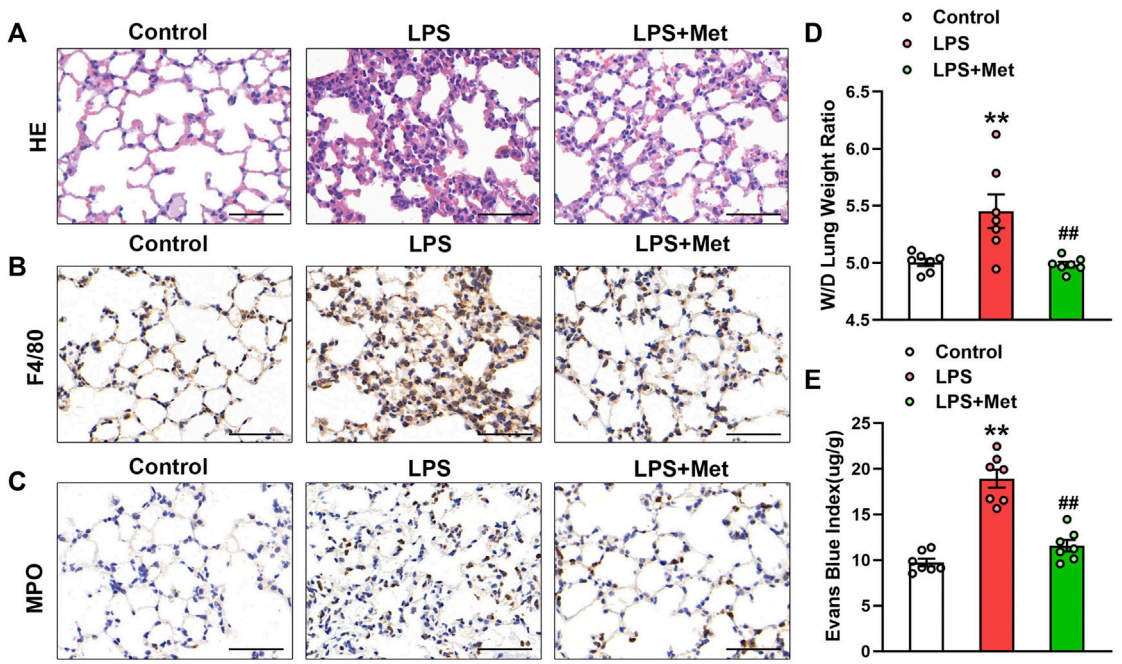

FIGURE 1 | Metformin ameliorates the morphological characteristics and vascular endothelial hyperpermeability of LPS-induced ALI in mice. Mice were subjected to LPS, with or without metformin treatment for 9 h. **(A)** Representative hematoxylin and eosin staining of the lung tissues. **(B)** Immunohistochemistry analysis was used to measure the intensity of F4/80. **(C)** Immunohistochemistry was used to measure the intensity of myeloperoxidase. **(D and E)** Lung W/D and Evans blue dye extravasation were determined as indexes of pulmonary edema. Original magnification, ×200. Scale bar, 50 μm. Data are presented as the mean ± SEM (n = 7). $^{**}p < 0.01$ vs. Control group, $\#\#p < 0.01$ vs. LPS group. Myeloperoxidase, MPO.

ELISA

The concentrations of IL-1β in lung tissues and cell supernatants were determined by enzyme-linked immunosorbent assay (ELISA) kits in accordance with the manufacturer's instructions (Elabscience Biotechnology Co., Ltd., Wuhan, China).

Statistical Analysis

All data are expressed as the mean ± standard error of mean (SEM). Differences among different groups were analyzed by one-way analysis of variance (ANOVA), followed by a *post-hoc* Tukey's multiple-comparison test using SPSS software. The significance level was set at $p < 0.05$.

RESULTS

Metformin Ameliorates LPS-Induced Lung Injury in Mice

To examine the effects of metformin on LPS-induced ALI, we assessed morphological characteristics, performed immunohistochemical analysis of F4/80 and MPO in lung tissues of mice to show the changes in terms of inflammation and neutrophils, and evaluated lung W/D and EBA to determine pulmonary endothelial permeability. Compared with the control group, LPS administration resulted in severe lung injury; in contrast, metformin pretreatment significantly improved LPS-induced lung injury, as reflected by decreased intra-alveolar and interstitial edema (**Figure 1A**). Metformin also strongly inhibited infiltration by macrophages and neutrophils (**Figures 1B and C**). LPS administration damaged the pulmonary vascular endothelium as evidenced by increased W/D ratio and degree of EBA extravasation, but these effects were also reduced by metformin (**Figures 1D and E**).

Metformin Suppresses LPS-Induced Endothelial Cell Pyroptosis and Vascular Adhesion Molecules *In Vivo*

To investigate whether the mitigation of lung injury by metformin was associated with pyroptosis, the expression levels of pyroptosis-related proteins were detected. As expected, the protein levels of NLRP3, activated caspase-1 (caspase-1 p20), and the N-terminal fragment of GSDMD and IL-1β level were significantly increased in lung tissues of mice exposed to LPS, and metformin pretreatment significantly decreased the levels of these pyroptosis-related proteins (**Figures 2A and B**). The results showed that the administration of LPS caused a significant increase in the expression of vascular adhesive molecules, including ICAM-1 and VCAM-1, while metformin pretreatment significantly decreased the expression levels of ICAM-1 and VCAM-1 (**Figure 2C**). To further demonstrate that pyroptosis occurred in pulmonary endothelium, CD31/NLRP3 and CD31/caspase-1 double staining were performed. As shown in **Figures 2D–G**, the percentage of NLRP3- and caspase-

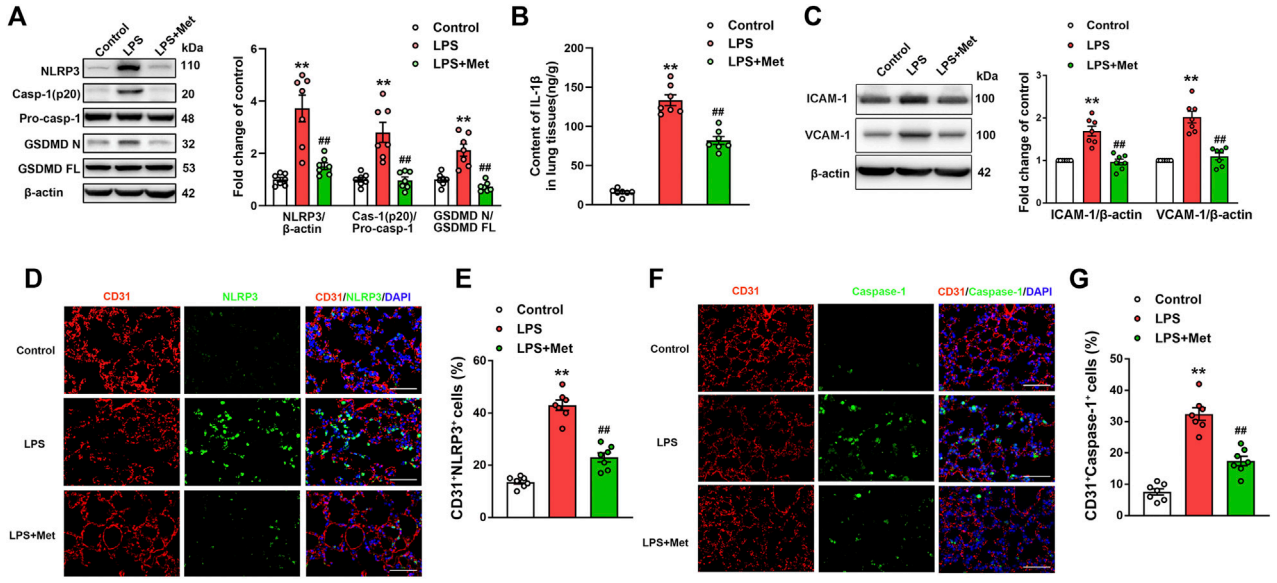

FIGURE 2 | Metformin reduces the LPS-induced release of pyroptotic proteins and vascular adhesion molecules in mouse lung tissues. **(A)** Western blotting was used to determine the levels of NLRP3, cleaved caspase 1 (p20), and N-terminal fragment of GSDMD. Indicative bands are shown. **(B)** ELISA was used to determine the protein levels of IL-1β. **(C)** Representative protein bands and corresponding histogram of ICAM-1 and VCAM-1 are shown. **(D)** Lung tissues were stained with NLRP3 (green) and CD31 (red). Nuclei were counterstained with 4'6-diamidino-2-phenylindole (DAPI) (blue). **(E)** Percentages of $CD31^{+}NLRP3^{+}$ cells are shown as histograms. **(F)** Lung tissues were stained with caspase-1 (green) and CD31 (red). Nuclei were counterstained with DAPI (blue). **(G)** Percentages of $CD31^{+}Caspase\text{-}1^{+}$ cells are shown as histograms. Original magnification, ×200. Scale bar, 50 μm. Data are presented as the mean ± SEM ($n = 7$). $^{**}p < 0.01$ vs. Control group, $\#\#p < 0.01$ vs. LPS group.

1-positive cells was markedly increased in the pulmonary endothelium of lung tissues following the LPS challenge, but the supplementation of metformin significantly decreased active NLRP3 and caspase-1-positive cells. Collectively, these results showed that metformin inhibited pulmonary EC pyroptosis and vascular adhesive molecules during LPS-stimulated lung injury.

Metformin Suppresses LPS-Induced Endothelial Cell Pyroptosis *In Vitro*

To further explore the role of metformin in LPS-induced endothelial injury, mouse lung ECs were exposed to LPS with or without metformin added. As shown in **Figure 3A**, the protein levels of NLRP3, cleaved caspase-1, and N-terminal fragment of GSDMD were increased in LPS-treated ECs. IL-1β in cell supernatant was also elevated after LPS administration (**Figure 3B**). Metformin pretreatment also inhibited the expression of ICAM-1 and VCAM-1 (**Supplementary Figure S2**). Furthermore, the immunofluorescence staining of NLRP3 and TUNEL staining, respectively, revealed that NLRP3-positive cells and apoptotic cells were remarkably increased by LPS treatment, whereas all these effects were attenuated after pretreatment with metformin (**Figures 3C–E**).

NLRP3 Inflammasome Induces Pyroptosis Activation in LPS-Treated ECs

NLRP3 inflammasome is well known for its involvement in the activation of caspase-1 and subsequent pyroptosis (Wang et al., 2019). To confirm our hypothesis, NLRP3 inhibitory experiments with the NLRP3 inhibitor MCC950 were performed. Notably, the results showed that MCC950 treatment significantly inhibited the LPS-induced increases in the protein levels of activated caspase-1 (p20) and N-terminal fragment of GSDMD, and the LPS-induced release of IL-1β was also suppressed by MCC950 treatment (**Figures 3F and G**). The expression levels of vascular adhesion molecules ICAM-1 and VCAM-1 were equally diminished following MCC950 treatment (**Supplementary Figure S3**). Moreover, the percentages of TUNEL-positive cells were reduced after the treatment with MCC950 in LPS-treated ECs (**Figures 3H and I**). Therefore, these data provided strong evidence that ECs pyroptosis in LPS-stimulated lung injury was mediated by NLRP3 inflammasome activation.

Effects of Metformin on the Expression of SIRT1/NF-κB Pathway *In Vivo* and *In Vitro*

Subsequently, we assessed the effects of metformin on the protein levels of SIRT1 in the lungs of the mouse ARDS model and LPS-treated pulmonary ECs. Western blot analysis indicated that the relative level of SIRT1 in the LPS group decreased to 43% of the control level, whereas further treatment with metformin increased it to nearly 75% of the control level (**Figure 4A**). Similarly, in pulmonary ECs exposed to LPS, the protein level of SIRT1 was decreased, while metformin administration restored the expression level of SIRT1 (**Figure 4B**). Phosphorylated NF-κB p65 subunit was increased, whereas IκB-α was decreased in the LPS group compared with the control group; however, metformin reversed these effects both *in vivo* (**Figure 4A**) and *in vitro* (**Figure 4B**). These results indicated that metformin increased the expression of SIRT1 and

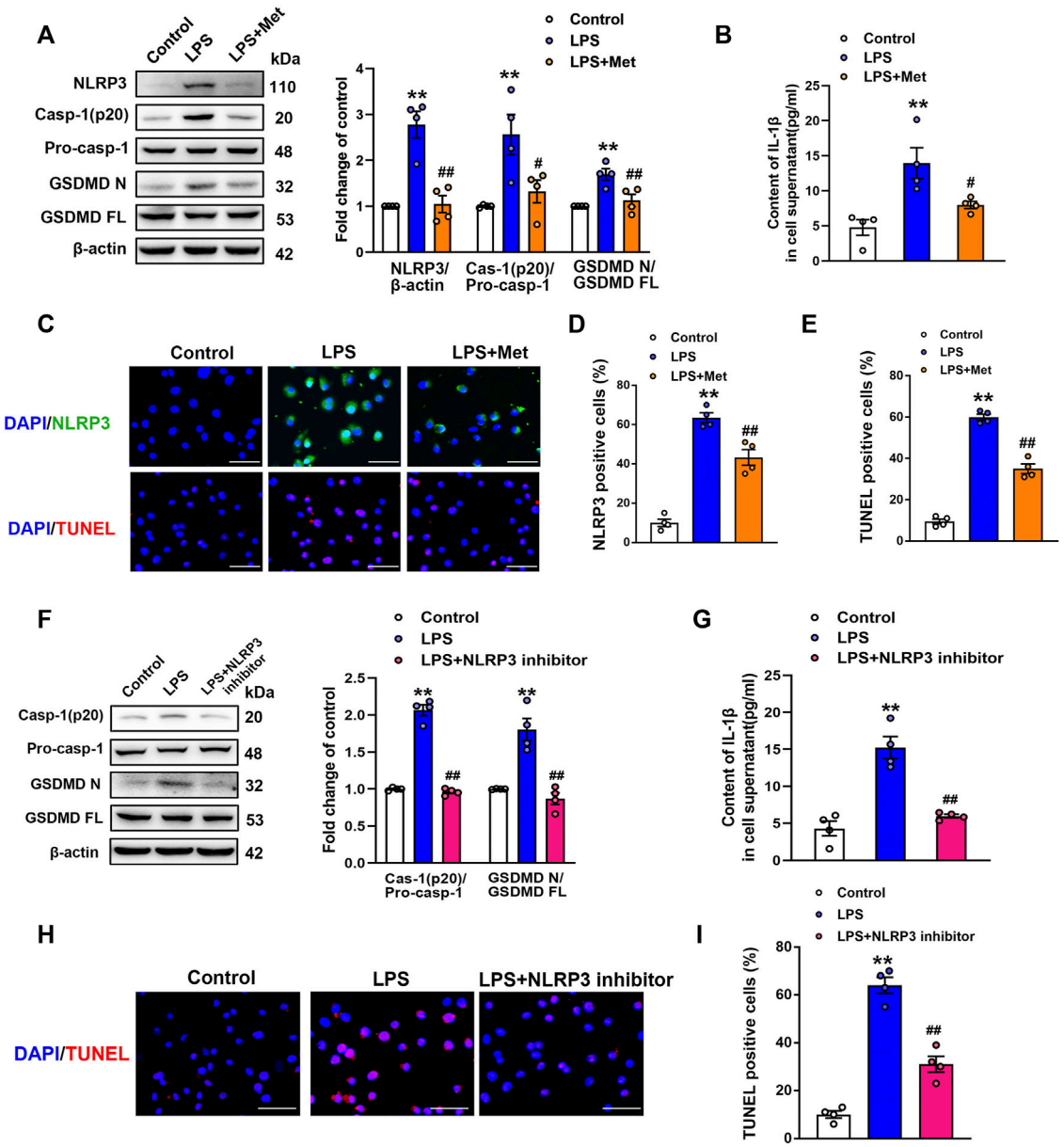

FIGURE 3 | Metformin and NLRP3 inhibitor reduce the LPS-induced release of pyroptotic proteins and inflammatory cytokines in primarily cultured pulmonary ECs of mice. Pulmonary ECs were pretreated with metformin (10 mM) and NLRP3 inhibitor (MCC950, 10 μM), and then ECs were exposed to LPS for 24 h. **(A)** Indicative protein bands of NLRP3, cleaved caspase 1 (p20), and N-terminal fragment of GSDMD. **(B)** ELISA was used to determine the protein levels of IL-1β in the supernatant. **(C)** ECs were stained with NLRP3 (green). Apoptotic cells were evaluated using TUNEL staining. The nuclei were stained blue using DAPI. **(D)** and **(E)** Percentages of NLRP3-positive cells and TUNEL-positive cells. **(F)** Effect of MCC950 pretreatment on the expression levels of pyroptosis-related proteins was analyzed by Western blotting. Quantitative analysis of pyroptosis-related protein expression was conducted. Representative bands are shown on the left of the histogram. **(G)** ELISA was used to determine the protein levels of IL-1β in supernatants. **(H)** DNA fragmentation was determined using TUNEL staining. The nuclei were stained blue using DAPI. **(I)** Percentage of TUNEL-positive cells. Magnification: ×200. Scale bar, 50 μm. Data are presented as the mean ± SEM ($n = 4$). $^{**}p < 0.01$ vs. Control group, $\#p < 0.05$, $\#\#p < 0.01$ vs. LPS group.

decreased the level of phosphorylated NF-κB p65. It has been reported that SIRT1 reduces NF-κB activity by decreasing the acetylation level of lysine 310 of the NF-κB p65 subunit; as expected, the enhancement of p65 lysine 310 acetylation after LPS administration was detected, but it decreased after metformin treatment both *in vivo* and *in vitro* (**Figures 4C and D**).

Inhibition of SIRT1 Eliminates the Protective Effect of Metformin on Endothelial Cell Pyroptosis *In Vitro*

A former study demonstrated that the activation of SIRT1 inhibited NLRP3 inflammasome activation and subsequent

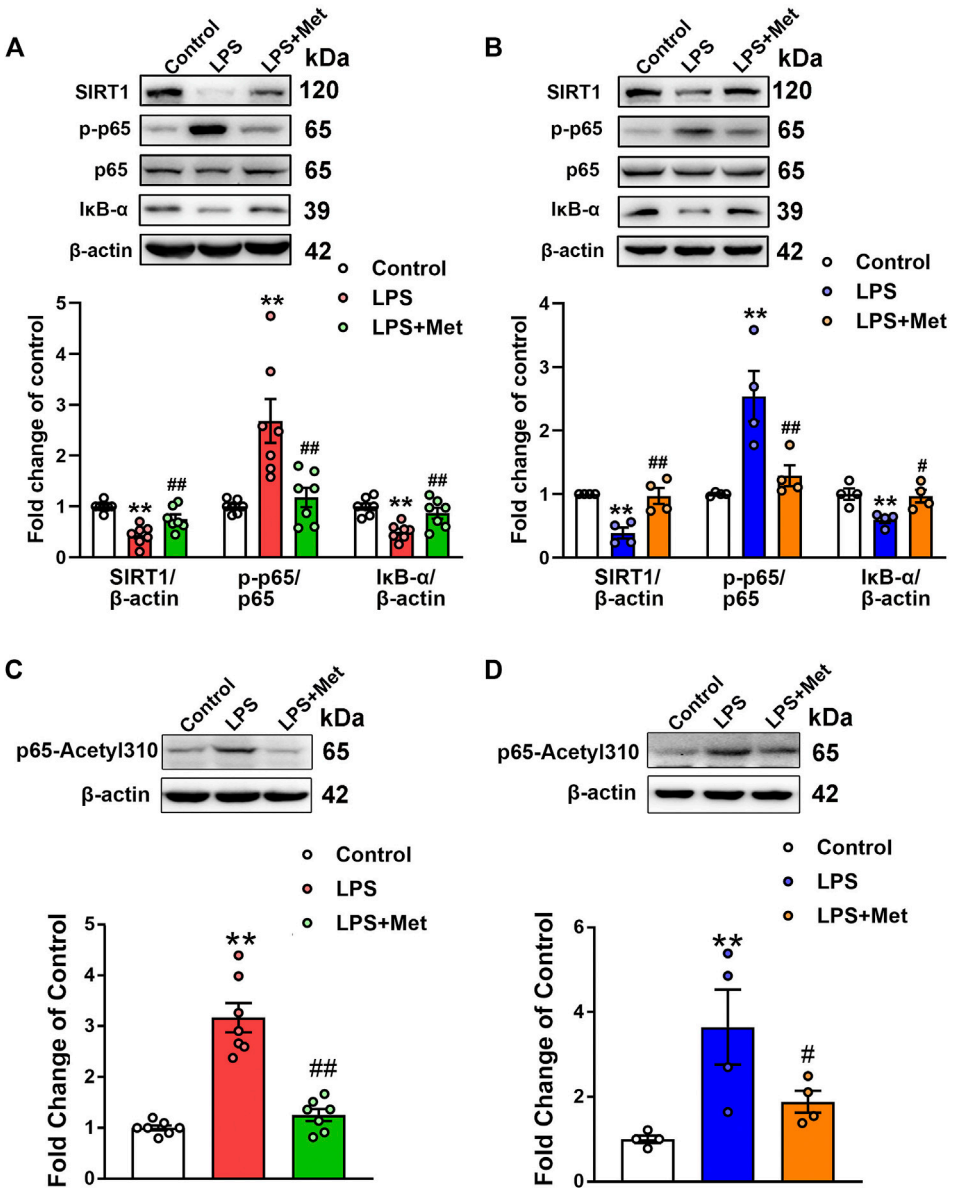

FIGURE 4 | Metformin suppresses the LPS-induced downregulation of SIRT1 both *in vivo* and *in vitro*. **(A)** Effects of metformin on the expression level of SIRT1 and NF-κB signaling pathway in pulmonary tissues of mice that received LPS intratracheally. Indicative bands are shown on the top of the histogram. Data are presented as mean ± SEM (n = 7). **(B)** Effects of metformin on the expression level of SIRT1 and NF-κB signaling pathway in primarily cultured pulmonary ECs. Representative bands are shown. Data are presented as mean ± SEM (n = 4). **(C)** Effects of metformin on the expression level of p65 lysine 310 acetylation in LPS-challenged mouse lung tissues. Data are presented as mean ± SEM (n = 7). **(D)** Effects of metformin on the expression level of p65 lysine 310 acetylation in LPS-treated pulmonary ECs. Data are presented as mean ± SEM (n = 4). $^{**}p < 0.01$ vs. Control group, #p <0.05, ##$p < 0.01$ vs. LPS group.

caspase-1 cleavage and IL-1β secretion (Li et al., 2017). In our experiment, we examined whether the inhibition of NLRP3 inflammasome mediated by metformin was regulated by SIRT1. The ECs were incubated with the SIRT1 inhibitor NAM before LPS and metformin treatment. Western blotting indicated that the protein levels of NLRP3, cleaved caspase-1, and N-terminal fragment of GSDMD were increased in the LPS group; however, these proteins decreased in the LPS + Met group and increased again in the LPS + Met + NAM group (**Figure 5A**). Furthermore, ELISA indicated that the suppression of SIRT1 reversed the effects of metformin on IL-1β levels in LPS-treated pulmonary ECs (**Figure 5B**). Similarly, treatment with NAM blocked the protective effect of metformin on LPS-induced expression of vascular adhesion molecules (**Supplementary Figure S4**). Phosphorylated NF-κB p65 subunit was increased, and IκB-α was decreased in the LPS + Met + NAM group compared with the LPS + Met group (**Figure 5C**). Moreover, p65 lysine

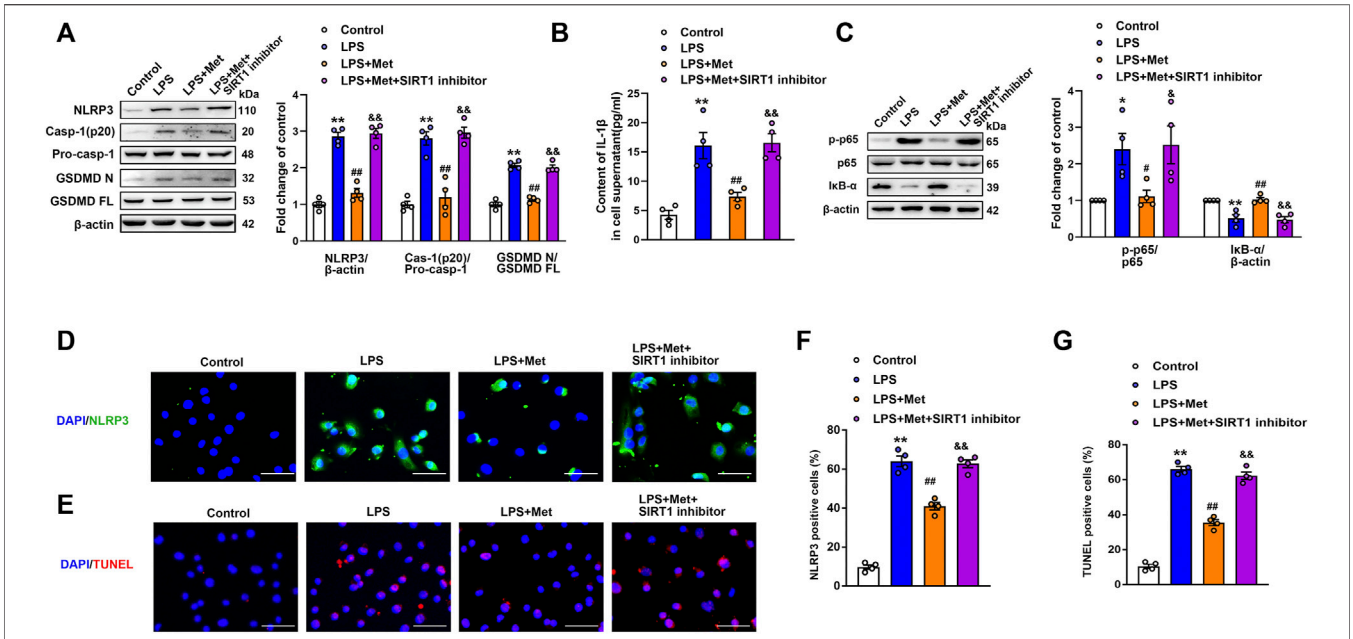

FIGURE 5 | The SIRT1 inhibitor nicotinamide prevents metformin from reducing LPS-induced pyroptosis in mice pulmonary ECs. **(A)** Western blotting analysis was used to determine the levels of NLRP3, cleaved caspase 1 (p20), and N-terminal fragment of GSDMD. Indicative bands are shown on the left of the histogram. **(B)** ELISA was used to determine the protein levels of IL-1β in supernatants. **(C)** Representative protein bands of NF-κB signaling pathway after pretreatment with NAM. **(D)** ECs were stained with NLRP3 (green). **(E)** Apoptotic cells were evaluated using TUNEL staining. The nuclei were stained blue using DAPI. **(F and G)** Percentage of NLRP3- and TUNEL-positive cells. Magnification: ×200. Scale bar, 50 μm. Data are presented as the mean ± SEM ($n = 4$). $^{*}p < 0.05$, $^{**}p < 0.01$ vs. Control group, $\#p < 0.05$, $\#\#p < 0.01$ vs. LPS group. $\&p < 0.05$, $\&\&p < 0.01$ vs. LPS + Met group.

310 acetylation was increased after SIRT1 inhibitor treatment (**Supplementary Figure S5B**). Meanwhile, SIRT1 siRNA was used to specifically knockdown the expression of SIRT1 in mouse pulmonary ECs; NF-κB p65 was assessed in nuclear lysates and cytoplasm, and representative bands are shown in **Supplementary Figure S6**. Furthermore, NLRP3 fluorescence intensity and TUNEL-positive endothelial cells, which were attenuated after treatment with metformin, were reversed by NAM administration (**Figures 5D–G**).

Inhibition of SIRT1 Reverses the Anti-Pyroptosis and Anti–Vascular Adhesion Molecules Effects of Metformin in Mice With LPS-Induced ALI

The role of the SIRT1 inhibitor in the anti-pyroptosis and anti–vascular adhesion molecules effects of metformin in LPS-induced ALI mice was further verified. As shown in **Figure 6A**, metformin significantly inhibited the expression levels of pyroptosis-associated proteins, including NLRP3, caspase-1 p20 fragment, and GSDMD p30 fragment, in the lung tissues of the mice challenged with LPS. However, when NAM was used to inhibit SIRT1, the anti-pyroptosis effects of metformin were suppressed. NAM also reversed the effects of metformin on IL-1β levels in the lungs of the mice exposed to LPS (**Figure 6B**). We also detected the protein levels of vascular adhesion molecules ICAM-1 and VCAM-1; the results indicated that after treatment with NAM, metformin no longer showed an inhibitory effect on vascular adhesion molecules (**Figure 6C**). The lung tissue level of the phosphorylated NF-κB p65 subunit was increased, whereas that of IκB-α was decreased in the LPS + Met + NAM group compared with the LPS + Met group (**Figure 6D**). The enhancement of p65 lysine 310 acetylation post-NAM treatment was also detected (Fig. S5A). $CD31^{+}$ $NLRP3^{+}$ and $CD31^{+}$ caspase-1^{+} cells were markedly reduced in lung tissues of ALI mice after treatment with metformin, and treatment with NAM reversed the inhibitory effect of metformin on NLRP3 and caspase-1 activation in the pulmonary endothelial cells of mice exposed to LPS administration (**Figures 6E–H**).

Inhibition of SIRT1 Eliminates the Protective Effect of Metformin on LPS-Induced Lung Injury in Mice

The SIRT1 inhibitor was used to evaluate the protective role of metformin on LPS-induced lung injury. As shown in **Figures 7A–C**, the treatment with NAM reversed the protective effects of metformin on LPS-stimulated lung injury, macrophage, and neutrophil infiltration. The W/D ratio and EBA extravasation were also elevated in the LPS + Met + NAM group compared with the LPS + Met group (**Figures 7D and E**), indicating that SIRT1 was a crucial facilitator in the protective effect of metformin in the lungs of LPS-induced ALI mice.

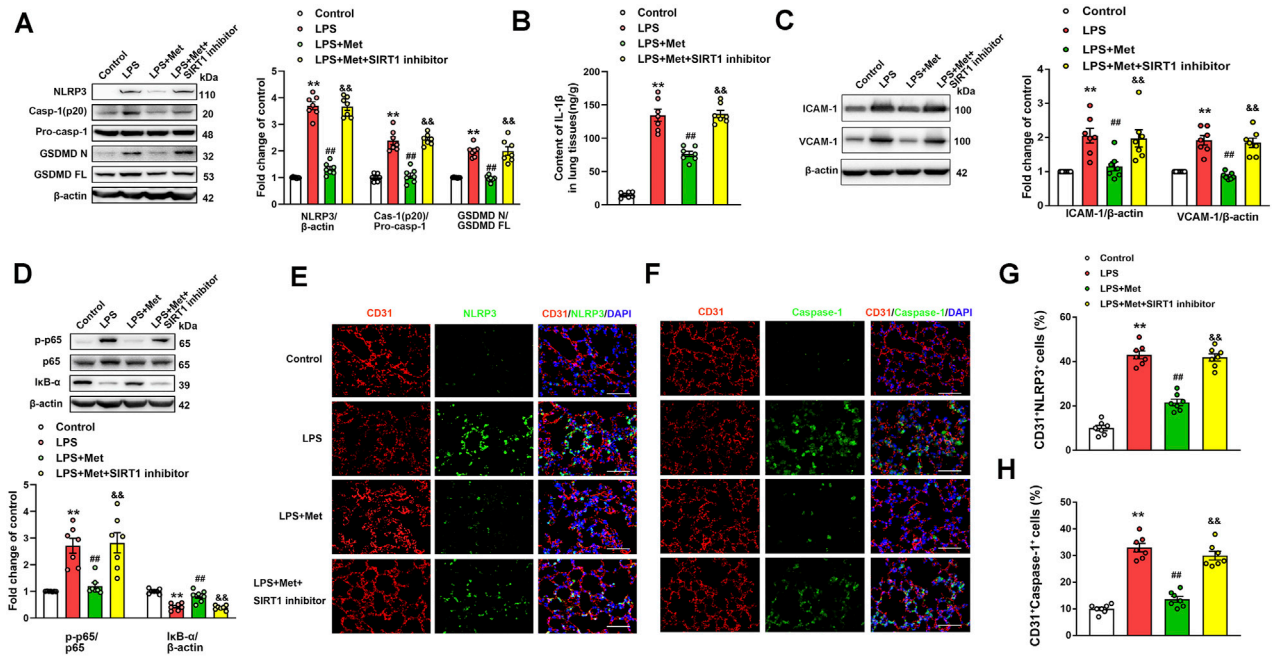

FIGURE 6 | The inhibition of SIRT1 prevents metformin from suppressing pyroptosis and vascular adhesion molecules in the lungs of LPS-induced ALI mice. **(A)** Represented pyroptosis-associated proteins in lung tissues of LPS-induced ALI mice after administration of NAM. **(B)** IL-1β protein level was detected. **(C)** Representative protein bands of ICAM-1 and VCAM-1 in lung tissue. **(D)** Representative protein bands of the NF-κB signaling pathway in lung tissues after pretreatment with NAM. **(E)** Lung tissues were stained with NLRP3 (green) and CD31 (red). Nuclei were counterstained with 4'6-diamidino-2-phenylindole (DAPI) (blue). **(F)** Lung tissues were stained with caspase-1 (green) and CD31 (red). Nuclei were counterstained with DAPI (blue). **(G)** Percentage of $CD31^{+}NLRP3^{+}$ cells. **(H)** Percentage of $CD31^{+}Caspase\text{-}1^{+}$ cells. Original magnification, ×200. Scale bar, 50 μm. Data are presented as the mean ± SEM ($n = 7$). $^{**}p < 0.01$ vs. Control group, $\#\#p < 0.01$ vs. LPS group. $\&\&p < 0.01$ vs. LPS + Met group.

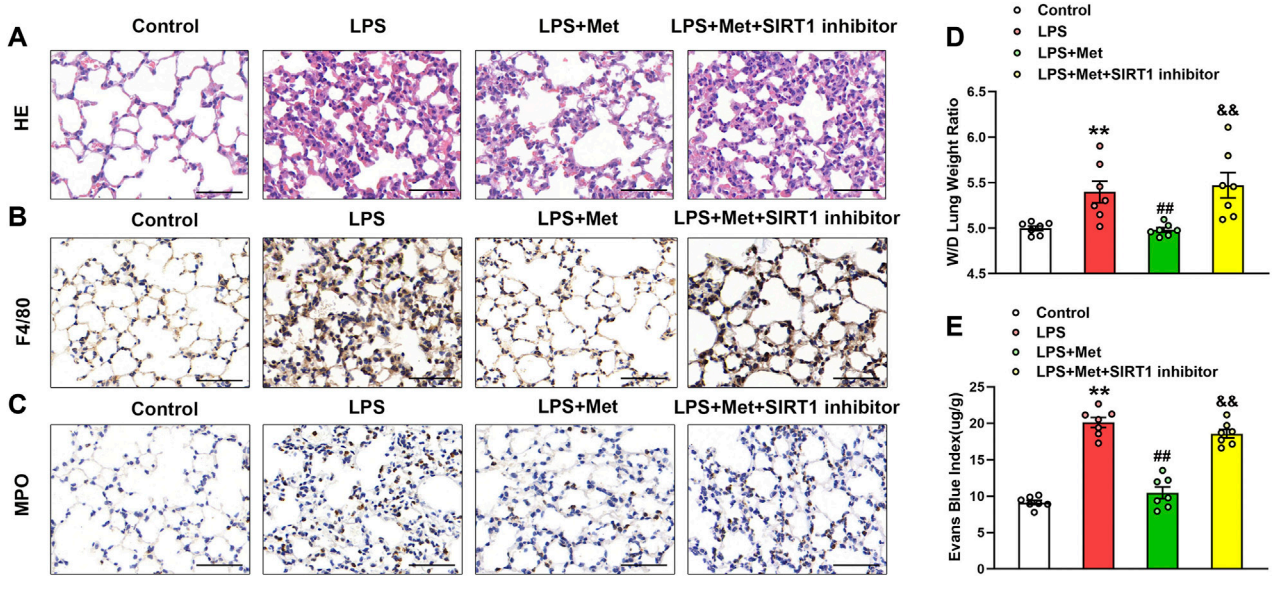

FIGURE 7 | The inhibition of SIRT1 prevents metformin from ameliorating the morphological characteristics and endothelial hyperpermeability of ALI. NAM (60 mg/kg) was administered 1 h before metformin administration. **(A)** Representative HE staining of lung tissues. **(B)** Immunohistochemistry analysis of F4/80. **(C)** Immunohistochemistry of MPO. **(D and E)** Lung W/D and Evans-blue dye extravasation were determined as indexes of pulmonary edema. Original magnification, ×200. Scale bar, 50 μm. Data are presented as the mean ± SEM ($n = 7$). $^{**}p < 0.01$ vs. Control group, $\#\#p < 0.01$ vs. LPS group. $\&\&p < 0.01$ vs. LPS + Met group.

DISCUSSION

In the current study, we illustrated that ECs pyroptosis plays a pivotal role in the pathogenesis of LPS-induced ARDS. We showed that the activation of pyroptosis was mediated by NF-κB, leading to elevated expression of NLRP3 and subsequent caspase-1 activation to produce and release inflammatory cytokines. Metformin, an antidiabetic drug, exhibited protective effects against LPS-induced ARDS *via* the activation of SIRT1, thereby inhibiting NF-κB/NLRP3 pathway–mediated pulmonary vascular ECs pyroptosis.

ARDS is a life-threatening lung injury of seriously ill patients, which is manifested by acute hypoxic respiratory failure and pulmonary inflammatory infiltrates (Diamond et al., 2021). A retrospective cohort study showed that metformin reduced mortality in COVID-19 patients in women with obesity or type 2 diabetes (Bramante et al., 2021). The protective effect of metformin may be attributed to its additional impact on inflammation (Valencia et al., 2017), given that the levels of high-sensitivity C-reactive protein after metformin treatment are reduced in women with diabetes compared with the placebo group (Haffner et al., 2005). Furthermore, short-term metformin treatment of non-diabetic subjects prevents acute inflammatory responses, such as ARDS. Researchers have demonstrated that metformin treatment prevents and ameliorates ARDS induced by LPS in mice, accompanied by abrogated NLRP3 inflammasome activation in macrophages, and attenuates pulmonary inflammation in COVID-19 patients (Xian et al., 2021). In the present study, we showed that metformin alleviated LPS-induced lung inflammation, including decreased MPO and macrophage infiltration. Notably, endothelial hyperpermeability in the lungs of LPS-induced ALI mice was also improved by metformin.

Metformin has been reported to improve vascular endothelial reactivity in type 2 diabetes patients with metabolic syndrome, which is a novel function in addition to its well-known antihyperglycemic effects (de Aguiar et al., 2006). Moreover, metformin protects against endothelial dysfunction in patients with metabolic syndrome by improving insulin resistance (Vitale et al., 2005). The effects of metformin in non-metabolic disease have also been studied. Current evidence suggests that concomitant administration of metformin during radiotherapy in rats decreases the expression of E-selectin, ICAM-1, and VCAM-1, thereby acting as a potent heart protector from endothelial dysfunction-induced damage (Karam and Radwan, 2019). There are multiple mechanisms by which metformin improves endothelial dysfunction, including the inhibition of an important mediator, LOX-1 signaling, thereby decreasing intracellular oxidative stress (Hattori et al., 2006; Xu et al., 2013). Other mechanisms underlying the protective effect of metformin in endothelial dysfunction also include inhibition of endothelial senescence and apoptosis (Arunachalam et al., 2014). In the present study, we found that metformin pretreatment effectively prevented pyroptosis in LPS-induced ARDS mice and LPS-treated lung ECs.

In eukaryotic cells, pyroptosis induced by inflammatory caspases serves as an innate immune strategy to protect against microbial infections (Bergsbaken et al., 2009; Jorgensen and Miao, 2015). Unlike the other forms of programmed cell death, here, the activation of caspases triggers lytic cell death, and GSDMD leads to pore formation, finally resulting in the cleavage of inflammatory cytokine IL-1β (Wallach et al., 2016). Unfettered pyroptosis can induce injury of multiple tissues, including ALI (Hou et al., 2018; Zeng et al., 2019); thus, targeting caspase-mediated pyroptosis in specific cell types, such as macrophages (Li et al., 2018), endothelial cells (Cheng et al., 2017), and epithelial cells (Zhang et al., 2018), may be a potential therapeutic strategy to alleviate inflammatory lung damage and organ failure, without degradation of the host defense barrier. Although the protective effects of metformin against lung injury have been well-demonstrated in various models (Tsaknis et al., 2012; Chen et al., 2015; Wu et al., 2018; Cheng et al., 2021), its protective effect against pulmonary ECs injury has not yet been reported. ECs line the surface of lung vasculature; thus, they are the first point of contact for pathogens and bacterial toxins and also the first point to respond to them. Vascular endothelial barrier refers to a semipermeable barrier that regulates the exchange of blood fluid and electrolytes across the blood vessel wall. At the blood–tissue interface, host defense is activated by an endothelial-based LPS detection system, which provides a defense mechanism. Therefore, the critical role of ECs in the systemic immune response to severe bacterial infection should be highlighted. Inflammasome and subsequent proinflammatory mediators release can be activated by administration of LPS into the lung tissue. It has been shown that LPS induces activation of inflammasome in mouse pulmonary ECs, thereby resulting in caspase-1 activation (Yang et al., 2016). In our study, mice lung tissues and ECs exposed to LPS showed increased expression levels of NLRP3 and cleaved GSDMD fragment and release of the proinflammatory cytokine IL-1β. Administration of metformin and NLRP3 inhibitor MCC950 remarkably decreased inflammasome activation and the level of pyroptosis-related indicators in LPS-treated pulmonary ECs and LPS-induced ALI mice, indicating that the potential therapeutic role of metformin in targeting the endothelial pyroptosis in ALI may be attributed to the activation of NLRP3 inflammasome. This is consistent with a recently published article that showed metformin abrogated macrophage NLRP3 inflammasome activation and pulmonary inflammation (Xian et al., 2021). Considering that metformin significantly inhibited macrophage inhibition, we detected the expression of vascular endothelial cell adhesion molecules ICAM-1 and VCAM-1 both *in vivo* and *in vitro*. We also examined the attachment of monocytes onto the activated endothelial cells. All these results suggested the underlying role of metformin in inhibiting macrophage infiltration.

K^+ efflux, reactive oxygen species (ROS) release, and lysosomal disruption can activate the NLRP3 inflammasome (Sutterwala et al., 2014). In addition, NF-κB is a central mediator of the priming signal of NLRP3 inflammasome activation; namely, activated NF-κB is translocated from cytoplasm to nucleus, whereby it transcriptionally activates the secretion of pro-IL-1β, pro-IL-18, and NLRP3, which are crucial for the induction of pyroptosis in several diseases (Li et al., 2019). Hattori et al. (2006) showed that metformin inhibited the cytokine-induced expression of proinflammatory and adhesion molecule genes by blocking NF-κB activation in vascular endothelial cells *via* AMPK activation. In this study, metformin

inhibited NF-κB phosphorylation in pulmonary tissues and mouse lung ECs following LPS treatment, indicating that metformin inhibited the NF-κB signaling pathway in LPS-induced pulmonary endothelial injury. SIRT1 has been reported to inhibit NF-κB by directly deacetylating the p65/RelA at lysine 310 (Yeung et al., 2004) or activating AMPK and PPARα, thus inhibiting the NF-κB pathway (Zhang et al., 2017). Notably, our study also demonstrated that the beneficial effects of metformin were mediated by SIRT1, as shown by the effects of the SIRT1 inhibitor NAM. Significant elevation of NF-κB phosphorylation and NLRP3-mediated pyroptosis-associated proteins due to inhibited SIRT1 expression by NAM was shown. Usually, NF-κB is bound in the cytoplasm by its inhibitor IκB. Upon stimulation, IκB is degraded so that NF-κB can translocate to the nucleus and stimulate inflammatory gene expression. In this study, SIRT1 inhibitors increased NF-κB p65 phosphorylation, showing that NF-κB p65 acts as a downstream target of SIRT1. Acetylation of the p65 at lysine 310 is a possible mechanism underlying the proinflammatory effect of the SIRT1 inhibitor (Schug et al., 2010). In this study, we also showed that SIRT1 reduced NF-κB activity by decreasing the acetylation level of lysine 310 of the NF-κB p65 subunit. However, we believe that it may not be the sole explanation because SIRT1 deletion inhibited the expression of IκB-α, which is an upstream signal of p65 nuclear translocation. Thus, further studies are warranted with regard to how SIRT1 regulates the NF-κB pathway.

In the present study, we observed elevated expression levels of NLRP3 and pyroptosis-associated proteins in LPS-treated endothelial cells and in the mouse lung tissues exposed to LPS. Furthermore, pyroptosis may play a crucial role in the development of LPS-induced inflammatory lung injury, whilst pulmonary endothelium is impaired and unable to provide barrier support effectively. Metformin recovered those detrimental changes, protected against endothelial dysfunction, and ultimately repaired the impaired lung functions, and the underlying mechanisms may be related to the activation of SIRT1. In summary, these results suggested that inhibition of endothelial pyroptosis and metformin treatment could be used as a novel therapeutic intervention strategy for ARDS treatment.

DATA AVAILABILITY STATEMENT

The raw data supporting the conclusions of this article will be made available by the authors, without undue reservation.

ETHICS STATEMENT

The animal study was reviewed and approved by the Ethical Committee of Xinhua Hospital, Shanghai Jiaotong University, School of Medicine.

AUTHOR CONTRIBUTIONS

YZ, YW, and LJ designed the experiments. HZ and SL performed the experiments and wrote the manuscript. KH participated in data assembly, analysis, and correction. All authors contributed to the article and approved the submitted version.

FUNDING

This work was financially supported by grants from the Shanghai Science and Technology Commission to YW (18YF1415500) and the National Natural Science Foundation of China to LJ (No. 82072209) and YW (No. 82002070).

ACKNOWLEDGMENTS

The authors thank LetPub (www.letpub.com) for its linguistic assistance during the preparation of this manuscript.

SUPPLEMENTARY MATERIAL

The Supplementary Material for this article can be found online at: https://www.frontiersin.org/articles/10.3389/fphar.2022.801337/full#supplementary-material

REFERENCES

Amato, M. B., Meade, M. O., Slutsky, A. S., Brochard, L., Costa, E. L., Schoenfeld, D. A., et al. (2015). Driving Pressure and Survival in the Acute Respiratory Distress Syndrome. *N. Engl. J. Med.* 372 (8), 747–755. doi:10.1056/NEJMsa1410639

Arunachalam, G., Samuel, S. M., Marei, I., Ding, H., and Triggle, C. R. (2014). Metformin Modulates Hyperglycaemia-Induced Endothelial Senescence and Apoptosis through SIRT1. *Br. J. Pharmacol.* 171 (2), 523–535. doi:10.1111/bph.12496

Bergsbaken, T., Fink, S. L., and Cookson, B. T. (2009). Pyroptosis: Host Cell Death and Inflammation. *Nat. Rev. Microbiol.* 7 (2), 99–109. doi:10.1038/nrmicro2070

Bramante, C. T., Ingraham, N. E., Murray, T. A., Marmor, S., Hovertsen, S., Gronski, J., et al. (2021). Metformin and Risk of Mortality in Patients Hospitalised with COVID-19: a Retrospective Cohort Analysis. *Lancet Healthy Longev.* 2 (1), e34–e41. doi:10.1016/S2666-7568(20)30033-7

Broz, P. (2019). Recognition of Intracellular Bacteria by Inflammasomes. *Microbiol. Spectr.* 7 (2), BAI-0003-2019. doi:10.1128/microbiolspec.BAI-0003-2019

Chen, X., Walther, F. J., Sengers, R. M., Laghmani, el H., Salam, A., Folkerts, G., et al. (2015). Metformin Attenuates Hyperoxia-Induced Lung Injury in Neonatal Rats by Reducing the Inflammatory Response. *Am. J. Physiol. Lung Cell Mol. Physiol.* 309 (3), L262–L270. doi:10.1152/ajplung.00389.2014

Cheng, D., Xu, Q., Wang, Y., Li, G., Sun, W., Ma, D., et al. (2021). Metformin Attenuates Silica-Induced Pulmonary Fibrosis via AMPK Signaling. *J. Transl. Med.* 19 (1), 349. doi:10.1186/s12967-021-03036-5

Cheng, K. T., Xiong, S., Ye, Z., Hong, Z., Di, A., Tsang, K. M., et al. (2017). Caspase-11-mediated Endothelial Pyroptosis Underlies Endotoxemia-Induced Lung Injury. *J. Clin. Invest.* 127 (11), 4124–4135. doi:10.1172/JCI94495

de Aguiar, L. G., Bahia, L. R., Villela, N., Laflor, C., Sicuro, F., Wiernsperger, N., et al. (2006). Metformin Improves Endothelial Vascular Reactivity in First-Degree Relatives of Type 2 Diabetic Patients with Metabolic Syndrome and Normal Glucose Tolerance. *Diabetes Care* 29 (5), 1083–1089. doi:10.2337/diacare.2951083

Diamond, M., Peniston, H. L., Sanghavi, D., and Mahapatra, S. (2021). *Acute Respiratory Distress Syndrome*. Treasure Island (FL): StatPearls.

Dong, W. W., Liu, Y. J., Lv, Z., Mao, Y. F., Wang, Y. W., Zhu, X. Y., et al. (2015). Lung Endothelial Barrier Protection by Resveratrol Involves Inhibition of

HMGB1 Release and HMGB1-Induced Mitochondrial Oxidative Damage via an Nrf2-dependent Mechanism. *Free Radic. Biol. Med.* 88 (Pt B), 404–416. doi:10.1016/j.freeradbiomed.2015.05.004

Gao, J., Yuan, J., Wang, Q., Lei, T., Shen, X., Cui, B., et al. (2020). Metformin Protects against PM2.5-induced Lung Injury and Cardiac Dysfunction Independent of AMP-Activated Protein Kinase α2. *Redox Biol.* 28, 101345. doi:10.1016/j.redox.2019.101345

Guérin, C., Reignier, J., Richard, J. C., Beuret, P., Gacouin, A., Boulain, T., et al. (2013). Prone Positioning in Severe Acute Respiratory Distress Syndrome. *N. Engl. J. Med.* 368 (23), 2159–2168. doi:10.1056/NEJMoa1214103

Haffner, S., Temprosa, M., Crandall, J., Fowler, S., Goldberg, R., Horton, E., et al. (2005). Intensive Lifestyle Intervention or Metformin on Inflammation and Coagulation in Participants with Impaired Glucose Tolerance. *Diabetes* 54 (5), 1566–1572. doi:10.2337/diabetes.54.5.1566

Han, S., and Mallampalli, R. K. (2015). The Acute Respiratory Distress Syndrome: From Mechanism to Translation. *J. Immunol.* 194 (3), 855–860. doi:10.4049/jimmunol.1402513

Hattori, Y., Suzuki, K., Hattori, S., and Kasai, K. (2006). Metformin Inhibits Cytokine-Induced Nuclear Factor kappaB Activation via AMP-Activated Protein Kinase Activation in Vascular Endothelial Cells. *Hypertension* 47 (6), 1183–1188. doi:10.1161/01.HYP.0000221429.94591.72

Heidari, B., Lerman, A., Lalia, A. Z., Lerman, L. O., and Chang, A. Y. (2019). Effect of Metformin on Microvascular Endothelial Function in Polycystic Ovary Syndrome. *Mayo Clin. Proc.* 94 (12), 2455–2466. doi:10.1016/j.mayocp.2019.06.015

Herman, F. J., and Pasinetti, G. M. (2018). Principles of Inflammasome Priming and Inhibition: Implications for Psychiatric Disorders. *Brain Behav. Immun.* 73, 66–84. doi:10.1016/j.bbi.2018.06.010

Hou, L., Yang, Z., Wang, Z., Zhang, X., Zhao, Y., Yang, H., et al. (2018). NLRP3/ASC-mediated Alveolar Macrophage Pyroptosis Enhances HMGB1 Secretion in Acute Lung Injury Induced by Cardiopulmonary Bypass. *Lab. Invest.* 98 (8), 1052–1064. doi:10.1038/s41374-018-0073-0

Ito, H., Kimura, H., Karasawa, T., Hisata, S., Sadatomo, A., Inoue, Y., et al. (2020). NLRP3 Inflammasome Activation in Lung Vascular Endothelial Cells Contributes to Intestinal Ischemia/Reperfusion-Induced Acute Lung Injury. *J. Immunol.* 205 (5), 1393–1405. doi:10.4049/jimmunol.2000217

Jia, C., Chen, H., Zhang, J., Zhou, K., Zhuge, Y., Niu, C., et al. (2019). Role of Pyroptosis in Cardiovascular Diseases. *Int. Immunopharmacol.* 67, 311–318. doi:10.1016/j.intimp.2018.12.028

Jorgensen, I., and Miao, E. A. (2015). Pyroptotic Cell Death Defends Against Intracellular Pathogens. *Immunol. Rev.* 265 (1), 130–142. doi:10.1111/imr.12287

Karam, H. M., and Radwan, R. R. (2019). Metformin Modulates Cardiac Endothelial Dysfunction, Oxidative Stress and Inflammation in Irradiated Rats: A New Perspective of an Antidiabetic Drug. *Clin. Exp. Pharmacol. Physiol.* 46 (12), 1124–1132. doi:10.1111/1440-1681.13148

Li, D., Ren, W., Jiang, Z., and Zhu, L. (2018). Regulation of the NLRP3 Inflammasome and Macrophage Pyroptosis by the P38 MAPK Signaling Pathway in a Mouse Model of Acute Lung Injury. *Mol. Med. Rep.* 18 (5), 4399–4409. doi:10.3892/mmr.2018.9427

Li, Y., Wang, P., Yang, X., Wang, W., Zhang, J., He, Y., et al. (2016). SIRT1 Inhibits Inflammatory Response Partly through Regulation of NLRP3 Inflammasome in Vascular Endothelial Cells. *Mol. Immunol.* 77, 148–156. doi:10.1016/j.molimm.2016.07.018

Li, Y., Yang, X., He, Y., Wang, W., Zhang, J., Zhang, W., et al. (2017). Negative Regulation of NLRP3 Inflammasome by SIRT1 in Vascular Endothelial Cells. *Immunobiology* 222 (3), 552–561. doi:10.1016/j.imbio.2016.11.002

Li, Z., Chen, D., Jia, Y., Feng, Y., Wang, C., Tong, Y., et al. (2019). Methane-Rich Saline Counteracts Cholestasis-Induced Liver Damage via Regulating the TLR4/NF-κB/NLRP3 Inflammasome Pathway. *Oxidative Med. Cell. Longev.* 2019, 6565283. doi:10.1155/2019/6565283

Lin, Z., Jin, J., Bai, W., Li, J., and Shan, X. (2018). Netrin-1 Prevents the Attachment of Monocytes to Endothelial Cells via an Anti-inflammatory Effect. *Mol. Immunol.* 103, 166–172. doi:10.1016/j.molimm.2018.08.021

Mathur, A., Hayward, J. A., and Man, S. M. (2018). Molecular Mechanisms of Inflammasome Signaling. *J. Leukoc. Biol.* 103 (2), 233–257. doi:10.1189/jlb.3MR0617-250R

Matthay, M. A., and Zemans, R. L. (2011). The Acute Respiratory Distress Syndrome: Pathogenesis and Treatment. *Annu. Rev. Pathol.* 6, 147–163. doi:10.1146/annurev-pathol-011110-130158

Nafisa, A., Gray, S. G., Cao, Y., Wang, T., Xu, S., Wattoo, F. H., et al. (2018). Endothelial Function and Dysfunction: Impact of Metformin. *Pharmacol. Ther.* 192, 150–162. doi:10.1016/j.pharmthera.2018.07.007

Papazian, L., Forel, J. M., Gacouin, A., Penot-Ragon, C., Perrin, G., Loundou, A., et al. (2010). Neuromuscular Blockers in Early Acute Respiratory Distress Syndrome. *N. Engl. J. Med.* 363 (12), 1107–1116. doi:10.1056/NEJMoa1005372

Park, C. S., Bang, B. R., Kwon, H. S., Moon, K. A., Kim, T. B., Lee, K. Y., et al. (2012). Metformin Reduces Airway Inflammation and Remodeling via Activation of AMP-Activated Protein Kinase. *Biochem. Pharmacol.* 84 (12), 1660–1670. doi:10.1016/j.bcp.2012.09.025

Peek, G. J., Mugford, M., Tiruvoipati, R., Wilson, A., Allen, E., Thalanany, M. M., et al. (2009). Efficacy and Economic Assessment of Conventional Ventilatory Support versus Extracorporeal Membrane Oxygenation for Severe Adult Respiratory Failure (CESAR): a Multicentre Randomised Controlled Trial. *Lancet* 374 (9698), 1351–1363. doi:10.1016/S0140-6736(09)61069-2

Schug, T. T., Xu, Q., Gao, H., Peres-da-Silva, A., Draper, D. W., Fessler, M. B., et al. (2010). Myeloid Deletion of SIRT1 Induces Inflammatory Signaling in Response to Environmental Stress. *Mol. Cell Biol.* 30 (19), 4712–4721. doi:10.1128/MCB.00657-10

Shi, J., Zhao, Y., Wang, K., Shi, X., Wang, Y., Huang, H., et al. (2015). Cleavage of GSDMD by Inflammatory Caspases Determines Pyroptotic Cell Death. *Nature* 526 (7575), 660–665. doi:10.1038/nature15514

Sutterwala, F. S., Haasken, S., and Cassel, S. L. (2014). Mechanism of NLRP3 Inflammasome Activation. *Ann. N. Y. Acad. Sci.* 1319, 82–95. doi:10.1111/nyas.12458

Tang, S., Huang, G., Fan, W., Chen, Y., Ward, J. M., Xu, X., et al. (2014). SIRT1-mediated Deacetylation of CRABPII Regulates Cellular Retinoic Acid Signaling and Modulates Embryonic Stem Cell Differentiation. *Mol. Cell* 55 (6), 843–855. doi:10.1016/j.molcel.2014.07.011

Tsaknis, G., Siempos, I. I., Kopterides, P., Maniatis, N. A., Magkou, C., Kardara, M., et al. (2012). Metformin Attenuates Ventilator-Induced Lung Injury. *Crit. Care* 16 (4), R134. doi:10.1186/cc11439

Vaez, H., Najafi, M., Toutounchi, N. S., Barar, J., Barzegari, A., and Garjani, A. (2016). Metformin Alleviates Lipopolysaccharide-Induced Acute Lung Injury through Suppressing Toll-like Receptor 4 Signaling. *Iran. J. Allergy Asthma Immunol.* 15 (6), 498–507.

Valencia, W. M., Palacio, A., Tamariz, L., and Florez, H. (2017). Metformin and Ageing: Improving Ageing Outcomes beyond Glycaemic Control. *Diabetologia* 60 (9), 1630–1638. doi:10.1007/s00125-017-4349-5

Vitale, C., Mercuro, G., Cornoldi, A., Fini, M., Volterrani, M., and Rosano, G. M. (2005). Metformin Improves Endothelial Function in Patients with Metabolic Syndrome. *J. Intern Med.* 258 (3), 250–256. doi:10.1111/j.1365-2796.2005.01531.x

Wallach, D., Kang, T. B., Dillon, C. P., and Green, D. R. (2016). Programmed Necrosis in Inflammation: Toward Identification of the Effector Molecules. *Science* 352 (6281), aaf2154. doi:10.1126/science.aaf2154

Wang, R. H., Sengupta, K., Li, C., Kim, H. S., Cao, L., Xiao, C., et al. (2008). Impaired DNA Damage Response, Genome Instability, and Tumorigenesis in SIRT1 Mutant Mice. *Cancer Cell* 14 (4), 312–323. doi:10.1016/j.ccr.2008.09.001

Wang, S., Yuan, Y. H., Chen, N. H., and Wang, H. B. (2019). The Mechanisms of NLRP3 Inflammasome/pyroptosis Activation and Their Role in Parkinson's Disease. *Int. Immunopharmacol.* 67, 458–464. doi:10.1016/j.intimp.2018.12.019

Wang, Y., Xu, C. F., Liu, Y. J., Mao, Y. F., Lv, Z., Li, S. Y., et al. (2017). Salidroside Attenuates Ventilation Induced Lung Injury via SIRT1-Dependent Inhibition of NLRP3 Inflammasome. *Cell Physiol. Biochem.* 42 (1), 34–43. doi:10.1159/000477112

Wu, K., Tian, R., Huang, J., Yang, Y., Dai, J., Jiang, R., et al. (2018). Metformin Alleviated Endotoxemia-Induced Acute Lung Injury via Restoring AMPK-dependent Suppression of mTOR. *Chem. Biol. Interact.* 291, 1–6. doi:10.1016/j.cbi.2018.05.018

Xian, H., Liu, Y., Rundberg Nilsson, A., Gatchalian, R., Crother, T. R., Tourtellotte, W. G., et al. (2021). Metformin Inhibition of Mitochondrial ATP and DNA Synthesis Abrogates NLRP3

Inflammasome Activation and Pulmonary Inflammation. *Immunity* 54 (7), 1463–e11. doi:10.1016/j.immuni.2021.05.004

Xiang, M., Shi, X., Li, Y., Xu, J., Yin, L., Xiao, G., et al. (2011). Hemorrhagic Shock Activation of NLRP3 Inflammasome in Lung Endothelial Cells. *J. Immunol.* 187 (9), 4809–4817. doi:10.4049/jimmunol.1102093

Xu, S., Ogura, S., Chen, J., Little, P. J., Moss, J., and Liu, P. (2013). LOX-1 in Atherosclerosis: Biological Functions and Pharmacological Modifiers. *Cell Mol. Life Sci.* 70 (16), 2859–2872. doi:10.1007/s00018-012-1194-z

Yang, J., Zhao, Y., Zhang, P., Li, Y., Yang, Y., Yang, Y., et al. (2016). Hemorrhagic Shock Primes for Lung Vascular Endothelial Cell Pyroptosis: Role in Pulmonary Inflammation Following LPS. *Cell Death Dis.* 7 (9), e2363. doi:10.1038/cddis.2016.274

Yeung, F., Hoberg, J. E., Ramsey, C. S., Keller, M. D., Jones, D. R., Frye, R. A., et al. (2004). Modulation of NF-kappaB-dependent Transcription and Cell Survival by the SIRT1 Deacetylase. *EMBO J.* 23 (12), 2369–2380. doi:10.1038/sj.emboj.7600244

Zeng, Y., Qin, Q., Li, K., Li, H., Song, C., Li, Y., et al. (2019). PKR Suppress NLRP3-Pyroptosis Pathway in Lipopolysaccharide-Induced Acute Lung Injury Model of Mice. *Biochem. Biophys. Res. Commun.* 519 (1), 8–14. doi:10.1016/j.bbrc.2019.08.054

Zhang, B., Zhou, X., Qiu, Y., Song, Y., Feng, F., Feng, J., et al. (2020). Clinical Characteristics of 82 Cases of Death from COVID-19. *PLoS One* 15 (7), e0235458. doi:10.1371/journal.pone.0235458

Zhang, W., Huang, Q., Zeng, Z., Wu, J., Zhang, Y., and Chen, Z. (2017). Sirt1 Inhibits Oxidative Stress in Vascular Endothelial Cells. *Oxid. Med. Cell Longev.* 2017, 7543973. doi:10.1155/2017/7543973

Zhang, Z., Shao, X., Jiang, N., Mou, S., Gu, L., Li, S., et al. (2018). Caspase-11-mediated Tubular Epithelial Pyroptosis Underlies Contrast-Induced Acute Kidney Injury. *Cell Death Dis.* 9 (10), 983. doi:10.1038/s41419-018-1023-x

Zhou, X., Wang, Q., Nie, L., Zhang, P., Zhao, P., Yuan, Q., et al. (2020). Metformin Ameliorates the NLPP3 Inflammasome Mediated Pyroptosis by Inhibiting the Expression of NEK7 in Diabetic Periodontitis. *Arch. Oral Biol.* 116, 104763. doi:10.1016/j.archoralbio.2020.104763

Conflict of Interest: The authors declare that the research was conducted in the absence of any commercial or financial relationships that could be construed as a potential conflict of interest.

Publisher's Note: All claims expressed in this article are solely those of the authors and do not necessarily represent those of their affiliated organizations, or those of the publisher, the editors, and the reviewers. Any product that may be evaluated in this article, or claim that may be made by its manufacturer, is not guaranteed or endorsed by the publisher.

Advantages of publishing in Frontiers

OPEN ACCESS
Articles are free to read for greatest visibility and readership

FAST PUBLICATION
Around 90 days from submission to decision

HIGH QUALITY PEER-REVIEW
Rigorous, collaborative, and constructive peer-review

TRANSPARENT PEER-REVIEW
Editors and reviewers acknowledged by name on published articles

Frontiers
Avenue du Tribunal-Fédéral 34
1005 Lausanne | Switzerland

Visit us: www.frontiersin.org
Contact us: frontiersin.org/about/contact

REPRODUCIBILITY OF RESEARCH
Support open data and methods to enhance research reproducibility

DIGITAL PUBLISHING
Articles designed for optimal readership across devices

FOLLOW US
@frontiersin

IMPACT METRICS
Advanced article metrics track visibility across digital media

EXTENSIVE PROMOTION
Marketing and promotion of impactful research

LOOP RESEARCH NETWORK
Our network increases your article's readership